Assembly of 3D DNA Architectures: Towards Minimal Design and Maximal Function

by

Christopher K. McLaughlin

A Thesis submitted to McGill University in partial fulfillment of the requirements of the degree of

Doctor of Philosophy

Department of Chemistry
McGill University
Montreal, Quebec, Canada

April 2012

I dedicate this thesis to my mother Marg, father Karl, sister Amanda and brother Jason for their continued love and support.

Abstract

DNA serves as the essential biomacromolecule responsible for encoding, transmitting and expressing genetic information in all forms of life. However, when taken out of this biological role, the unique self-assembling properties, information rich content and easy means of chemical synthesis make DNA an ideal material for solving some of the challenging problems in chemical construction at the nanometer length scale. The emerging field of *supramolecular DNA assembly* presents chemical solutions to DNA construction, by synthetically modifying DNA with small molecules and supramolecular motifs. This thesis specifically examines how DNA building blocks modified with synthetic organic, inorganic and polymeric molecules can be designed to efficiently assemble into well-defined 3D structures. In part 1, a modular assembly strategy is developed whereby 2D DNA triangles are efficiently prepared and connected to create the first triangular prismatic structure that can be site-specifically coordinated with transition metals. In part 2, selective introduction of sequence symmetry is utilized to both simplify design and generate an expanded set of 3D DNA geometries in a mild, facile and high yield manner. In parts 3 and 4, a 3D DNA construction method that assembles a minimum number of DNA strands in near quantitative yield, to give a scaffold with a large number of single-stranded arms, is introduced. As demonstrated in part 3, site-specific hybridization of DNA-polymer conjugates to the single-stranded arms of this 3D-DNA scaffold gives efficient access to nanostructured DNA-block copolymer cages with enhanced nuclease resistance. In part 4, it is demonstrated that unfunctionalized 3D DNA cubes efficiently accumulate in the cytoplasm of human cervical cancer cells (HeLa) without the aid of any transfection agent. Collectively, this work develops 'DNA-economic' strategies to assemble 3D DNA structures in a facile manner and excellent yield. These assembly methods lay the foundation for fundamental assessment and future integration of 3D DNA structures as cellular probes or drug delivery tools and as a means to help solve some of the challenges facing researchers in biophysics and nanoscience.

Rèsumè

L'ADN est une biomacromolécule essentielle qui sert à encoder, transmettre et exprimer l'information génétique contenue dans toutes les formes de vie. Toutefois, à

l'extérieur de ce contexte biologique, les propriétés uniques d'auto-assemblage, le contenu riche en information et les méthodes de synthèse chimique simples qui sont associées à l'ADN en font un matériau idéal pour résoudre certains des grands défis dans la construction à l'échelle nanométrique. Le domaine émergent de l'*assemblage supramoléculaire de l'ADN* présente des solutions chimiques pour la construction de nanostructures au moyen de l'ADN, en modifiant celui-ci synthétiquement avec des molécules organiques et des motifs supramoléculaires. Cette thèse examine spécifiquement comment des blocs de construction d'ADN modifiés avec des molécules synthétiques organiques, inorganiques et des polymères peuvent être conçus pour s'assembler en structures 3D bien définies et de manière efficace. Dans la 1^{e} partie, une stratégie d'assemblage modulaire est développée. Celle-ci permet de relier des triangles d'ADN bidimensionnels préparés de façon efficace pour créer la première structure prismatique triangulaire en 3D qui peut être coordonnée en des lieux spécifiques avec des métaux de transition. Dans la 2^{e} partie, l'introduction sélective de symétrie dans les séquences est utilisée pour à la fois simplifier la conception et pour générer un ensemble élargi de géométries d'ADN en 3D d'une manière simple et haute en rendement. Dans les 3^{e} et 4^{e} parties, une méthode de construction d'ADN en 3D qui assemble un nombre minimal de brins dans un rendement presque quantitatif pour donner une structure comportant un grand nombre de sections en ADN simple-brin est introduite. Comme démontré dans la 3^{e} partie, l'hybridation spécifique de conjugués d'ADN-polymère aux sections en simple-brin de cet échafaudage d'ADN tridimensionnel permet l'assemblage efficace de cages nanostructurées d'ADN-copolymère séquencé avec une résistance améliorée aux nucléases. Dans la 4^{e} partie, il est démontré que des cubes d'ADN en 3D non-fonctionnalisés s'accumulent efficacement dans le cytoplasme de cellules humaines du cancer du col de l'utérus (HeLa) sans l'aide d'un agent de transfection. Collectivement, ce travail développe des stratégies «économiques en ADN» pour assembler des structures d'ADN en 3D d'une manière simple et avec un excellent rendement. Ces méthodes d'assemblage jettent les bases pour l'évaluation fondamentale et l'intégration future de structures d'ADN en 3D en tant que sondes cellulaires, outils d'administration de médicaments et moyens pour aider à résoudre certains des défis auxquels sont confrontés les chercheurs en biophysique et nanosciences.

Acknowledgments

My research time at McGill has been filled from day 1, with family, friends and colleagues; all of which have contributed to my life and academic journey.

I would first like to thank my supervisor and mentor, Hanadi Sleiman, for her support throughout my research. Her enthusiasm in research and endless creativity provided an ideal environment for exploring creative means of self-assembly. I thank her greatly for the encouragement, insight, attention to detail and impact on my development as a scientist.

To my first research mentor at McGill, Faisal Aldaye, I can't thank you enough. Your hard work and dedication on a daily to basis to discovery and analysis was inspiring. If it didn't work, we tried it again. Also, to Hua Yang whom I had the extreme pleasure of working side by side to the end of my first project/publication, I thank you for your hard work and motivating spirit. It took us awhile, but the journey was oh-so sweet.

I am forever in debt to Graham Hamblin, with whom I was lucky enough to work with on multiple projects. No matter what the code name, the mission was eventually completed. And though the battle scars may endure, the stories will live on forever.

To all my lab mates over the years (and there have been many), I thank you for putting up with me and trying your best to infuse my daily routine with scientific discussion, dedicated assistance and most of all copious amounts of humour. Thank you and good luck to you all.

To all the personnel at the electron microscopy center, I thank you for your dedication and assistance over the years as I embarked on my (unfinished) structural quest. I thank Dr. Kelly Sears and Dr. Hojatollah Vali for the countless times microscope expertise was required. I thank, Dr. Driss Mountassif, Lucien Fabre and Dr. Mihnea Bostina for their assistance and insight with cryo-EM. I especially thank Dr. Isabelle Rouiller whom took countless hours of her own time to personally train me to both freeze and acquire cryo-EM images. This journey is just starting and there is so much more I am sure you all could teach me.

I thank the crew of P. Farb, K. Luska, M. Huot and J. Fuller. Whether the classification be gentlemen and scholars, slap-stick comedians and athletes or ruffians and topers, you have reserved a place in my heart (there is room for you all, don't worry). Remember, time stops and the game is over only when the scorers table has been McBoomed.

What is life without music? Not much in my opinion. And so I am eternally grateful to Dr. Rock and The Ox for the many shared musical moments. The Ox, for his dystopian shredding and lead singer swagger, always fun to watch. Dr. Rock, for the surging beats and locked in rhythms, always a pleasure. And not to forget our 4th member, the south shore criminal, JCON for his never ending smile and supply of 'string' supported musical attack. Everyone will one day long to hear tales of the adventures of Le Moondog. Not one note to many, ever.

It would be remiss to not thank departmental chair Professor R. B. Lennox and building director N. Trempe for their dedicated work over the years to ensure the refurbishment of OM. The moves kept me on my toes, but the end result has been amazing. Moreover, to Chantal Marotte for the countless answered questions, explanations and navigation through the minefield of paper work and for her always friendly/approachable demeanor. You are the greatest. I would also like to acknowledge the Chemistry Department and University for financial support through scholarships and departmental awards.

And last but not least, to my entire extended family who has supported me during this academic process. I believe a number of you have already spent my first paycheck from the 'real world'. Still might be awhile before we get to that evening out… To my father and mother, this part of my life journey would not have been completed without your love and support. I am indebted to you both for both of your unwavering and unconditional support and to the way in which your respective hard working ways have motivated me to push forward. I can't ever thank you enough.

Contribution of authors

All papers presented in chapters 1 - 6 were co-authored with Prof. Hanadi F. Sleiman (Department of Chemistry, McGill University), who acted as research advisor.

As outlined below, contributions from a variety of colleagues to assist in both the preparation and characterization of materials for successful publishing were required.

Chapter 1: Contains work from a review written on the field of supramolecular DNA assembly. Christopher McLaughlin wrote, edited and prepared figures for the manuscript. Graham Hamblin assisted in writing, editing and graphical preparation for the manuscript.

Chapter 2: Christopher McLaughlin, contributed to project design, developed method of 3D assembly, characterized 3D structures using enzymatic experiments, helped performed metallation studies, performed electron microscopy, performed fluorescence experiments and prepared/edited manuscript. Hua Yang contributed to project design, performed synthesis of dpp DNA, characterized metallated DNA products (CD, UV/Vis and PAGE), and prepared/edited manuscript. Faisal Aldaye contributed to both project design and preliminary PAGE studies. Andrzej Rys prepared dpp phosphoramidite. Graham Hamblin assisted with electron microscopy and helped prepare graphics. Dr. Isabelle Rouiller assisted with electron microscopy studies.

Chapter 3: Christopher McLaughlin, contributed to project design, developed method of 3D assembly, completed all final PAGE studies, characterized 3D structures using enzymatic experiments and prepared/edited manuscript. Graham Hamblin assisted with project design and preliminary PAGE characterization of 3D structures, generated graphics and helped prepare/edit manuscript. Hua Yang and Faisal Aldaye assisted with project design.

Chapter 4: Christopher McLaughlin contributed to project design, developed method of 3D assembly, completed all final PAGE studies, characterized 3D structures using enzymatic experiments, DLS and cryo-EM, performed DNA-polymer conjugation and characterization, carried out nuclease studies and prepared/edited manuscript. Graham Hamblin contributed to design and development of 3D assembly, performed preliminary PAGE investigations, prepared graphics and edited manuscript. Kevin Hanni synthesized polymer. Justin Conway performed AFM studies. Karina Carneiro assisted with MALDI characterization of DNA-polymer conjugate. Manoj Nayak prepared monomers used for polymer synthesis. Dr. Hassan Bazzi helped design polymer.

Chapter 5: Christopher McLaughlin contributed to project design, developed method of 3D assembly, completed all final PAGE studies, characterized 3D structures using enzymatic experiments, prepared 3D structure for cell studies, labeled DNA with Cy5, developed FRET system and prepared/edited manuscript. Johans Fakhoury contributed to project design, carried out all cell studies (confocal microscopy and flow cytometry) and prepared/edited manuscript.

Appendix 1: Christopher McLaughlin contributed to project design, performed DNA gold nanoparticle (AuNP) conjugations, developed extension strand method for AuNP characterization, performed agarose gel electrophoresis and TEM characterization of AuNP-DNA conjugates and prepared/edited manuscript. Yongqiang Wen contributed to project design, performed DNA gold nanoparticle (AuNP) conjugations, assembled AuNP-DNA structures and bis-AuNP-DNA structures, performed agarose gel electrophoresis and TEM characterization of AuNP-DNA conjugates and prepared/edited manuscript. Pik Kwan Lo and Hua Yang assited with project design and DNA synthesis.

Table of contents

List of Figures

List of Tables

List of abbreviations

AFM	Atomic force microscopy
AGE	Agarose gel electrophoresis
AuNP	Gold nanoparticle
CD	Circular dichroism
CH2Cl2	Dichloromethane
CPG	Controlled pore glass
Cryo-EM	Cryogenic electron microscopy
DLS	Dynamic light scattering
DMF	Dimethyl formamide
DMSO	Dimethyl sulfoxide
dpp	diphenylphenanthroline
ds	double-stranded
EDTA	Ethylenediaminetetraacetic acid
EtOH	Ethanol
FRET	Forster (or fluorescence) resonance energy transfer
GPC	Gel permeation chromatography
LS	Linking strand
MALDI	Matrix-assisted laser desorption ionization
Min	Minute
MW	Molecular weight
PAGE	Polyacrylamide gel electrophoresis
PDI	Polydispersity index
PEG	Poly(ethylene)glycol
ROMP	Ring-opening metathesis polymerization
TAE	Tris-acetate-EDTA
TBE	Tris-boric acid-EDTA
TEM	Transmission electron microscopy
THF	Tetrahyrdofuran
rt	Room temperature
RS	Rigidifying strand
ss	single-stranded
UV/Vis	Ultraviolet-visible
1D	One dimensional
2D	Two dimensional
3D	Three dimension

Chapter 1: Introduction

Parts of this chapter have been reproduced with permission from; "Supramolecular DNA assembly", McLaughlin, C. K., Hamblin, G. D. and Sleiman, H. F. *Chem. Soc. Rev.,* **2011**, 40, 5647-5646. Royal Society of Chemistry (2011).

1.1 Manipulating matter – A nano-revolution?

Numerous scientific disciplines, ranging from materials science, chemistry, biology and engineering, have contributed significant advancements to the organization of matter within the Ångstrom and micron size regimes. With the utmost of precision, an ever-expanding array of synthetic strategies is being utilized to prepare complex molecules that continue to revolutionize our understanding of the world. In parallel, leaps and bounds in micron-scale fabrication have enabled the generation of advanced materials and electronic components, which in turn have fundamentally changed the ways in which humans interact both with each other and the natural world. Such advances in the ability to exert control over matter would suggest that little in the way of exploration could be possible in chemical construction. But what about the middle of the road? In terms of length-scale, tucked neatly between that of Ångstrom and micron is the nanometer size regime; a place where some of the most fascinating structural and functional feats have been realized, and challenges in chemical construction still remain.

Generally speaking, development and research of materials or structures within the dimensions from 1-100 nm fall under the umbrella of the fields nanoscience and nanotechnology (Fig. 1.1).[1] Although debate is ongoing over the environmental/health implications of this field[2,3], the surge of fundamental research dedicated over the past two decades towards engineering functional

systems at the molecular scale has been astounding. Part of the basic scientific foundation for exploring such avenues of chemical construction has been the discovery that novel phenomena begin to appear at this size scale that are not observed in bulk materials. Moreover, complexity within the nanometer size regime has been evolved over millions of years in the natural world.[4] Due in part to the advancement of more precise analytical tools, insight into some of the inner working of nature has unveiled a molecular landscape that derives precise organization of functional components using a balance of covalent and non-covalent strategies. The breadth of detail on how biological systems and machines operate in such an elegant manner has thus provided ample inspiration for nanotechnologists and nanoscientists in their pursuit to manipulate matter at the nanoscale.

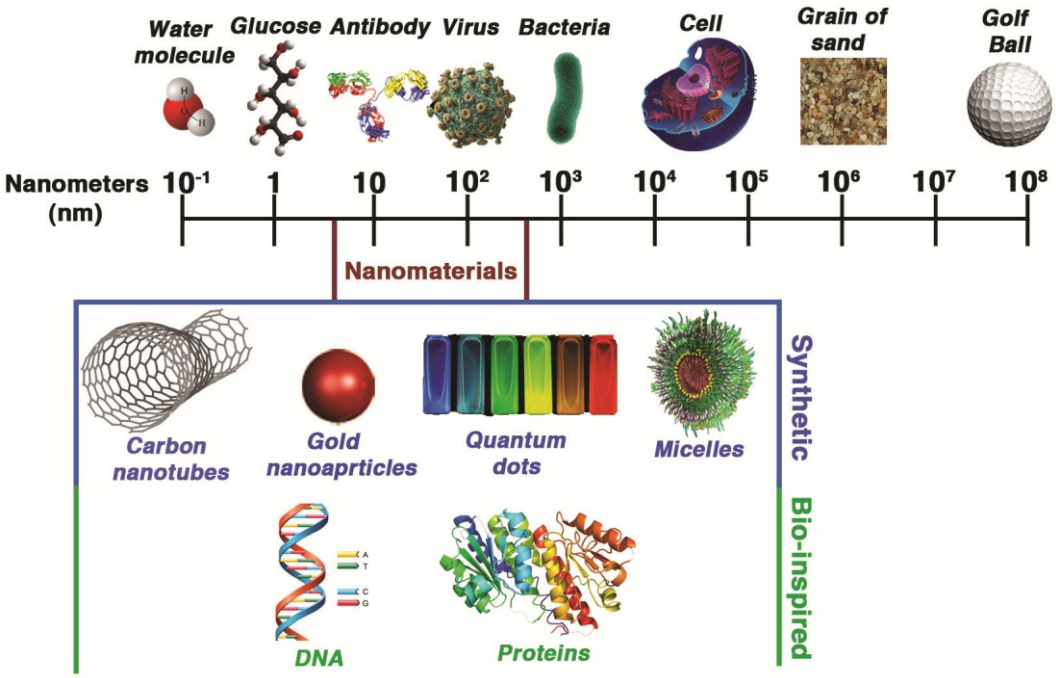

Figure 1.1 The regime of nanoscience/nanotechnology. Materials or structures designed with dimensions roughly between 1 – 100 nm can offer advantageous properties over bulk counterparts.

Generating materials within the nanometer regime can be divided roughly into two approaches. The first, 'top-down' assembly typically creates nano-sized

structures from larger entities. Advancements in micropatterning techniques, such as photolithography, and more advanced microchip manufacturing, have, however, pushed top-down assembly techniques to ever more precise positioning of molecules.[5,6] Alternatively, the second approach – bottom-up assembly or self-assembly- uses the concepts of molecular recognition to drive spontaneous assembly of molecular components.[7] This latter design principle, involves the harnessing of molecular forces that do not involve strict covalent bond forming interactions and where spontaneous association of molecular components can be used to prepare complex and functional structures. It is within this second approach that the framework developed in this thesis to help solve challenges of chemical construction is derived.

1.2 Deoxyribonucleic acid (DNA)

Of the naturally evolved systems, DNA is widely recognized as the carrier of our genetic code, with obvious ties to biology, evolution and medicine. But chemically speaking, it is just as fascinating. DNA is possibly the most efficient self-assembling material known, undergoing rapid, high fidelity association according to exceptionally simple base-pairing rules.[8] Through a cooperative balance of hydrogen-bonding, π-stacking and other non-covalent forces, a single strand of DNA can find its complement in solution with extraordinary selectivity (Fig. 1.2a). The bioploymer is comprised of simple heterocyclic units (nucleobases) attached to a deoxyribose sugar and connected by phosphodiester bonds. As shown in Fig. 1.2b, each of the nucleobases, adenine (A), cytosine (C), guanine (G) and thymine (T), are designed to selectively hydrogen-bond into base pairs (bp) A:T and C:G. Two hybridized strands run in opposite directions to each other and therefore exist in an anti-parallel arrangement within the B-form (right-hand helical) duplex, resulting in a thermodynamically stable structure, due in part to the stacking interactions between the aromatic bases, selective hydrogen bonds and minimal helical distortion.[9] Additionally, the persitence length of double-stranded (ds) DNA in this helical form is ca. 50 nm,[10] making it ideal for assembling materials on the nanometer length scale. Lastly, DNA is not only a biocompatible material with a host of molecular biology tools available for

manipulation and analysis, but can also be synthesized easily via now well-developed solid-phase chemical techniques.[11,12] Though many self-assembling molecules are known, it is extremely rare to have such control over the programmability and the resulting product. This precise assembly code and in conjunction with the structural properties of the resulting double helices make DNA an ideal candidate for complex chemical construction.

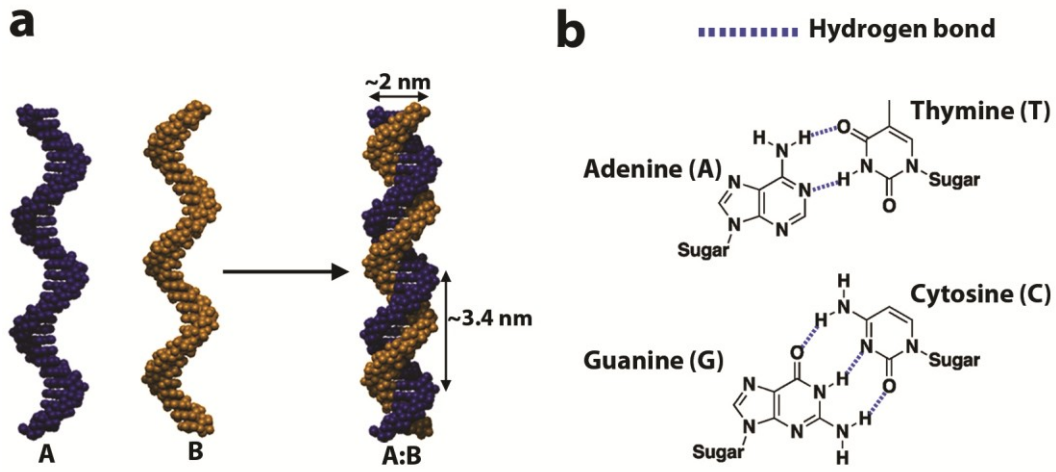

Figure 1.2 Structural properties of the DNA. a, Two DNA strands (A and B) hybridize in a cooperative, anti-parallel orientation to form the B-DNA duplex. A complete turn of the helix spans 10.5 bases and is ca. 3.4 nm in length. Individual base pairs (bp) are spaced 0.34 nm apart. The helix is 2 nm in diameter. **b,** Specific examples of the hydrogen bonds that result in the DNA duplex between nucleobases; Adenine (A):Thymine (T) and Guanine(G):Cytosine(C).

1.3 Structural DNA nanotechnology

Although many researchers have explored the properties of nucleic acids over the past 30 years, the removal of DNA from its biological context and intial exploration as a material for higher-order nanoscale assembly can be traced back to Seeman and co-workers in early 1980's.[13] Formally referred to as structural DNA nanotechnology, researchers in this field have utilized the unique properties of DNA in a varitey of chemical construction applications.[14] Early work focused on generating ordered structures from a Holliday junction modified with short single-stranded overhangs (sticky-ends) (Fig. 1.3a). This naturally occuring four-

way branched junction was found to be flexible for use in assembly of ordered materials.[15] This necessitated design of the more rigid double-crossover motif (DX), shown in Fig. 1.3b.[16] A variety of DX junctions, along with appropriate sticky-ends, could then be used to generate well-defined 2D crystalline lattices with control over size, shape and periodicity (Fig. 1.3b).[17] Using similar principles a number of different 'tiles' have been prepared, including multi-crossover molecules, triple crossover[18] and four-, eight-, and 12-helix planar tiles[19,20], and shown to self-assemble into well-defined lattices.[14]

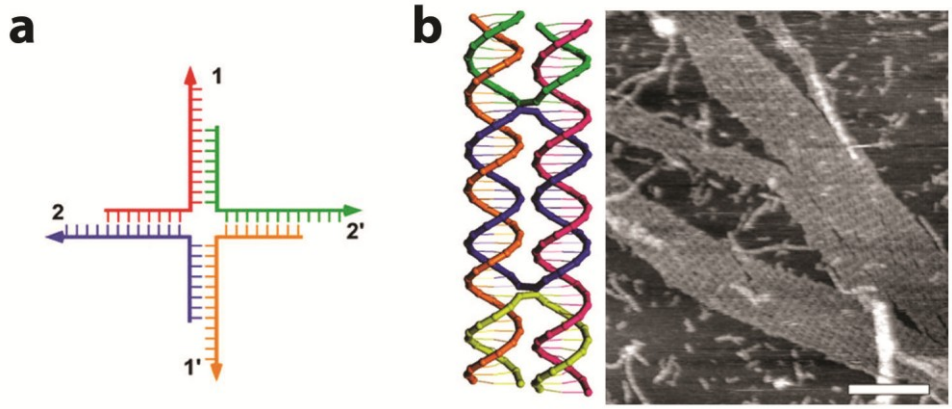

Figure 1.3 Initial motifs used in structural DNA nanotechnology assembly. a, Classical Holliday junction consisting of four strands with 'sticky-ends' (labeled 1, 2, 1', 2') available for additional hybridization. **b,** Double crossover (DX) tile (left) designed to be more rigid and shown to assemble to into ordered 2D lattices (right). Adapted with permission from reference 17 (ACS publishing, 1991).

1.3.1 DNA-tile based assembly in 2D

To date, numerous examples of 2D lattices made with a variety of different tile structures have been utilized to organize materials on the nanometer length scale.[14] In 2003 the first example of a two-dimensional protein array was demonstrated. Here, four-way branched DNA tiles were designed that could assemble into long-range two-dimensional square networks.[21] Modification of each tile with biotin allowed selective interaction with streptavidin. In subsequent work, a four-tile system was used to control the periodicity of the aptamer binding

sites within the large 2D-array that was assembled with sequence uniqueness between rows.[22] As shown in Fig. 1.4a, tiles could be selectively addressed with two different aptamers, one specific to thrombin and the second to platelet-derived growth factors, to generate alternating rows of proteins. The same group has also used DNA tile self-assembly to generate micrometer-sized two-dimensional arrays that carry nucleic acid probes and barcoded fluorescent dyes to achieve multiplexed detection.[23] Numerous examples of highly ordered arrays of gold nanoparticles using tile-based DNA assembly have also been demonstrated.[14] One such example from Seeman and co-workers is shown in Fig. 1.4b.[24] Here, an extended rhombic lattice is constructed from two sequence asymmetric double-crossover triangular tiles. Two different sizes of gold nanoparticles with DNA strands were mono-functionalized with DNA strands that could be incorporated into the triangular tiles prior to 2D assembly. Excellent organization of the gold nanoparticles was achieved as characterized by the TEM images in Fig. 1.4b.

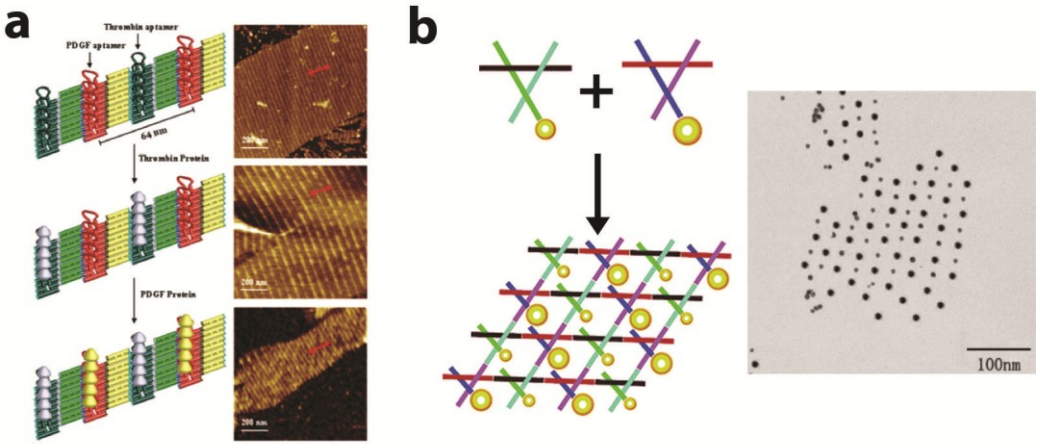

Figure 1.4 Organization on planar 2D arrays. a, A four-tile system is used to selectively organize 2 sets of aptamers into alternating rows that can subsequently be functionalized with thrombin and platelet-derived growth factors. Adapted with permission from reference 22 (ACS publishing, 2007). **b,** Gold nanoparticles functionalized with single DNA stands, incorporated into triangular tiles and assembled into a rhombic lattice. Adapted with permission from reference 24 (ACS publishing, 2006).

1.3.2 DNA-tile based assembly in 3D

Control over the assembly and positioning of other nanoscale materials has also been achieved using non-planar 2D arrays. These systems take advantage of selective curvature to generate either nanotubular or discrete 3D arrangements of DNA-tiles.[25] For example, DNA tiles, such as the DX[26], have been induced to cyclize by rationally programming a specific non-zero degree of curvature within each tile. A second approach, where the triple-crossover junction[27] was initially used by LaBean and co-workers, involves programming different dsDNA sequences such that they will assemble into a closed helix bundle with a fixed number of helices. Yan and coworkers have also demonstrated that gold nanoparticle-DNA conjugates can be used in this manner to induce curvature in DNA-tiles through size-dependent steric repulsion effects.[28] The resulting DNA tubes display a unique helical arrangement of two sizes of nanoparticles with resulting architectures being controlled by the spatial positioning within each starting DNA-tile. More recently, the Liu and Yan utilized a 7-helix bundle nanotubular structure to organize fluorescent molecules in a manner to promote efficient energy transfer.[29] As shown in Fig. 1.5a, nanometer scale spatial organization of three different fluorophores can be achieved on the helical scaffolds. Using time-resolved fluorescence analysis by time-correlated single-photon counting (TCSPC) energy transfer, this artificial light-harvesting system could be observed on the picosecond time scale. In addition, Seeman, Mao, and coworkers recently demonstrated that the branched, rigid DNA triangular motifs with short sticky ends could be used to create the first self-assembled 3D-DNA crystal.[30]

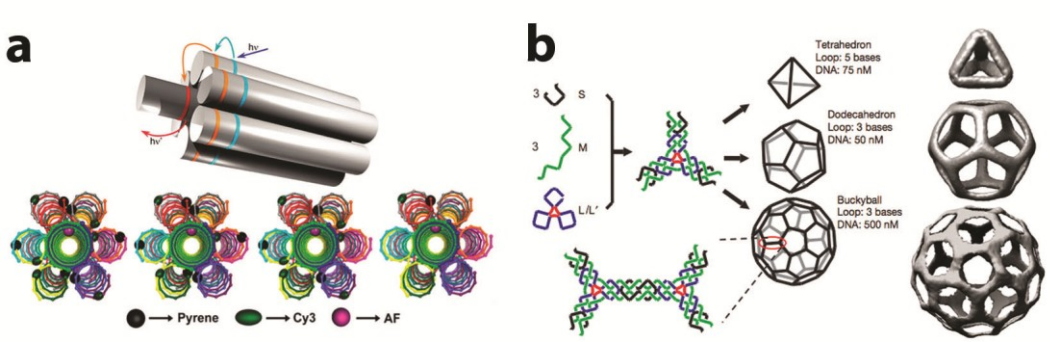

Figure 1.5 DNA-tile based assembly of nanotubes and discrete polyhedra. a, A 7-helix bundle is modified with three different fluorescent molecules in a manner that generates efficient energy transfer. Adapted with permission from reference 29 (ACS publishing, 2011). **b,** Three types of DNA polyhedra (tetrahedron, dodecahedron and buckyball) are assembled from a single 'DNA star' motif in a concentration dependent fashion. Final single-particle reconstructions for each structure are shown on the right. Adapted with permission from reference 34 (Nature publishing group, 2008).

DNA-tiles have also been designed to assemble into closed, discrete 3D structures.[31] Using some preliminary elements of structural DNA nanotechnology, Seeman produced the first 3D DNA objects - a structure with connectivity of a cube[32] and a truncated octahedron[33] - although both structures were generated in low yields. Mao and co-workers have pioneered this work by creating 'DNA star motifs', a subset of DNA nanostructures with 3, 4, 5, or 6 branches, that are programmed to assemble into a number of different polyhedra with diameters ranging from ~ 20 - 80 nm. The first example utilized at single motif to generate 3 DNA polyhedra in a concentration dependent fashion with characterization by cryogenic electron microscopy (cryo-EM) and single-particle reconstruction (Fig. 1.5b).[34] With this method, however, it should be noted that assembly to create the smaller structures, such as the tetrahedron, requires very low concentrations (50 nM) and long anneal times (48 hr). Additional work by this group has demonstrated that tuning the flexibility within the sequence symmetric star motifs can be used to control DNA-polyhedra formation.[35,36]

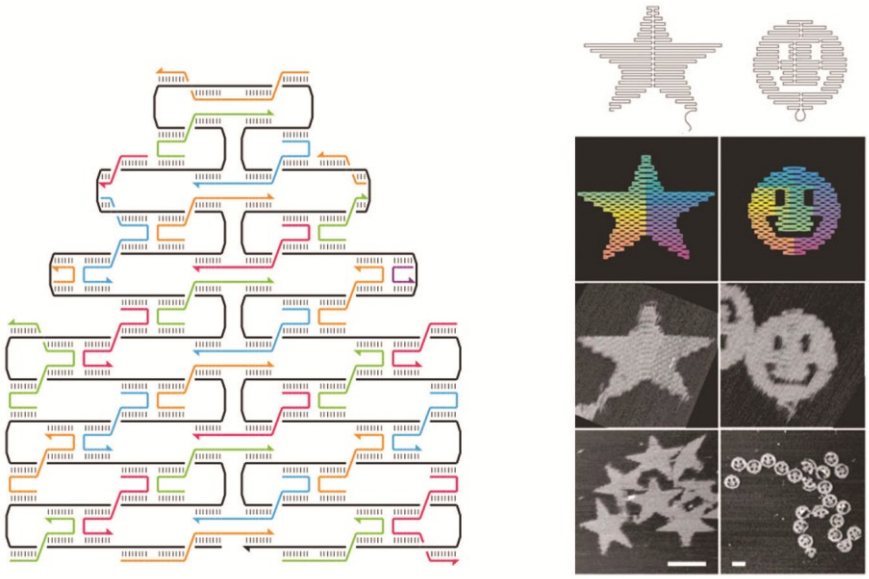

Figure 1.6 DNA origami. Virus genomic DNA is strategically folded (left) with 100s of staple strands and crossover duplex interactions. Depending on how the staple strands are designed to hybridize with the scaffold, numerous 2D assemblies are produced and characterized by AFM (right). Adapted with permission from reference 37 (Nature publishing group, 2006).

1.4 DNA origami: an explosion of 2D and 3D self-assembly

In 2006, P. Rothemund changed the landscape of chemical construction with the development of 'DNA-origami'; a self-assembly technique that utilizes a combination of computational design and DNA folding to generate discrete 2D and 3D structures.[37,38] In this method, a single continuous ssDNA template (or 'scaffold'), typically obtained from viral genomic DNA of up to thousands of bases in length, is simultaneously folded with a number of 'helper' or 'staple' strands into a computationally designed arrangement. Using the same genomic DNA strand, variation in staple strand composition was first used to generate a variety of 2D assemblies as shown in Fig. 1.6.[37] The double-helical DNA domains, which comprise the DNA-origami structures, yield a spatial resolution of approximately 6 nm. Because each staple-strand is unique, these strands can be modified for use in additional assembly and positioning.[39] Depending on the packing and spatial arrangement of DNA required, assembly typically requires high salt concentrations and long anneal times. Since its inception, numerous

examples of chemical construction using self-assembly on modified DNA-origami structure have been demonstrated and recently reviewed.[38-40] Here, focus will be placed on highlighting specific examples of DNA origami that represent its use in molecular organization and 3D structure assembly.

1.4.1 Organization and chemical control with 2D DNA origami substrates

DNA origami has been utilized as a platform for a variety of single-molecule applications, such as chemical synthesis, positioning nanoparticles and as platforms for label-free detection of nucleic acids.[41] One of first applications of DNA origami for single-molecule analysis was from Yan and co-workers.[42] Here, an assay for label-free RNA hybridization on DNA origami was developed with detection achieved by atomic force microscopy AFM. As outlined in Fig. 1.7a, ssDNA was placed on origami substrates that were complementary to the RNA targets. These molecularly positioned 'capture' strands were then used to simultaneously hybridize with analytes. The resulting substrates could then be analyzed for specific RNA/DNA pairs by AFM. Gothelf and co-workers have also made steps towards using DNA origami structures as locally addressable solid supports.[43] In this work, single-molecule analysis of chemical reactions is performed through a series of cleavage and formation of individual chemical bonds (Fig. 1.7b). The chemical reactions shown in Fig. 1.7b (top) allow for specific positioning of streptavidin onto the DNA origami substrate. Depending on subsequent chemical conditions, the site-specific loss of streptavidin can be visualized by AFM (Fig. 1.7b – bottom). Although AFM is not the most practical of detection methods, these examples reveal the positional power of DNA origami for single molecule analysis.

More recent investigations into how DNA origami can be used as a programmable and nanometer-precise scaffold have focused on the selective organization of nanoparticles,[44] viruses[45] and proteins[46]. Liedl et al. recently demonstrated the potential of DNA origami for generating plasmonic nanostructures by arranging nanoparticles in close proximity such that they are helically aligned and can be detected by circular dichroism (CD). Similar multi-

chromophore arrangments as outlined for DNA-tiles have also been recently developed on an origami substrate.[47] Here, the 2D arrangement allows for a fourth fluorescent molecule to be integrated into the scaffold at multiple locations, allowing for excitation energy to be directed to specific dye molecules.

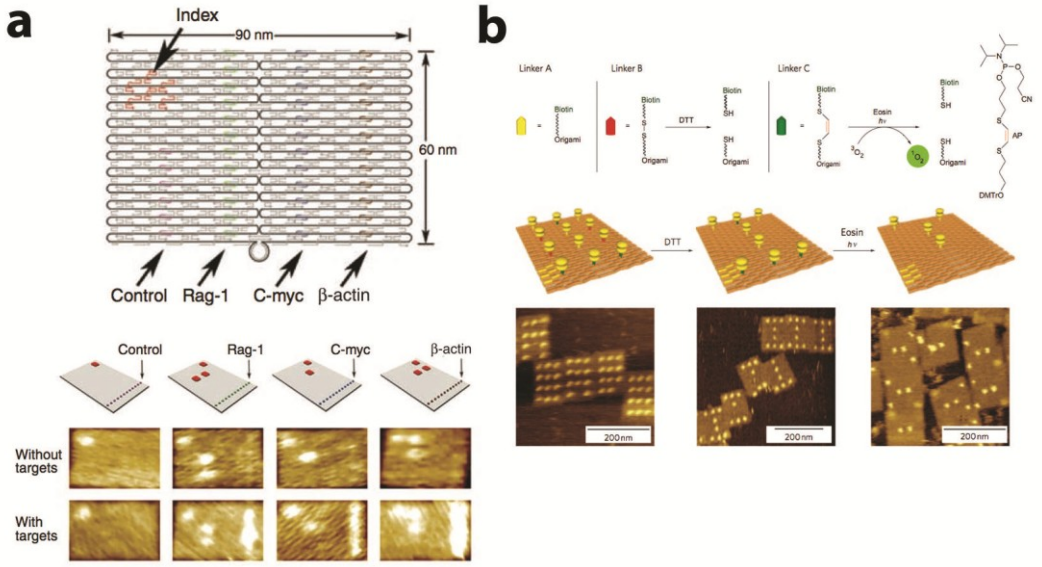

Figure 1.7 Single molecule analyses on DNA origami. a, Origami substrate (top row) designed for recognition of target RNA by hybridization with probe DNA strands (middle row). 'Index' parameter allows for substrate to be properly oriented for AFM analysis. Hybridization to the RNA target generates a protrusion that can be visualized as a bright spot (increased height) by AFM (bottom panels). Adapted with permission from reference 42 (Science, 2008). **b,** Using three different biotinilytated functional groups (top row), streptavidin can be positioned onto a origami surface (middle row). Depending on subsequent chemcical conditions, each linker can be selectively cleaved resulting in a distinct protein pattern characterized by AFM (bottom row). Adapted with permission from reference 43 (Nature publishing group, 2010).

1.4.2 DNA-origami used to assemble 3D structures

The demonstration of DNA origami in 2006 set into motion a race between researchers eager to produce 3D structures that utilize this self-assembly technique. Starting in 2009, various strategies began to appear that individually tailored the method to fold or curve DNA origami structures into closed 3D

topologies.[44] Shih and co-workers reported 3D origami construction that generates a dense parallel arrangement of helices into a honeycomb lattice (Fig. 1.8a).[48] Although a number of architectures are produced with this method, significantly long assembly times and low yields for the more complex structures does occur. Recently this group has reported improvements on purification procedures to isolate the more complex assemblies.[49] Kjems, Gothelf and co-workers reported the preparation of a DNA origami box by connecting six planar origami sheets at the edges to create the closed structure (Fig. 1.8b, top).[50] By integrating hinges along one of the edge lengths, opening of the box lid could be controlled by selective hybridization to complementary DNA strands, referred to as 'keys', and monitored by FRET (Fig. 1.8b, bottom). This mechanism for opening/closing 3D origami structures was recently incorporated by Church and co-workers into a structure designed to be selectively opened upon interaction with specific membrane receptors.[51] Similar origami box designs have also been reported by Komiyama[52] and Sugiyama and co-workers[53]. In addition, a related strategy to construct a hollow DNA origami triangular pyramid, with an estimated internal cavity volume of 1.5×10^{-23} m^3, was reported by Yan and co-workers.[54]

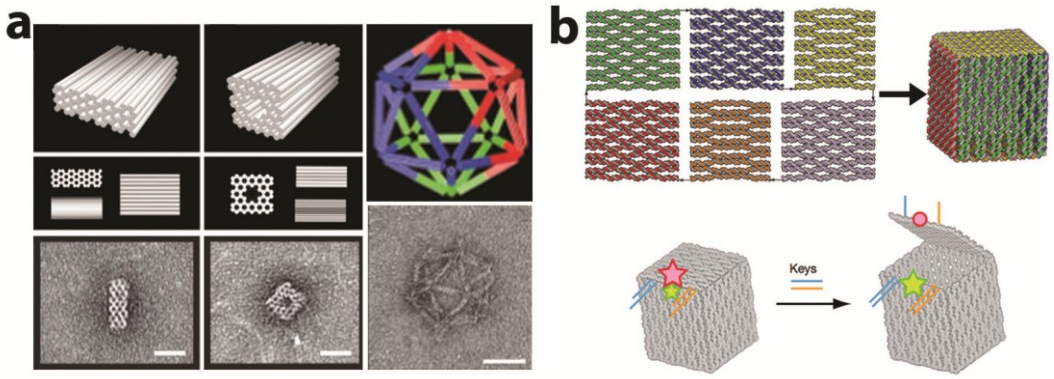

Figure 1.8 3D DNA origami structures. a, Three examples of 3D structures designed using a honey comb lattice assembly method that packs and folds DNA origami into dense units. Adapted with permission from reference 48 (Nature publishing group, 2009). **b,** Folding of six interconnected 2D origami sheets into a 3D DNA box (top). Opening of the box lid can be controlled by addition of DNA 'keys' and detected by FRET (bottom). Adapted with permission from reference 50 (Nature publishing group, 2009).

1.5 Alternative methods for 3D nucleic acid assembly

Outside the use of DNA-tile based assembly and DNA origami, alternative design strategies that employ DNA folding have been developed to generate well-defined 3D structures.[25,55] Typically, these methods rely on simpler folding of encoded DNA to generate 3D structures on the nanometer length scale. Joyce and co-workers reported synthesis of an octahedron using a DNA-origami like folding strategy.[56] The structure was confirmed using cryo-EM and single particle analysis. In 2005 Turberfield and co-workers developed a strategy to prepare a DNA tetrahedron from four single-stranded oligonucleotides.[57] Assembly in this case was demonstrated to be stereoselective and demonstrated the chiral purity of the DNA-tetrahedron prepared. This method, however, does require low assembly concentrations (50 nM) for best yields and purification to isolate the DNA structure from misassembled materials. Knudsen and coworkers generated a 3D-DNA octahedron from eight DNA strands that was covalently closed by T4 polynucleotide kinase ligation.[58] In 2009, work by Krishnan and coworkers reported the construction of icosahedral DNA structures in modest yield using an annealing strategy involving DNA star motifs.[59]

1.6 Supramolecular DNA assembly

While the motifs typically used in structural DNA nanotechnology, mainly DNA-tiles and DNA origami, have provided an impressive range of ways to manipulate and organize matter on the nanometer length scale, methods of assembly can be low yielding and require time consuming purification of complex architectures. In addition, generation of more complex structures typically requires expanding pools of DNA to generate highly DNA-dense nucleic acid materials. Combined with the fact that DNA displays limited intrinsic functionality, strategic synthetic modification of this biopolymer could help to expand the repertoire of motifs for chemical construction and help to alleviate the requirements for DNA-rich designs necessary to maintain proportional structural expansion.

In parallel to structural DNA nanotechnology, an important and now mature

research area that has significantly contributed to bottom-up construction is *supramolecular chemistry*. Over the last forty years, this field has developed an in-depth understanding of non-covalent interactions. It has evolved a toolbox of synthetic organic and inorganic molecules that use these interactions to spontaneously assemble into remarkably diverse architectures.[60,61] Because the component molecules can possess intrinsic functionality, such as redox, photophysical, magnetic and catalytic properties, they allow the rational design of complex function into the final assemblies. However, while supramolecular chemistry can successfully organize symmetrical structures and periodic assemblies, its ability to achieve the programmable positioning of components into any deliberately designed structure, whether symmetric or asymmetric, is less well developed.

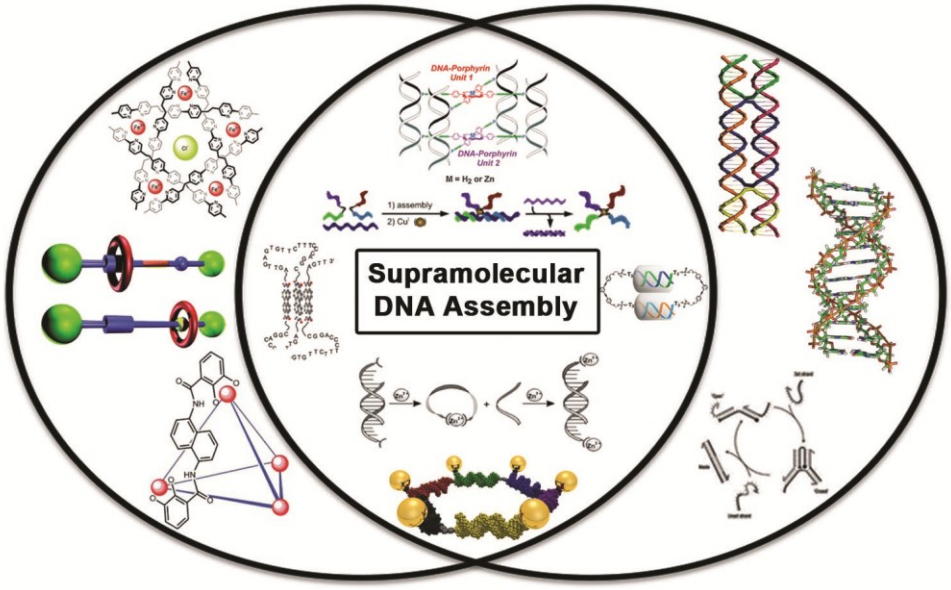

Figure 1.9 Supramolecular DNA assembly. The union of supramolecular chemistry with structural DNA nanotechnology gives rise to a new area with materials and biological applications. Reproduced with permission from reference 63 (Royal Society of Chemistry reference, 2011).

Bringing together the programmability of DNA with the structural and functional diversity achieved by supramolecular chemistry, is now being explored by numerous researchers in a new emerging area recently termed 'supramolecular DNA assembly'.[55,62,63] Blending together DNA building blocks with synthetic

organic and inorganic molecules, the field of DNA nanotechnology is gaining new structural motifs and can impart functionality to the typically passive DNA structures. (Fig. 1.9) By adding DNA to its toolbox, the field of supramolecular chemistry acquires the ability to position components into any programmable pattern, in order to engineer sophisticated function. Thus, this new area is poised to enrich both fields with completely new structures and new applications in both biology and materials science.

In the following sections, seminal and recent research in this field is outlined, with specific focus on the underlying advantages of synthetic insertions in two- and three-dimensional nanostructures.

1.6.1 Using synthetic insertions to modify DNA assembly

The simplest chemical insertions into DNA strands are able to alter its hybridization and control its self-assembly outcome. By incorporating molecules with specific geometries at the insertion points, basic linear duplexes can be oriented relative to each other in a unique manner, combining the self-assembly properties of DNA with the structural versatility of synthetic groups. The result is the introduction of new construction motifs for nanotechnology.

An early example of this is illustrated by the work of Bergstrom and coworkers, which employs two-arm vertices.[64] The vertex centers around a single tetrahedral carbon and is connected to two single-stranded (ss) DNA linkers via rigid p-(2-hydroxyethyl)phenylethynylphenyl spacer units (Fig. 1.10a). In this case, self-complementary ssDNA linkers were included, so that their hybridization would yield discrete macrocycle formation. Because any number of monomers can associate, a ladder of oligomeric products results, with the primary product a function of monomer concentration. Increasing flexibility by introducing non-pairing thymine residues between the DNA-vertex bond disfavoured oligomerization. Though not emphasized in Bergstrom's article, this may be evidence that DNA assembly was indeed manipulated by the synthetic insertion. The group of von Kiedrowski constructed a tris-branched

oligonucleotide containing a flexible vertex and three identical DNA strands.[65] They showed that it can assemble under kinetic conditions into a dimeric structure, in which the vertices are connected by three DNA double helices, along with other higher-order structures.

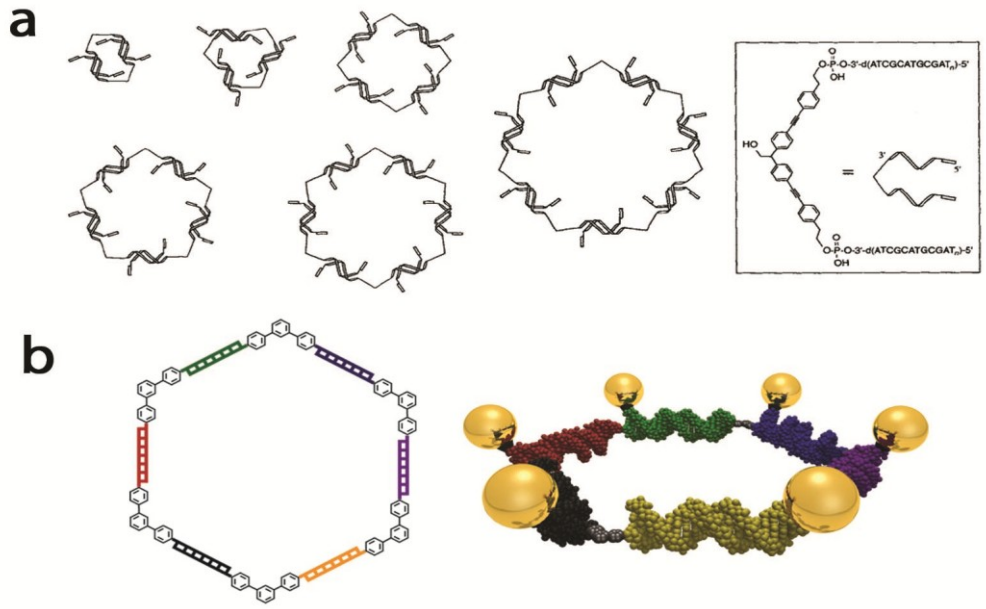

Figure 1.10 DNA modification with organic vertices. a, An organic vertex is incorporated into DNA to prepare bis-DNA building blocks that undergo macrocycle formation. Reproduced from reference 64 with permission from Wiley-VCH. **b,** Asymmetric DNA building blocks with organic vertices are used to prepare discrete hexagons that can assemble gold nano- particles. Reproduced from reference 66 with permission from Wiley-VCH.

With the aim of obtaining a single, well-defined product, Sleiman and co-workers developed DNA-conjugated organic vertices, in which the arms are no longer self-complementary or identical to one another (Fig. 1.10b).[66] A *m*-terphenyl-based chemical insertion is a significantly more rigid vertex, and linker sequences were designed to ensure the hexamer was the only product available that satisfied Watson–Crick base-pairing. The result is a very narrow product distribution, comprised of predominantly the DNA hexagon shown schematically in Fig. 1.10b-left. This system was used as a scaffold for organizing gold nanoparticles (AuNPs) into a discrete 2D structure (Fig. 1.10b-right). The synthetically modified DNA strands were conjugated to nanoparticles prior to

assembly, allowing them to template the formation of a cyclic hexamer of AuNPs.

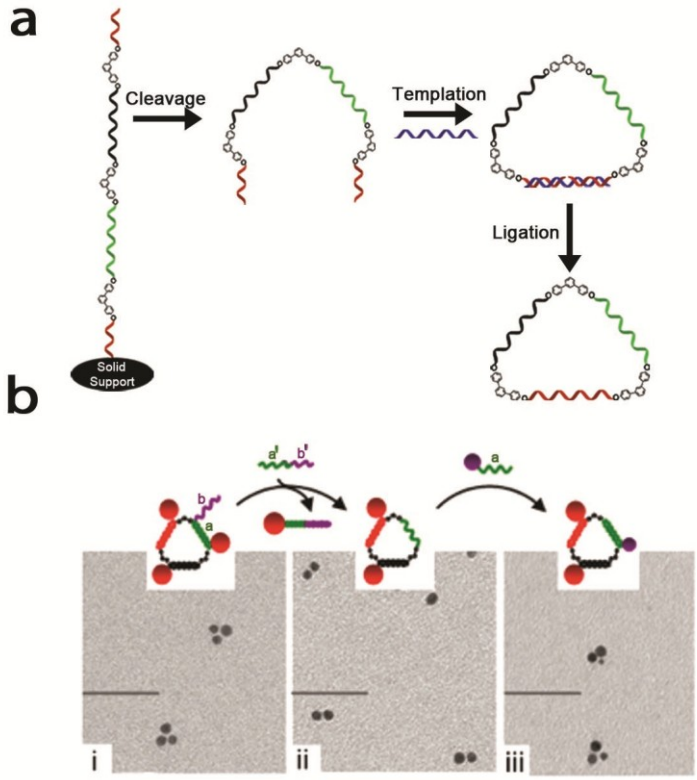

Figure 1.11 Single-stranded DNA polygons. (a) Synthetic vertices are incorporated into the growing DNA strand on a solid-support, followed by cleavage and a templated ligation to yield the ssDNA structure. (b) DNA- AuNP conjugates can be organized onto the single-stranded scaffold in a discrete manner and subjected to 'write/ erase' experiments. Adapted with permission from reference 67. Copyright 2007 American Chemical Society.

Subsequently, this group constructed cyclic DNA polygons, composed of single-stranded DNA arms and rigid m-terphenyl corner units (Fig. 1.11).[67] For example, a DNA ss triangle was synthesized by on-column incorporation of three m-terphenyl insertions into a DNA strand, followed by templated joining together of its two extremities by a phosphodiester linkage (Fig. 1.11a). Using this simple strategy, ss DNA squares, pentagons and hexagons were also selectively constructed. These could then be used as templates for the positioning of materials by hybridization to their single-stranded arms. For example, these templates were used to position gold nanoparticles into a diverse array of polygonal assemblies. Because of their single-stranded and fully cyclic nature, these could serve as

dynamic templates that allowed writing, erasing, and structurally switching nanoparticle assemblies, using externally added DNA strands (Fig.1.11b). Monoconjugation of DNA to AuNPs and subsequent self-assembly into well-defined 2D and 3D nanostructures demonstrates the high degree of positional control that DNA allows.[68] These nanoparticle assemblies are being explored as dynamic, tailorable nano-electronic and plasmonic substrates.

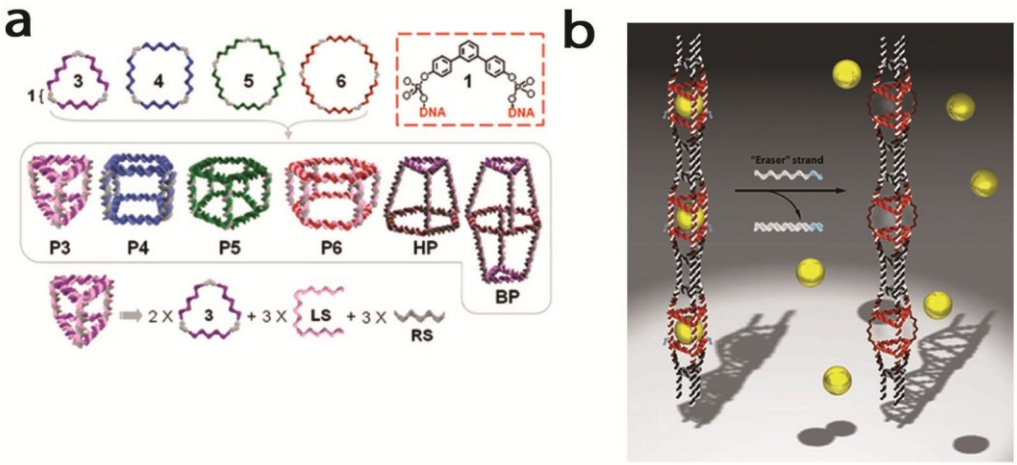

Figure 1.12 DNA cycles used to prepare 3D DNA structures. Dynamic DNA cycles allow the preparation of (a) 3D prisms (Adapted with permission from reference 69. Copyright 2007 American Chemical Society) and (b) nanotubes that can be used for nanoscale organization.

Using the single-stranded DNA polygons described above, Aldaye and Sleiman pushed DNA assembly into 3D by demonstrating the construction of a library of DNA polyhedra, including triangular prisms, cubes, pentagonal and hexagonal prisms, heteroprisms and biprisms (Fig. 1.12a).[69] This was done by connecting the DNA polygons top and bottom, using linking strands, in quantitative yields. These DNA cages were also shown to be structurally expanded and contracted between three different sizes, using externally added DNA strands. Recently, our group has also developed simple methods to build 3D-DNA structures from a minimum number of commercially available DNA strands, in quantitative yields.[70,71] Moreover, a cubic structure produced with maximal amounts of ssDNA sites[71] could be selectively hybridized with DNA-

polymer conjugates, which conferred some stability to nuclease degradation.

Expanding 3D assembly to long-range ordered structures, Sleiman and co-workers reported a modular approach for the synthesis of DNA nanotubes through assembly of DNA 2D polygons longitudinally.[72] This method gave ready control of the geometry, size and stiffness of these assemblies, and ability to generate these in single-stranded and 'open', and double-stranded and 'closed' forms. Modification of the assembling units led to the demonstration of these DNA nanotubes ability to encapsulate gold nanoparticles and selectively release this cargo (Fig. 1.12b).[73] When a specific DNA strand is added, it removes the strands that close the nanotube, and the nanoparticle cargo is released. Utilizing synthetically modified DNA polygons additionally allowed precise control of the length of DNA nanotubes.[74] More recently, rolling circle amplification (RCA) was used to generate a continuous single-stranded DNA template that allowed DNA nanotubes preparation with increased stability and length.[75] These constructs were also shown undergo selective uptake by a human cervical cancer cell line (HeLa).

Through selective chemical modification of DNA with synthetic junctions, unique hybrid DNA templates can be prepared and assembled into well-defined materials with potential applications for drug delivery, nanowire growth, and as interconnects or tracks for molecular motors.

1.6.2 Boosting complexity with branched molecules

Expanding the central core to a three- or four-arm structure appended with DNA creates a more diverse range of possible orientations and hybridized structures. Shchepinov,[76] von Kiedrowski[77], Sawai[78] and Nguyen/Schatz[79,80] have reported three-way organic junctions on which DNA can grow by standard phosphoramidite chemistry. If self-complementary strands are used, the resulting junctions self-assemble into wire- frame cages, analogous to the cryptands of classic host–guest chemistry. These cages are more thermodynamically stable than the corresponding unbranched duplexes, suggesting a highly cooperative assembly due to the vertex effectively preorganizing the linking strands. Again here, self-complementarity results in a concentration-dependent product

distribution rather than a single assembly. Tris-branched motifs using a 1,3,5-tri-substituted benzene vertex also allow unique sequences to be addressed on each arm of the synthetic insertion.[81] Such insertions led to a small hexagonal nanostructure that could be modified with FRET (fluorescence resonance energy transfer) pairs at pre-determined positions along the DNA scaffold. More recently, this same modification was used to create an asymetric four-ring network assembled in a one-step annealing process, which can be covalently ligated using site-specific click chemistry.[82] von Kiedrowski and coworkers have used a benzene scaffold to create tris-oligonucleotide branched linkers with $C3_h$ symmetry that could be used to prepare a 3D DNA dodecahedron (Fig. 1.13a).[77]

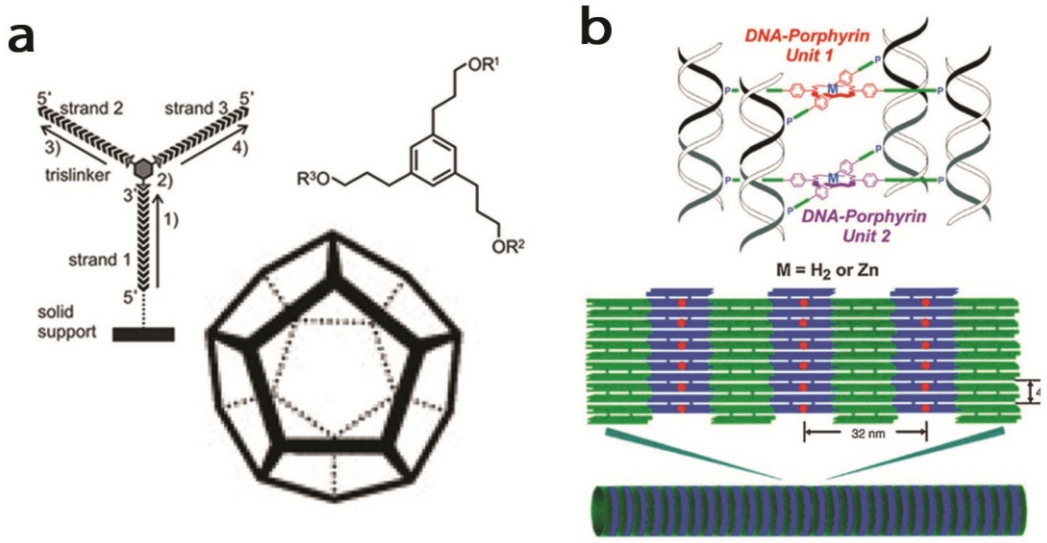

Figure 1.13 Branched DNA systems. a, A DNA dodecahedron prepared from a tris-branched junction. Reproduced from ref. 77 with permission from Wiley-VCH. **b,** Rolled up tiles can be prepared using a porphyrin-DNA four-way junction. Reproduced from ref. 84 with permission from Wiley-VCH.

Bao and coworkers further explored organic molecule-DNA hybrid structures by looking at mono-, bis- and tris-branched aromatic compounds that do not require traditional phosphoramidite chemistry.[83] Cross-coupling routes using iso-thiocyanate-'click' and amide coupling strategies produced hybrid structures containing polyethylene glycol (PEG), poly(p-phenylene ethynylene) (PPE), and benzene-tricarboxylate and single-stranded DNA that could then be

enzymatically elongated to prepare micrometre-sized double-stranded systems.

Endo, Majima, Seeman[84] and Shchepinov[76] have succeeded in creating functional higher-order branching junctions as well. Rather than discrete cages, these junctions template extended systems with significant cross-linking. But using careful design, assembly can be controlled to yield well-defined structures. Fig. 1.13b illustrates an elegant example of this, where a porphyrin- based four-way junction is combined with a DNA tile system known to form 2D arrays.[84] One of the tiles was tagged with an extra strand, complementary to the junction branches. This tagging preorganized the tile into circular tetramers, ensuring that subsequent tile association led to rolled up nanotubes rather than the flat sheets normally observed.

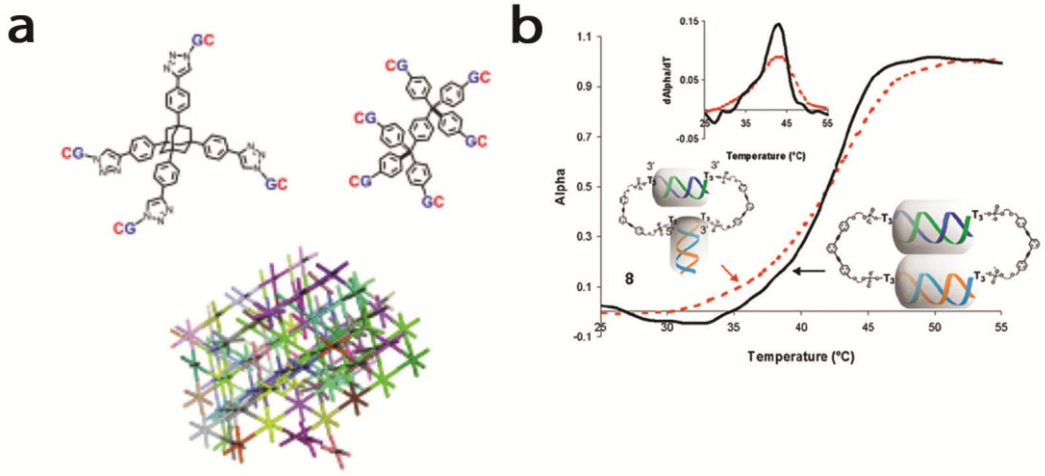

Figure 1.14 Branched organic insertions and DNA assembly. a, Tetra-substituted organic vertices modified with two bases can be used to create macroscopic materials. Reproduced from ref. 85 with permission from Wiley-VCH. **b,** Theoretical and experimental work with bis DNA-organic vertices illustrates the enhanced cooperativity of nanostructure assembly. Adapted with permission from ref. 87. Copyright 2010 American Chemical Society.

Extending the synthetic core to a tetra-substituted building block produces a DNA hybrid structure with an additional element of self-assembly. In an attempt to examine the possibility of DNA crystallization, Richert and coworkers pre-oriented DNA of various sequence lengths onto a tetrahedral core.[85] Through a two base-pair interaction on each arm, a cross-linked material assembled in a stable and selective way (Fig. 1.14a). It should be noted that a hallmark in

structural DNA nanotechnology was recently achieved with Seeman and coworkers preparing the first self-assembled DNA crystals.[30] Although the DNA crystals were made without synthetic modification, they exhibited similar properties to the tetrahedral DNA hybrid and remarkable stability through the two base-pair interaction. These features support the unique characteristics of 3D DNA materials and the different rules for their construction. More recently, synthetic cores have been expanded to six DNA arms with a pseudo-octahedral structure and an adamantane derivative.[86]

Seminal research from Schatz and Nguyen has provided key insights into some of the nanostructures generated from bis-[79] and tris-branched[80,87] rigid organic cores (Fig. 1.14b). The DNA-hybrid structures formed using these synthetic insertions display unique cooperativity due to neighboring-duplex interactions and increased effective concentrations. Using a blend of molecular modeling and experimental techniques, these researchers are generating useful models to help define some of the cooperative and thermodynamic aspects of DNA-hybrid materials, thus assisting in future design strategies.

1.6.3 Incorporating transition metal vertices

While the DNA-synthetic hybrids outlined in previous sections rely on organic insertions, another important self-assembly approach takes advantage of transition metal-based environments.[88] Transition metal centers provide access to a rich diversity of coordination geometries, bond angles and functional characteristics unavailable in traditional carbon-based systems. Nature derives electrostatic stabilization, biomolecular stability/folding and functional diversity by harnessing the properties of transition metal centres.[89] As illustrated in Fig. 1.15a, modification of oligonucleotides with either metal-complexes as vertices, or transition metal coordinating ligands allows researchers to create nanomaterials with added redox, catalytic, photochemical and synthetic properties.[90] What's more, the strong binding displayed by certain coordination environments can significantly stabilize DNA materials.[91] A diverse selection of ligand

modifications, such as those shcmetatically shown in Fig. 1.15a, has allowed researchers to explore the selective coordination of many different transition metals within DNA.[90,92]

Early examples of direct metal-complex insertions into DNA (Fig. 1.13ai), where the coordination environment influenced the arrangement of DNA strands, were reported by the groups of Sleiman[93,94] and McLaughlin[95,96]. In 2004 a two-way DNA junction based on a $[Ru(bpy)_3]^{2+}$ insertion was used to template predominantly dimeric DNA-metal macrocycles (Fig. 1.15b).[94] A larger cyclic product distribution was observed when the metal was absent, leaving a more flexible bipyridine vertex. This illustrates the role of the metal in directing the assembly process and favouring one product out of several pre-existing possibilities. While direct insertion of metal complexes as vertices creates a wealth of geometric and coordination environments, it should be noted that these metals must be sufficiently inert to withstand automated DNA synthesis conditions.

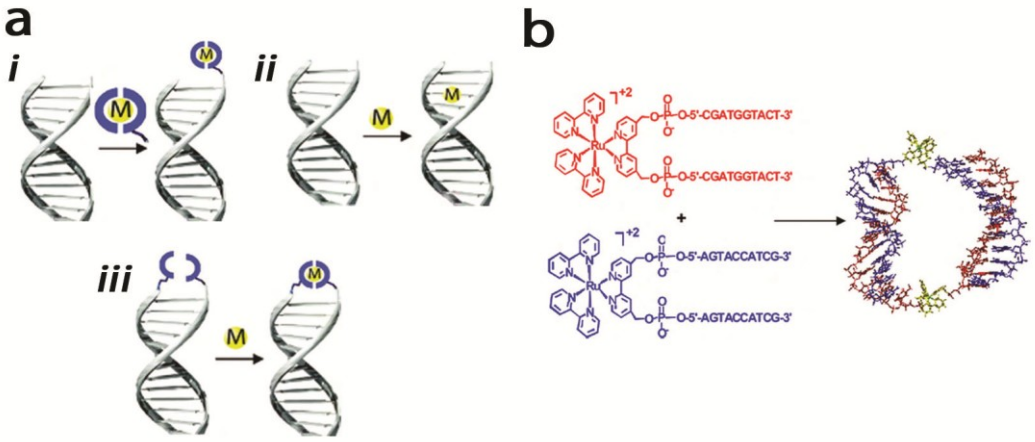

Figure 1.15 Modification of DNA with metals. **a,** Methods to site-specifically incorporate metals into DNA. (i) Metal binding to unmodified DNA. (ii) Attachment of metal complexes to DNA. (iii) Metal binding to ligand-modified DNA. Reproduced from ref. 90 with permission from Elsevier publishing. **b,** Metal complexes can be introduced into DNA to form branched motifs that assemble into dimeric nanostructures. Reproduced from ref. 94 with permission from Wiley-VCH.

An alternative strategy is to directly modify DNA with ligands (Fig. 1.15aii and aiii). Researchers can then use the ligand-metal interaction or templating

ability of DNA to form stable metal coordination environments within a variety of 2D and 3D nanostructures. A particularly important example of this strategy involves the preparation of artificial nucleobases that are capable of metal binding, and their use to create multi-metal 'metallobase-paired' DNA.[92] In this way, problems incorporating metal-complexes into DNA via solid-phase synthesis can be avoided.

Han and co-workers demonstrated that ssDNA end-modified with a terpyridine ligand could be used to drive assembly upon addition of specific metals.[97] When Fe^{2+} was added to this system, the ligand-metal coordination brought together two strands of DNA into metal-bound branched molecules (Fig. 1.16a). For this process to result in assembly, the two arms of a given dimer must be unique. A purification step was therefore necessary in order to separate the heterodimer from the homodimer side products. This approach gave the researchers dual modes of control over the assembly process; both metal coordination and predesigned base-pairing could be used to define the final product.

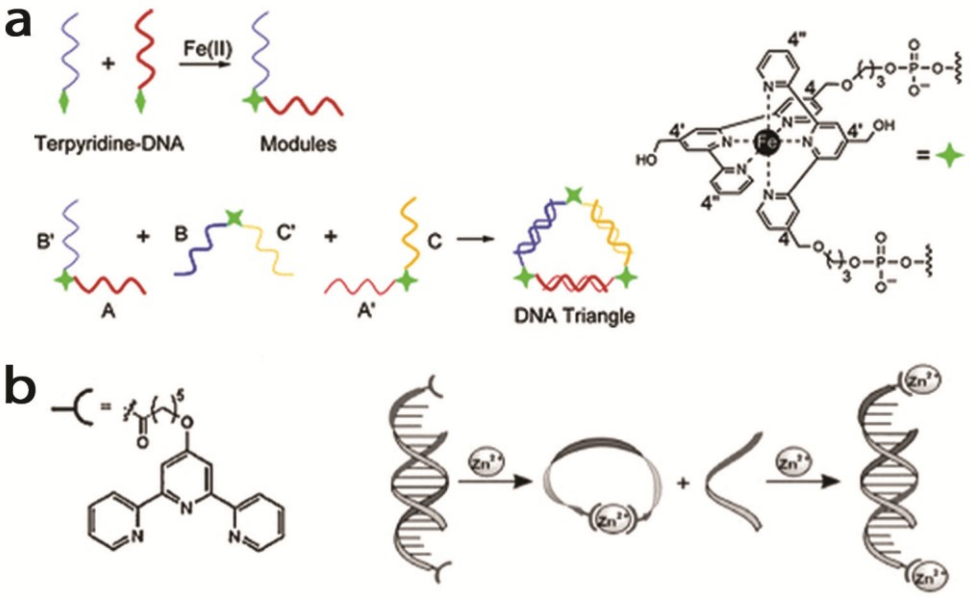

Figure 1.16 Modification of DNA with metals coordinating ligands. **a,** Terpyridine modified DNA drives the formation of a DNA triangle using Fe^{2+} coordination. Adapted with permission from ref. 97. Copyright 2004 American Chemical Society. **b,** Zn^{2+} drives the opening and closing of DNA cycles. Adapted with permission from ref. 98. Copyright 2005 American Chemical Society.

A system devised by Kramer and co-workers[98] used a short DNA sequence doubly end-modified with terpyridine derivatives, creating a system that would cyclize upon addition of metals such as Fe^{2+}, Zn^{2+} and Ni^{2+} (Fig. 1.16b). Here, the thermodynamics of the metal-coordination were strong enough to displace a complementary DNA strand and allow the system to cyclize. The stimuli-responsiveness of this structure was in turn demonstrated by adding excess metal, which opened the cyclized structure and restored the duplex DNA. Sugimoto and co-workers have used ligand insertions to assemble higher order structures. In the presence of Ni^{2+} ions, bipyridine- modified G-quadruplexes change from a anti-parallel to parallel structure, resulting in intermolecular association to form 'G-wires'. This type of metal-mediated self-assembly could be reversed upon addition of EDTA.[99] These contributions show an impressive level of dynamic control and specificity in such supramolecular interactions.

Another approach to incorporate transition metal vertices involves site-specifically inserting ligands into the DNA back- bone and using DNA self-assembly to generate environments that bind and stabilize transition metals. An early example by Gothelf and co-workers showed modular assembly of DNA-programmed linear and branched conjugated nanostructures using a metal-salen interaction.[100] Yang and Sleiman have selectively incorporated a range of reactive transition metals into DNA-templated junctions.[91] This involves the creation of an architecture in which the ligand environment is in close contact with DNA, allowing the DNA double helix and the metal complex to synergistically stabilize each other (Fig. 1.17a). This results in metallated DNA junctions with unusually high stability (e.g., 40 °C melting temperature increase for a 10-base DNA duplex upon single metal incorporation).

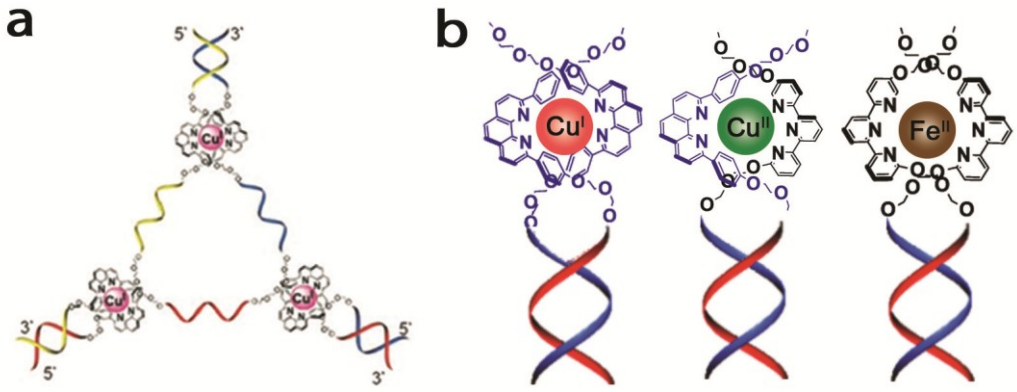

Figure 1.17 Metal DNA complexes and structures. a, Site-specifically incorporating diphenylphenanthroline (dpp) into DNA templates nanostructures with highly stable duplexes. Reproduced from ref. 91 with permission from Wiley-VCH. **b,** Using two different ligand insertions, selective coordination environments can be templated with DNA. Reproduced from ref. 101 with permission from Wiley-VCH.

The real potential of DNA lies in its ability to organize different transition metals in precise locations within a nano structure. With this in mind, Sleiman and co-workers recently reported the DNA-templated creation of three different ligand environments.[101] Each of these binds a specific transition metal ion, with enhancement of the stability of DNA (Fig. 1.17b). Moreover, when the 'incorrect' metal ion is placed within one of these ligand environments, 'error correction' spontaneously occurs. Thus, the metal adjusts its oxidation state, displaces a relatively labile metal to form a more stable complex, or causes reorganization of the coordination site to create the favored ligand complex.

Using this method, Sleiman and co-workers have also reported the construction of a metal-DNA cage, with site-specific incorporation of transition metals in the vertices of this structure (Fig. 1.18a).[102] This class of materials brings together the properties of metal–organic frameworks (MOF), such as metal-mediated redox, photochemical, magnetic or catalytic control on encapsulated guest molecules, with the programmability of DNA and its facile chemical and structural variation. This method will be detailed further in Chapter 2.

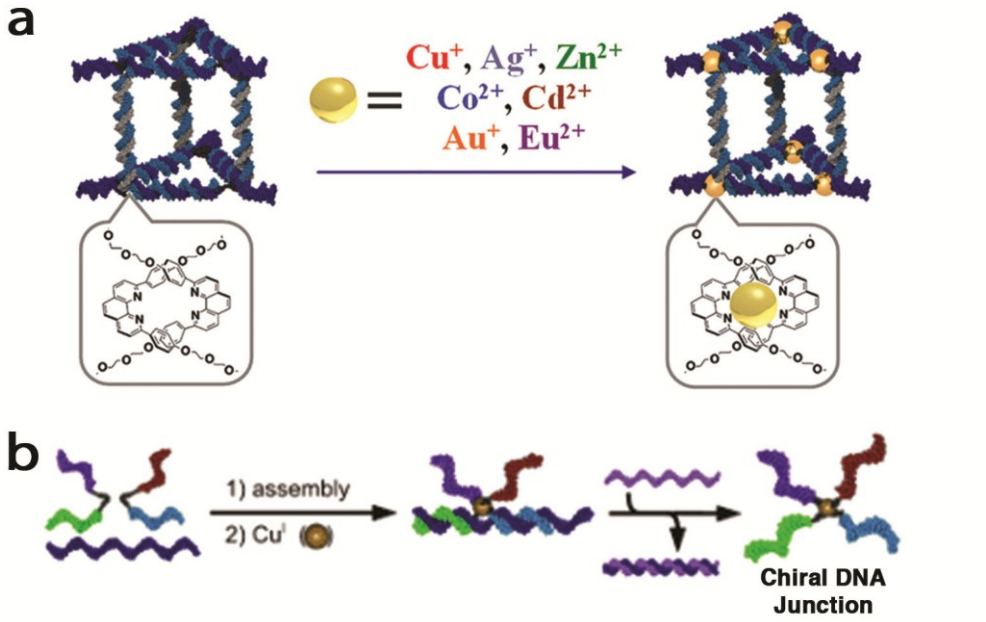

Figure 1.18 Metal DNA complexes and structures in 3D. a, Metal-DNA cage structure with selective coordination environments templated in 3D. **b,** Chiral four-way metal-DNA junction formed via templated assembly of modified sequences. Reproduced from ref. 103 with permission from Wiley-VCH.

One of the consequences of using metal-DNA hybrid systems is the ability to create 'DNA-economical' structures, where the metal coordination geometry defines the geometry of the vertex, and the DNA strands give programmable regions that can used as building blocks for 2D and 3D structures. Towards this goal, Sleiman and co-workers recently developed a DNA-templated method to create chiral metal-DNA junctions.[103] By modifying DNA strands with a phenanthroline ligand and templating using a minimal amount of DNA, we generated a chiral DNA junction with a transition metal at the branch point (Fig. 1.18b). This junction contains four different single-stranded DNA arms, making it a unique synthon for further self-assembly. Its information content and precise spatial arrangement of DNA were then used to construct metal-DNA triangular rungs that could be assembled into the first metal-DNA nanotubular structure.

The functions of such multi-metallic systems have yet to be examined in detail, but these initial studies have shown that transition metals can be selectively incorporated to generate monodisperse and highly stabilized DNA structures with preserved self-assembly properties, smaller sizes and dynamic character. Future

applications envisaged for metal-containing DNA materials include catalysis, sensing, nanoelectronics and artificial photosynthesis systems.

1.6.4 Using molecules to drive DNA self-assembly

So far, discussion within the context of supramolecular DNA assembly has focused on hybrid DNA systems, where assembly properties are still primarily determined by DNA Watson–Crick base pairing. Synthetic insertions have the additional potential to introduce new assembly features into DNA, that complement or possibly even override DNA's own base-pairing. Because of the wealth of supramolecular motifs that have been achieved in the last four decades, this nascent area holds great potential towards expanding DNA nanotechnology into completely new structures.

A number of research groups have used DNA as a scaffold to organize polyaromatic molecules into π-stacked arrays.[104] This was achieved either by replacing the natural DNA bases with artificial polyaromatic molecules, or by site-specifically attaching aromatic chromophores to these bases. Unique photophysical properties, unusual stabilities and biodetection applications can result from this mode of DNA modification.[104,105] Hydrogen bonding has also been used to reprogram DNA hybridization into a five-stranded structure by replacing the nucleobases with iso-guanine, resulting in pentameric assemblies.[106]

Perylene diimide-oligonucleotides have been shown to form either duplex or hairpin structures based on the choice of DNA sequences used.[107] Wagenknecht has used Y-shaped DNA junctions end-terminated with perylene units to drive self-assembly in 2D.[108] Extended aromatic insertions of this type can produce specific interactions with other hydrophobic materials. As an example, porphyrin modifications can anchor a DNA hexagon to a lipid membrane, yielding a dynamic yet surface-bound assembly (Fig. 1.19a).[109] The weak anchoring allows DNA components to migrate and adjust to their environment without leaving the membrane surface. This could serve as an important step towards self-repairing or stimuli-responsive materials.

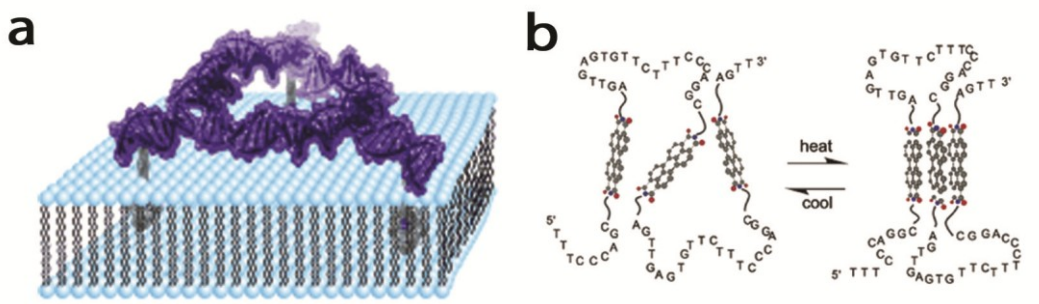

Figure 1.19 Self-assembly via chemical modification. a, Porphyrin-DNA modifications can be used to selectively attach DNA nanostructures to lipid vesicles. Reproduced from ref. 109 with permission from Wiley- VCH. **b,** DNA foldamers yield folded structures through p-stacking interactions. Adapted with permission from ref. 110. Copyright 2003 American Chemical Society.

DNA foldamers are an interesting example of the effect of synthetic insertions on self-assembly. A foldamer is a polymer that wraps into a highly specific conformation under given conditions, using a number of non-covalent interactions between its monomer units. Synthetic insertion of hydrophobic perylene units within a hydrophilic DNA chain can drive folding processes, to yield a final product that is different from the standard double helix.[110] This folded structure places the perylene units into a π-stacked aromatic core. This behaviour was even more favourable with increasing temperature (a condition that normally denatures secondary and tertiary structures), due to endothermic folding enthalpies. With careful sequence planning, the group designed a star-shaped foldamer that is stable across a wide temperature range; at low temperatures DNA base-pairing maintains the structure, while at high temperatures hydrophobic effects fill this role (Fig. 1.19b). Nucleic acids are known to carry out some catalytic functions, which means that highly stable hybrids with well-defined folding have exciting implications for mimicking folded, functional proteins.

1.6.5 DNA block copolymers and higher order assembly

To increase the long-range order of assembled structures, researchers are working to covalently attach biomolecules to polymers. The resulting products show new biological and self assembly properties and are being explored for a

variety of applications, from therapeutics and drug delivery, to tissue engineering and materials science.[111-113] In the context of supramolecular DNA assembly, DNA-lipid, block copolymer[114] and dendrimer conjugates[115,116] have been prepared and can assemble into a number of interesting morphologies. The amphiphilic nature of these materials has yielded interesting micellar assemblies that can be further manipulated with the recognition properties of DNA. We direct the reader to recent reviews that outline some of the properties of biohybrid materials prepared by attaching lipids or polymers to DNA.[111,114,117]

Switchable self-assembled structures have been created using polypropyleneoxide (PPO) and polyethylene glycol (PEG) block copolymers with short DNA tails.[118] Alone, these structures formed star micelles with hydrophobic cores and oligonucleotide coronas. But when long template strands composed of repeating complement sequences to the DNA block are added, a new arrangement was formed. Elongated assemblies of duplex DNA were linked by repeating hydrophobic cores, as shown in Fig. 1.20a, with size defined by the choice of template strand. It is important to note that adding shorter complementary sequences did not disrupt the micelle in this design, making such structures amenable to functionalization. The organized DNA within these micelle structures has also been used to template the assembly of the Cowpea Chlorotic Mottle Virus (CCMV) capsid, which traps or encapsulates hydrophobic and hydrophilic molecules in the core of the particle.[119] Dynamic character was shown by Gianneshi and co-workers, who designed a PEG-DNA-brush block copolymer with the ability to shift between spherical and cylindrical shaped micelles with the addition of complementary DNA strands or DNAzymes (Fig. 1.20b).[120]

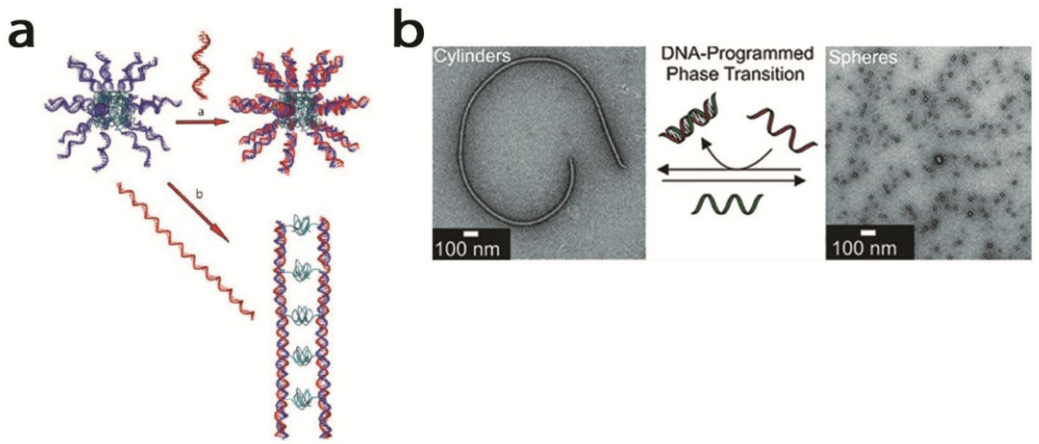

Figure 1.20 DNA-block copolymer conjugates. a, Micelles assemble using amphiphiles made of DNA and block copolymers. Reproduced from ref. 118 with permission from Wiley-VCH. **b,** Using specific DNA inputs, a PEG-DNA-brush polymer can shift shape between spherical and cylindrical micelles. Reproduced from ref. 120 with permission from Wiley-VCH.

Carneiro and Sleiman employed the self-assembling properties of short oligoethylene glycol (OEG) units arranged in a dendritic fashion.[121] By modifying the ends of DNA strands with these dendritic structures and hybridizing the strands into a duplex, a block-copolymer architecture was formed (Fig. 1.21). These hybrid structures, composed of a dsDNA core surrounded by the OEG dendritic structure (Fig. 1.21-top), self-assembled into long-range fibers in organic solvents by end-to-end stacking of the DNA strands. Through simple modification of the deposition conditions, the fibers could also assemble into long-range ordered 2D networks (Fig. 1.21-bottom). The Liu group created an amphiphilic DNA-dendron hybrid, containing a hydrophobic dendron attached to a DNA single strand. In aqueous media, this molecule assembles into nanofibers, containing a hydrophobic dendron core and a single-stranded DNA corona, and these morphologies were shown to encapsulate hydrophobic guest molecules.[116] Recently, the groups of Tan[122] and Mirkin[123] have also demonstrated that self-assembled polyvalent DNA structures display efficient cellular uptake and thus may prove to be candidates for drug delivery applications. In particular, Mirkin has demonstrated such polyvalent structures composed of DNA targeted for mRNA can regulate gene expression via the antisense pathway.[123]

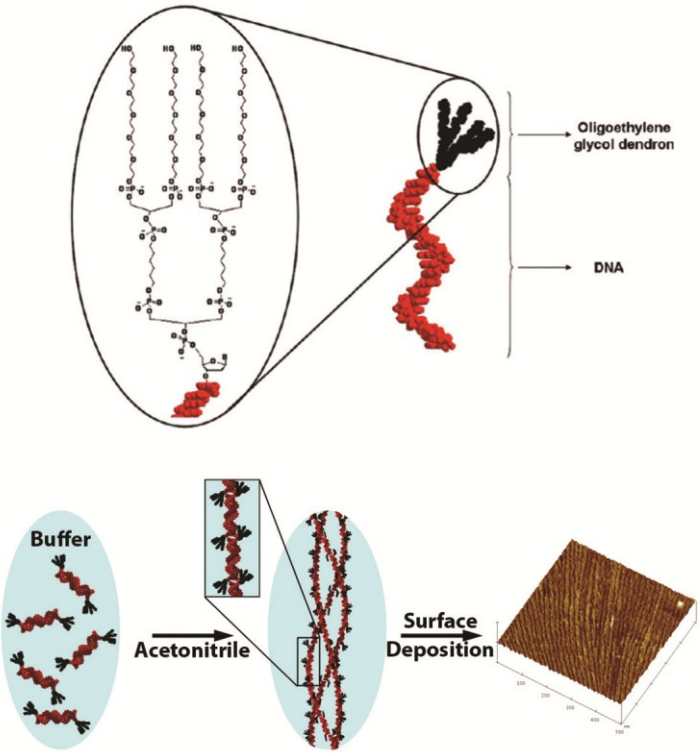

Figure 1.21 Long-range assembly of a dendritic DNA motif. Covalently modifying DNA with dendritic oligoethylene moieties enables self-assembly of long-range fibers. Adapted with permission from ref. 121. Copyright 2010 American Chemical Society.

By tuning the hydrophilic and hydrophobic properties of the organic insertion, DNA conjugates can be designed to exhibit unique properties that are not possible in the individual components themselves. The result is a supramolecular system that can display dynamic and thermoresponsive characteristics as well as the ability to achieve long-range ordering of materials at the nanometre length-scale in a well-defined manner.

1.6.6 Dynamic control of over DNA self-assembly

The description of supramolecular DNA assembly has thus far focused on covalent modification with molecules that impart structural or self-assembling properties to DNA nanostructures. In this final section, discussion is shifted to molecules that can *dynamically* control DNA assembly, either through covalent insertion or non-covalent interactions. In DNA nanomachines, control over DNA

motion occurs in the presence of externally added DNA strands, enzymes, or in response to pH or ion changes.[124] The use of synthetic molecules to effect DNA structural switching or modification can significantly widen the spectrum of dynamic control available for further tuning the assembly of 2D and 3D nanostructures.

One of the ways to control DNA assembly is by developing molecules that 'repair' DNA mismatches and restore DNA hybridization. Nakatani and co-workers introduced a small synthetic ligand, a naphthyridinecarbamate dimer (NCD), that acts as a 'molecular glue' in DNA nanofabrication.[125] Recently, this molecule was used to modulate DNA hybridization and form a DNA tetrahedron (Fig. 1.22a).[126] This method requires that key structural sequences involved in nanostructure formation be altered with GG mismatches. The set of component DNA strands are designed to assemble into a tetrahedral structure only in the presence of the small molecule NCD, which selectively binds at the GG-mismatch site. Upon coordination, NCD increases the thermal stability of dsDNA and allows 3D assembly to take place. Another method to control DNA assembly is to specifically block or disrupt the hydrogen bonding interactions required for strands to associate. A photocaged thymidine residue has been incorporated into DNA by standard synthesis conditions, disrupting hydrogen bonding.[127] In this site-specific, covalent modification strategy, DNA hybridization was restored by irradiating to 'decage' thymine's hydrogen bonding face.

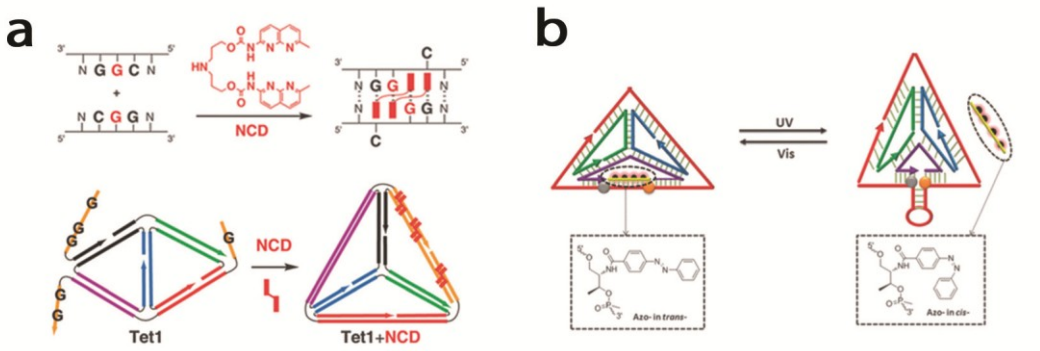

Figure 1.22 Molecule mediated DNA self-assembly. a, Small molecules can selectively interact with GG mismatches sites, allowing for open- ing/closing of 3D DNA nanostructures. Reproduced from ref. 126 with permission from the Royal Society of Chemistry. **b,** Incorporating azobenzenes into a 3D DNA tetrahedron allows reversible cycling of structure. Reproduced from ref. 131 with permission from the Royal Society of Chemistry.

Within the supramolecular toolbox, molecules that undergo photoswitchable behaviour provide impressive dynamic control over self-assembly properties.[128] The thermodynamically favoured association of the DNA duplex, for example, can be overridden by altering the conformation of molecules that interact with it. Some of the most commonly used molecules are azobenzene and its derivatives, where photo-isomerization between cis and trans forms provides enough motion to destabilize duplex formation.[129] Dynamic control over two- dimensional systems, such as a DNA hairpin, has been achieved, revealing that the correct placement and number of azobenzene derivatives is paramount to initiating high levels of assembly control.[130,131] Tan and co-workers recently switched 3D DNA assembly with an azobenzene derivative.[131] In this example, the shape of a DNA tetrahedron can be reversibly controlled by alternately irradiating with different wavelengths of light (Fig. 1.22b).

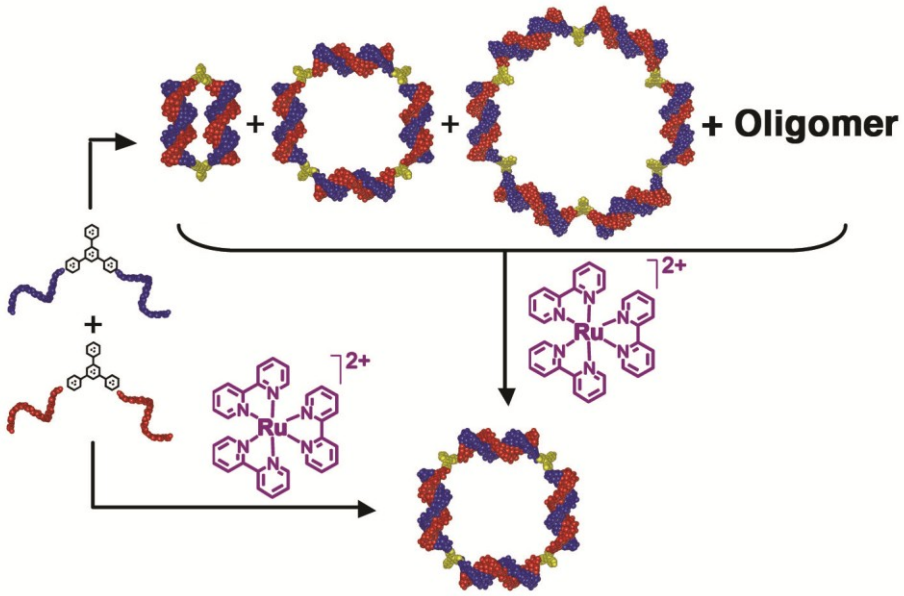

Figure 1.23 Molecule mediated assembly. Small molecule ruthenium tris-bypyridine ($Ru(bpy)_3^{2+}$) is used to selectively control the 2D DNA nanostructure formation of branched symmetric starting materials. Adapted with permission from ref. 134. Copyright 2007 American Chemical Society.

An alternative approach to controlling 2D and 3D DNA assembly is to use molecules that can selectively template how specific nanostructures are formed from a dynamic equilibrium of constituents. This method is based on the highly successful area of dynamic combinatorial chemistry.[132,133] It can result in correcting assembly errors and reducing the number of strands required to prepare complex DNA nanostructures. Aldaye and Sleiman demonstrated this strategy by constructing 5,5'- branched DNA building blocks, containing a rigid organic vertex and two identical DNA arms.[134] In the absence of template, the assembly of one of these molecules with its complementary partner produces a large number of cyclic nanostructures, from dimer to square to hexamer to oligomers. When the molecule ruthenium tris-bipyrdine ($Ru(bpy)_3^{2+}$) is added, the entire library converges into a square product in quantitative yields (Fig. 1.23). It remains unclear as to why the small molecule guest assists in converting the molecular library to one product. This may be due to interactions with the major/minor groves, intercalation to the duplex structures upon formation or even more selective host-guest interactions between the small molecule and void volume

within the structure. While further mechanistic investigation is underway, this example illustrates the ability of externally added molecules to dramatically affect DNA self-assembly and result in clean formation of a single product from a small number of symmetrical DNA strands.

Small molecules that can change the properties of DNA hybridization are a powerful means of generating 2D and 3D nanostructures with dynamic character. These can be applied as 'error-correcting' tools for DNA self-assembly and as stimuli-responsive systems for drug delivery and biosensing.

1.7 Context and scope of thesis research

In summary, the use of DNA as a material outside its normal genomic context has given researchers a great deal of positional control within the nanoscale. Examples from the field of structural DNA nanotechnology, either using DNA-tile or DNA origami approaches, have thus far demonstrated unique bottom-up assembly of nanoparticles, proteins and 3D structures. However, these methods ultimately require increasing amounts of nucleic acids for more complex structures to be prepared. In contrast, combining the superior self-assembly properties of DNA with the functional elements of synthetic organic and inorganic molecules within the field of supramolecular DNA assembly has allowed creation of nanostructures that display properties far greater than the sum of their parts. Within this context, the scope of the research presented in this thesis is aimed at solving problems in chemical construction through selective modification of DNA with synthetic molecules. In retrospect, what we have shown might go beyond synthetic insertions. The inspiration of supramolecular chemistry helped us to develop new approaches towards DNA construction, which did away with interweaving duplexes to go into 2D and 3D. This is what allowed us to generate DNA minimal strategies, and importantly for the field, it allowed us to assemble DNA nanostructures with a large number of ss units. These (a) give assemblies in quantitative yields often at room temperature, (b) provide the ready ability to functionalize with additional macromolecules, and (c) give intrinsic dynamic character to the resulting structures.

In chapter 2, the design and assembly of the first metal-DNA 3D architecture is reported. A face-centered assembly approach is developed that allows connection of two DNA triangles into a well-defined triangular prismatic (**TP**) structure. Each triangle is synthetically modified to contain DNA-templated ligand environments that selectively coordinate and position transition metals. The coordination at pre-programmed positions and stabilizing role for transition metals integrated into a 3D DNA framework is demonstrated. This allowed for facile preparation of a 3D DNA prism from strands that are enriched due to the metal coordination ability and resulting structural stability.

In chapter 3, a modular approach to generate geometrically diverse 3D DNA prismatic structures in a rapid and high-yielding manner is described. Balancing the incorporation of sequence uniqueness and symmetry results in triangular (**TP**), rectangular (**RP**), and pentagonal prism (**PP**) formation without compromising the potential for nanostructure addressability. It is also demonstrated that the use of full sequence symmetry promotes intra- rather than intermolecular association of strands upon assembly of DNA structures. This method gives access to 3D DNA structures in near quantitative yields, room temperature assembly, assembly at higher concentrations and ease of functionalization.

In chapter 4, 3D-DNA construction is pushed further to generate a structure that requires a minimum number of DNA strands to produce a scaffold with a large number of single-stranded arms. This DNA frame is produced in quantitative yields and used as a core structure to organize materials in 3D. Ring-opening metathesis polymerization (ROMP) is used to generate block copolymers that are covalently attached to DNA strands. Site-specific hybridization of these DNA-polymer chains on the single-stranded arms of the 3D-DNA scaffold gives efficient access to DNA-block copolymer cages. These biohybrid cages possess polymer chains that are programmably positioned in three dimensions on a DNA core and display increased nuclease resistance as compared to unfunctionalized DNA cages. This ‘DNA-minimal’ method thus represents one of the highest

yielding means to generate 3D DNA structures with a maximal amount of single-stranded regions for additional functionalization.

Finally, the cell uptake properties of DNA nanocubes assembled from four 80-base single strands and decorated with Cy3 and/or Cy5-modified complementary strands are investigated in chapter 5. It is demonstrated that these 3D DNA cubes efficiently accumulate in the cytoplasm of human cervical cancer cells (HeLa) without the aid of any transfection agent, whereas single stranded and double stranded DNA cytoplasmic accumulation is acutely absent. A sequence asymmetric DNA cube variant was also assembled, which showed excellent cell uptake when labeled with only a single fluorophore. The results in this chapter suggest that the intracellular accumulation of nucleic acid particles without the aid of viral or non-viral vectors could be achieved if DNA strands are packaged into compact globular particles. This finding is of significance in the area of nucleic acid delivery, and will allow the implementation of nucleic acid therapies without the use of potentially toxic transfection agents.

1.8 References

(1) Lu, W.; Lieber, C. M. *Nat. Mater.* **2007**, *6*, 841.

(2) Krug, H. F.; Wick, P. *Angewandte Chemie-International Edition* **2011**, *50*, 1260.

(3) Maynard, A. D.; Warheit, D. B.; Philbert, M. A. *Toxicol Sci* **2011**, *120 Suppl 1*, S109.

(4) Sahoo, S. K.; Parveen, S.; Panda, J. J. *Nanomedicine* **2007**, *3*, 20.

(5) Craighead, H. *Nature* **2006**, *442*, 387.

(6) Salaita, K.; Wang, Y.; Mirkin, C. A. *Nat. Nanotechnol.* **2007**, *2*, 145.

(7) Whitesides, G. M.; Mathias, J. P.; Seto, C. T. *Science* **1991**, *254*, 1312.

(8) Mandelkern, M.; Elias, J. G.; Eden, D.; Crothers, D. M. *J Mol Biol* **1981**, *152*, 153.

(9) a) Watson, J.D.; Crick, F. H. C.; Nature **1953**, *171*, 737. b) Record Jr, M. T.; Mazur, S. J.; Melançon, P.; Roe, J. H.; Shaner, S. L.; Unger, L. *Annu. Rev. Biochem* **1981**, *50*, 997.

(10) Lu, Y.; Weers, B.; Stellwagen, N. C. *Biopolymers* **2001**, *61*, 261.

(11) a) Alvarado-Urbina, G.; Sathe, G. M.; Liu, W.C.; Gillen, M.F.; Duck, P.D.; Bender, R.; Ogilvie, K.K. *Science* **1981**, 270. b) Caruthers, M. H. *Acc. Chem. Res.* **1991**, *24*, 278.

(12) Kwak, M.; Herrmann, A. *Chem. Soc. Rev.* **2011**, *40*, 5745.

(13) Seeman, N. C. *J Theor Biol* **1982**, *99*, 237.

(14) Lin, C.; Liu, Y.; Yan, H. *Biochemistry* **2009**, *48*, 1663.
(15) Kallenbach, N. R.; Ma, R. I.; Seeman, N. C. *Nature* **1983**, *305*, 829.
(16) Fu, T. J.; Seeman, N. C. *Biochemistry* **1993**, *32*, 3211.
(17) Winfree, E.; Liu, F.; Wenzler, L. A.; Seeman, N. C. *Nature* **1998**, *394*, 539.
(18) LaBean, T. H.; Yan, H.; Kopatsch, J.; Liu, F. R.; Winfree, E.; Reif, J. H.; Seeman, N. C. *J. Am. Chem. Soc.* **2000**, *122*, 1848.
(19) Reishus, D.; Shaw, B.; Brun, Y.; Chelyapov, N.; Adleman, L. *J. Am. Chem. Soc.* **2005**, *127*, 17590.
(20) Ke, Y. G.; Liu, Y.; Zhang, J. P.; Yan, H. *J. Am. Chem. Soc.* **2006**, *128*, 4414.
(21) Park, S. H.; Yin, P.; Liu, Y.; Reif, J. H.; Labean, T. H.; Yan, H. *Nano Lett.* **2005**, *5*, 729.
(22) Chhabra, R.; Sharma, J.; Ke, Y.; Liu, Y.; Rinker, S.; Lindsay, S.; Yan, H. *J. Am. Chem. Soc.* **2007**, *129*, 10304.
(23) Lin, C.; Liu, Y.; Yan, H. *Nano Lett.* **2007**, *7*, 507.
(24) Zheng, J. W.; Constantinou, P. E.; Micheel, C.; Alivisatos, A. P.; Kiehl, R. A.; Seeman, N. C. *Nano Lett.* **2006**, *6*, 1502.
(25) Lo, P. K.; Metera, K. L.; Sleiman, H. F. *Curr. Opin. Chem. Biol.* **2010**, *14*, 597.
(26) Rothemund, P. W.; Ekani-Nkodo, A.; Papadakis, N.; Kumar, A.; Fygenson, D. K.; Winfree, E. *J. Am. Chem. Soc.* **2004**, *126*, 16344.
(27) Liu, D.; Park, S. H.; Reif, J. H.; LaBean, T. H. *Proc. Natl. Acad. Sci. USA* **2004**, *101*, 717.
(28) Sharma, J.; Chhabra, R.; Cheng, A.; Brownell, J.; Liu, Y.; Yan, H. *Science* **2009**, *323*, 112.
(29) Dutta, P. K.; Varghese, R.; Nangreave, J.; Lin, S.; Yan, H.; Liu, Y. *J. Am. Chem. Soc.* **2011**, *133*, 11985.
(30) Zheng, J.; Birktoft, J. J.; Chen, Y.; Wang, T.; Sha, R.; Constantinou, P. E.; Ginell, S. L.; Mao, C.; Seeman, N. C. *Nature* **2009**, *461*, 74.
(31) Zhang, C.; He, Y.; Su, M.; Ko, S. H.; Ye, T.; Leng, Y.; Sun, X.; Ribbe, A. E.; Jiangh, W.; Mao, C. *Faraday Discuss* **2009**, *143*, 221.
(32) Chen, J. H.; Seeman, N. C. *Nature* **1991**, *350*, 631.
(33) Zhang, Y. W.; Seeman, N. C. *J. Am. Chem. Soc.* **1994**, *116*, 1661.
(34) He, Y.; Ye, T.; Su, M.; Zhang, C.; Ribbe, A. E.; Jiang, W.; Mao, C. *Nature* **2008**, *452*, 198.
(35) Zhang, C.; Su, M.; He, Y.; Zhao, X.; Fang, P. A.; Ribbe, A. E.; Jiang, W.; Mao, C. *Proc. Natl. Acad. Sci. USA* **2008**, *105*, 10665.
(36) Zhang, C.; Ko, S. H.; Su, M.; Leng, Y.; Ribbe, A. E.; Jiang, W.; Mao, C. *J. Am. Chem. Soc.* **2009**, *131*, 1413.
(37) Rothemund, P. W. *Nature* **2006**, *440*, 297.
(38) Castro, C. E.; Kilchherr, F.; Kim, D. N.; Shiao, E. L.; Wauer, T.; Wortmann, P.; Bathe, M.; Dietz, H. *Nat. Methods* **2011**, *8*, 221.
(39) Nangreave, J.; Han, D.; Liu, Y.; Yan, H. *Curr. Opin. Chem. Biol.* **2010**, *14*, 608.

(40) Michelotti, N.; Johnson-Buck, A.; Manzo, A. J.; Walter, N. G. *Wiley Interdiscip. Rev. Nanomed. Nanobiotechnol.* **2012**, *4*, 139.

(41) Rajendran, A.; Endo, M.; Sugiyama, H. *Angewandte Chemie-International Edition* **2012**, *51*, 874.

(42) Ke, Y.; Lindsay, S.; Chang, Y.; Liu, Y.; Yan, H. *Science* **2008**, *319*, 180.

(43) Voigt, N. V.; Torring, T.; Rotaru, A.; Jacobsen, M. F.; Ravnsbaek, J. B.; Subramani, R.; Mamdouh, W.; Kjems, J.; Mokhir, A.; Besenbacher, F.; Gothelf, K. V. *Nat. Nanotechnol.* **2010**, *5*, 200.

(44) Torring, T.; Voigt, N. V.; Nangreave, J.; Yan, H.; Gothelf, K. V. *Chem. Soc. Rev.* **2011**, *40*, 5636.

(45) Stephanopoulos, N.; Liu, M. H.; Tong, G. J.; Li, Z.; Liu, Y.; Yan, H.; Francis, M. B. *Nano Lett.* **2010**, *10*, 2714.

(46) Nakata, E.; Liew, F. F.; Uwatoko, C.; Kiyonaka, S.; Mori, Y.; Katsuda, Y.; Endo, M.; Sugiyama, H.; Morii, T. *Angew. Chem. Int. Ed.* **2012**, *51*, 2421.

(47) Stein, I. H.; Steinhauer, C.; Tinnefeld, P. *J. Am. Chem. Soc.* **2011**, *133*, 4193.

(48) Douglas, S. M.; Dietz, H.; Liedl, T.; Hogberg, B.; Graf, F.; Shih, W. M. *Nature* **2009**, *459*, 414.

(49) Bellot, G.; McClintock, M. A.; Lin, C.; Shih, W. M. *Nat. Methods* **2011**, *8*, 192.

(50) Andersen, E. S.; Dong, M.; Nielsen, M. M.; Jahn, K.; Subramani, R.; Mamdouh, W.; Golas, M. M.; Sander, B.; Stark, H.; Oliveira, C. L.; Pedersen, J. S.; Birkedal, V.; Besenbacher, F.; Gothelf, K. V.; Kjems, J. *Nature* **2009**, *459*, 73.

(51) Douglas, S. M.; Bachelet, I.; Church, G. M. *Science* **2012**, *335*, 831.

(52) Kuzuya, A.; Komiyama, M. *Chem. Commun.* **2009**, 4182.

(53) Endo, M.; Hidaka, K.; Kato, T.; Namba, K.; Sugiyama, H. *J. Am. Chem. Soc.* **2009**, *131*, 15570.

(54) Ke, Y.; Sharma, J.; Liu, M.; Jahn, K.; Liu, Y.; Yan, H. *Nano Lett.* **2009**, *9*, 2445.

(55) Aldaye, F. A.; Palmer, A. L.; Sleiman, H. F. *Science* **2008**, *321*, 1795.

(56) Shih, W. M.; Quispe, J. D.; Joyce, G. F. *Nature* **2004**, *427*, 618.

(57) Goodman, R. P.; Schaap, I. A.; Tardin, C. F.; Erben, C. M.; Berry, R. M.; Schmidt, C. F.; Turberfield, A. J. *Science* **2005**, *310*, 1661.

(58) Andersen, F. F.; Knudsen, B.; Oliveira, C. L.; Frohlich, R. F.; Kruger, D.; Bungert, J.; Agbandje-McKenna, M.; McKenna, R.; Juul, S.; Veigaard, C.; Koch, J.; Rubinstein, J. L.; Guldbrandtsen, B.; Hede, M. S.; Karlsson, G.; Andersen, A. H.; Pedersen, J. S.; Knudsen, B. R. *Nucleic Acids Res.* **2008**, *36*, 1113.

(59) Bhatia, D.; Mehtab, S.; Krishnan, R.; Indi, S. S.; Basu, A.; Krishnan, Y. *Angew. Chem. Int. Ed.* **2009**, *48*, 4134.

(60) Lehn, J. M. *Supramolecular Chemistry: Concepts and Perspectives : a Personal Account Built Upon the George Fisher Baker Lectures in Chemistry*

at Cornell University [and The] Lezione Lincee, Accademia Nazionale Dei Lincei, Roma; VCH, 1995.

(61) Vicens, J.; Vicens, Q. *Journal of Inclusion Phenomena and Macrocyclic Chemistry* **2011**, *71*, 251.

(62) Aldaye, F. A.; Sleiman, H. F. *Pure Appl. Chem.* **2009**, *81*, 2157.

(63) McLaughlin, C. K.; Hamblin, G. D.; Sleiman, H. F. *Chem. Soc. Rev.* **2011**, *40*, 5647.

(64) Shi, J. F.; Bergstrom, D. E. *Angewandte Chemie-International Edition in English* **1997**, *36*, 111.

(65) Scheffler, M.; Dorenbeck, A.; Jordan, S.; Wüstefeld, M.; Von Kiedrowski, G. *Angew. Chem. Int. Ed.* **1999**, *38*, 3312.

(66) Aldaye, F. A.; Sleiman, H. F. *Angew. Chem. Int. Ed.* **2006**, *45*, 2204.

(67) Aldaye, F. A.; Sleiman, H. F. *J. Am. Chem. Soc.* **2007**, *129*, 4130.

(68) Zhang, T.; Yang, Z.; Liu, D. *Nanoscale* **2011**, *3*, 4015.

(69) Aldaye, F. A.; Sleiman, H. F. *J. Am. Chem. Soc.* **2007**, *129*, 13376.

(70) McLaughlin, C. K.; Hamblin, G. D.; Aldaye, F. A.; Yang, H.; Sleiman, H. F. *Chem. Commun.* **2011**, *47*, 8925.

(71) McLaughlin, C. K.; Hamblin, G. D.; Hanni, K. D.; Conway, J. W.; Nayak, M. K.; Carneiro, K. M.; Bazzi, H. S.; Sleiman, H. F. *J. Am. Chem. Soc.* **2012**, *134*, 4280.

(72) Aldaye, F. A.; Lo, P. K.; Karam, P.; McLaughlin, C. K.; Cosa, G.; Sleiman, H. F. *Nat. Nanotechnol.* **2009**, *4*, 349.

(73) Lo, P. K.; Karam, P.; Aldaye, F. A.; McLaughlin, C. K.; Hamblin, G. D.; Cosa, G.; Sleiman, H. F. *Nat. Chem.* **2010**, *2*, 319.

(74) Lo, P. K.; Altvater, F.; Sleiman, H. F. *J. Am. Chem. Soc.* **2010**, *132*, 10212.

(75) Hamblin, G. D.; Carneiro, K. M.; Fakhoury, J. F.; Bujold, K. E.; Sleiman, H. F. *J. Am. Chem. Soc.* **2012**, *134*, 2888.

(76) Shchepinov, M. S.; Mir, K. U.; Elder, J. K.; Frank-Kamenetskii, M. D.; Southern, E. M. *Nucleic Acids Res.* **1999**, *27*, 3035.

(77) Zimmermann, J.; Cebulla, M. P.; Monninghoff, S.; von Kiedrowski, G. *Angew. Chem. Int. Ed.* **2008**, *47*, 3626.

(78) Kuroda, T.; Sakurai, Y.; Suzuki, Y.; Nakamura, A. O.; Kuwahara, M.; Ozaki, H.; Sawai, H. *Chem. Asian J.* **2006**, *1*, 575.

(79) Stepp, B. R.; Gibbs-Davis, J. M.; Koh, D. L.; Nguyen, S. T. *J. Am. Chem. Soc.* **2008**, *130*, 9628.

(80) Prytkova, T. R.; Eryazici, I.; Stepp, B.; Nguyen, S. B.; Schatz, G. C. *J. Phys. Chem. B* **2010**, *114*, 2627.

(81) Tumpane, J.; Sandin, P.; Kumar, R.; Powers, V. E. C.; Lundberg, E. P.; Gale, N.; Baglioni, P.; Lehn, J. M.; Albinsson, B.; Lincoln, P.; Wilhelmsson, L. M.; Brown, T.; Norden, B. *Chem. Phys. Lett.* **2007**, *440*, 125.

(82) Lundberg, E. P.; Plesa, C.; Wilhelmsson, L. M.; Lincoln, P.; Brown, T.; Norden, B. *ACS Nano* **2011**, *5*, 7565.

(83) Lee, J. K.; Jung, Y. H.; Tok, J. B.; Bao, Z. *ACS Nano* **2011**, *5*, 2067.

(84) Endo, M.; Seeman, N. C.; Majima, T. *Angew. Chem. Int. Ed.* **2005**, *44*, 6074.

(85) Meng, M.; Ahlborn, C.; Bauer, M.; Plietzsch, O.; Soomro, S. A.; Singh, A.; Muller, T.; Wenzel, W.; Brase, S.; Richert, C. *ChemBioChem* **2009**, *10*, 1335.

(86) Singh, A.; Tolev, M.; Meng, M.; Klenin, K.; Plietzsch, O.; Schilling, C. I.; Muller, T.; Nieger, M.; Bräse, S.; Wenzel, W.; Richert, C. *Angew. Chem. Int. Ed.* **2011**, *50*, 3227.

(87) Eryazici, I.; Prytkova, T. R.; Schatz, G. C.; Nguyen, S. T. *J. Am. Chem. Soc.* **2010**, *132*, 17068.

(88) Leininger, S.; Olenyuk, B.; Stang, P. J. *Chem. Rev.* **2000**, *100*, 853.

(89) Cowan, J. A. *Chem. Rev.* **1998**, *98*, 1067.

(90) Yang, H.; Metera, K. L.; Sleiman, H. F. *Coord. Chem. Rev.* **2010**, *254*, 2403.

(91) Yang, H.; Sleiman, H. F. *Angew. Chem. Int. Ed.* **2008**, *47*, 2443.

(92) Clever, G. H.; Shionoya, M. *Coord. Chem. Rev.* **2010**, *254*, 2391.

(93) Vargas-Baca, I.; Mitra, D.; Zulyniak, H. J.; Banerjee, J.; Sleiman, H. F. *Angew. Chem. Int. Ed.* **2001**, *40*, 4629.

(94) Mitra, D.; Di Cesare, N.; Sleiman, H. F. *Angew. Chem. Int. Ed.* **2004**, *43*, 5804.

(95) Stewart, K. M.; McLaughlin, L. W. *J. Am. Chem. Soc.* **2004**, *126*, 2050.

(96) Stewart, K. M.; Rojo, J.; McLaughlin, L. W. *Angewandte Chemie-International Edition* **2004**, *43*, 5808.

(97) Choi, J. S.; Kang, C. W.; Jung, K.; Yang, J. W.; Kim, Y. G.; Han, H. *J. Am. Chem. Soc.* **2004**, *126*, 8606.

(98) Goritz, M.; Kramer, R. *J. Am. Chem. Soc.* **2005**, *127*, 18016.

(99) Miyoshi, D.; Karimata, H.; Wang, Z. M.; Koumoto, K.; Sugimoto, N. *J. Am. Chem. Soc.* **2007**, *129*, 5919.

(100) Gothelf, K. V.; Thomsen, A.; Nielsen, M.; Clo, E.; Brown, R. S. *J. Am. Chem. Soc.* **2004**, *126*, 1044.

(101) Yang, H.; Rys, A. Z.; McLaughlin, C. K.; Sleiman, H. F. *Angew. Chem. Int. Ed.* **2009**, *48*, 9919.

(102) Yang, H.; McLaughlin, C. K.; Aldaye, F. A.; Hamblin, G. D.; Rys, A. Z.; Rouiller, I.; Sleiman, H. F. *Nat. Chem.* **2009**, *1*, 390.

(103) Yang, H.; Altvater, F.; de Bruijn, A. D.; McLaughlin, C. K.; Lo, P. K.; Sleiman, H. F. *Angew. Chem. Int. Ed.* **2011**, *50*, 4620.

(104) Bandy, T. J.; Brewer, A.; Burns, J. R.; Marth, G.; Nguyen, T.; Stulz, E. *Chem. Soc. Rev.* **2011**, *40*, 138.

(105) Ruiz-Carretero, A.; Janssen, P. G.; Kaeser, A.; Schenning, A. P. *Chem. Commun.* **2011**, *47*, 4340.

(106) Chaput, J. C.; Switzer, C. *Proc. Natl. Acad. Sci. USA* **1999**, *96*, 10614.

(107) Zheng, Y.; Long, H.; Schatz, G. C.; Lewis, F. D. *Chem. Commun.* **2005**, 4795.

(108) Menacher, F.; Stepanenko, V.; Wurthner, F.; Wagenknecht, H. A. *Chem. Eur. J.* **2011**, *17*, 6683.

(109) Borjesson, K.; Lundberg, E. P.; Woller, J. G.; Norden, B.; Albinsson, B. *Angew. Chem. Int. Ed.* **2011**, *50*, 8312.

(110) Wang, W.; Wan, W.; Zhou, H. H.; Niu, S.; Li, A. D. *J. Am. Chem. Soc.* **2003**, *125*, 5248.

(111) Fuks, G.; Mayap Talom, R.; Gauffre, F. *Chem. Soc. Rev.* **2011**, *40*, 2475.

(112) Webber, M. J.; Kessler, J. A.; Stupp, S. I. *J. Intern. Med.* **2010**, *267*, 71.

(113) Holzwarth, J. M.; Ma, P. X. *J. Mater. Chem.* **2011**, *21*, 10243.

(114) Kwak, M.; Herrmann, A. *Angew. Chem. Int. Ed.* **2010**, *49*, 8574.

(115) Liu, H.; Torring, T.; Dong, M.; Rosen, C. B.; Besenbacher, F.; Gothelf, K. V. *J. Am. Chem. Soc.* **2010**, *132*, 18054.

(116) Wang, L.; Feng, Y.; Sun, Y.; Li, Z.; Yang, Z.; He, Y.-M.; Fan, Q.-H.; Liu, D. *Soft Matter* **2011**, *7*, 7187.

(117) Patwa, A.; Gissot, A.; Bestel, I.; Barthelemy, P. *Chem. Soc. Rev.* **2011**, *40*, 5844.

(118) Ding, K.; Alemdaroglu, F. E.; Borsch, M.; Berger, R.; Herrmann, A. *Angew. Chem. Int. Ed.* **2007**, *46*, 1172.

(119) Kwak, M.; Minten, I. J.; Anaya, D. M.; Musser, A. J.; Brasch, M.; Nolte, R. J.; Mullen, K.; Cornelissen, J. J.; Herrmann, A. *J. Am. Chem. Soc.* **2010**, *132*, 7834.

(120) Chien, M. P.; Rush, A. M.; Thompson, M. P.; Gianneschi, N. C. *Angew. Chem. Int. Ed.* **2010**, *49*, 5076.

(121) Carneiro, K. M.; Aldaye, F. A.; Sleiman, H. F. *J. Am. Chem. Soc.* **2010**, *132*, 679.

(122) Wu, Y. R.; Sefah, K.; Liu, H. P.; Wang, R. W.; Tan, W. H. *Proc. Natl. Acad. Sci. USA* **2010**, *107*, 5.

(123) Cutler, J. I.; Auyeung, E.; Mirkin, C. A. *J. Am. Chem. Soc.* **2012**, *134*, 1376.

(124) Krishnan, Y.; Simmel, F. C. *Angew. Chem. Int. Ed.* **2011**, *50*, 3124.

(125) Dohno, C.; Nakatani, K. *Chem. Soc. Rev.* **2011**, *40*, 5718.

(126) Dohno, C.; Atsumi, H.; Nakatani, K. *Chem. Commun.* **2011**, *47*, 3499.

(127) Lusic, H.; Young, D. D.; Lively, M. O.; Deiters, A. *Org. Lett.* **2007**, *9*, 1903.

(128) Mayer, G.; Heckel, A. *Angewandte Chemie-International Edition* **2006**, *45*, 4900.

(129) Beharry, A. A.; Woolley, G. A. *Chem. Soc. Rev.* **2011**, *40*, 4422.

(130) Liang, X.; Mochizuki, T.; Asanuma, H. *Small* **2009**, *5*, 1761.

(131) Han, D.; Huang, J.; Zhu, Z.; Yuan, Q.; You, M.; Chen, Y.; Tan, W. *Chem. Commun.* **2011**, *47*, 4670.

(132) Lehn, J. M. *Chem. Soc. Rev.* **2007**, *36*, 151.

(133) Corbett, P. T.; Leclaire, J.; Vial, L.; West, K. R.; Wietor, J. L.; Sanders, J. K.; Otto, S. *Chem. Rev.* **2006**, *106*, 3652.

(134) Aldaye, F. A.; Sleiman, H. F. *J. Am. Chem. Soc.* **2007**, *129*, 10070.

Chapter 2: Design, Self-Assembly and Site-specific Metallation of a 3D DNA Structure

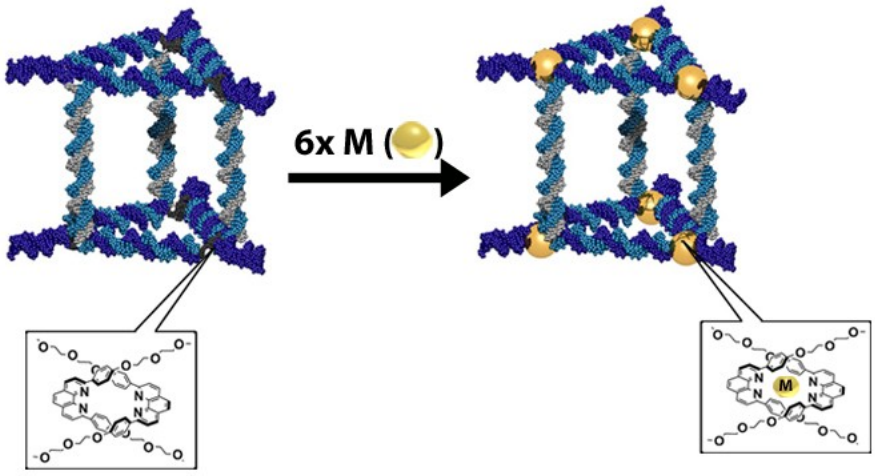

The majority of this chapter has been published as; "Metal-nucleic acid cages", *Yang, H., *McLaughlin, C. K., Aldaye, F. A., Hamblin, G. D., Rys, A. Z., Rouiller, I., and Sleiman, H. F. *Nature Chem.,* **2009**, 1, 390-396 (*Both authors contributed equally to this work).

2.1 Abstract

In chapter 2, the quantitative construction of metal–DNA cages, with the site-specific incorporation of a range of metals within a three-dimensional DNA architecture is reported. Oligonucleotide strands containing specific environments suitable for transition-metal coordination were first organized into two DNA triangles that could then be assembled into a DNA prism with linking strands. Subsequently, the metal centers incorporated at pre-programmed locations within the prismatic assembly were coordinated with copper and silver. Assembly and metal coordination are characterized using circular dichroism, thermal denaturation studies, fluorescence spectroscopy, and gel electrophoresis mobility assay experiments. This ability to position transition metals within a three-dimensional framework could lead to metal–DNA hosts with applications for the

encapsulation, sensing, modification and release of biomolecules and nanomaterials.

2.2 Introduction

The emergence of DNA as a programmable and addressable material for organizing matter on the nanometer length-scale has led to its incorporation into a variety of one- and two-dimensional structures.[1-4] More recently, access to three-dimensional (3D) structures that incorporate DNA as a structural scaffold[5-8] has opened the door for applications in 3D nanoscale organization,[9,10] and biomolecule encapsulation[11,12] and as potential drug delivery vehicles[13]. As outlined in Chapter 1 though, while the intrinsic properties of DNA offer high 'information rich' content, the biopolymer does not possess functional properties such as sizeable conductivity in devices, redox, photoactivity or magnetic properties.

In the natural world, function has evolved through selective coordination of transition metals.[14] Examples where metal use is intimately linked with the processes of life include metalloenzymes, subunits responsible for transduction of photons in photosynthesis and functional groups for storage and release of oxygen.[14] Thus, transition metals serve as an ideal candidate to be incorporated into DNA structures as a means of enhancing both structural and functional properties. Transition metals can be selectively introduced into DNA by direct insertion of metal complexes, through modification of the nucleobases with metal-binding ligands or by direct introduction of metal-binding ligands into the phosphodiester backbone.[15] Although the means of incorporation have been varied, the structures produced have been thus far limited to simple 1D and 2D examples, while more complex assemblies, such as 3D metallated DNA structures, have not been reported.

The value of selectively metallating 3D DNA structures is rooted in their potential as a new class of materials that combine the programmable nature of nucleic acids with the functional properties inherent to transition metals. Such structures could be tuned to encapsulate guest molecules, resulting in switchable

pore sizes (via redox, photochemical or magnetic control), catalytic activity or luminescence sensing.[16-18] The discrete objects produced could also act as building blocks for extended networks or materials, analogous to metal-organic frameworks.[19-21] However, in contrast to these coordination driven polymers or supramolecular metallo-cages,[16-18] these structures offer variability over pore size, geometry, chemistry and addressability via simple DNA modification and design.[1-4] In addition, programmable incorporation of metals can be done in a symmetric or asymmetric fashion within these well-defined 3D structures.

In this chapter, the design and assembly of the first metal-DNA 3D architecture is reported. Triangles are first assembled in excellent yield and each contains three DNA-templated ligand environments that selectively coordinate and position transition metals. A face-centered assembly approach is then employed to connect two DNA triangles into a well-defined triangular prismatic (**TP**) structure. Characterization by circular dichroism (CD), thermal denaturation studies, fluorescence spectroscopy, electron microscopy and gel mobility shift assays reveals both selective coordination at pre-programmed positions and a stabilizing role for transition metals integrated into a 3D DNA framework.

2.3 Design Strategy

In creating 3D metal-DNA structures, two main challenges must be overcome. First, the 3D DNA architecture should be created in an efficient manner that is designed to contain specific positions amenable to modification. Second, the modification sites must be able to bind metals without disruption of the DNA construct. Meeting the latter criteria requires a selective ligand coordination environment that circumvents non-specific metal interactions with either the nucleobases or the highly negatively charged phosphodiester backbone.

As outlined in Fig. 2.1, the modular method developed in this chapter allows both efficient self-assembly and selective metallation of a 3D DNA structure. This method requires only six unique DNA strands, labeled **1a**, **1b**, **1c** and **2a**, **2b**, **2c**, that are selectively modified by standard phoshoramidite chemistry to incorporate bis-2,9-diphenyl-1,10-phenanthroline (dpp) ligands (**3**) at

two positions within each strand (Fig. 2.1a, see experimental section for sequences/synthesis). These strands have been designed to contain two 10 base sequences that are complementary to a single 10 base region on each respective strand (shown as X:X', Y:Y' and Z:Z' in Fig. 2.1a). Ligand **3** is selectively inserted within each strand after each of these complementary regions that act to self-assemble 2D structures. For example, annealing strands **1a-1c** (Fig. 2.1a) both generates triangle **T1** and templates three bis-dpp coordination environments (shown on far right) that can coordinate metals. In an identical fashion dpp modified strands **2a-2c** assemble to create the triply dpp modified triangle **T2**. Each of these geometric objects then becomes a 'face' of the desired triangular prism (**TP**). These prismatic faces are connected by three linking strands (**LSa-c**), as shown in Fig. 2.1b, that each hybridize to a single-stranded region of **T1** and **T2** to create **TP-S**. The remaining single-stranded sections of each **LS** are then sequestered by complementary rigidifying strands (**RSa** or **RSb**), generating a fully double-stranded structure **TP**. This 3D DNA structure thus possesses six metal-coordination junctions that are pre-organized to site-specifically bind transition metals to produce **TP.M$_6$**.

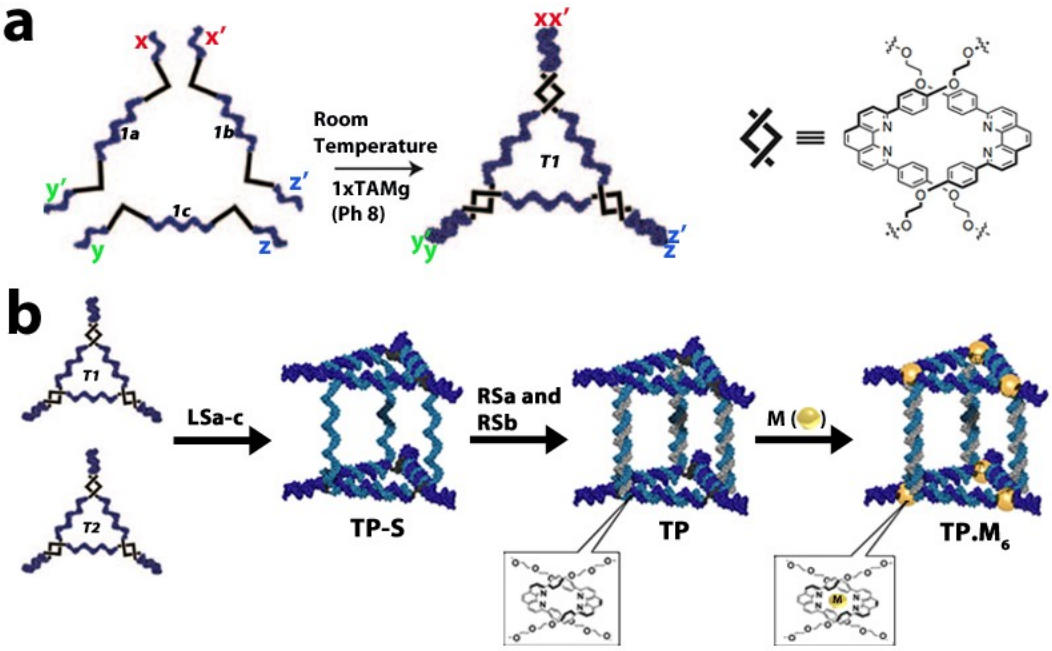

Figure 2.1 Schematic representation of the 2D and 3D assembly strategy. a, Three separate oligonucleotide strands (**1a**, **1b**, and **1c**), designed to have 10 base complementary ending sequences (X:X', Y:Y', and Z;Z'), are modified to include dpp (**3**) vertexes. Upon hybridization the strands combine to form triangle **T1** in which the dpp ligands are arranged in three pairs suitable for the coordination of a transition metal (DNA-templated dpp–dpp metal coordination site shown on far right). Triangle 2 (**T2**) is formed in an identical fashion. **b,** Triangles **T1** and **T2** are annealed with three linking strands **LSa-c** to first create single-stranded prismatic structure **TP-S**. The three remaining single-stranded regions are then hybridized to rigidifying strands **RSa** or **RSb** to generate fully double-stranded **TP**, which now contains six dpp-dpp ligand environments available for metal coordination.

2.4 Results and Discussion

2.4.1 2D DNA Assembly

Assembly of **T1** and **T2**, as shown in Figure 2.1a, was achieved by sequentially adding dpp-modified strands together in stochiometric ratios. As an example, sequential addition of **T1** component strands **1a-1c** at room temperature led to quantitative formation of the DNA triangle as analyzed by polyacrylamide gel electrophoresis (PAGE) performed under non-denaturing conditions (Figure 2.2a, from now on referred to as 'native PAGE'). As opposed to a sequential addition, strands **1a-c** and **2a-c** could also be added together quickly, allowed to anneal for 10 minutes and quantitative yields were still obtained. Our lab had

previously developed methods for the synthesis of DNA cycles by ligation of acyclic intermediates,[6,22] but ultimately suffered from poor yields, formation of intermolecular byproducts and generally required lengthy purification. The methodology developed here overcomes these issues, resulting in quantitative formation of a DNA cycle at room temperature without the requirement for further purification. The connectivity of the closed triangles was confirmed using an enzymatic digestion assay with exonuclease VII (ExoVII). This enzyme is unique in that it acts on either the 5' or 3' termini (bi-directional) of single-stranded open-form DNA.[23] If each triangle is truly a closed system, then ExoVII should not be able to digest the 2D DNA structures. As shown in Figure 2.2b, native PAGE analysis of **T1** (Lane 1) shows no degradation after ExoVII treatment (Lane 2). In contrast, an open control system **1a1b** (Lane 3) is completely digested (lane 4) by ExoVII under identical conditions.

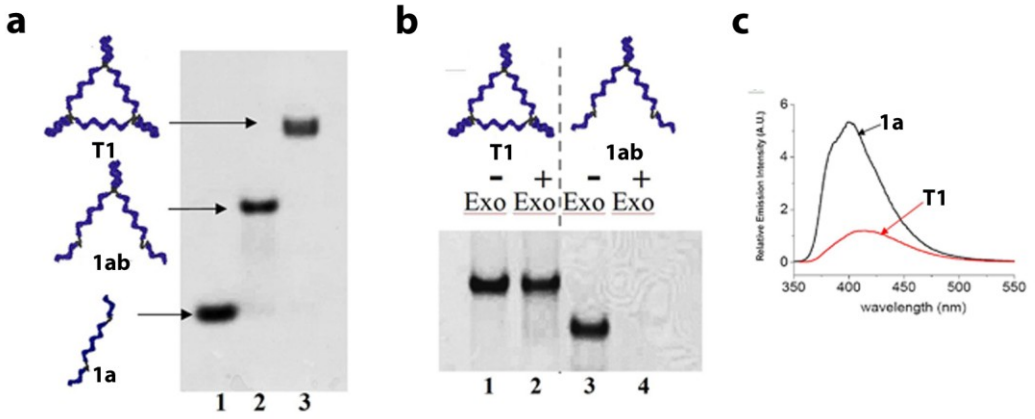

Figure 2.2 Construction and characterization of DNA triangle T1. a, Native PAGE (8% polyacrylamide) analysis for triangle **T1** formation. Lane 1 – **1a**, Lane 2 – **1a1b** and Lane 3 – **1a1b1c** (**T1**). **b,** Assessment of the connectivity of **T1** using enzymatic digestion with exonuclease VII (ExoVII). Upon treatment of **T1** (lane 1) with ExoVII, no digestion is observed (lane 2), whereas the open intermediate **1a1b** (lane 3) is fully digested (lane 4). **c,** Luminescence spectra obtained for the singly bis-dpp-modified **1a** and for triangle **T1**. A red shift in the emission maximum, accompanied by a decrease in intensity, is observed in forming **T1**.

The assembled 2D structures were further characterized by fluorescence spectroscopy (Fig. 2.2c). This technique was used to probe the emission

properties of the dpp ligands that were selectively inserted into each triangle component strand. For example, excitation at 341 nm for strand **1a**, which contains two dpp ligands, displays a broad emission peak with λ_{max} = 402 nm. Upon hybridization with the two remaining triangle building blocks **1b** and **1c**, the emission spectrum is red-shifted (λ_{max} = 416) and reduced in intensity. This pattern is consistent with the close proximity of each pair of dpp ligands and π-π interactions that result in non-radiative decay.[24,25] The emission characteristics of the dpp-dpp junction are also of diagnostic interest as they are expected to change depending on metal coordination.

2.4.2 Metallation of 2D DNA structures T1 and T2

The facile and efficient preparation of triangles **T1** and **T2** resulted in the templation of dpp-dpp ligand environments that can now be utilized for site-specific metal binding.[22] Each of the three templated environments shown in Fig. 2.3 is designed to selectively coordinate transition metals, especially copper(I) and silver(I).[24]

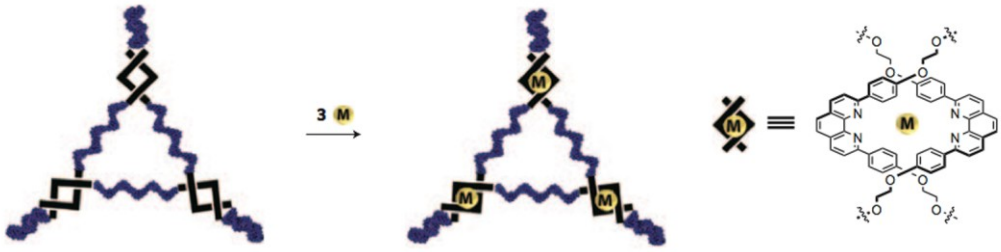

Figure 2.3 Schematic representation of the site-specific metallation of DNA triangle T1. Assembly of **T1** creates a discrete DNA template with three well-defined dpp–dpp junctions. Upon metallation, three transition metals are incorporated into the structure at these pre-determined positions. M= Cu^{+} or Ag^{+}

Each triangle junction was first metallated using either a Cu(I) ($Cu(MeCN)_4PF_6$ or Cu(II) ($CuSO_4$) source, the latter of which required *in situ* reduction with triscarboxyethylphosphine; TCEP) or Ag(I) ($Ag(NO_3)$), to create **T1.Cu(I)$_3$**, **T2.Cu(I)$_3$**, **T1.Ag(I)$_3$** or **T2.Ag(I)$_3$**. Metallation was first examined

using denaturing PAGE analysis. Typically, the 4M urea conditions used for this type of analysis lead to disassembly of DNA structures as shown in Fig. 2.4a- lane 1 for unmetallated **T1**. Without metal coordination, only the component strands **1a**-**1c** are observed using this technique. Alternatively, assembly of strands **1a**, **1b** and **1d** (where **1d** has no dpp ligand modifications) and addition of copper generates two bands (Fig. 2.4a, lane 2); the faster moving band corresponding to the unmetallated sequence **1d** and the slower moving band resulting from metal stabilization of the open dimer **1a1b**. This simple experiment demonstrates that coordination of metals is selective only to the templated ligand environment and not the singly-modified junctions. As an example, metallation of triply modified **T1** to generate **T1.Cu(I)$_3$** and **T1.Ag(I)$_3$** leads to a single band of significantly reduced mobility (Fig. 2.4a, lanes 3 and 4, respectively). This initial analysis by PAGE shows both efficient metal coordination and that, despite denaturation of the 10 base pair templating interactions, there is significant stabilization of the modified DNA junctions.

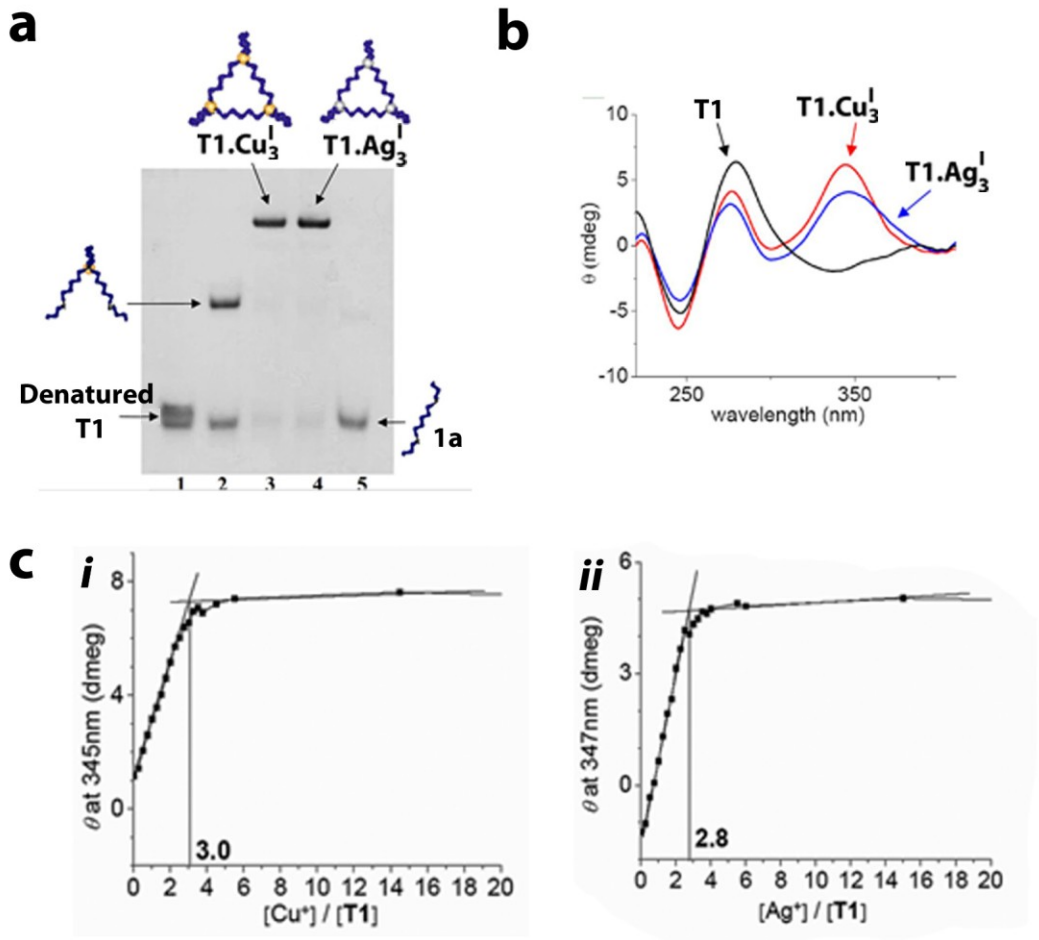

Figure 2.4 Characterization of metallated T1. a, Denaturing PAGE (12% acrylamide) analysis for metallated triangles **T1·Cu(I)$_3$** and **T1·Ag(I)$_3$**. Whereas the non-metallated **T1** (lane 1) is broken down into component strands **1a-c** under these conditions, **T1.Cu(I)$_3$** and **T1.Ag(I)$_3$** (lanes 3 and 4, respectively) resist denaturation owing to the metallation reaction, which has occurred at each of the DNA-templated dpp–dpp junctions. Lane 2 shows a control DNA construct with two building blocks **1a** and **1b** held together by metal coordination. **b,** Circular dichroism spectra for **T1**, **T1.Cu(I)$_3$** , and **T1.Ag(I)$_3$**. **c,** CD titration curves obtained for ***i*** **T1.Ag$^{I}_{3}$** and ***ii*** **T1.Cu$^{I}_{3}$**. The peak where spectral data was collected is shown on each y-axis.

Metallation could also be easily observed by CD spectroscopy as shown in Fig. 2.4b. The CD spectrum for **T1** shows a large positive peak at 260 nm corresponding to the right-handed helical B-DNA found in the hybridized templating regions. Upon metallation with copper or silver, a peak corresponding to the ligand-centered transition is clearly observed at approximately 350 nm for both **T1.Cu(I)$_3$** and **T1.Ag(I)$_3$**. It should be noted here that initial development of modified dpp **3** (Fig. 2.13) was done in a manner to allow for maximal interaction

of the templated dpp-dpp ligand environment with the right-handed helical B-DNA duplex, thus increasing the chance of chiral transfer after metal coordination and ultimately permitting a unique means of characterization by CD spectroscopy.[22] In addition to single spectrum analysis, CD titration experiments were also performed on **T1** with copper and silver (Figure 2.4c). For both copper (Fig. 2.4ci) and silver (Fig. 2.4cii) CD signal saturation occurred at almost exactly 3 equivalents of added metal, further indicating selective binding at the dpp junctions. Similar results were obtained for **T2**. Investigations are ongoing to determine a binding constant for this DNA-templated ligand environment.

To help quantify the degree of stabilization that resulted from coordination of silver or copper, UV/vis thermal denaturation experiments were performed on **T1.Cu(I)$_3$** and **T1.Ag(I)$_3$**. Each structure was prepared at an overall concentration of 3.5 μM in TAMg buffer (40mM tris, 12 mM $MgCl_2$, pH 8, adjusted with acetic acid). Monitoring absorbance at 260 nm upon heating for each structure produced the denaturation curves shown in Fig. 2.5a. The average melting temperature (Tm) for unmetallated **T1** was calculated to be 49 °C, which is on par for the 10 bp duplexes that form the closed structure. On the other hand, the denaturation curves are shifted to higher temperatures for **T1.Ag(I)$_3$** and **T1.Cu(I)$_3$**, with calculated Tm values of 56 °C and 76 °C, respectively. Significant stabilization of the DNA structure is thus observed due to copper coordination. As a control experiment, denaturation curves were obtained for a short unfunctionalized 10mer duplex (5'-CCAGCGACAC + complement) with and without the addition of Cu(I). It is clear from the overlap of the denaturation curves found in Fig. 2.5b that addition of metal does not affect duplex structure and site-specific metal coordination at the dpp-dpp junctions is responsible for the stabilization observed.

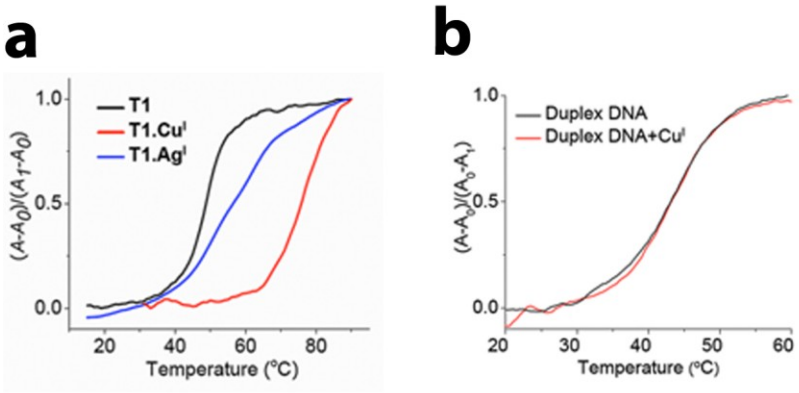

Figure 2.5 Spectral characterization of metallated T1 and T2. a, Thermal denaturation curves obtained for non-metalated **T1** (-),**T1.CuI3** (-), and **T1.AgI3** (-) and **b,** Comparision between thermal denaturation curves for a short duplex (10mer) with (-) and without (-) copper added.

2.4.3 Design, Assembly and Characterization of 3D DNA structure TP

With full characterization of metallated **T1** and **T2** achieved, attention is now shifted to the construction of the 3D DNA structures. For this project, the desired polygon **TP** was efficiently assembled using the face-centered approach outlined previously in Fig. 2.1b. Sequential assembly of fully double-stranded **TP** is outlined in the native gel mobility analysis in Fig. 2.6a. The first **TP**-intermediate can be obtained by initially linking the two faces (**T1** and **T2**) together (Fig. 2.6a, lane 2) with a single linking strand **LSa**. Although this first weakly held intermediate partially disproportionates under the non-denaturing PAGE conditions, subsequent addition of **LSb** and **LSc** (Fig, 2.6a, lanes 3 and 4) produces a stable 3D product in excellent yield, which now contains three flexible single-stranded regions (lane 4, **TP-S**). Final addition of the three rigidifying strands leads to formation of the more rigid **TP** structure (lane 5) at room temperature, with inner volume dimensions of approximately 25–30 nm^3 based on modeling studies (Fig. 2.6b).

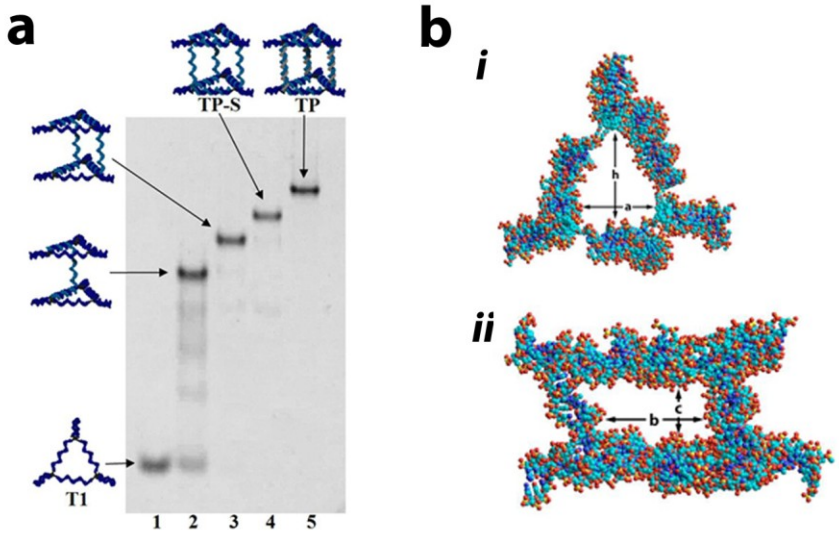

Figure 2.6 Assembly of the triangular prism TP. a, Native PAGE analysis of **TP** assembled using a face-centered approach. Starting from T1 (lane 1), adding **T2** with each linking strand in a sequential manner (**LSa**, lane 2; **LSb**, lane 3; **LSc**, lane 4) results in the discrete single-stranded intermediate **TP-S** (lane 5). This product is rigidified with sequences **RSa–b** to generate **TP** in excellent yield. **b,** Approximate dimensions of **TP** based on modeling. *i*, A top-view of **TP** with the triangular face labeled with height (h ≈ 5 nm) and base (a ≈ 5 nm) markers. *i*, Side-view of **TP** showing one of the rectangular sides labeled with height (c ≈ 3 nm) and width (b ≈ 4 nm) markers.

Selective enzymatic digestions using both mung bean nuclease (MBN) and ExoVII show the correct connectivity of **TP** (Fig. 2.7). After treatment with MBN, an endonuclease selective for degrading single-stranded over double-stranded DNA,[23] the rigid capsule remains fully intact (lane 2), whereas the intermediate **TP-S**, which has three single-stranded regions, is digested (lane 5). Both **TP** and **TP-S** are unaffected by the addition of the exonuclease ExoVII (lanes 3 and 6) indicating the cyclic and closed nature of these 3D products. As an additional control experiment, we prepared a deliberately open and rigidified capsule (**TP-O**), where one of the linking strands is not complementary to the triangle **T1** side and thus cannot hybridize to form a closed structure. The partially open **TP-O** has a different gel mobility from the closed structure **TP** (lane 7), consistent with a different degree of compactness for this molecule. Furthermore, **TP-O** is partially degraded by both Exo-VII and MBN (lanes 8 and 9), consistent with digestion of the unhybridized single-stranded decanucleotide portion.

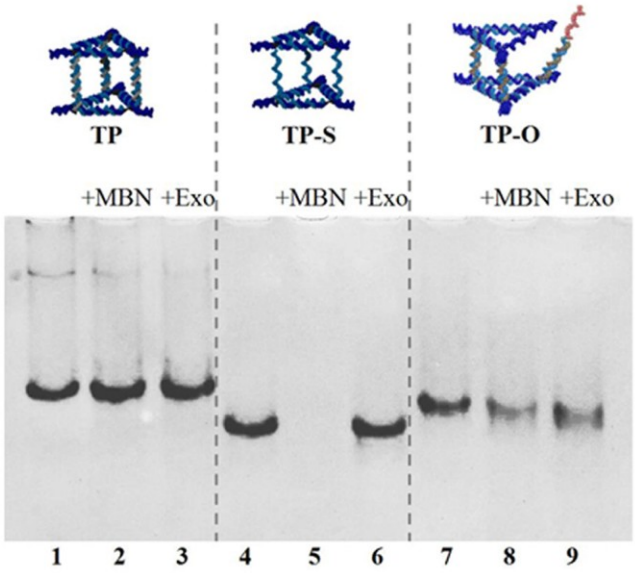

Figure 2.7 Characterization of triangular prism TP using enzyme digestions. Assessment of the connectivity of **TP** using enzymatic digestions with mung bean nuclease (MBN) and exonuclease VII (ExoVII) and analysis by native PAGE; Lane 1 – **TP**, Lane 2 **TP** + MBN, lane 3 – **TP** + ExoVII, lane 4 – **TP-S**, lane 5 – **TP-S** + MBN, lane 6 – TP-S + ExoVII, lane 7 - **TP-O**, lane 8 – **TP-O** + MBN and lane 9 - **TP-O** + ExoVII.

In addition to PAGE analysis and enzymatic digestion experiments, transmission electron microscopy (TEM) was used to help obtain a clearer structural picture of the 3D DNA polygon. Best imaging results were obtained when a 40 nM concentration of **TP** was deposited onto grids that had been glow discharged in the presence of amyl amine followed by staining with uranyl acetate. A typical TEM field of view is shown in Fig. 2.8a where a number of single particles with dimensions in agreement with that of the **TP** cage can be observed within the field of view. Images selected from the negative stained data, shown in Fig. 2.8b, reveal a number of projections that are in agreement with the size determined from modeling **TP**. Some of the particles observed did appear to be broken or distorted which is likely do to denaturation caused by the low pH of uranyl acetate or structural artifacts from the staining process.[26] EM imaging under negative staining conditions did however provide direct visual evidence of the structural dimensions of **TP** which agree with the *in silico* generated model. Although the technique of cryo-EM has proved ideal for characterizing soft

materials, especially DNA self-assembled structures,[27] the correct grid preparation and imaging conditions for the small **TP** structure have yet to be determined. Further EM investigations are currently being pursued to better elucidate the exact structure of these 3D DNA polygons.

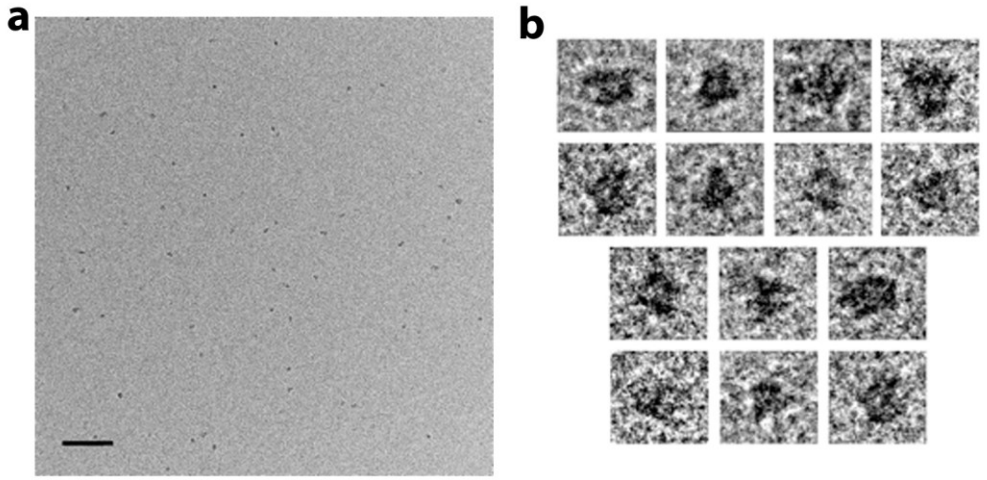

Figure 2.8 TEM images of negatively stained TP cages. a, A typical field of view obtained for **TP** (40 nM) deposited onto a 400 mesh carbon coated copper grid subsequently stained with a 2% solution of uranyl acetate. Scale bar shown is 100 nm. **b,** Representative particles obtained from the negative-staining TEM data for **TP**. Dimensions of the box used to select each particle are ca. 22 x 22 nm.

Before outlining the 3D DNA metallation results, it is pertinent to backtrack slightly and address some of the design optimization that was required for linking strands **LSa–c**, which serve as the interconnects between the two triangles in the final **TP** structure. The first linking strand design (**LS_T**, Fig. 2.9a) contained two non-base pairing thymidine residues between the sequences that connect triangles **T1** and **T2**. However, these linking strands led to only modest product yields of the DNA cage (Fig. 2.9b, lane 1) and a structure that was not stable under enzymatic conditions (Fig. 2.9b, lanes 2 and 3). The hypothesis here was that the thymidine spacer was both sterically demanding and may have introduced additional repulsive electrostatic interactions at connection points, resulting in destabilization of hybridization to each single-stranded triangle (**T1** or **T2**). Although the correct product was formed, the resulting structure was likely more prone to partial denaturation of the linking strands, thus resulting in

accessibility to enzymatic digestion. The thymidine residues were first replaced with a short triethylene glycol insertion (**LSEG**, Fig. 2.9a). This second generation design would hopefully add flexibility at the junction where hybridization takes place and ultimately solve some of the destabilizing steric/electrostatic effects observed with the $\mathbf{LS_T}$. The use of $\mathbf{LS_{EG}}$**a-c** led to excellent product formation (Figure 2.9c) and correct connectivity assayed by nuclease digestion. Although this linking strand modification led to the desired product in excellent yield, site-specific metal coordination (as will be discussed in subsequent sections) was difficult. As evidenced by the CD data shown in Fig. 2.9d, a large excess of copper was required to promote saturation of the signal. Although difficult to prove, the close proximity of the triethylenglycol insertions to the dpp ligand environment may have generated a 'crown ether'-like structure that was able to sequester metal ions or effectively block access to the dpp-dpp ligand environment. To address this problem, a third linking strand variant was prepared where the triethylene glycol linker was replaced with a 1,6-hexanediol derivative (**LS**, Fig. 2.9a). This eliminated metal complexation problems while retaining quantitative assembly and correct connectivity, and was therefore used for the construction of DNA cage **TP**.

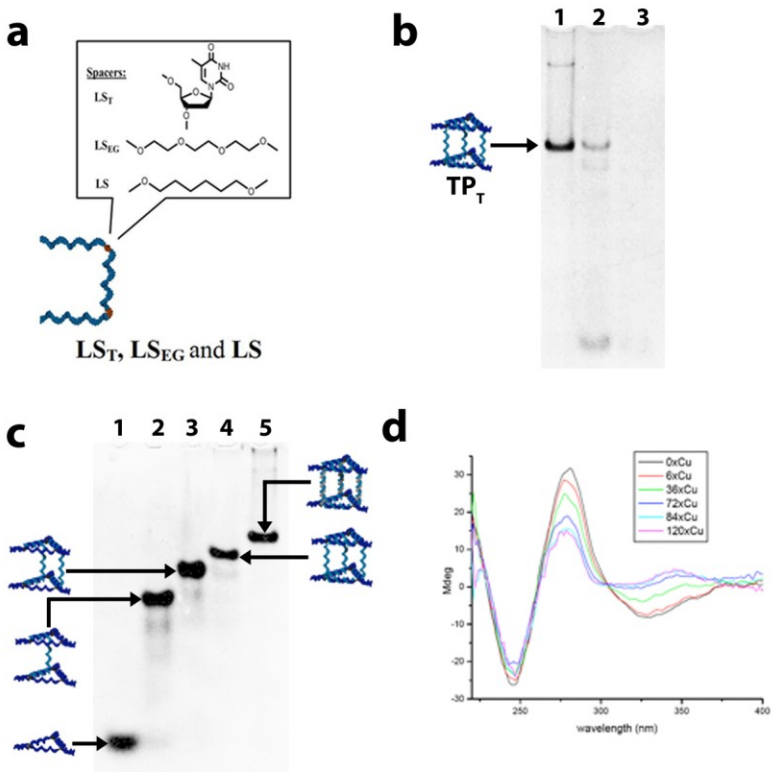

Figure 2.9 Design of Linking strands. a, Modifications made to the linking strands; bis-thymidine (**LS$_T$**), hexaethyleneglycol (**LS$_{EG}$**) and hexyl chain incorporation (**LS**), which were used to assemble **TP**. **b,** Native PAGE characterization (7%) of 3D structure **TP$_T$** prepared from LS$_T$a-c**TP$_T$** (lane 1) and the results of digestion with MBN (lane 2) and ExoVII (lane 3). **c,** 7% non-denaturing PAGE characterization of 3D structure **TP$_{EG}$** prepared by starting from **T1** (lane 1) and sequentially adding **LS$_{EG}$a** (lane 2), **LS$_{EG}$b** (lane 3), **LS$_{EG}$c** (lane 4) and finally **RSa** and **RSb** (lane 5). **d,** CD titration experiment for **TP$_{EG}$** which reveals a disruption of site-specific metal binding for this 3D architecture.

2.4.4 Metallation of 3D DNA structure TP

With the fully characterized **TP** in hand, site-specific metallation was next examined using the methods developed in Section 2.4.2. Denaturing PAGE analysis on the metallated form of the 3D DNA polygon, **TP.M$_6$**, is shown in Fig. 2.10a. As expected, non-metallated **TP** fully dissociates under denaturing conditions to yield bands corresponding to its structural constituents, **RS**, **LS**, and the six triangle components **1a-1c** and **2a-2c** (Fig. 2.10a, lane 1). After addition of Cu(I) and Ag(I), denaturing PAGE shows two bands of reduced mobility (Fig. 2.10a, lanes 2 and 3, respectively) corresponding to the undissociated metallated triangles **T1** and **T2**. Although the linking strand interactions remain the same, selective coordination of metals to the individual prismatic faces provides

excellent structural stability. In addition to PAGE, fluorescence spectra of **TP.Cu(I)$_6$** and **TP.Ag(I)$_6$** show a reduction in intensity and red-shift of the ligand-centered emission, consistent with site-specific metallation of these ligand junctions (Fig. 2.10b).[24]

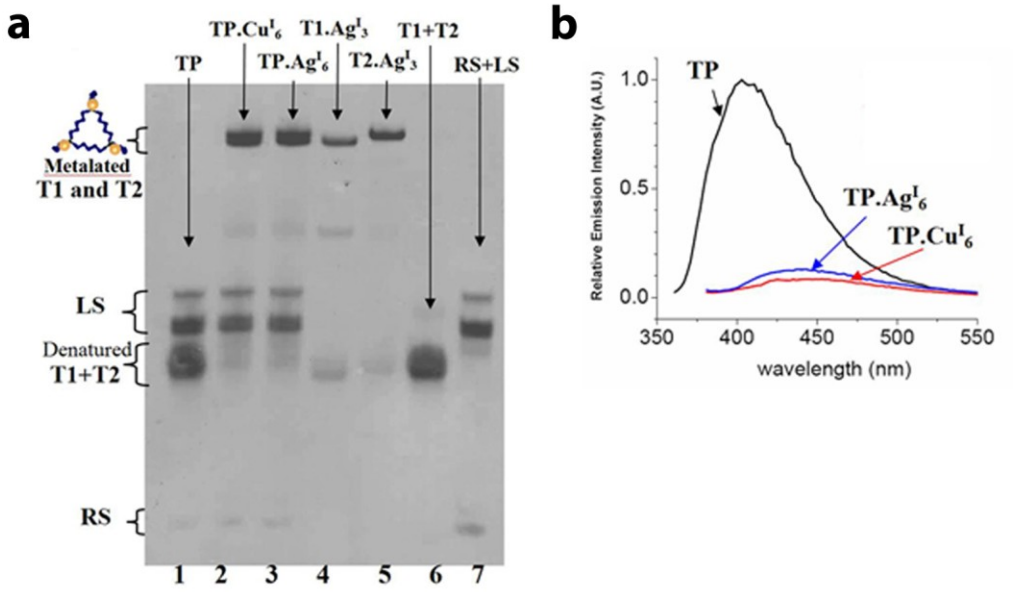

Figure 2.10 Characterization by denaturing PAGE and fluorescence spectroscopy of the site-specific metallation of TP to form TP.M$_6$ a, Denaturing PAGE analysis of **TP**, **TP.Cu(I)$_6$** and **TP.Ag(I)$_6$**; Lane 1 - **TP**, lane 2 - **TP.Cu(I)$_6$** , lane 3 - **TP.Ag(I)$_6$**, lane 4 - **T1.Cu(I)$_3$**, lane 5 - **T1.Ag(I)$_3$**, lane 6 – mixture of unmetallated **T1** and **T2** and lane 7 – mixture of **RSa**, **RSb**, and **LSa-c**. **b,** Luminescence spectra recorded for **TP**, **TP.Cu(I)$_6$** , and **TP.Ag(I)$_6$**, which show a decrease in intensity and red shift in the emission spectra upon metallation of the 3D cages.

Alternatively, Cu(I) and Ag(I) coordination in **TP.M$_6$** could be observed by CD spectroscopy (Figure 2.11a). Upon metallation with Cu(I) and Ag(I), a band with a positive Cotton effect at ca. 350 nm was observed for the chiral induction imposed on the dpp-dpp junctions contained within each prismatic face (Fig. 2.11a). A CD titration was again performed, this time on **TP.Cu(I)$_6$**, to show selective and stable metal coordination of the 3D DNA structure. The binding curve reveals signal saturation after the addition of six equivalents of metal (Fig. 2.11b). The importance of the strong chiral induction that occurs upon metallation

with copper and silver cannot be overstated, as the strong CD signal provides a diagnostic signature for such site-specifically modified DNA structures.

A more direct measure of the stability gained from this unique dpp-metal-dpp interaction was provided by thermal denaturation analysis. In Fig. 2.11c **TP** exhibits a melting curve with a melting temperature (Tm) of 41 °C, which is increased to 50 °C after addition of six equivalents of Ag(I). The melting curve after addition of Cu(I) is striking in that it now exhibits two distinct transitions at 49 °C and 76 °C. The latter Tm corresponds well to that of metallated triangles **T1.Cu(I)**$_3$ and **T2.Cu(I)$_3$**. It would appear that metallation of the DNA cage not only significantly stabilizes the clipping strands that are held together by base pairing and metal coordination, but may also add thermal stability to the non-metallated linking strands that hybridize to each single-stranded triangle, as the transition at 49 ^{o}C is due to denaturation of the linking strands from the 3D triangles. Without a more detailed structural picture, one can only speculate as to the reason for this observed stabilization. One hypothesis could be that the tight chiral environment imposed upon metallation of the dpp-dpp junction somehow influences, potentially via π-stacking, the terminal sections of each 10 base pair duplex to prevent fraying of these hybridized sections that hold the two faces in place. This may however also be attributed to variation in the sequences used for assembly i.e. differing G:C content and thus varying Tm values are expected. Nonetheless, these results illustrate the important structural role that metal–DNA junctions can play in DNA nanotechnology, lending much needed stability to the resulting DNA architectures.

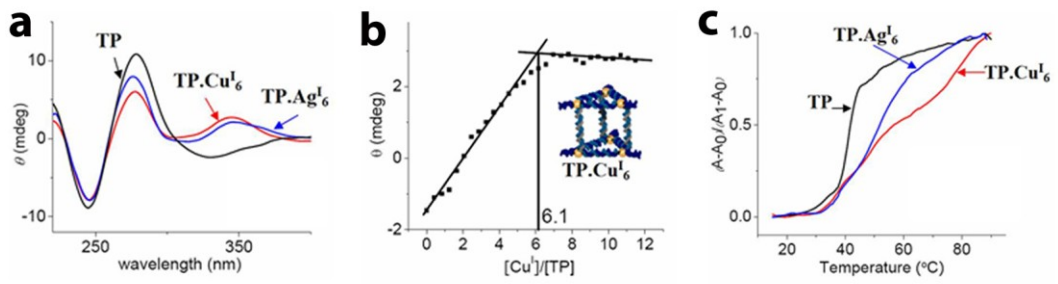

Figure 2.11 Characterization by CD spectroscopy and thermal denaturation of the site-specific metallation of TP to form TP.M$_6$ a, Circular dichroism spectra recorded for **TP**, **TP.Cu(I)$_6$** and **TP.Ag(I)$_6$**. **b,** Binding stoichiometry obtained from a circular dichroism titration experiment for **TP.Cu(I)$_6$**, which shows six equivalents of copper binding to reach signal saturation. **c,** Thermal denaturation curves for **TP** (Tm = 41 °C), **TP.Cu(I)$_6$** (Tm ≈ 49 and 76 °C) and **TP.Ag(I)$_6$** (Tm ≈ 50 °C).

An alternative assembly strategy, in which the 2D DNA triangles are first metallated and then used to directly assemble the metal–DNA 3D objects, was also examined (Fig. 2.12a). Native PAGE analysis (Fig. 2.12b) shows quantitative formation of **TP.Cu(I)$_6$** and CD spectroscopy shows this product to possess identical spectral signatures to the metallo-cage generated by titrating the 'apo' structure **TP** with six equivalents of metal ions (Fig. 2.12c). This method will be especially useful for bringing together DNA polygons that have been functionalized with different transition metals into multi-metallic 3D DNA structures.

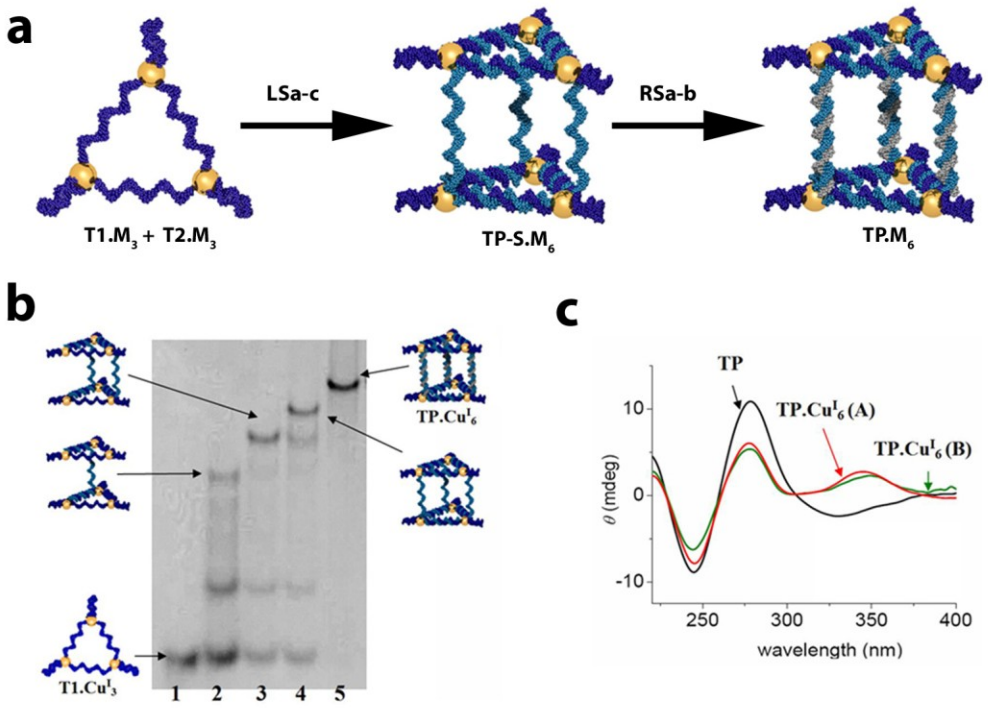

Figure 2.12 Pre-metallation of T1 and T2 and their assembly into TP.Cu(I)$_6$. a, A schematic representation outlining the assembly of a metallated 3D structure **TP.M$_6$** starting from the fully metallated triangles **T1.M$_3$** and **T2.M$_3$**. **b,** Native PAGE analysis for the sequential assembly of **TP.Cu(I)$_6$** starting from metallated triangles **T1.Cu(I)$_3$** and **T2.Cu(I)$_3$**. **c,** CD spectra recorded for **TP** and **TP.Cu(I)$_6$**, starting from the 'apo' 3D structure (A) or using pre-metallated triangles (B).

2.5 Conclusions

In this chapter, efficient and facile preparation of the first metal–nucleic acid 3D structure has been demonstrated. This was accomplished through a face-centered approach, by first quantitatively generating DNA triangles with ligand environments at each of their vertices, and then assembling these triangles using linking strands into a 3D prismatic cage. This structure contains six ligand pockets that are pre-organized by DNA templation, and proved to be excellent coordination environments. Stoichiometric metallation of the cages gave significant stabilization to these constructs, including significant resistance towards chemical (4 M urea) and thermal denaturation conditions. Although only two types of metals are presented here, the ligand environment is amenable to modification in a manner that will allow for selective and site-specific

coordination of various other metals. With this, transition metals have the potential to bring much needed functionality, such as redox, photoactivity, magnetic and catalytic properties, as well as increased stability to previously passive 3D DNA constructs. Applications of these metallated DNA cages include stimuli-responsive host molecules for proteins and nanoparticles, as well as building blocks for a new generation of extended metal–nucleic acid frameworks.

2.6 Experimental Section

2.6.1 General

Toluene and ether were dried by refluxing over Na and dichloromethane was dried by refluxing over CaH_2. 1,10-N,N-phenanthroline, p-bromoanisole, tert-BuLi, MnO_2, 4-methoxyltritylchloride, chlorodiethyleneglycol, anhydrous pyridine, HCl, triethylamine, diisopropylethylamine, dimethylaminopyridine, ethylenediaminetetracetic acid (EDTA), trichloroacetic acide (TCA), StainsAll®, acetic acid, tris(hydroxymethyl)-aminomethane (Tris), formamide, amyl amine and urea were used as purchased from Aldrich. Acetic acid, boric acid, and $MgCl_2 \cdot 6H_2O$ were purchased from Fisher Scientific and used without further purification. 2- cyanoethyl diisopropylchloro-phosphoramidite, nucleoside (dA,T,dC,dG) derivatized 500 Å and 1000Å LCAA-CPG supports with loading densities between 25-40 μmol/g, and 5-ethylthiotetrazole for automated DNA synthesis were purchased from ChemGenes Incorporated. Sephadex G-25 (super fine, DNA grade) was purchased from Amersham Biosciences. Mung Bean Nuclease (MBN, source: Mung Bean Sprouts) and Exonuclease VII (ExoVII, source: recombinant) were purchased from BioLynx Incorporated. Carbon coated 400 mesh copper EM grids were purchased from SPI.

2.6.2 Instrumentation

^{1}H-NMR spectra were obtained using a Mercury 400 MHz NMR spectrometer. ^{13}C-NMR spectra were obtained using a Mercury 300 MHz NMR spectrometer. ^{31}P-NMR spectra were obtained using a Gemini 200 MHz NMR spectrometer. Standard automated oligonucleotide solid- phase synthesis was performed on a Perspective Biosystems Expedite 8900 DNA synthesizer. UV/Vis experiments and thermal denaturing experiments were conducted on a Varian Cary 300 biospectrophotometer. Gel

electrophoresis experiments were carried out on an acrylamide 20 X 20 cm vertical Hoefer 600 electrophoresis unit. Fluorescence experiments were carried out on a PTI (Photon Technology International) TimeMaster Model C-720F spectrofluorimeter. Circular dichroism experiments were collected on a JASCO J-810 or JASCO J-815 spectropolarimeter at 20 ^{o}C. Enzymatic digestions were conducted using a Flexigene Techne 60 well thermocycler. EM measurements were performed on a Technai G2 F20 microscope operating at 200 keV and equipped with a Gatan Ultrascan 4k x 4k CCD camera. All measurements were performed under low dose conditions.

2.6.3 Synthesis and incorporation of non-standard phosphoramidites

The dpp-phosphoramidite (**3**) was synthesized according to a previously reported procedure.[22,24] ^{31}P-NMR: 149.7(s), HR-ESI: 1013.4613 (theoretical mass: 1013.4597). The 1,6-hexanediol (C6)-phosphoramidite (**4**) and triethyleneglycol (TEG)-phosphoramidite (**5**) were purchased from ChemGenes Incorporated and used as received. It should be noted that molecule **4** is no longer available and has been replaced with a hexaethylene glycol derivative.

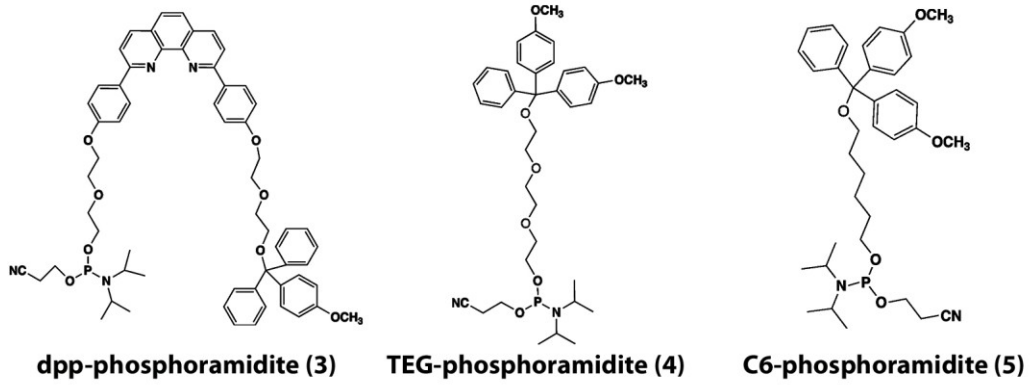

Figure 2.13 Phosphoramidites 3, 4 and 5 used for selective incorporation into oligonulceotides.

2.6.4 DNA synthesis

DNA synthesis was performed on a 0.5 μmol scale, starting from the required nucleotide modified 500Å or 1000 Å LCAA-CPG solid-support. Phosphoramidte derivatives of **3-5** were coupled on the growing oligonulceotide chain as an artificial base with a prolonged coupling time of 5min. The coupling efficiency was monitored after

trityl group removal. All sequences were fully deprotected in concentrated ammonium hydroxide (55 ^{o}C, 16 hours). Crude oligonucleotide products were purified on 15-24% polyacrylamide/8M urea polyacrylamide gels (PAGE; up to 20 OD260 of crude DNA per gel) at constant current of 30 mA, using 0.09M Tris-Boric acid (TB) buffer (pH 8.3). Following electrophoresis, gels were wrapped in plastic, placed on a fluorescent TLC plate and illuminated with a UV lamp (254nm). The bands were quickly excised, and the gel pieces were crushed and incubated in 10 mL of sterilized water at 55 ^{o}C for 16 hours. Samples were then dried to 1.5 mL, desalted using size exclusion chromatography (Sephadex G-25), and quantified (OD260) using UV-vis spectroscopy. The purity of all DNA strands was confirmed by analytical denaturing PAGE analysis.

2.6.5 DNA sequence design

Table 1 below summarizes all sequences used to prepare both 2D structures **T1** and **T2** and 3D structure **TP**. The sequences for each component strand were initially compiled from two previously optimized sequence pools[6,22] and refined iteratively to minimize potential secondary interactions, both within strands and between strands, using Integrated DNA Technology's (IDT) software program OligoAnalyzer. In addition, the possibility for intramolecular folding was tested using the same company's m-fold program. Both programs can be accessed free of charge via the link http://www.idtdna.com/site. Sequence design, especially for strands involving 10 base pair interactions, typically involved a G:C content of at least 40-50% so as to maintain stability at room temperature.

Table 2.1: Oligonucleotides prepared for the assembly of 2D and 3D DNA structures T1, T2 and TP.

Name	Sequence (5' → 3')
1a	TCTAGGAGAC **3** ACATTAGGTA **3** CTTTCAACTT
1b	AAGTTGAAAG **3** GTTTGCTGGG **3** GTGATGTCAT
1c	ATGACATCAC **3** CCGCCGATTA **3** GTCTCCTAGA
2a	TCTGGTAGAT **3** AACTCTTGAA **3** CTTTCAACTT
2b	AAGTTGAAAG **3** CCTGCTCATA **3** GTGGTGTCAT
2c	ATGACACCAC **3** GAAACGACAA **3** ATCTACCAGA
***LSa**	TAATCGGCGG **5** TTTATTAAAGTCTCAGT **5** TTGTCGTTTC
***LSb**	CCCAGCAAAC **5** TTTATTAAAGTCTCAGT **4** TTCAAGAGTT

***LSc**	TACCTAATGT **5** TCACAGAATACCTCTCT **5** TATGAGCAGG
RSa	CTGAGACTTTAATAA
RSb	GAGAGGTATTCTGTG

*Linking strands shown contain C6 phosphoramidite **5**. These identical sequences (**LSa-c**) were originally tested with both a double-thymidine incertion and TEG phosphoramidite **4** spacer as outlined in section 2.3.3.

2.6.6 Assembly of DNA structures T1, T2 and TP

T1 and **T2** were assembled at room temperature by addition of equimolar amounts of component strands **1a-1c** and **2a-2c**, respectively, at a final concentrations of 5-20 μM in tris (40 mM)-acetic acid (18 mM)-$MgCl_2$ (12 mM) buffer (TAMg, pH 8). Equimolar amounts of each linking strand **LSa–c** were then sequentially added to the 2D triangles and annealed at room temperature for 5 minutes in TAMg to yield the single stranded triangular prism **TP-S**. Subsequent addition of equimolar amounts of rigidifying strands **RSa** (x2) and **RSb** yielded near quantitative formation of **TP** at room temperature.

2.6.6 Optimization of enzymatic digestion assays

As outlined in section 2.3.3, connectivity of the 2D and 3D products was determined using selective enzymatic digestions with Exonuclease VII (ExoVII) and/or mung bean nuclease (MBN). Enzymatic assays were performed in TAMg buffer at 15 °C for 2 hr on approximately 0.05 nmol total of DNA. Linear, single-stranded open-form DNA (0.05 nmoles) was first dissolved in 10 uL of 1xTAMg buffer. ExoVII optimization experiments were then performed by digesting DNA with various amounts of enzyme. As shown in Figure 2.14a, 5 units (U) of ExoVII were required to completely digest the control DNA mixture at 15 °C for 2 hrs.

A similar procedure was performed with MBN, except both ssDNA and dsDNA were used to optimize digestion. MBN is selective for the digestion of ssDNA over dsDNA by a factor of 30,000.[23] MBN digestion conditions were also optimized at 15 °C for 2 hr in a 1xTAMg buffer system. As can be seen in Figure 14b, ssDNA is almost completely degraded with 20U of (Figure 2.14bi, lane 5) while the dsDNA control is not degraded at this enzyme concentration (Figure 2.14bii, lane 5).

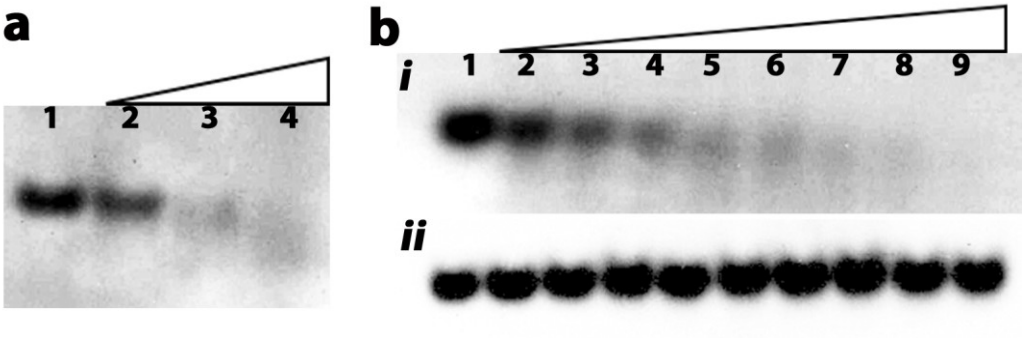

Figure 2.14 Enzyme optimization experiments. a, 8% native PAGE characterization of 0.05 nmole of linear DNA in TAMg buffer after digestion with various units (U) of ExoVII; Lane 1-0 U, lane 2-1U, lane 3-3 U and lane 4-5 U. **b,** 8% native PAGE characterization of 0.05 nmole of linear open form ssDNA (***i***) and dsDNA (***ii***) in TAMg buffer after digestion with increasing units (U) of MBN. The lane assignments in both ***i*** and ***ii*** are the same: lane 1-0 U, lane 2- 5 U, lane 4-10 U, lane 5- 15 U, lane 6-20 U, lane 7- 25 U, lane 8- 30 U, lane 9- 35 U, lane 10- 40 U.

2.6.7 Transition metal incorporation and characterization

In general, after assembly of **T1**, **T2** and **TP**, transition metal incorporation was achieved by addition of an appropriate metal salt in either a phosphate (10 mM NaH_2PO_4–Na_2HPO_4 , pH 7.2) or TAMg buffer system followed by incubation at room temperature for 15 minutes. For example;

Preparation of T1.Ag^{I}_3 and T2.Ag^{I}_3

0.342nmol of **T1** or **T2** were made in phosphate buffer (10mM NaH_2PO_4-Na_2HPO_4, pH 7.2) or TAmg buffer (Tris-Acetic acid, 12mM $MgCl_2$, pH 8). After incubation at room temperature for 15 min, 1.03 ml of 1 mM silver nitrate solution was added. Incubation was conducted at room temperature, for 15 minutes.

Preparation of T1.Cu^{I}_3 and T2.Cu^{I}_3

0.342nmol of **T1** or **T2** were made in phosphate buffer (10mM NaH_2PO_4-Na_2HPO_4, pH 7.2) or TAMg buffer (Tris-Acetic acid, 12mM $MgCl_2$, pH 8). After incubation at room temperature for 15 min, 1.03ml of 1mM $Cu(CH_3CN)_4PF_6$ acetonitrile solution (or $CuSO_4$ and TCEP·HCl (Tris[2-carboxyethyl]phosphine hydrochloride 1:2 mixture, water solution, final Cu^{I} concentration 1mM) was added.

As outlined in the results and discussion section (2.3), a variety of techniques were used to characterize the metallated DNA constructs; including native and denaturing PAGE, thermal denaturation studies, circular dichroism spectroscopy, luminescence and UV/vis spectroscopy. Denaturing PAGE (12%, 4 M urea, 200 V, 15 mA) was performed in a TB buffer at 4 °C. Thermal denaturation was achieved by heating metallated products from 15–90 °C (0.5 °C /min) and monitoring at 260 nm. Melting temperature values were calculated from the first derivative of the absorbance versus temperature curves.

2.7 References

(1) Gothelf, K. V.; Labean, T. H. *Org. Biomol. Chem.* **2005**, *3*, 4023.

(2) Lin, C.; Liu, Y.; Rinker, S.; Yan, H. *ChemPhysChem* **2006**, *7*, 1641.

(3) Aldaye, F. A.; Palmer, A. L.; Sleiman, H. F. *Science* **2008**, *321*, 1795.

(4) Seeman, N. C. *Mol. Biotechnol.* **2007**, *37*, 246.

(5) Shih, W. M.; Quispe, J. D.; Joyce, G. F. *Nature* **2004**, *427*, 618.

(6) Aldaye, F. A.; Sleiman, H. F. *J. Am. Chem. Soc.* **2007**, *129*, 13376.

(7) Goodman, R. P.; Heilemann, M.; Doose, S.; Erben, C. M.; Kapanidis, A. N.; Turberfield, A. J. *Nat. Nanotechnol.* **2008**, *3*, 93.

(8) He, Y.; Ye, T.; Su, M.; Zhang, C.; Ribbe, A. E.; Jiang, W.; Mao, C. *Nature* **2008**, *452*, 198.

(9) Mastroianni, A. J.; Claridge, S. A.; Alivisatos, A. P. *J. Am. Chem. Soc.* **2009**, *131*, 8455.

(10) Mitchell, N.; Schlapak, R.; Kastner, M.; Armitage, D.; Chrzanowski, W.; Riener, J.; Hinterdorfer, P.; Ebner, A.; Howorka, S. *Angew. Chem. Int. Ed.* **2009**, *48*, 525.

(11) Erben, C. M.; Goodman, R. P.; Turberfield, A. J. *Angew. Chem. Int. Ed.* **2006**, *45*, 7414.

(12) Bhatia, D.; Mehtab, S.; Krishnan, R.; Indi, S. S.; Basu, A.; Krishnan, Y. *Angew. Chem. Int. Ed.* **2009**, *48*, 4134.

(13) Chang, M.; Yang, C. S.; Huang, D. M. *ACS Nano* **2011**, *5*, 6156.

(14) Crichton, R. R. *Biological Inorganic Chemistry* ; Elsevier Science, 2008.

(15) Yang, H.; Metera, K. L.; Sleiman, H. F. *Coord. Chem. Rev.* **2010**, *254*, 2403.

(16) Seidel, S. R.; Stang, P. J. *Acc. Chem. Res.* **2002**, *35*, 972.

(17) Yoshizawa, M.; Fujita, M. *Pure Appl. Chem.* **2005**, *77*, 1107.

(18) Pluth, M. D.; Bergman, R. G.; Raymond, K. N. *Science* **2007**, *316*, 85.

(19) Rowsell, J. L. C.; Spencer, E. C.; Eckert, J.; Howard, J. A. K.; Yaghi, O. M. *Science* **2005**, *309*, 1350.

(20) Chandler, B. D.; Cramb, D. T.; Shimizu, G. K. *J. Am. Chem. Soc.* **2006**, *128*, 10403.
(21) Ghosh, S. K.; Kaneko, W.; Kiriya, D.; Ohba, M.; Kitagawa, S. *Angew. Chem. Int. Ed.* **2008**, *47*, 8843.
(22) Yang, H.; Sleiman, H. F. *Angew. Chem. Int. Ed.* **2008**, *47*, 2443.
(23) Rittié, L.; Perbal, B. *Journal of Cell Communication and Signaling* **2008**, *2*, 25.
(24) Armaroli, N.; Decola, L.; Balzani, V.; Sauvage, J. P.; Dietrichbuchecker, C. O.; Kern, J. M.; Bailal, A. *J. Chem. Soc., Dalton Trans.* **1993**, 3241.
(25) Champin, B.; Mobian, P.; Sauvage, J. P. *Chem. Soc. Rev.* **2007**, *36*, 358.
(26) Ohi, M.; Li, Y.; Cheng, Y.; Walz, T. *Biol Proced Online* **2004**, *6*, 23.
(27) Sander, B.; Golas, M. M. *Microsc. Res. Tech.* **2011**, *74*, 642.

2.8 Introduction to Chapter 3

The methodology developed in chapter 2 to make a 3D polygon provided insight into how selective chemical modifications could be used to augment the structural properties of DNA as a nanomaterial. It became clear, though, that diversifying the methodology would require an expanded pool of DNA sequences to achieve more complex structures. This philosophy had become commonplace in the field of structural DNA nanotechnology whereby large amounts of DNA were used to produce dense DNA structures. Towards a more 'DNA economic' approach to generate well-defined 3D architectures, sequence symmetry, in tandem with selective synthetic modification, were tested. Chapter 3 thus describes a simple and quantitative method to generate DNA cages of deliberately designed geometry from readily available starting strands. It is demonstrated that balancing the incorporation of sequence uniqueness and symmetry in a face-centered approach to 3D construction can result in triangular (TP), rectangular (RP), and pentagonal prisms (PP) without compromising the potential for nanostructure addressability.

Chapter 3: A Facile, Modular and High Yield Method to Assemble Three-Dimensional DNA Structures

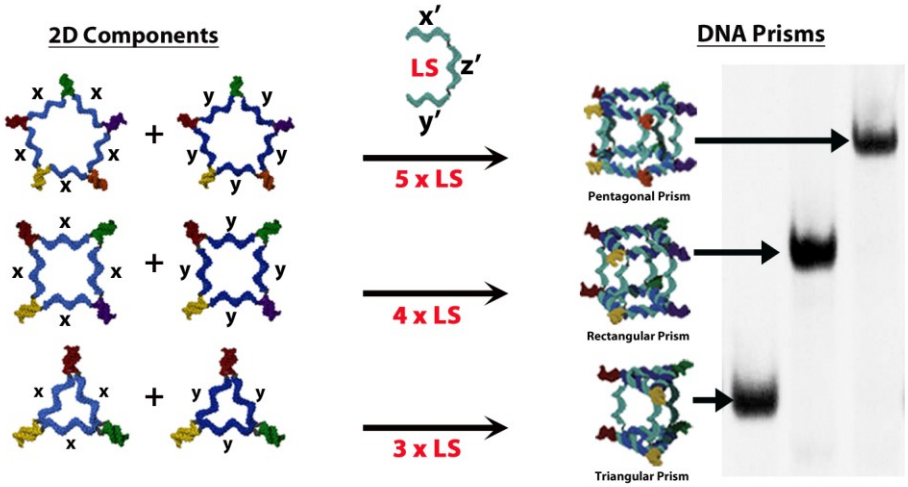

Reproduced with permission from; "A facile, modular and high yield method to assemble three-dimensional DNA structures", McLaughlin, C. K., Hamblin, G. D., Aldaye, F. A., Yang, H. and Sleiman, H. F. *Chem. Commun.,* **2011**, 47, 8925-8927. Royal Society of Chemistry (2011).

3.1 Abstract

A rapid and high-yielding method to generate DNA cages of deliberately designed geometry is described in this chapter. Balancing the incorporation of sequence uniqueness and symmetry in a face-centered approach to 3D construction results in triangular (**TP**), rectangular (**RP**), and pentagonal prisms (**PP**) without compromising the potential for nanostructure addressability. It is also demonstrated that the use of full sequence symmetry promotes intra- rather than intermolecular association of strands upon assembly of DNA structures.

3.2 Introduction

The construction of three-dimensional (3D) assemblies is a long-standing goal in supramolecular chemistry. These structures hold great potential as tools to control the reactivity of guest molecules,[1-3] templates for the growth of new materials,[4] vehicles for drug delivery to diseased cells,[5,6] gas storage substrates,[7] and scaffolds for organization.[8] While a number of methods have been used to generate 3D-assemblies, access to structures with deliberately designed size and shape, and with independently addressable subunits has been challenging.

In this chapter, a facile method is developed to generate 3D-DNA cages, with finely controlled geometry, symmetric or asymmetric positioning oligonucleotides, and the ability to incorporate single-stranded regions as structurally switchable units. This method relies on commercially available DNA strands, and involves room temperature assembly in minutes to produce 3D structures in excellent yield.

Beyond the subset of structures that derive their rigidity from triangular faces (such as DNA tetrahedra and octahedra), [9-16] there are three general methods to assemble 3D-DNA structures. The first involves the use of 'DNA origami', where a long single strand of DNA is folded into a desired structure, through addition of short 'staple strands'.[17] While this can result in excellent shape control,[10,18-22] DNA origami uses hundreds of different staple strands and long assembly times (days), and yields large, DNA-dense structures. The second approach relies on the assembly of identical branched DNA subunits into DNA cages. [23,24] The full rigidity of these branch points is used to pre-program curvature such that self-assembly converges into a single 3D-DNA structure. The resulting cages are stiff, double stranded and fully symmetric. The third approach relies on the assembly of single-stranded DNA polygons with organic corner units, as faces of prismatic structures, and their linking into 3D-DNA cages. [25-29] However, the method requires laborious ligation of DNA polygons and is fully asymmetric in its design, i.e. all assembling strands are different from each other in sequence.

The interest here was in developing an assembly strategy that could be

readily used by other laboratories, and that relied both on simple sequence design and the ability to purchase oligonucleotides from commercial sources. As such, a method to create DNA polygons from readily obtainable starting materials with no need for ligation or complicated synthetic insertions was sought. It was also asked whether sequence symmetry could be introduced within the structures. The challenge is to maximize the number of identical DNA sequences used, in order to reduce errors and simplify the assembly process, yet to retain some strategically positioned unique sequences that allow access to DNA cages with programmed geometries and independently addressable subunits. This required careful examination of the efficiency of the 3D-assembly upon progressive introduction of symmetry elements within the structures.

3.3 Results and discussion

3.3.1 Assembly and characterization of 2D DNA polygons

A method to assemble DNA polygons containing single-stranded arms was first examined (Fig. 3.1). This was achieved by using DNA strand, such as **1**, which possess a central sequence x, flanked by two 10-base sequences at either side that can bring together the polygons by hybridization (shown as different colors in Fig. 3.1). This method was initially developed with the self-assembly of DNA triangles,[30] but was not expanded to include variability in the polygon structures. A key component in the design of each building block is the use of a C6-alkyl spacer that separates the three DNA regions in these building blocks. This helps to reduce electrostatic and steric crowding at the junctions upon assembly of each DNA strand.[26]

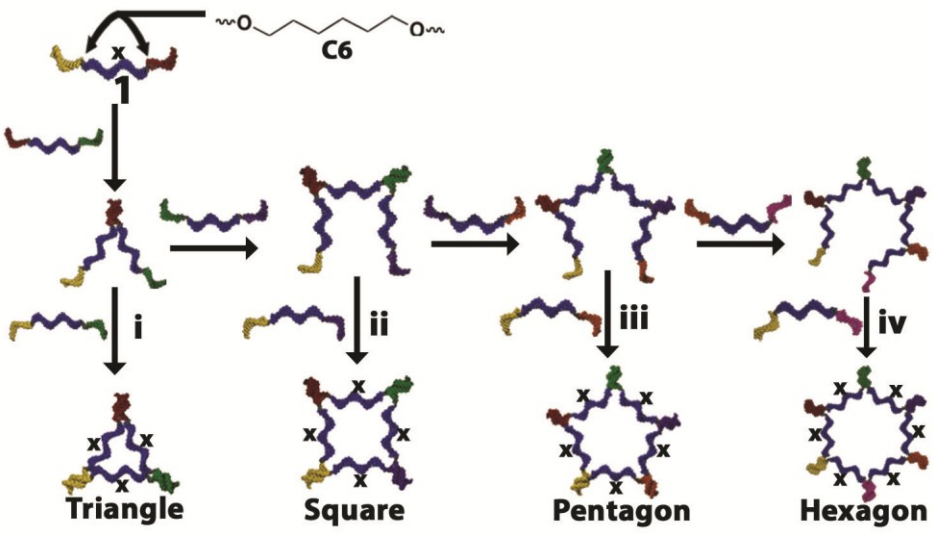

Figure 3.1 Assembly of triangles, squares, pentagons, and hexagons. Regions of the same colour denote identical duplex DNA sequences.

Using three such complementary strands, a triangle was first assembled with single-stranded arms at room temperature in quantitative yields, as determined by native polyacrylamide gel electrophoresis (PAGE) (Fig. 3.2a). A square could be accessed equally efficiently by keeping two of these strands, and designing two others that can close to form a tetramer (Fig. 3.2b). The process was also quantitative for a pentagon and a hexagon (Fig. 3.2c and d, respectively). It should be noted that these structures possess identical sequences x within the interior of the polygon (as shown in Fig. 3.1), and as such significantly reduce the sequence-space, cost and errors that arise from the assembly. On the other hand, each of the double stranded extremities in these polygons has a unique sequence (see coloured duplexes in Fig. 3.1), allowing them to be independently addressable (i.e. they can be symmetrically or asymmetrically functionalized at each of their vertices). The C6-alkyl spacer is commercially available, and thus the component strands can be readily obtained commercially without the need for an in-house DNA synthesizer. Thus a small set of strands can be designed to interact in a modular fashion, resulting in a number of DNA polygons with single-stranded arms. Similar self-assembly was observed for structures **T2**, **S2**, **P2** and **H2** except the interior regions were given a new sequence y. While the focus of the design here is to connect each pair of polygons to yield a 3D DNA structure, the single-

stranded regions can easily be functionalized with other materials to generate a unique set of DNA-hybrid materials with well-defined geometries.

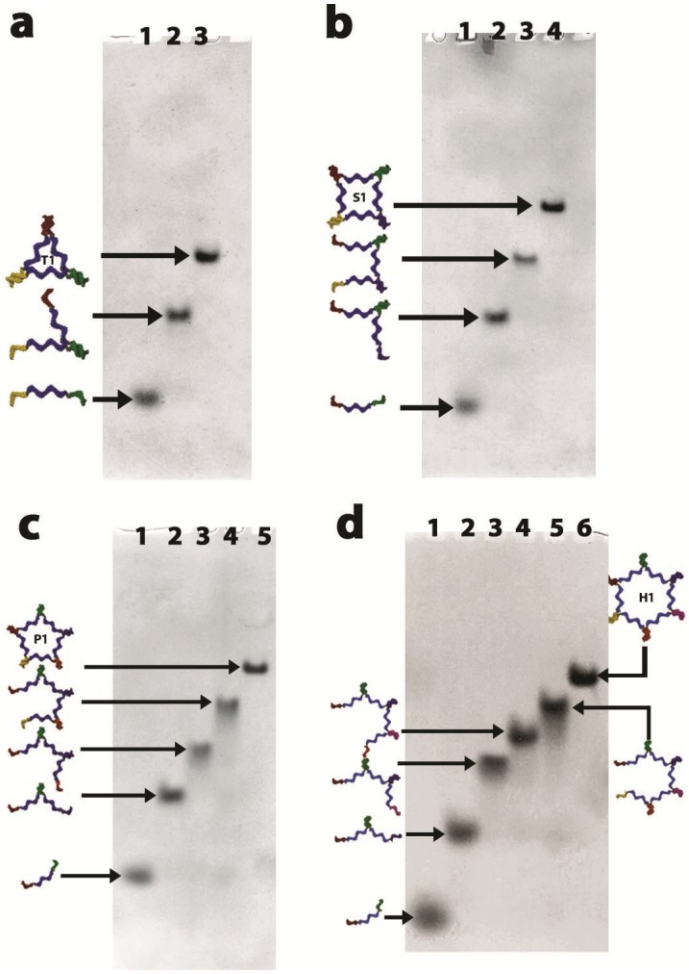

Figure 3.2 Sequential assembly and native PAGE analysis of T1, S1, P1 and H1. a, Lane 1- T1a, Lane 2- T1aT1b, Lane 3- T1aT1bT1c i.e. **T1**. **b,** Lane 1- S1a, Lane 2- S1aS1b, Lane 3- S1aS1bS1c, Lane 4- S1aS1bS1cS1d i.e. **S1**. **c,** Lane 1- P1a, Lane 2- P1aP1b, Lane 3- P1aP1bP1c, Lane 4- P1aP1bP1cP1d, Lane 5- P1aP1bP1cP1dP1e i.e. **P1**. **d,** Lane 1- H1a, Lane 2- H1aH1b, Lane 3- H1aH1bH1c, Lane 4- H1aH1bH1cH1d, Lane 5- H1aH1bH1cH1dH1e and Lane 6- H1aH1bH1cH1dH1eH1f i.e. **H1**. (It should be note that T1a = S1a = P1a = H1a, etc. See section 3.6.3 for sequence details)

3.3.2 Assembly and characterization of 3D DNA structures

Initial 3D DNA studies focused on the assembly of a pseudo-symmetric DNA cage, with different polygons top and bottom (Fig. 3.3). For example, a triangular prism **TP** with this strategy would come from two triangles **T1** and **T2**,

each containing three identical internal sequences (x for **T1** and y for **T2**). It would have a pseudo-C3v geometry, but would still have three different sites of attachment on the vertices of the triangles. Note that the external DNA sequences that are used to bring together the cyclic structures (colored duplexes in Fig. 3.3) can be re-used in the top and bottom polygons. To bring the two polygons together, a single linking strand **LS1** with three regions was used: the top and bottom regions of **LS1** possess sequences x' and y', complementary to the sides of the top and bottom polygons, respectively, and the middle region is a 15-base sequence z' that would act as a spacer between these two polygons and form the edges of the prism. As with the strands that make up the polygons (Fig. 3.1), these three regions in **LS1** are separated by C6-alkyl spacers.

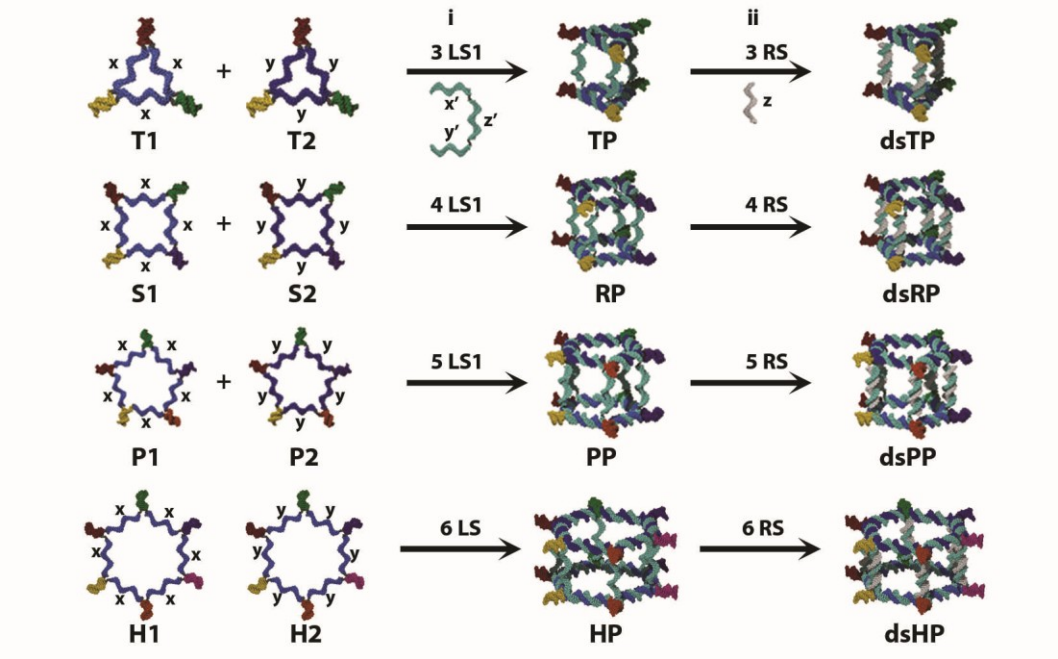

Figure 3.3 Self-assembly strategy for preparing 3D DNA prismatic structures. Triangles (**T1** and **T2**), squares (**S1** and **S2**), pentagons (**P1** and **P2**) and hexagons (**H1** and **H2**) are connected (i) to form DNA prisms **TP**, **RP**, **PP** and **HP** respectively. The remaining single-stranded regions are then sequestered to form fully double-stranded structures (ii) **dsTP**, **dsRP**, **dsPP** and **dsHP**. **LS1** = linking strand 1, **RS** = rigidifying strand.

Sequential room temperature assembly of each pair of 2D DNA building blocks, **T1**/**T2**, **S1**/**S2** and **P1**/**P2**, with the correct equivalents of **LS1** showed

clean and near quantitative DNA prism formation (Fig. 3.4). Structures were also assembled at room temperature in only 10 minutes and at final 3D concentrations between 2-10 μM. These structures thus mark a key advancement in 3D DNA assembly, as typical concentrations for previous structures are restricted to <0.5 μM to prevent higher order assemblies from forming and typically require long annealing times with elevated temperatures. Also, **LS1** can be added in a stepwise manner (e.g. **T1** + **LS1** + **T2** → **TP**) or directly to the pair of polygons (e.g. **T1**/**T2** + **LS1** → **TP**) to generate each prismatic structure. Discussion regarding the assembly of **HP** will be addressed in subsequent sections.

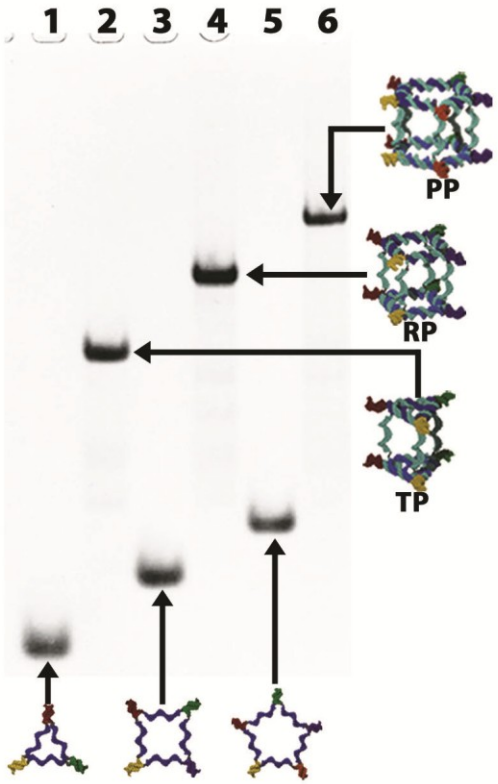

Figure 3.4 Characterization of 3D DNA prismatic structures. Assembly and native PAGE analysis (6%) of 3D DNA prisms; Lane 1 - **T1**, lane 2 - **TP**, lane 3 - **S1**, lane 4 - **RP**, lane 5 - **P1** and lane 6 - **PP**.

As shown in Fig. 3.2ii, construction of each prism leaves a set of 15-base spacer arms between the polygons that can be rigidified using a single complementary DNA strand **RS** to yield the fully double-stranded products **dsTP**,

dsRP and **dsPP**. To confirm that each structure is fully assembled and closed (i.e. the linking strands are fully bound to the top and bottom polygons), selective enzymatic digestions, using ExoVII and MBN (Fig. 3.5), were performed as outlined previously.[26] Structure **TP** (Fig. 3.5a, lane 1) remains intact after digestion with ExoVII (Fig. 3.5a, lane 2) but is digested with MBN (Fig. 3.5a, lane 3) due to the single-stranded regions that comprise each prismatic structure's connecting region. As shown in Fig. 3.5a, **dsTP** (lane 4) also remains undigested after ExoVII treatment (lane 5) but is further stabilized against MBN addition (lane 6) due to the double-stranded nature of the sequences that connect the prismatic faces. Similar results were obtained for **RP** (Fig. 3.5b, lanes 1 - 3) and **dsRP** (Fig. 3.5b, lanes 4 - 6), as well as **PP** (Fig. 3.5c, lanes 1 - 3) and **dsPP** (Fig. 3.5c, lanes 4 - 6) after nuclease treatment, showing the correct connectivity.

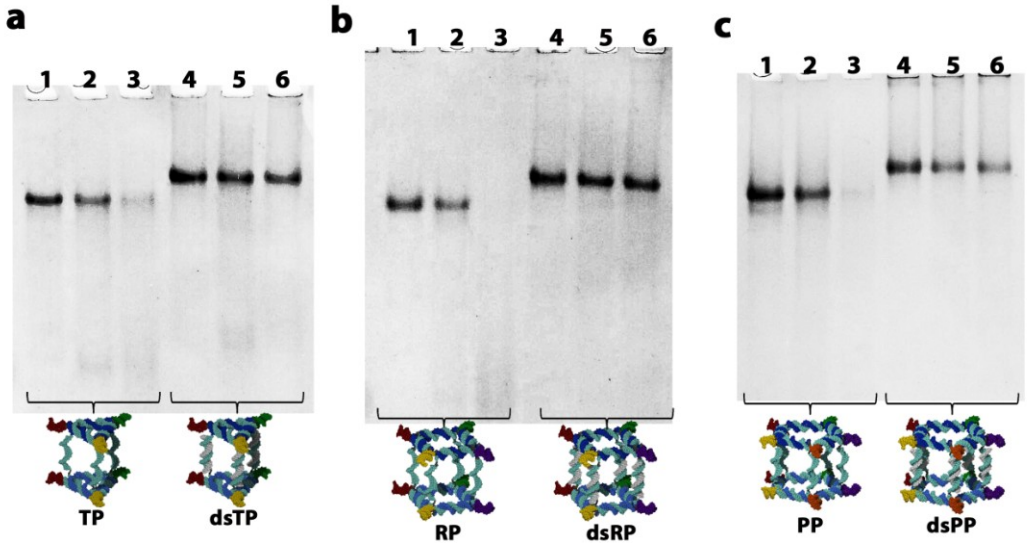

Figure 3.5 Connectivity analyses of 3D structures using nucleases ExoVII and MBN. a, TP (lane 1) was subjected to treatment with ExoVII (lane 2) and MBN (lane 3). Similar analysis was performed on **dsTP** (lane 4 - no enzyme, lane 5 - ExoVII, lane 6 - MBN). **b,** The connectivity of the second 3D construct **RP** was analyzed using similar enzymatic protocols: **RP** (lane 1 - no enzyme, lane 2 - ExoVII, lane 3 - MBN) and **dsRP** (lane 4 - no enzyme, lane 5 - ExoVII, lane 6 - MBN). **c,** Enzymatic protocols repeated on the final structures **PP** (lane 1 - no enzyme, lane 2 - ExoVII, lane 3 - MBN) and **dsPP** (lane 4 - no enzyme, lane 5 - ExoVII, lane 6 - MBN).

Overall, a small number of strands can now be assembled at room temperature into 3D-DNA structures in excellent yield. Partial incorporation of

symmetry, defined as using identical sequences x or y within each respective polygon, allows one to diversify 3D structure by strategically reusing sequences that serve a structural role in assembly. Thus, the facile and efficient manner in which **TP**, **RP** and **PP** can be designed and prepared gives easy access to structures that can be further site-specifically modified with a number of synthetic and bio-macromolecules to yield geometrically well-defined arrangements on the nanometer length scale.

3.3.3 Construction of hexagonal prism HP

Missing from the previous section was discussion of the assembly of hexagonal prism **HP** from 2D starting materials **H1** and **H2** (Fig. 3.6a). The yield for **HP** was substantially reduced as compared to the other 3D structures (Fig. 3.6b, lane 1). From the native PAGE analysis in Fig. 3.6b, it appears that **HP** is only partially stable and disassembles to a species of intermediate mobility between that of the desired 3D structure and a single 2D hexagon (lane 2). Judging by the absence of any leftover single-stranded hexagons in lane 1, it can be surmised that this intermediate structure contains hybridized linking strands on a single polygon, either **H1** or **H2**. One possible explanation for this observation is that full hybridization of the six linking strands between **H1** and **H2** imparts strain to the overall assembly, resulting in weaker 10 base duplex interactions. This could mean that HP is formed in solution, but weakened connectivity causes disassembly under analysis conditions. Alternatively, the six linking strands on a single hexagon may be misaligned or sterically crowded, making hybridization to each of the single-stranded regions of the second hexagon difficult.

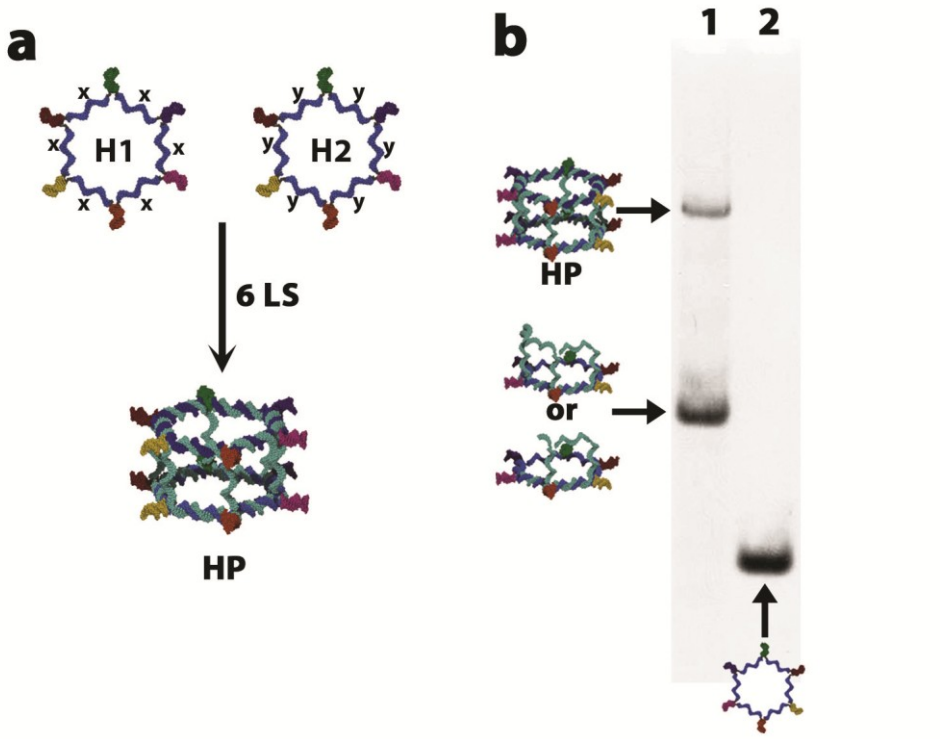

Figure 3.6 Assessment of 3D assembly for a hexagonal prism (HP). a, schematic representation of HP assembly from sequence symmetric 2D polygons H1 and H2. **b,** Assembly and native PAGE analysis (6%) of **HP** formation; Lane 1 – product mixture resulting from **H1** + **LS1** (6 eqv.) + **H2** and lane 2 – **H1**.

To more clearly understand 3D assembly using hexagons, a series of 2D derivatives that contain a ten-thymidine (T10) tract where **LS1** would normally bind were generated (Fig. 3.7a). This substitution effectively knocks out hybridization to the linking strands **LS1** wherever the T10 tracts are placed within the hexagon structure. The modular way in which 2D polygons are generated additionally allowed placement of the T10 sequence tracts in a well-defined orientation, making it easier to examine the effects on 3D assembly. Each new hexagon, **H3**-**H7**, was prepared with one, two or three T10 sequences. It should be noted that the binding sequence that is retained in each of the modified hexagons is identical to the sequence used in **H1** i.e. sequence x. As shown in Fig. 3.7a, this would then allow assembly of hexagonal prism structures both varying number and orientation of linking strand **LS1**.

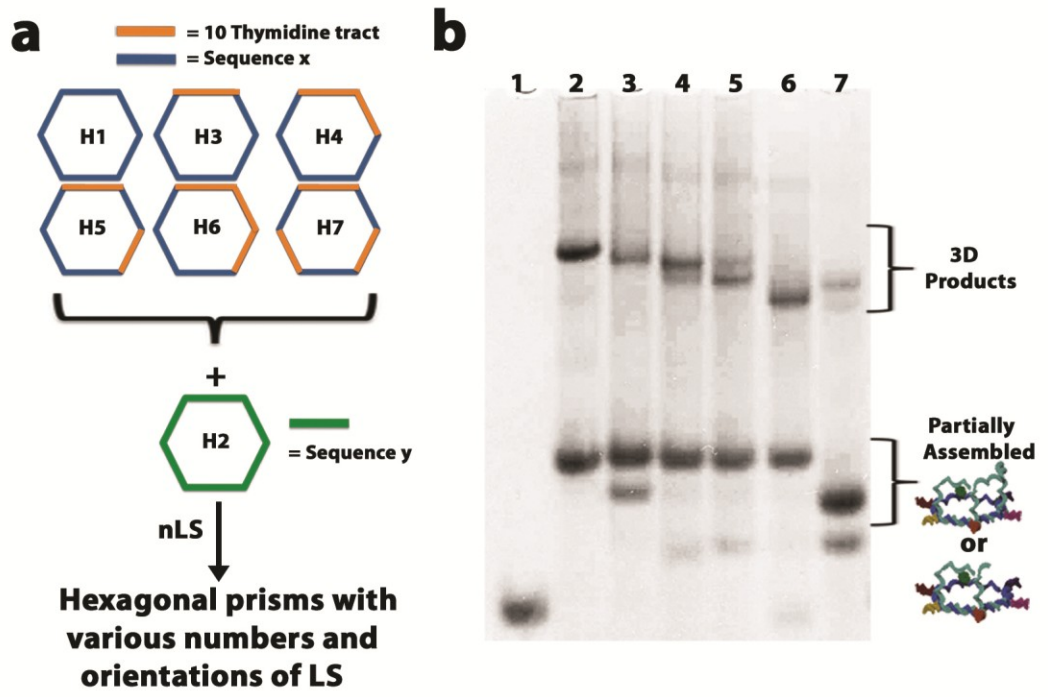

Figure 3.7 Variation in HP assembly through modification of hexagon H1. a, Schematic representation of modified hexagons containing sequence x (shown in blue) that should undergo selective coordination to **LS1** and hexagon **H2** to produce various hexagonal prismatic structures. The 10mer duplexes have been removed from the schemes for clarity. **b,** Native PAGE analysis (6%) of various HP structures; Lane 1- **H1**, Lane 2- **H1** + 6 eqv **LS1** + **H2**, Lane 3- **H3** + 5 eqv **LS1** + **H2**, Lane 4- **H4** + 4 eqv **LS1** + **H2**, Lane 5– **H5** + 4 eqv **LS1** + **H2**, Lane 6 - **H6** + 3 eqv **LS1** + **H2** and Lane 7 - **H7** + 3 eqv **LS1** + **H2**.

As shown in Fig. 3.7b, 3D assembly using each hexagon pair results in a distribution of products as analyzed by native PAGE. In each of Lanes 2-7 there appears to be a distribution between the slower moving 3D products and what appears to be a hexagon with a specific number of linking strands bound to it (schematically represented on the side of the gel). Removing half of the binding sites in an effort to reduce steric crowding/strain, as is the case with **H6** (Lane 6) and **H7** (Lane 7), and addition of **H2** still resulted in poor 3D product formation. Despite pre-organization of the linking strands within each hexagon structure, sterics may still be playing a role upon addition of the second hexagon **H2**. In addition, **H2** contains 6 binding sites for the pre-organized linking strands to coordinate with, potentially making it difficult for a single orientation to be preferred. This could result in initial assembly errors that both destabilize the

structure and prevent correct orientation of the linking strands. As was observed in the initial **HP** assembly (Fig. 3.7b, lane 1) no hexagon starting materials are left over in each of lanes 2-8, indicating that initial assemblies were indeed formed. Errors in **LS1** binding likely destabilize each structure, leading to instability of the 3D products.

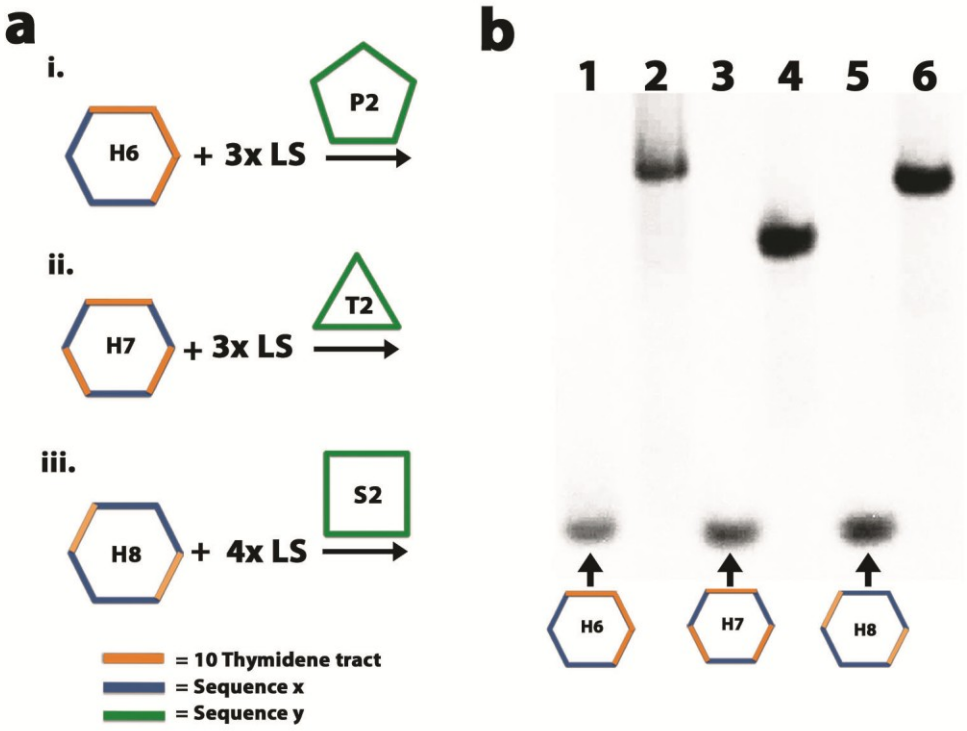

Figure 3.8 Formation of heteroprisms. a, Schematic representations (i-iii) of hexagons derived from **H1** that can be assembled into heteroprisms using selective coordination of **LS1** and the second set of polygons, **T2**, **S2**, and **P2**. **b,** Native PAGE analysis (6%) of heteroprism formation; Lane 1- **H6**, lane 2- **H6** + 3 eqv **LS1** + **P2**, lane 3- **H7**, lane 4 – **H7** + 3 eqv **LS1** + **T2**, lane 5 – **H8** and lane 6 – **H8** + 4 eqv **LS1** + **S2**.

Alternatively, to test whether the number of binding sites on the 2nd polygon face would impact product yields, 3D preparation was performed using **P2**, **T2** and **S2** instead of **H2**. Each assembly experiment is schematically represented in Fig. 3.8a and would formally allow the preparation of heteroprisms with different geometries. In Fig. 3.8ai, hexagon **H6** is designed to bind three adjacent linking strands that could best hybridize to available sites on **P2**. Similarly, the design of **H7** (Fig. 3.8aii) and **H8** (Fig. 3.8aiii) make it possible to

coordinate triangle **T2** and square **S2**, respectively. For each of these designs, a 3D structure is formed in excellent yield (Fig. 3.8b, lanes 2, 4, and 6, respectively). These experiments thus suggest that the number of available coordination sites on the 2nd polygon is important in determining how effectively the pre-organized linking strands can bind to yield a closed prismatic structure. Thus, tuning the linking strand orientation on each hexagon through selective incorporation of thymine residues could be used to generate a scaffold that can coordinate a variety of geometrically diverse DNA polygons. Such heteroprisms could be additionally modified due to the multitude of single-stranded regions that remain after 3D formation. Further investigations are underway to modify **H2** in a manner that will promote efficient assembly of hexagonal prismatic structures.

3.3.4 Potential cooperativity in 3D DNA prism assembly

Unlike previous approaches which use highly rigid building blocks to generate 3D-DNA structures,[23,24] the method described here introduces sequence symmetry into flexible DNA building blocks. In principle, this flexibility could lead to assembly errors. Remarkably, there is a near absence of by-products in 3D-assembly, indicating that cooperative assembly may be at play. To probe this question, triangles **T1** and **T2** were brought together with increasing amounts of linking strand **LS1** as shown in Fig. 3.9a. Interestingly, PAGE analysis indicated that the triangular prism is produced in high yields at both low and high relative amounts of **LS1** with very few side-products (Fig. 3.9b).

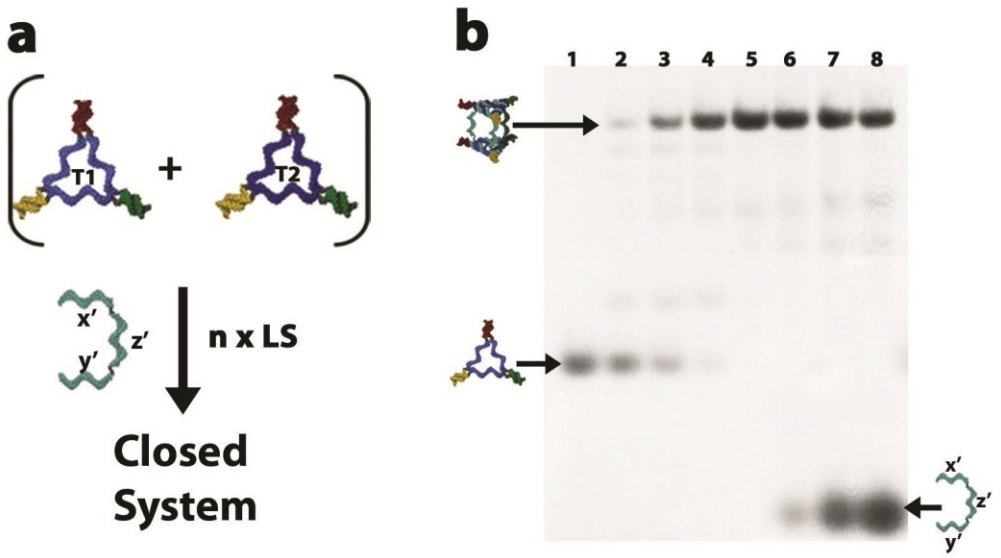

Figure 3.9 Preliminary assessment of cooperativity in 3D DNA assembly. a, Schematic representation of the assembly of 3D DNA structure **TP** by adding increasing equiv. of **LS1** to a 1:1 mixture of **T1** and **T2**. **b,** Native PAGE (6%) analysis.; Lane 1 - (**T1**+**T2**) + 0**LS1**, lane 2 - (**T1**+**T2**) + 0.5**LS1**, lane 3 - (**T1**+**T2**) + 1**LS1**, lane 4 - (**T1**+**T2**) + 2**LS1**, lane 5 - (**T1**+**T2**) + 3**LS1**, lane 6 - (**T1**+**T2**) + 6**LS1**, lane 7 - (**T1**+**T2**) + 12**LS1** and lane 8 - (**T1**+**T2**) + 18**LS1**. b,

To expand on these experiments, **LS1** was also added prior to the addition of **T2** to determine whether the individual binding strengths of the two polygons would play a role in determining the extent of cooperative behaviour. It should be noted that the single-stranded regions x and y in the two triangles **T1** and **T2** are different sequences, and thus contain different binding strengths to the respective complementary regions on **LS1**. This means that, even when all strands are simultaneously added, the triangle with the greater binding strength may assemble with the three linking strands first, and this is then followed by the second triangle. To further probe the assembly process, a sequential assembly experiment was designed.

As shown schematically in Fig. 3.10a, a given ratio of **LS1** should yield a full distribution of products, **i-iii**, that are pre-organized to bind **T2** to create bi-facial structures. Thus, even with less than a stochiometric amount of **LS1** ($n<3$), the full prismatic structure could form. Alternatively, when the amounts of **LS1** in solution are $n > 3$, one could envisage a range of products, unless selective binding to the second polygon takes place. To explore this potential

disproportionation, various equivalents of **LS1** were added to the starting template **T1**, followed by **T2** addition and analysis of the product distributions by PAGE (Fig. 3.10b). In all experiments where the equivalents of **LS1** are changed from 0.5 – 18 (Fig. 3.10b, Lanes 2-8) the major product observed is the 3D prism **TP**.

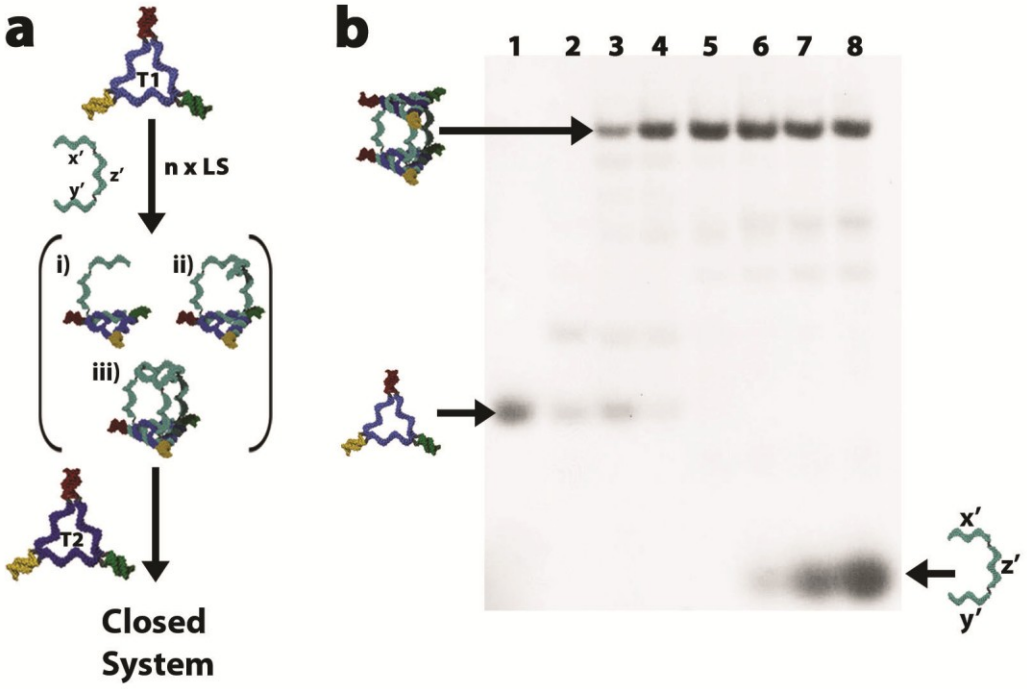

Figure 3.10 Variation in 3D DNA assembly to try and elucidate cooperativity. a, Schematic representation of the assembly of 3D prism **TP** by pre-coordination of various equivalents of **LS1** to **T1** followed by the addition of **T2**. **b,** Products analyzed by native PAGE from addition of **LS1** to **T1**, followed by addition of **T2**; In lanes 1-8 only the number of equivalents of **LS1** are changed; Lane 1- 0 **LS1** eqv, lane 2 – 0.5 **LS1**, lane 3 – 1 **LS1**, lane 4 – 2 **LS1**, lane 5 – 3 **LS1**, lane 6 – 6 **LS1**, lane 7 – 12 **LS1** and lane 8 – 18 **LS1**.

The above experiments result in nearly identical outcomes, irrespective of the assembly strategy employed. Although difficult to elucidate what exactly are the cooperative contributions to the 3D assembly mechanism, structure **iii** in Fig. 3.10a does indeed represent a stable prismatic intermediate, suggesting that products with maximal linking strand content are favoured by this face-centered assembly method. In addition, the highly pre-organized nature of this intermediate allows successful binding of the second polygon even in the presence of both low and excess linking strands, making it a selective chelate for 3D prismatic

formation. Because the single-stranded regions x and y in the two triangles **T1** and **T2** have different sequences, the different binding strengths do seem to play a role in assembly. Based on the above experiments, it is likely that the three linking strands bind first to the triangle that provides the highest duplex stability, resulting in selective formation of this chelating intermediate with three pre-organized linking strands that can then efficiently bind to the second triangle. Further sequence modifications, assembly experiments and structural studies will help to better distill the cooperative elements at play in this modular 3D DNA synthesis strategy.

3.3.5 Additional symmetry incorporated into 3D DNA prism assembly

It was next examined whether an additional symmetry element could be introduced into this 3D-assembly strategy. This was achieved by modifying the linking strand to contain two x' sequences (**LS2**) and would result in identical polygons, top and bottom, within any 3D structure formed. Structures produced in this manner would thus have pseudo-D_{nh} symmetry, for example pseudo-D_{3h} triangular prisms. In the case of **TP** formation, however, there may be two possible assembly mechanisms (Fig. 3.11a); (1) Three linking strands can bring together two triangles to generate 3D structure **TP** (Fig. 3.11ai) or (2) The linking strand can use its two x' extremities to bind intramolecularly to a single triangle, and two such triangles can then be brought together using a third linking strand (Fig. 3.11aii). This generates a structure which is the formal ‘isomer’ of a triangular prism.

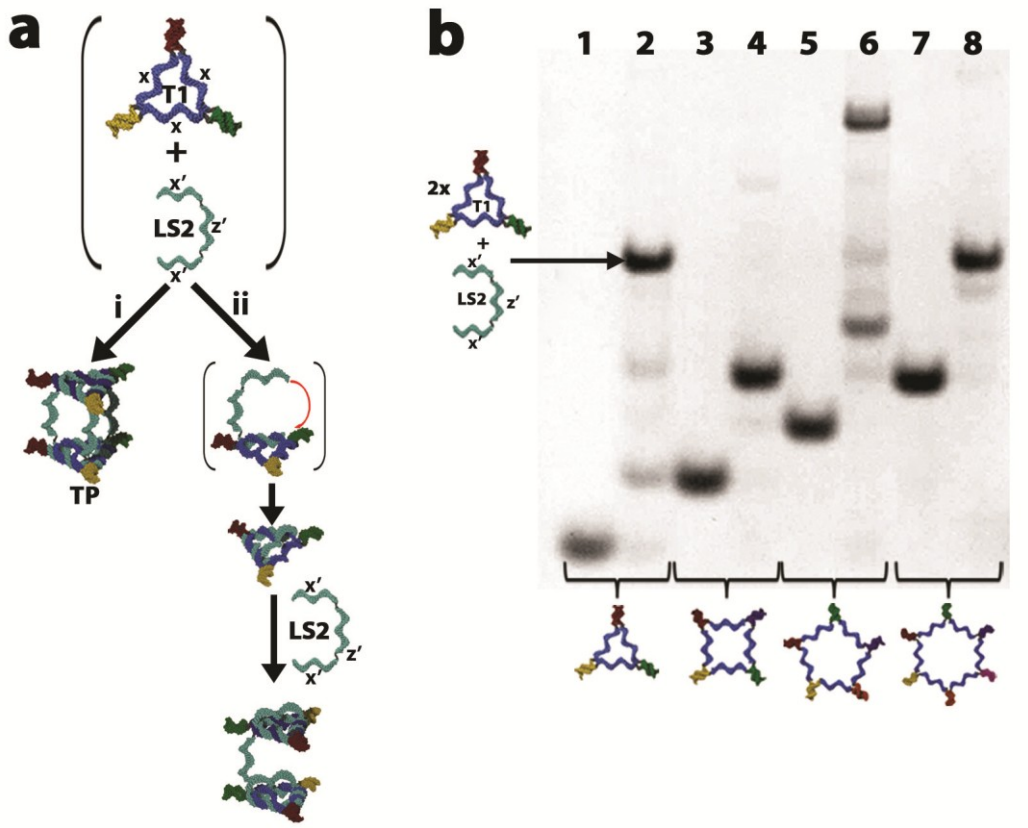

Figure 3.11 Effect of additional symmetry on 3D DNA formation. a, Schematic representation of proposed 3D assembly for **TP** using additional symmetry elements. In pathway i, **TP** is fully formed via connecting two triangles with three points of interaction with **LS2**. In ii, **LS2** interacts initially with T1 to yield an intermediate that then undergoes intramolecular hybridiziation (red arrow) to sequester the remaining open end. This intramolecularly bound triangle thus blocks two binding sites, leaving only a single sequence for LS2 to anneal. LS2 then connects two of these triangles to form a closed product.. **b,** Native PAGE analysis of 2D polygon assembly with symmetric linking strand **LS2**; Lane 1 - **T1**, lane 2 - 2**T1** + 3**LS2**, lane 3- **S1**, lane 4 - 2**S1** + 4**LS2**, lane 5 - **P1**, lane 6 - 2**P1** + 5**LS2**, lane 7 - **H1**, and lane 8 - 2**H1** + 6**LS2**.

Assembly of identical triangles, squares, pentagons and hexagons was performed and analyzed by native PAGE, which revealed an interesting 'odd–even' effect (Fig. 3.11b). The structures with an odd number of sides (e.g., triangles, pentagons) showed bands of similar lower mobility as those of the prismatic cages (Fig. 3.11b, Lanes 2 and 6). The structures with an even number of sides showed only a single band of higher mobility and no lower mobility bands ascribed to the assembly of two polygons (Fig. 3.11b, Lanes 4 and 8).

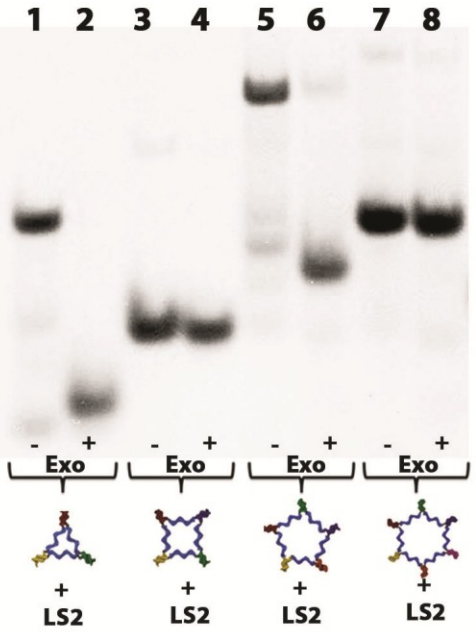

Figure 3.12 ExoVII characterization of symmetric DNA structures. Products analyzed by native PAGE from addition of **LS2** to **T1**, **S1**, **P1** and **H1** before and after the addition of exonuclease VII (ExoVII). Lane 1- **T1** + **LS2**, Lane 2 – **T1** + **LS2** + ExoVII, Lane 3- **S1** + **LS2**, Lane 4 – **S1** + **LS2** + ExoVII, Lane 5- **P1** + **LS2**, Lane 6 – **P1** + **LS2**+ ExoVII, Lane 7 - **H1** + **LS2** and Lane 8 – **H1** + **LS2** + ExoVII.

Interestingly, the lower mobility bands for the odd-sided structures were no longer resistant to exonuclease treatment (Fig. 3.12), as was the case for the prismatic cages outlined in section 3.3.2. Based on these studies, it is proposed that a linking strand with two identical x' extremities prefers to bind intramolecularly to each individual polygon. With an even number of sides, all the binding sites are occupied with linking strands, thus two polygons cannot be assembled together (Fig. 3.13ai). These intramolecularly bound structures created from **S1** and **H1**, though, are very stable and exonuclease resistant. Such structures may find use for the generation of more complex 3D-DNA structures. Alternatively, with an odd number of sides, one binding site remains, and an additional linking strand can link two such polygons together into a structure (Fig. 3.13aii), which is too weakly bound to resist enzymatic degradation. Whether the number of binding sites is odd or even, it is also of note that intramolecular

association produces a single product. Although the orientation of the linking strands are not known for these intramolecular products, a number of plausible structures are outlined in Fig. 3.13b.

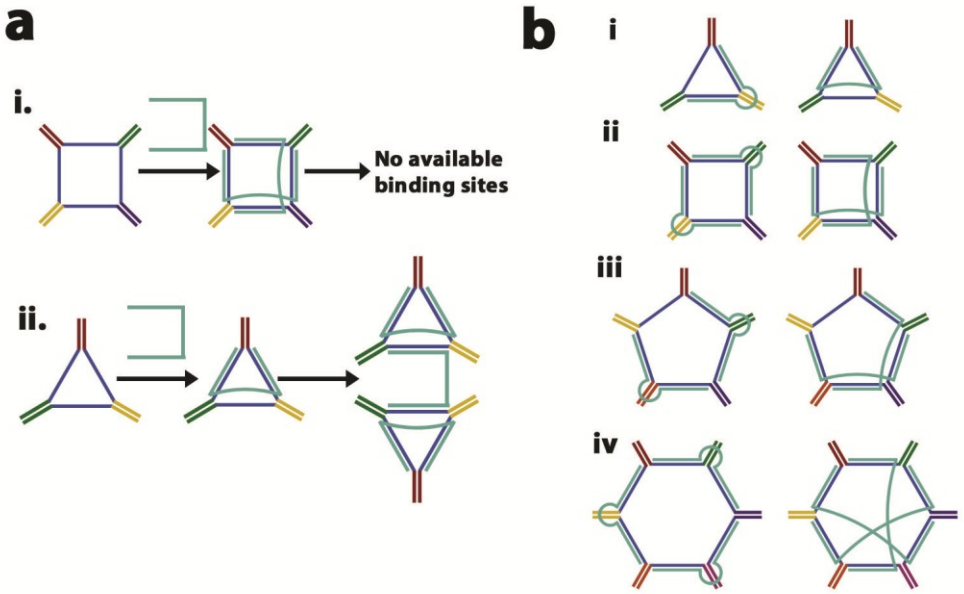

Figure 3.13 Products from intramolecular binding of LS2. a, Representations of proposed final structures for i (**S1** + 2**LS2**) and ii (2**T1** + 3**LS2**). **b,** Schematic representations of intramolecular products from **LS2** assembly with i) **T1**, i) **S1**, i) **P1** and i) **H1**.

To further demonstrate that an intramolecular process was competing with intermolecular association of the prismatic faces, two additional triangles **T3** and **T4** were designed, such that they contain two identical arms for intramolecular hybridization of a linking strand (shown in green for **T3** and in red for **T4** in Fig. 3.14a), and one different unique sequence on their interior. In comparison, **T1** has three identical internal arms (of sequence labeled *x* in Fig. 3.3a) that permit intramolecular association of **LS2** (**T1**·**LS2**, Fig. 3.14ai. Thus, triangle **T3** has one arm of sequence *x* and two arms of sequence *y*, while **T4** has one arm of sequence *x* and two arms of a new sequence *z*. Binding a linking stand **LS3** that is selective for hybridization to the two strands *y* in **T3**, leaves behind an empty binding site on **T3** with sequence *x* (**T3**·**LS3**, Fig. 3.14aii). Similarly, binding a linking stand **LS4** that is selective for hybridization to the two strands *z* in **T4**, also leaves

behind an empty binding site on **T4** with sequence *x* (**T4·LS4**, Fig. 3.14aiii). This sequence adjustment allows the assembly of an authentic sample of the proposed open structure (Fig. 3.14bi), where the two free single-stranded arms on **T3·LS3** and **T4·LS4** can be joined together with linking strand **LS2** that possesses two *x'* extremities (Fig. 3.14bii). .

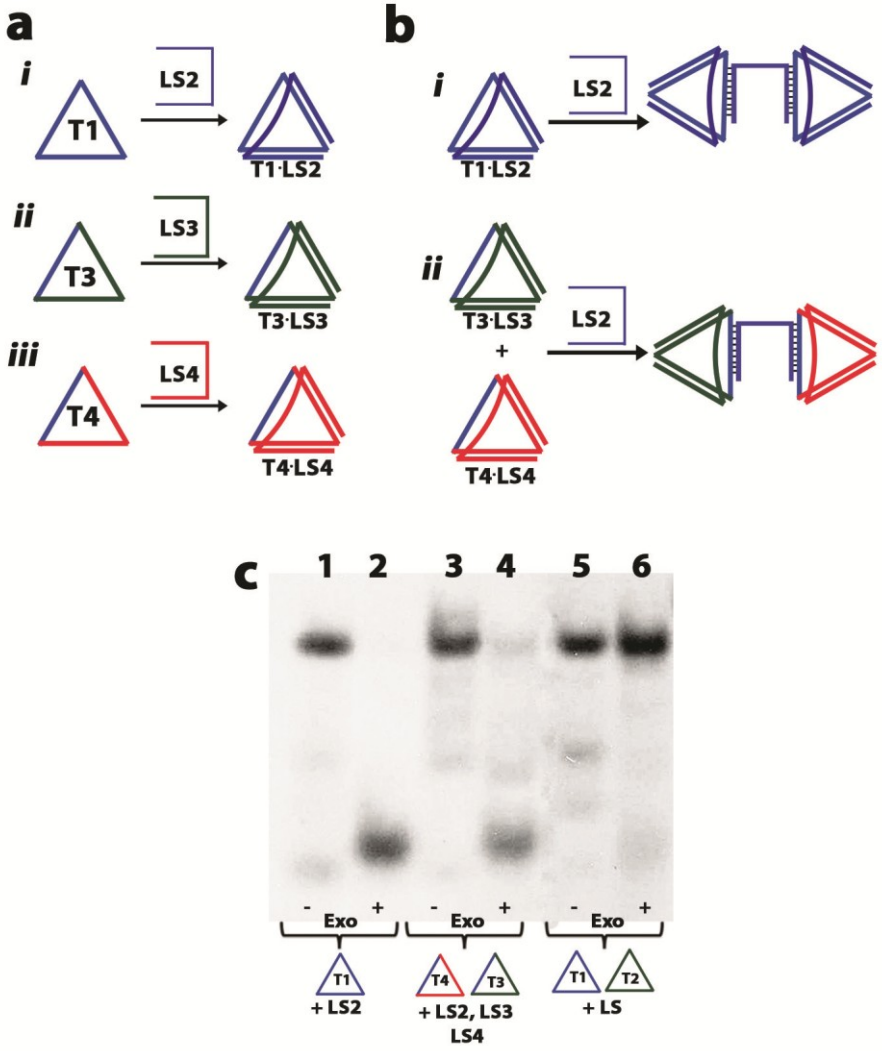

Figure 3.14 Elucidation of intramolecular binding using modified triangles. a, Schematic representation of triangles used to assemble intramolecular products **T1·LS2**, **T3·LS3** and **T4·LS5**. **b,** Schematic representations for the proposed intramolecular product (i) and authentic standard for intramolecular product (ii) **c,** Products analyzed by native PAGE before and after ExoVII treatment; Lane 1 – **T1** + **LS2**, lane 2 – **T1** + **LS2** + ExoVII, lane 3 – (**T3** + **LS3**) + (**T4** + **LS4**) + **LS2**, lane 4 – (**T3** + **LS3**) + (**T4** + **LS4**) + **LS2** + ExoVII, lane 5 – **T1** + **LS1** + **T2** and lane 6 – **T1** + **LS1** + **T2** + ExoVII.

Assembly and enzymatic studies were performed as shown in Fig. 3.14c to confirm the intramolecular association that results from full sequence symmetry. Addition of **LS2** to **T1** again generates a band of slower mobility (Lane 1) that is degraded by ExoVII (Lane 2). We then pre-mixed **T3**/**LS3** and **T4/LS4** and added **LS2** to link them. A product with identical mobility by PAGE was observed (Lane 3) and similarly underwent degradation after ExoVII treatment (Lane 4). Interestingly, preparation of our previously characterized triangular prism **TP** using asymmetric linking strand **LS1** and triangles **T1** and **T2** results in a band with identical mobility (Lane 5) as observed for the symmetric products, but that resists ExoVII degradation (Lane 6). Although formal isomers of each other with presumably different shapes, each set of products displays a similar mobility by PAGE analysis. The ExoVII results, though, clearly indicate instability of the products and further suggest the presence of an intramolecular mechanism that eliminates intermolecular binding sites between polygons. Additional design, in tandem with detailed PAGE and structural studies, are underway to elucidate the intramolecular binding process and characterize the unique products formed under these highly sequence symmetric conditions.

3.4 Conclusions

In conclusion, the efficient generation of a number of 3D-prismatic DNA structures at room temperature, in minutes and in excellent yields has been demonstrated in this chapter. By using sequence symmetry in strategic locations, the assembly strategy is simplified, and errors are minimized. On the other hand, by preserving sequence uniqueness in locations that guide the assembly, the prepared 3D-DNA cages remain available for asymmetric, site-specific functionalization. For these flexible systems, it demonstrated that there is a limit beyond which sequence symmetry cannot be increased, as intramolecular processes compete. Overall, this gives rapid and modular access to DNA cages, which are DNA-economic, possess independently addressable subunits, and can contain single-stranded, dynamic components. This will expand their applications

as biological host structures, scaffolds for 3D-patterning and templates for the growth of shape-controlled materials.

3.5 Experimental section

3.5.1 General

StainsAll®, acetic acid, tris(hydroxymethyl)-aminomethane (Tris), formamide and urea were used as purchased from Aldrich. Acetic acid, and boric acid were purchased from Fisher Scientific and used without further purification. Nucleoside (dA,T,dC,dG) derivatized 500 Å and 1000Å LCAA-CPG supports with loading densities between 25-40 μmol/g, 5-ethylthiotetrazole, 1,6-hexanediol phosphoramidite and reagents used for automated DNA synthesis were purchased from ChemGenes Incorporated. Sephadex G-25 (super fine, DNA grade) was purchased from Amersham Biosciences. Mung Bean Nuclease (MBN, source: Mung Bean Sprouts) and Exonuclease VII (ExoVII, source: recombinant) were purchased from BioLynx Incorporated. 1xTB buffer is composed of 0.09M Tris and Boric acid (TB) with a pH ~8.3. 1xTAEMg buffer is composed of 45 mM Tris, 12.5 mM $Mg(OAc)_2 \cdot 6H_2O$ and 2 mM EDTA. The pH was adjusted to 8 using glacial acetic acid.

3.5.2 Instrumentation

Standard automated oligonucleotide solid-phase synthesis was performed on a Perspective Biosystems Expedite 8900 DNA synthesizer or Mermade MM6 synthesizer from Bioautomation. Gel electrophoresis experiments were carried out on an acrylamide 20 X 20 cm vertical Hoefer 600 electrophoresis unit. Enzymatic digestions were conducted using a Flexigene Techne 60 well thermocycler.

3.5.3 Oligonucleotides prepared for 2D and 3D DNA assembly

DNA synthesis was performed on a 1 μmole scale, starting from the required nucleotide modified 500Å or 1000 Å LCAA-CPG solid-support (isobutyrl-dG, benzoyl-dC, benzoyl-dA). Additionally, a 1,6 hexanediol phosphoramidte (**C6**) was site-specifically incorporated into each sequence and coupled onto the growing oligonucleotide chain as an artificial base with a prolonged coupling time of 5min. The coupling efficiency was

monitored after trityl removal. All sequences were fully deprotected in concentrated ammonium hydroxide (55 °C, 16 hours). Crude products were purified on 15% polyacrylamide/8M urea polyacrylamide gels (PAGE; up to 20 OD_{260} of crude DNA per gel) at constant current of 30 mA for 2 hours, using 0.09M Tris-Boric acid (TB) buffer (pH 8.3). Following electrophoresis, the plates were wrapped in plastic and placed on a fluorescent TLC plate and illuminated with a UV lamp (254nm). The bands were quickly excised, and the gel pieces were crushed and incubated in 10 mL of sterile water at 55 °C for 16 hours. Samples were then dried to 1.5 mL, desalted using size exclusion chromatography (Sephadex G-25), and quantified (OD_{260}) using UV-vis spectroscopy.

Table 3.1 Oligonucleotides synthesized. A hexane diol spacer (**C6**) was site-specifically incorporated into select sequences using a commercially available phosphoramidite.

Name	Sequence (5' → 3')
T1a	TCTAGGAGAC**C6**GTCCAGACTC**C6**CTTTCAACTT
T1b/S1b/P1b/H1b	AAGTTGAAAG**C6**CCGCCGATTA**C6**GTGATGTCAT
T1c/S1c	ATGACATCAC**C6**CCGCCGATTA**C6**GTCTCCTAGA
S1a/P1a/H1a	AGGTTTGCTG**C6**CCGCCGATTA**C6**CTTTCAACTT
S1d/P1d/H1d	TCTAGGAGAC**C6**CCGCCGATTA**C6**CAGCAAACCT
P1c/H1c	ATGACATCAC**C6**CCGCCGATTA**C6**TTCGTCACTA
P1e	TAGTGACGAA**C6**CCGCCGATTA**C6**GTCTCCTAGA
H1e	CGAGTGTCAG**C6**CCGCCGATTA**C6**GTCTCCTAGA
H1f	TAGTGACGAA**C6**CCGCCGATTA**C6**CTGACACTCG
T2a	TCTAGGAGAC**C6**GAAACGACAA**C6**CTTTCAACTT
T2b/S2b/P2b/H2b	AAGTTGAAAG**C6**GAAACGACAA**C6**GTGATGTCAT
T2c/S2c	ATGACATCAC**C6**GAAACGACAA**C6**GTCTCCTAGA
S2a/P2a/H2a	AGGTTTGCTG**C6**GAAACGACAA**C6**CTTTCAACTT
S2d/P2d/H2d	TCTAGGAGAC**C6**GAAACGACAA**C6**CAGCAAACCT
P2c/H2c	ATGACATCAC**C6**GAAACGACAA**C6**TTCGTCACTA
P2e	TAGTGACGAA**C6**GAAACGACAA**C6**GTCTCCTAGA
H2e	CGAGTGTCAG**C6**GAAACGACAA**C6**GTCTCCTAGA
H2f	TAGTGACGAA**C6**GAAACGACAA**C6**CTGACACTCG
H1aT10	AGGTTTGCTG**C6**TTTTTTTTTT**C6**CTTTCAACTT

H1bT10	AAGTTGAAAG**C6**TTTTTTTTTT**C6**GTGATGTCAT
H1dT10	TCTAGGAGAC**C6**TTTTTTTTTT**C6**CAGCAAACCT
H1fT10	TAGTGACGAA**C6**TTTTTTTTTT**C6**CTGACACTCG
T3a	TCTAGGAGAC**C6**GTCCAGACTC**C6**CTTTCAACTT
T3b	AAGTTGAAAG**C6**GTCCAGACTC**C6**GTGATGTCA
T3c	ATGACATCAC**C6**GTCCAGACTC**C6**GTCTCCTAGA
LS1	TAATCGGCGG**C6**TTATTAAAGTCTCAG**C6**TTGTCGTTTC
LS2	TAATCGGCGG**C6**TTATTAAAGTCTCAG**C6**TAATCGGCGG
LS3	TTGTCGTTTC**C6**TTATTAAAGTCTCAG**C6**TTGTCGTTTC
LS4	GAGTCTGGAC**C6**TTATTAAAGTCTCAG**C6**GAGTCTGGAC
RS	CTGAGACTTTAATAA

3.5.4 Assembly of 2D DNA polygons

Equimolar amounts of each building block (6.7×10^{-12} moles) were added together at room temperature in 1xTAEMg buffer and allowed to anneal for a total of 5-10 minutes to form discrete products. For each structure, addition of successive component strands generated a discrete intermediate that results from the bimolecular interaction of the 10 base sequences that act to 'clip' the vertices of each 2D polygon together. Addition of the final component strand produces the desired cyclic polygon in a quantitative fashion. After confirming the individual assemblies, stock solutions of each polygon were made by taking 0.70 nmoles of the component strands and adding them together with 10 µL of 10xTAEMg buffer and giving a 10 minute hybridization time before use. The total volume was adjusted to 100 µL with autoclaved water (18.2 MΩ) to give a final 2D DNA polygon **(T1/T2, S1/S2, P1/P2** and **H1/H2)** concentration of 7 µM.

3.5.5 Assembly of 3D DNA prisms

As described in the previous section, each 2D polygon was prepared as a 7 µM stock solution in 1xTAEMg buffer. Stock solutions of both linking strand **LS1** and **RS** were prepared in 1xTAEMg buffer, but at concentrations of 21 µM, 28 µM, 35 µM, and 42 µM. As an example, the step-wise 3D assembly of **TP** is achieved by taking 1 µL of **T1** (7 µM) and adding 1 µL of **LS1** (21 µM). After a 3-5 minute wait time at room

temperature, the triangle is pre-loaded with 3 linking strands now ready for binding with the second polygon. The second triangle **T2** (1 μL, 7 μM) is then added to the mixture, with an additional 3-5 minute wait time, to generate single-stranded 3D prism **TP** (Fig.. Finally, the intervening sequences can be made double-stranded by addition of **RS** (1 μL, 21 μM) to generate **dsTP** (Fig. S4a, Lane 4). Each prismatic structure is generated using a similar protocol, except the correct **LS1**/**RS** stock solutions are used to maintain stoichiometric ratios. 3D structures are left for 5 minutes after addition of the polygons and linking strands, and then are ready for use.

3.5.6 Characterization of 3D constructs using selective enzymatic digestions

Enzymatic protocols used to carry out the characterization of **TP** and **RP** were performed as previously reported.[25,26] The closed, cyclic connectivity of each 3D prism was confirmed using Exonuclease VII (ExoVII) digestion. ExoVII is selective for the digestion of single-stranded open DNA, over that of cyclic closed DNA. In a typical experiment 0.05 nmoles of DNA (total), is placed in 10 uL of TAEMg buffer and subjected to 5 U of ExoVII at 15 °C for 2 hrs. In addition to ExoVII treatment, connectivity of the 3D constructs was further confirmed using mung bean nuclease (MBN). MBN is selective for the digestion of single-stranded DNA over double- stranded DNA by a factor of 30,000. Digestions were again performed as previously reported by addition of 20U of MBN to 0.05 nmoles of DNA (total) in a 1xTAEMg buffer system and allowing the digestion to proceed for 2 hr at 15 °C.

3.6 References

(1) Ajami, D.; Rebek, J., Jr. *Nat. Chem.* **2009**, *1*, 87.

(2) Brown, C. J.; Bergman, R. G.; Raymond, K. N. *J. Am. Chem. Soc.* **2009**, *131*, 17530.

(3) Murase, T.; Horiuchi, S.; Fujita, M. *J. Am. Chem. Soc.* **2010**, *132*, 2866.

(4) Scharnagl, N.; Lee, S.; Hiebl, B.; Sisson, A.; Lendlein, A. *J. Mater. Chem.* **2010**, *20*, 8789.

(5) Vance, D.; Martin, J.; Patke, S.; Kane, R. S. *Adv. Drug Deliv. Rev.* **2009**, *61*, 931.

(6) Scheinberg, D. A.; Villa, C. H.; Escorcia, F. E.; McDevitt, M. R. *Nat. Rev. Clin. Oncol.* **2010**, *7*, 266.

(7) Furukawa, H.; Yaghi, O. M. *J. Am. Chem. Soc.* **2009**, *131*, 8875.

(8) Sharma, J.; Chhabra, R.; Cheng, A.; Brownell, J.; Liu, Y.; Yan, H. *Science* **2009**, *323*, 112.

(9) Chen, J. H.; Seeman, N. C. *Nature* **1991**, *350*, 631.

(10) Shih, W. M.; Quispe, J. D.; Joyce, G. F. *Nature* **2004**, *427*, 618.

(11) Goodman, R. P.; Schaap, I. A.; Tardin, C. F.; Erben, C. M.; Berry, R. M.; Schmidt, C. F.; Turberfield, A. J. *Science* **2005**, *310*, 1661.

(12) Erben, C. M.; Goodman, R. P.; Turberfield, A. J. *Angew. Chem. Int. Ed.* **2006**, *45*, 7414.

(13) Zimmermann, J.; Cebulla, M. P.; Monninghoff, S.; von Kiedrowski, G. *Angew. Chem. Int. Ed.* **2008**, *47*, 3626.

(14) Goodman, R. P.; Heilemann, M.; Doose, S.; Erben, C. M.; Kapanidis, A. N.; Turberfield, A. J. *Nat. Nanotechnol.* **2008**, *3*, 93.

(15) Bhatia, D.; Mehtab, S.; Krishnan, R.; Indi, S. S.; Basu, A.; Krishnan, Y. *Angew. Chem. Int. Ed.* **2009**, *48*, 4134.

(16) Lo, P. K.; Metera, K. L.; Sleiman, H. F. *Curr. Opin. Chem. Biol.* **2010**, *14*, 597.

(17) Rothemund, P. W. *Nature* **2006**, *440*, 297.

(18) Andersen, E. S.; Dong, M.; Nielsen, M. M.; Jahn, K.; Subramani, R.; Mamdouh, W.; Golas, M. M.; Sander, B.; Stark, H.; Oliveira, C. L.; Pedersen, J. S.; Birkedal, V.; Besenbacher, F.; Gothelf, K. V.; Kjems, J. *Nature* **2009**, *459*, 73.

(19) Kuzuya, A.; Komiyama, M. *Chem. Commun.* **2009**, 4182.

(20) Douglas, S. M.; Dietz, H.; Liedl, T.; Hogberg, B.; Graf, F.; Shih, W. M. *Nature* **2009**, *459*, 414.

(21) Dietz, H.; Douglas, S. M.; Shih, W. M. *Science* **2009**, *325*, 725.

(22) Liedl, T.; Hogberg, B.; Tytell, J.; Ingber, D. E.; Shih, W. M. *Nat. Nanotechnol.* **2010**, *5*, 520.

(23) He, Y.; Ye, T.; Su, M.; Zhang, C.; Ribbe, A. E.; Jiang, W.; Mao, C. *Nature* **2008**, *452*, 198.

(24) Ko, S. H.; Su, M.; Zhang, C.; Ribbe, A. E.; Jiang, W.; Mao, C. *Nat. Chem.* **2010**, *2*, 1050.

(25) Aldaye, F. A.; Sleiman, H. F. *J. Am. Chem. Soc.* **2007**, *129*, 13376.

(26) Yang, H.; McLaughlin, C. K.; Aldaye, F. A.; Hamblin, G. D.; Rys, A. Z.; Rouiller, I.; Sleiman, H. F. *Nat. Chem.* **2009**, *1*, 390.

(27) Aldaye, F. A.; Palmer, A. L.; Sleiman, H. F. *Science* **2008**, *321*, 1795.

(28) Aldaye, F. A.; Lo, P. K.; Karam, P.; McLaughlin, C. K.; Cosa, G.; Sleiman, H. F. *Nat. Nanotechnol.* **2009**, *4*, 349.

(29) Lo, P. K.; Karam, P.; Aldaye, F. A.; McLaughlin, C. K.; Hamblin, G. D.; Cosa, G.; Sleiman, H. F. *Nat. Chem.* **2010**, *2*, 319.

(30) Yang, H.; Sleiman, H. F. *Angew. Chem. Int. Ed.* **2008**, *47*, 2443.

3.7 Introduction to Chapter 4

The approaches developed in chapters 2 and 3 show that assembly of 3D DNA structures containing additional single-stranded sites is a new method in DNA nanotechnology to give quantitative yields, room temperature assembly, assembly at higher concentrations and ease of functionalization. Given the fact that the field of DNA nanotechnology typically uses highly DNA dense and double-stranded structures, we wondered whether we can go the other way: how 'DNA-minimal' can we go? In this way, design and development of a 3D DNA construction method that brings together many single-stranded DNA arms into well-defined geometries is highly desirable. As with the methods discussed so far, the 3D DNA method should be both 'economic' in design and maximize addressability and organization of components on the nanometer length scale.

Chapter 4: Three-Dimensional Organization of Block Copolymers on "DNA-Minimal" Scaffolds

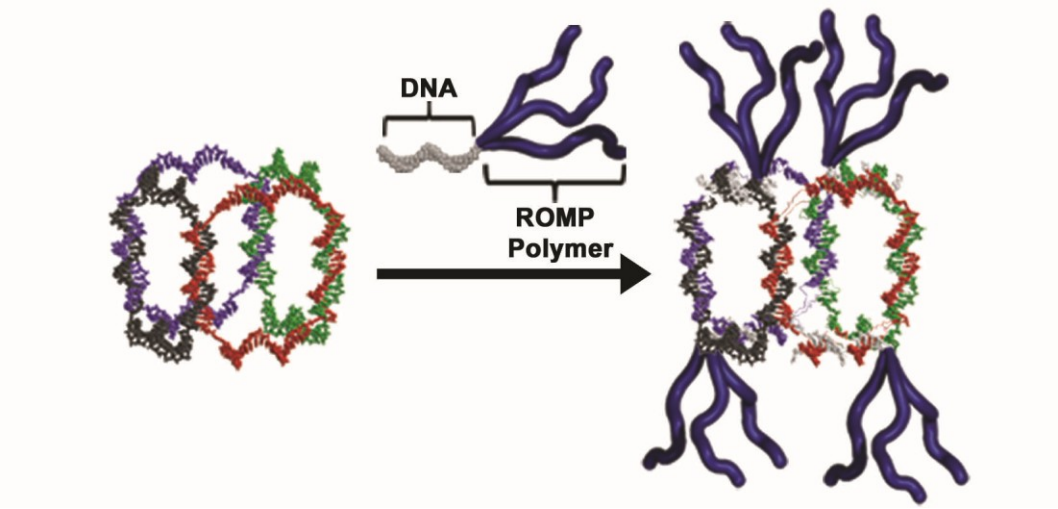

Reproduced with permission from; "Three-Dimensional Organization of Block Copolymers on "DNA-Minimal" Scaffolds", McLaughlin, C. K., Hamblin, G. D., Hanni, K. D., Conway, J. W., Nayak, M. K., Carneiro, K. M., Bazzi, H. S. and Sleiman, H. F. *J. Am. Chem. Soc.,* **2012**, 134, 4280-4286. American Chemical Society (2012).

4.1 Abstract

In this chapter, a 3D-DNA construction method that assembles a minimum number of DNA strands in quantitative yield, to give a scaffold with a large number of single-stranded arms, is introduced. This DNA frame is used as a core structure to organize materials in 3D as the shell. Ring-opening metathesis polymerization (ROMP) is used to generate block copolymers that are covalently attached to DNA strands. Site-specific hybridization of these DNA-polymer chains on the single-stranded arms of the 3D-DNA scaffold gives efficient access to DNA-block copolymer cages. These biohybrid cages possess polymer chains that are programmably positioned in three dimensions on a DNA core and display increased nuclease resistance as compared to unfunctionalized DNA cages.

4.2 Introduction

Three-dimensional (3D) DNA structures hold promise for numerous applications, from biological probes and drug delivery tools to organizational scaffolds. Unlike most nanomaterials, they provide fine control over geometry, precise and monodisperse sizes, symmetric or asymmetric positioning of molecules, and molecule-responsive switching of structure.[1-3] Conventional methods to make 3D-DNA structures, such as DNA origami[4-9] or tile-based assembly,[10-17] result in double- stranded, DNA-dense structures. Typically, these types of structures lack geometrically positioned single-stranded DNA, making placement of materials difficult in a selective and well-defined manner.

In this chapter, 3D-DNA assembly is approached from an alternative, "DNA-economic" perspective: Can a minimum number of DNA strands be used to create geometrically well- defined 3D-scaffolds, which contain a large number of single- stranded arms? These scaffolds would be able to act as a core structure that guides the site-specific organization of other materials as their shell. This method simply uses DNA to guide other functional structures into three-dimensional arrangements, but the materials generated can be richer in other functionalities than previously reported 3D-DNA structures.

Synthetic polymers are a particularly attractive class of materials with which to "coat" 3D-DNA scaffolds. They can be engineered for stability, biocompatibility, cell penetrating ability, increased circulation time, and decreased toxicity, and they can introduce multiple functionalities into typically passive DNA structures.[18-21] Polymers with attached DNA strands have previously been made[22,23] and were found to associate into responsive micellar structures and ordered nanofibers. [24-29] Recent work has also explored the use of DNA−polymer conjugates in a number of materials science[28,30] and biological[31-33] applications.

Construction of a new class of biohybrid materials, where synthetic polymer chains are programmably positioned in three-dimensions using DNA cages as scaffolds, is outlined in this chapter. A cubic DNA structure, containing eight

single-stranded arms, is generated in a facile manner and excellent yield using only a minimum number of component strands. Polymer−DNA conjugates are synthesized through covalent attachment of a ROMP block copolymer to a short DNA strand. These conjugates efficiently hybridize to the individual arms of the DNA scaffolds to produce block-copolymer DNA cages that are more nuclease-resistant than the unfunctionalized DNA cages, making them potential candidates for applications such as responsive biological probes and drug delivery tools.

On a fundamental level, block copolymers are able to undergo self-assembly into a number of useful morphologies, which can be typically controlled by polymer composition, block compatibility, and solvent conditions.[34] The block copolymer-DNA cages shown here introduce new parameters to control morphology, such as the geometry of the DNA scaffold, the 3D-orientation of the polymer chains, and the environmentally responsive nature of DNA assembly. They can thus expand the morphological range that can be obtained from these materials.

4.3 Results and discussion

4.3.1 Design, assembly and characterization of DNA cube C

The strategy presented simplifies the design of 3D-DNA structures and allows for maximized functionality using single-stranded sequences. Fig. 4.1a shows this approach for synthesizing a DNA cube, illustrating that when one DNA strand hybridizes with the next, its two extremities form a pseudocatenated, cyclic structure. Thus, if a cube is required, four such DNA strands (C1−C4) are connected to each other, with the fourth strand hybridizing to the first to close the cube. Each of these cyclized strands is one face of the final 3D-structure. This approach is inspired by the early and seminal contributions of Seeman and co-workers to 3D DNA assembly.[10] However, in contrast to this previous process, this method results in quantitative assembly yields, does not require ligation steps, and, for the first time, produces 3D-structures with a maximum number of single-stranded regions for further functionalization. Cube **C** is comprised of four 80-

nucleotide strands containing four hexanediol (C6) insertions at the junctions where the structure makes the square. Previous reports showed that these insertions increase flexibility and reduce strain, allowing formation of the self-assembled DNA structure in higher yield. [35,36]

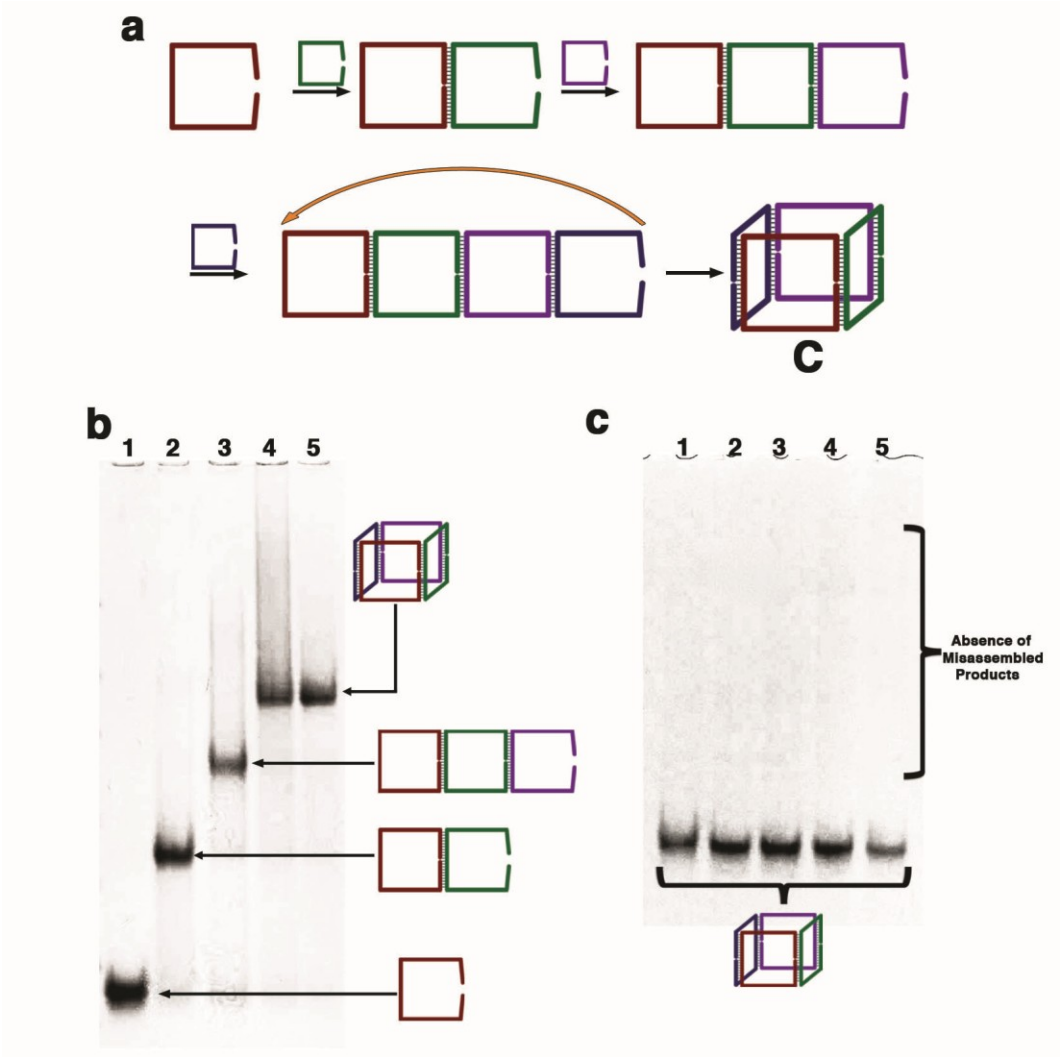

Figure 4.1 3D DNA design and assembly. **a,** Schematic representation of the stepwise self-assembly of DNA cube **C**. **b,** Native PAGE analysis of the assembly of **C** under native conditions using four component DNA strands C1−C4; Lane 1 C1, lane 2 - C1 + C2, lane 3 - C1 + C2 + C3, lane 4 - C1 + C2 + C3 + C4 (i.e. **C**) and lane 5 - C1 + C2 + C3 + C4 after a slow anneal cycle. **c,** Assembly of strands C1-C4 and native PAGE analysis; Lane 1- 250 nM, lane 2- 500nM, lane 3- 1.25 μM, lane 4 – 2.5 μM and lane 5 - 5 μM

The DNA cube scaffold was assembled from these component strands at room temperature in a sequential manner and monitored by polyacrylamide gel electrophoresis (PAGE) under native conditions (Fig. 4.1b). Successive additions of the four component strands generated bands of reduced mobility, indicating successful hybridization of each component (lanes 1−4) to produce the 3D nanostructure in excellent yield (lane 4). Heating to 95 °C and slowly cooling the four component strands together in one pot over 3 h yielded quantitative formation of **C** at a final concentration of 1.25 μM (lane 5). Additional experiments also revealed clean assembly of **C** at higher concentrations (up to 5 μM, Fig. 4.1c). This again contrasts our methods with 3D DNA strategies from other labs, which require very low starting DNA concentrations. The connectivity of **C** was confirmed using digestion with exonuclease VII (ExoVII). This bidirectional nuclease selectively cleaves single-stranded, open form DNA structures over closed form DNA assemblies. DNA cube **C** did not degrade after ExoVII was added, confirming the closed nature of the assembled 3D-product (Fig. 4.2).

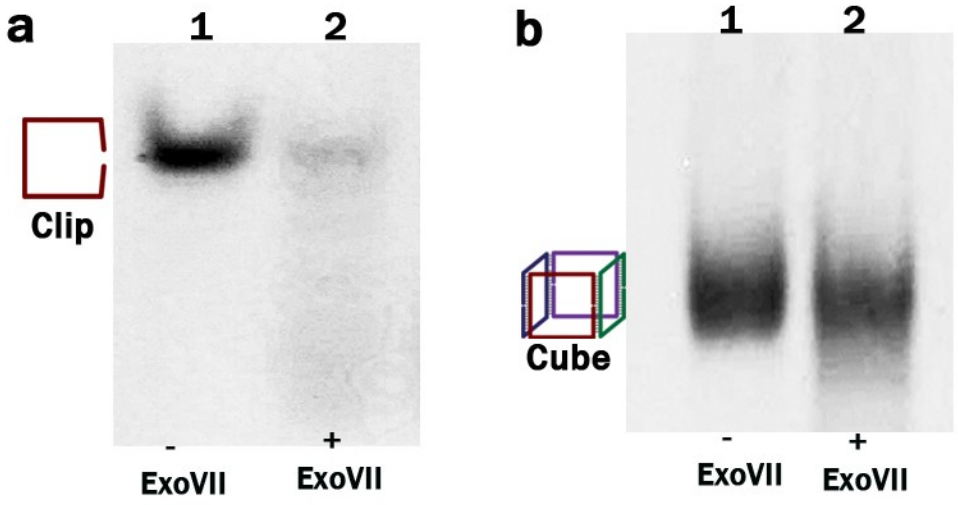

Figure 4.2 Connectivity analyses using ExoVII. Both a single clip (a) and DNA cube (b) were (Lane 1, respectively) were subjected to treatment with ExoVII (Lane 2, respectively). Enzymatic digestions were both analyzed by PAGE under native conditions (6%).

The assembled DNA cage contains eight single-stranded regions, each 20 bases long, that can be used for further self- assembly (Fig. 4.3a). Each of these regions can possess a different DNA sequence, allowing the independent, site-specific positioning of different functional groups on this frame. In the first iteration of the DNA cube, the design was simplified such that sequence symmetry was introduced into the single-stranded regions on both the top and the bottom faces (Fig. 4.3a). As indicated in Figure 4.3a, each 80 unit strand is designed in such a way that four strands of sequence **a** assemble on one cube face and four strands of sequence **b** assemble on the opposite face. We used native PAGE analysis to verify that all eight sides are available to hybridize with the complementary DNA (cDNA) strands (Fig. 4.3b). Adding 4 equiv of complementary strand **a′** to **C** (lane 1) cleanly generates a structure with four occupied sites (lane 2). Adding complementary strand **b′** yields the fully double-stranded product, referred to as **dsC**, in excellent yield (lane 3). Dynamic light scattering (DLS) was performed to evaluate the physical dimensions of **C** in solution (Fig. 4.3c). An apparent hydrodynamic radius of 5.5 ± 0.6 nm was determined for **C**, which matches well with the calculated theoretical Rh value of 5.8 nm.

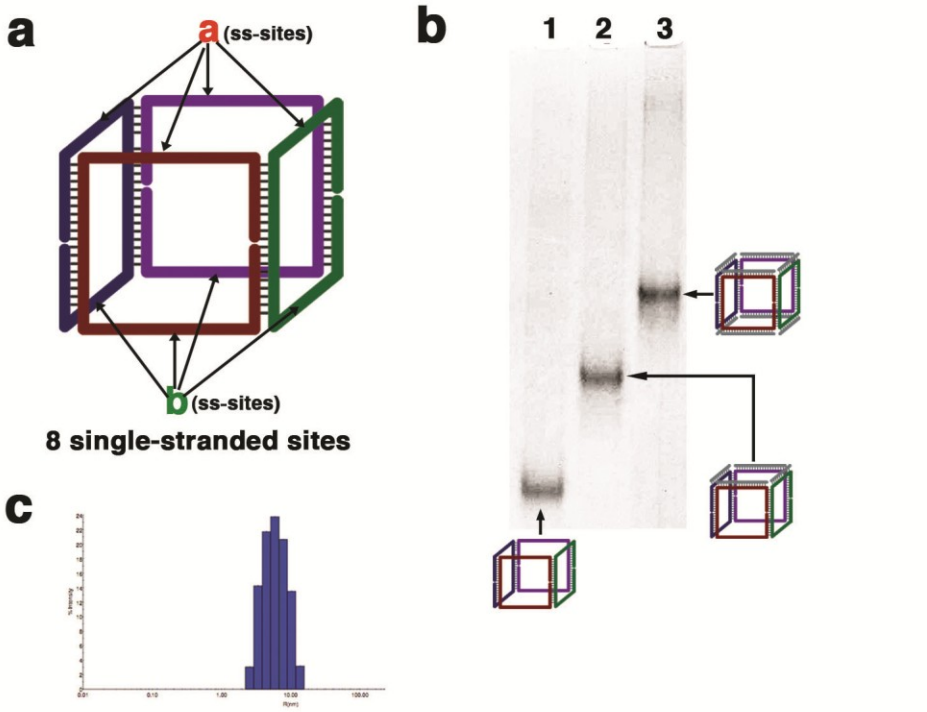

Figure 4.3 Characterization of DNA cube of C. a, Schematic representation of DNA cube **C** showing sequence symmetry within each single-stranded face. The top face contains 4x sequence **a**, and the bottom face displays 4x sequence **b**. **b,** PAGE analysis under native conditions showing the hybridization of complement sequences to the single-stranded regions on the DNA cube; Lane 1 – **C**, lane 2 - **C** + 4×**a′**, lane 3 - **C** + 4×**a′** + 4×**b′**. **c,** Dynamic light scattering (DLS) results obtained for single-stranded DNA cube **C**. An average hydrodynamic radius (Rh) of 5.5 ± 0.6 nm was obtained.

The strongest evidence for the formation of the 3D cubic architecture was provided by cryogenic electron microcopy (cryo-EM), a technique that helps to preserve the native environment of self-assembled structures.[5,11,13,17,37] To generate more uniform contrast, cryo-EM imaging was performed on fully double-stranded DNA cube **dsC**, where each of the eight single-stranded regions is hybridized with complementary strands (4× **a′**, 4× **b′**). A typical cryo-EM field of view (Fig. 4.4a) shows numerous single particles, some of which have been enclosed as the areas of contrast within the red squares. Closer inspection of these individual projections reveals a cubic geometry (Fig. 4.4b) that supports the assigned structure, with each area of contrast displaying dimensions that fit one or more of the 20 unit duplex DNA regions of the structures. Imaging of single-stranded cube **C** (data not shown) was similar to those obtained for the fully

double-stranded system. The major distinction here, though, is that it was more difficult to visualize a detailed projection of the 3D structure embedded in the vitreous ice. Cryo-EM analysis, in tandem with single-particle reconstruction techniques, is currently underway to try and obtain a detailed electron density map for these self-assembled 3D DNA structures.

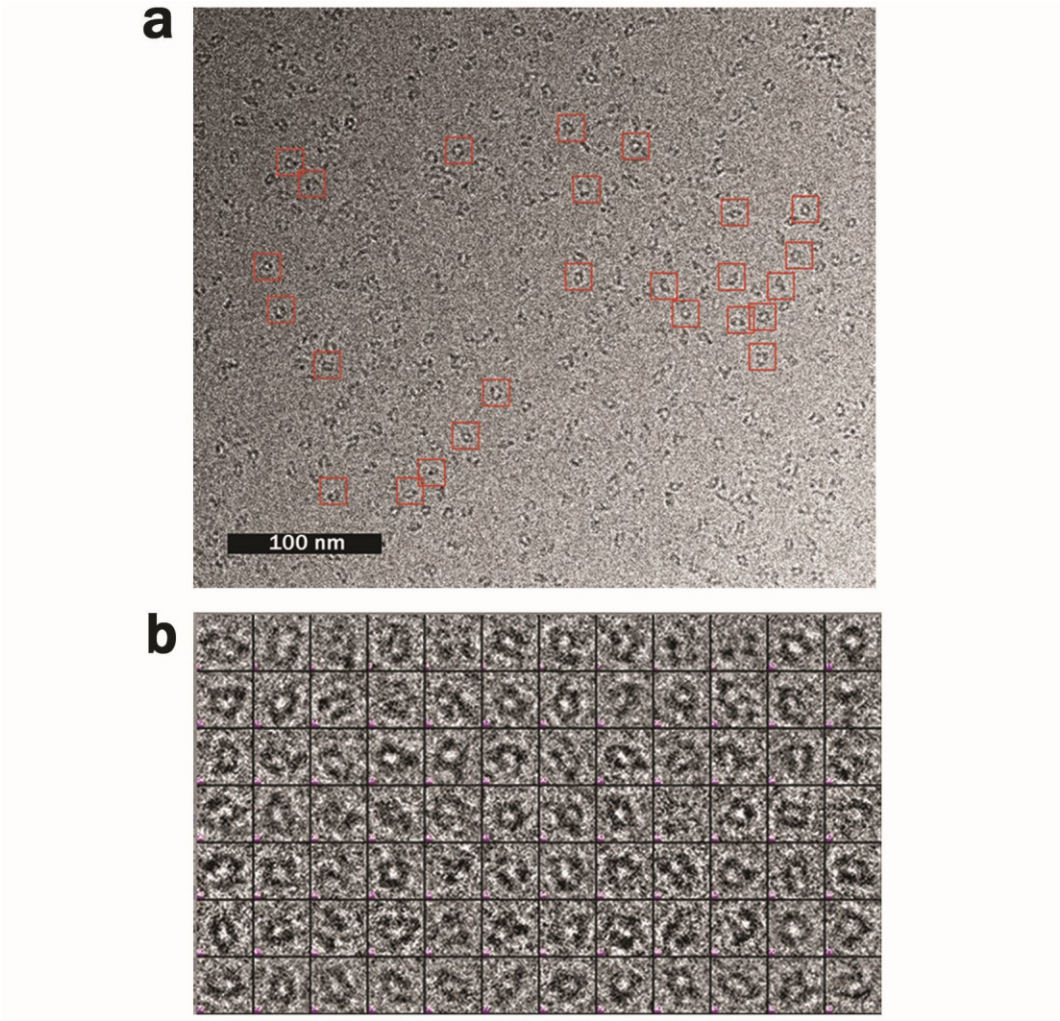

Figure 4.4 Analysis of dsC by cryo-EM. **a,** Typical cryo-EM field of view generated after imaging **dsC** (7 μM). Red boxes enclose areas of contrast that are assigned to the cubic DNA structure. **b,** Collected cryo-EM projections that correlate well with the modeled dimensions of **dsC** and reveal detailed facets of the designed cubic structure.

In addition, atomic force microscopy (AFM) imaging of **dsC** is consistent across a range of concentrations under dry conditions. A typical AFM field of view (Fig. 4.5a) shows relatively uniform particles with a narrow size distribution.

Height measurements on this architecture revealed an average value of 0.6 ± 0.2 nm. The small height value in combination with the ability to see an interior cavity in certain projections indicates that the structure likely strongly adsorbs to the mica substrate and becomes dehydrated to cause flattening.[13,17] Similar results were obtained for single-stranded **C**, although the structures showed less uniform contrast by cryo-EM imaging as compared to **dsC** (Fig. 4.5b). Analysis of AFM images for **C** revealed a slightly smaller average height (0.4 ± 0.2 nm) than that obtained for the **dsC**. Still, it should be noted that AFM imaging under dehydrated conditions is not ideal for small, flexible soft materials such as 3D DNA cubes as it is difficult to obtain reliable structural dimensions. The cryo-EM data provided in Figure 4.4 better allow for elucidation of structural features in the expected size regime for these types of self-assembled objects.

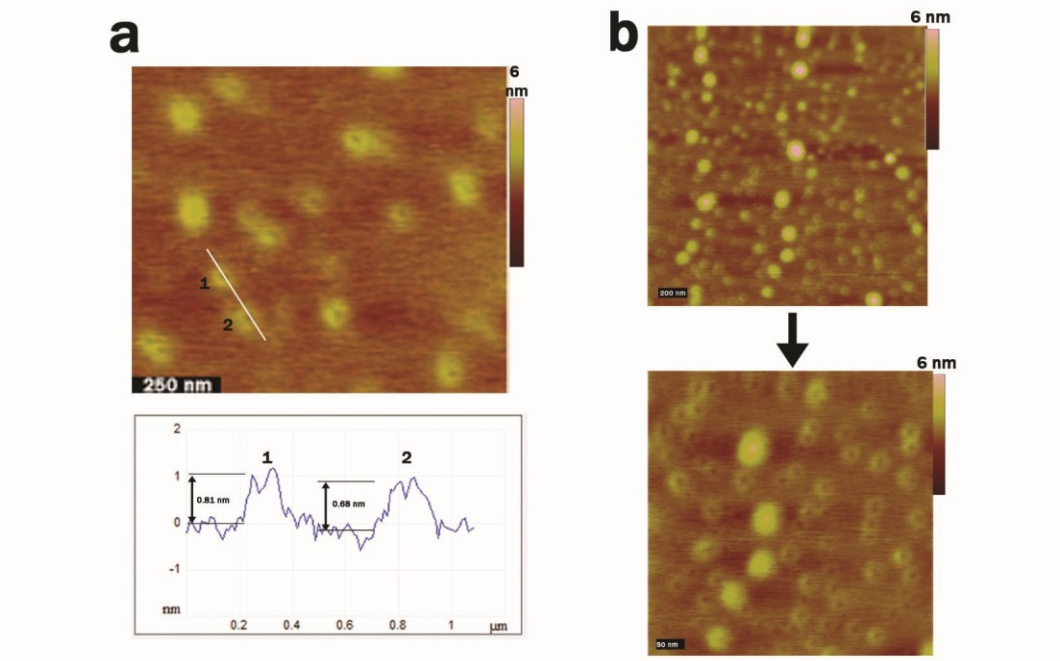

Figure 4.5 Characterization of DNA cubes by AFM. a, Top: Typical AFM field of view (height image) obtained for **dsC** showing the relatively monodisperse nature of the DNA architecture. The white line indicates where a height measurement was taken for structures labeled 1 and 2. Bottom: Height analysis of structures 1 and 2. **b,** Top - Typical AFM field of view (2 µm) obtained for cube **C**. Bottom – zoom in on the AFM field of view. Analysis of the structures reveal an average height of 0.4 ± 0.2 nm.

4.3.2 Synthesis and conjugation of ROMP polymer to DNA

With the single-stranded DNA cube **C** in hand, a DNA block copolymer capable of site-specifically hybridizing to this structure could be prepared (Figure 4.6a). A short diblock copolymer **P** was synthesized by living ring-opening metathesis polymerization (ROMP) of ring-strained, substituted oxanorbornene imide monomers (Figure 4.6a).[38] The first block contains macromonomers, each substituted with a long polyethylene glycol $(PEG)_{44}$ chain, while the second block contains an N-hydroxysucciminimide activated carboxylic acid substituent. Polymerization was carried out using the generation III Grubbs catalyst in dichloromethane under inert atmosphere. NMR analysis revealed a final polymer composition consistent with the monomer to initiator ratio used, and gel permeation chromatography (GPC) showed a narrow molecular weight distribution (polydispersity index PDI = 1.13, Figure 4.6b). This data is consistent with the living character of the ROMP reaction used to generate diblock copolymer **P**,[38] now amenable for conjugating to DNA.

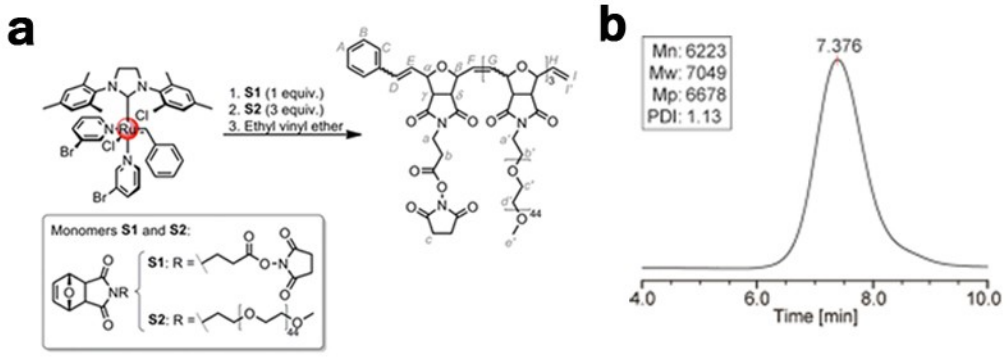

Figure 4.6 Synthesis and characterization of polymer P. a, Schematic representation for the preparation of polymer **P** using ROMP. **b,** GPC trace obtained for **P** in DMF. PDI was measured as 1.13.

Even with a narrow molecular weight distribution, synthetic polymers do not rival the monodisperse nature of biological macromolecules such as DNA. Thus, conjugation of ROMP polymers with DNA could help to isolate more monodisperse conjugates. Diblock polymer **P** was reacted with 3′-amine-functionalized DNA strand **D** in a borate buffer (0.1 M, pH 8) at room

temperature for 2 days as indicated in Figure 4.7a. Analysis of the reaction mixture by PAGE under denaturing conditions revealed the presence of two main products significantly retarded in mobility as compared to the amine-DNA starting material (Figure 4.7bi, denoted by red arrows). The slowest moving band was isolated to give a clean product, as observed by denaturing PAGE (Figure 4.7bii). Analysis by matrix assisted laser desorption ionization (MALDI) mass spectrometry indicated a molecular weight that matches the theoretical mass of a $(PEG)_3$−$(DNA)_1$ conjugate, which contains one DNA strand and three PEG repeat units (Fig. 4.7c). Although the yields were moderate for solution-based attachment of DNA to the activated ROMP polymer, the conjugate is more monodisperse due to the uniform nature of DNA, and to the ability to separate the conjugates by gel electrophoresis.

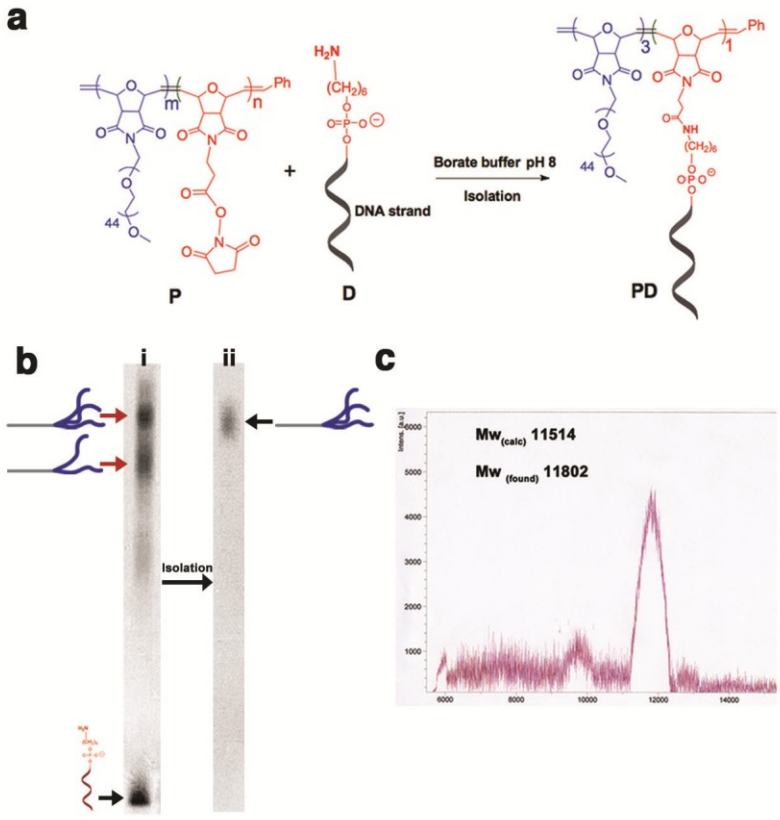

Figure 4.7 Polymer conjugation to DNA. a, Schematic representation of the conjugation between amine modified DNA **D** and diblock copolymer **P**. **b,** Denaturing PAGE analysis (12%) of the crude conjugation mixture. (i) Black arrow denotes starting material, and red arrows denote major products formed. Isolation of the slowest moving species and reanalysis by PAGE (ii) reveals the pure conjugate product **PD**. **c,** MALDI spectrum obtained for **PD**.

4.3.3 Organization of conjugate PD onto DNA cubes

To demonstrate the capacity of these DNA structures for programmable 3D-organization, asymmetric versions of the cube **C1a**−**C3a** with precisely positioned binding sites of sequence a that are complementary to block copolymer−DNA conjugate **PD** were prepared (Figure 4.8a). Poly(thymidine) tracts (T14) were incorporated into specific single-stranded positions of the cubes to eliminate binding of polymer−DNA conjugate **PD**. Structure **C1a**, containing only one binding site, was first hybridized with 1 equiv of the **PD**. This resulted in a single band by PAGE under native conditions (Figure 4.8b, lane 2) with reduced mobility as compared to unsubstituted cube **C** (Figure 4.8b, lane 1). This structure was assigned to the singly substituted cube **C1a-PD$_1$**, with one site occupied by PEG$_3$-ROMP polymer **P**.

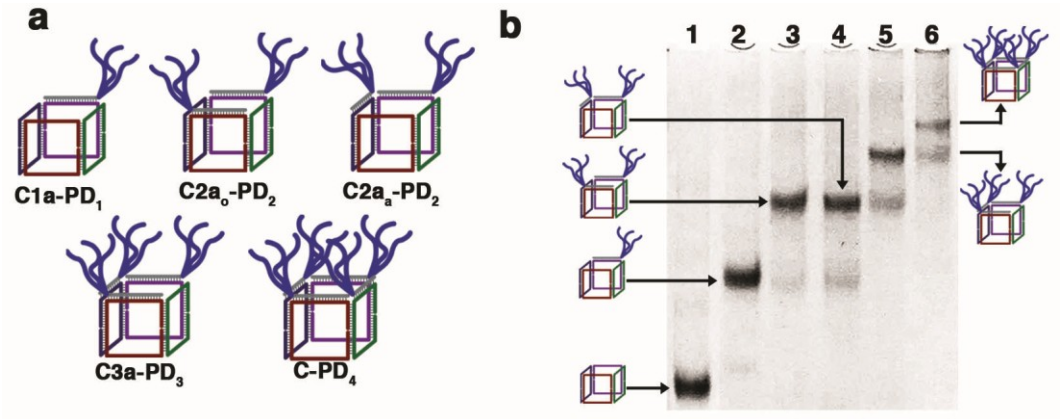

Figure 4.8 Organizing DNA−polymer conjugate onto 3D DNA scaffold. a, Schematic representations of DNA cubes with site-specifically arranged polymer conjugate **PD**. **b**, Native PAGE analysis of cubes **C1a**−**C3a** hybridized to DNA−polymer conjugate **PD**; Lane 1 – **C**, lane 2 - **C1a** + 1 equiv of **PD**, lane 3 - **C2a$_o$** + 2 equiv of **PD**, lane 4 - **C2a$_a$** + 2 equiv of **PD**, lane 5 - **C3a** + 3 equiv of **PD** and lane 6 – **C** + 4 equiv of **PD**.

Because of the programmability of the single-stranded regions, two **a** binding sites could be positioned in either an opposite (**C2a$_o$**) or an adjacent (**C2a$_a$**) orientation within a cubic face. Hybridization with 2 equiv of **PD** to **C2a$_o$** (Figure 4.8b, lane 3) gave a near quantitative yield of a single band of reduced

mobility as compared to the monosubstituted cube, indicating that a DNA cube had been generated with two PEG_3-ROMP polymers site-specifically positioned on opposite faces (**C2a$_o$-PD$_2$**). Adding the DNA−polymer conjugate to **C2a$_a$** also generated disubstituted cube **C2a$_a$-PD$_2$** in good yield (Figure 4.8b, lane 4). A small amount of monosubstituted cube was observed in this case, suggesting that the six adjacent PEG chains on this cube may be sterically crowded, thus slightly reducing the yield.

When a cube containing three adjacent binding sites (**C3a**) was hybridized with 3 equiv of **PD**, a major band that is assigned to trisubstituted cube **C3a-PD$_3$** with nine PEG_{44} chains was observed, along with a minor band with the same mobility as a disubstituted cube (Figure 4.8b, lane 5). With four adjacent binding sites (**C**), tetrasubstituted cube **C-PD$_4$** with 12 PEG_{44} chains was obtained, showing a more sizable band for a trisubstituted byproduct (Figure 4.8b, lane 6). As a control, 20 equiv of **PD** was added to **C** and resulted in no change to the product distribution, indicating that stoichiometry was not a contributing factor (Fig. 4.9). The trend in electrophoretic mobilities for each polymer-bound 3D-DNA architecture indicates that sterics may influence hybridization, especially when binding sites are arranged in an adjacent fashion.

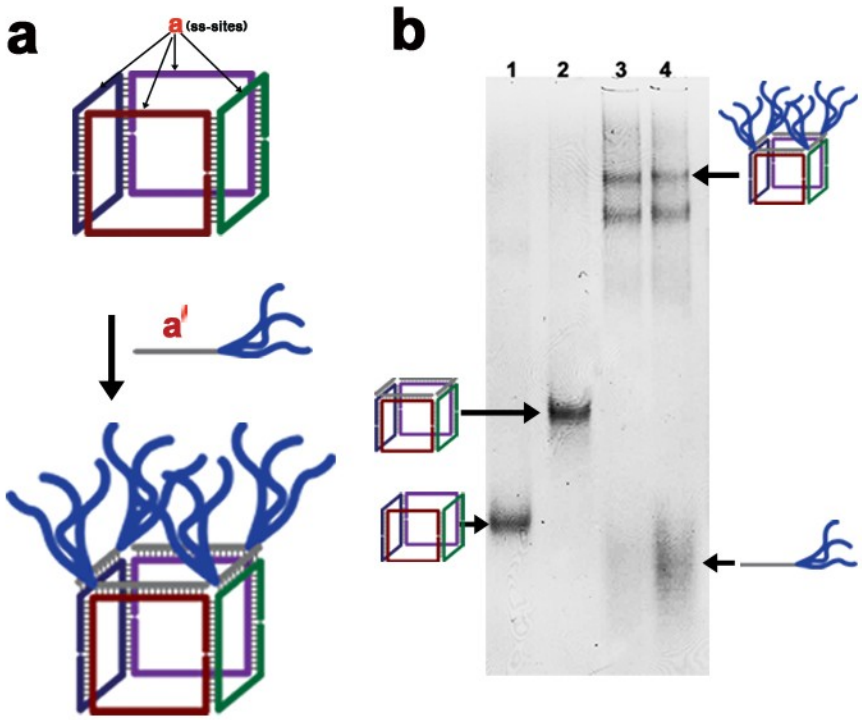

Figure 4.9 a, Schematic representation of cube **C** with 4 available **a** binding sites that can hybridize to DNA-polymer conjugate **PD** creating a structure with 4 organized polymers on a single cubic face. **b**, Native PAGE analysis of DNA-polymer addition to **C**; Lane 1 – **C**, Lane 2 – **C** + **a'** (1:1, **a'**:**C**), Lane 3 – **C** + Polymer conjugate (1:1, **PD**:**C**) and Lane 4 - **C** + Polymer conjugate (5:1, **PD**:**C**)

To test how orientation of the single-stranded regions may influence hybridization to our DNA−polymer conjugate, cubic structure **C4a$_o$**, which orients sequence a on opposite sides of the top and bottom cubic faces as depicted in Fig. 4.10a, was prepared. Such an arrangement could help to offset the steric effects from DNA−polymer conjugate binding. As compared to binding two polymer−DNA conjugates (Fig. 4.10b, lane 1), native PAGE analysis of this new arrangement reveals a major band that can be assigned to cube **C4a$_o$-PD$_4$** with four polymers bound (lane 2), and a smaller amount of the triply bound species.

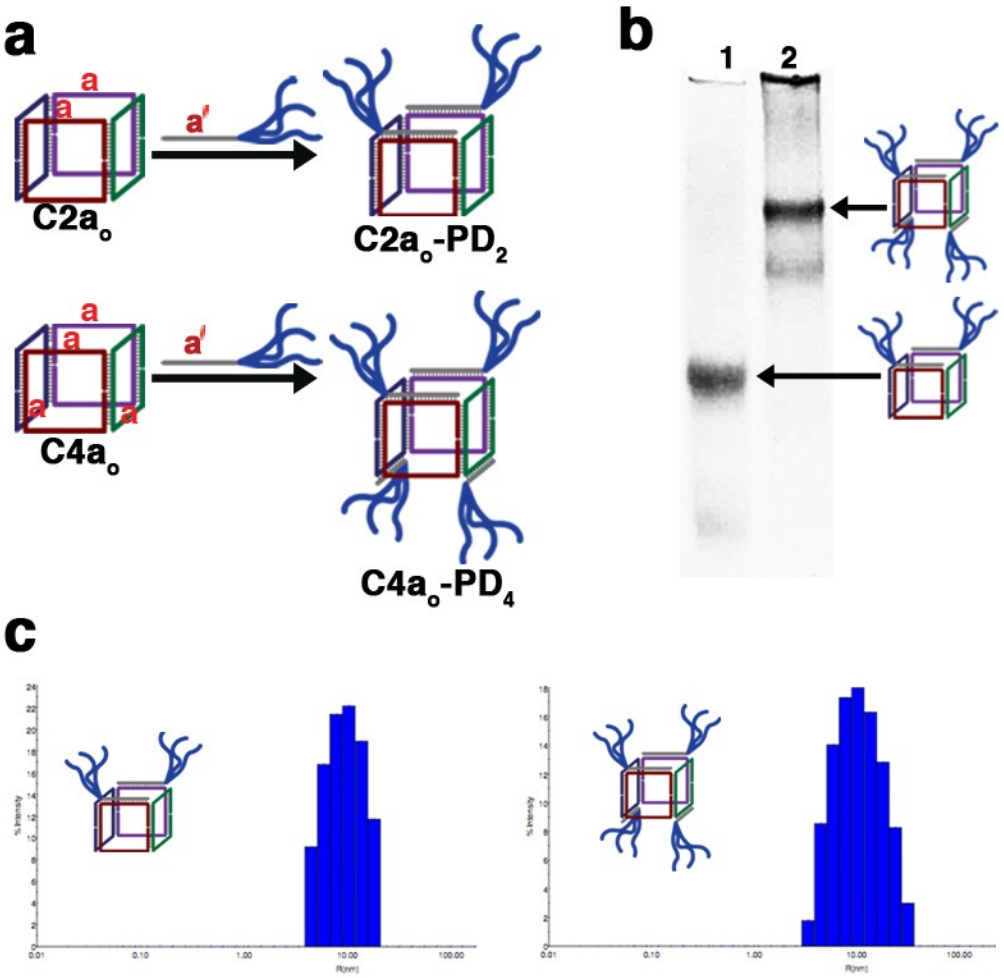

Figure 4.10 Programmable organization of DNA−polymer conjugates onto a 3D scaffold. **a,** To help reduce sterics and maximize the number of DNA−polymer conjugates bound to the DNA cube, structure **C4a$_o$** was designed to place two single-stranded sites on one cubic face and two sites perpendicular to these on the opposite face. **b,** Native PAGE analysis of DNA-containing cubes **C2a$_o$-PD$_2$** (lane 1, 2 equiv of **PD**) and **C4a$_o$-PD$_4$** (lane 2, 4 equiv of **PD**). **c,** Typical DLS histograms obtained for (left) **C2a$_o$-PD$_2$** and (right) **C4a$_o$-PD$_4$**. The 1xTAEMg buffer peak has been removed in each case.

In addition to PAGE, DLS studies showed that the DNA cube size increases as varying amounts of polymer were added (Fig. 4.10c). The average experimental Rh values of 8.9 ± 1.0 nm (**C2a$_o$-PD$_2$**) and 10.5 ± 1.2 nm (**C4a$_o$-PD$_4$**). These results indicate successful hybridization of the DNA−polymer conjugate onto the 3D-DNA scaffold.

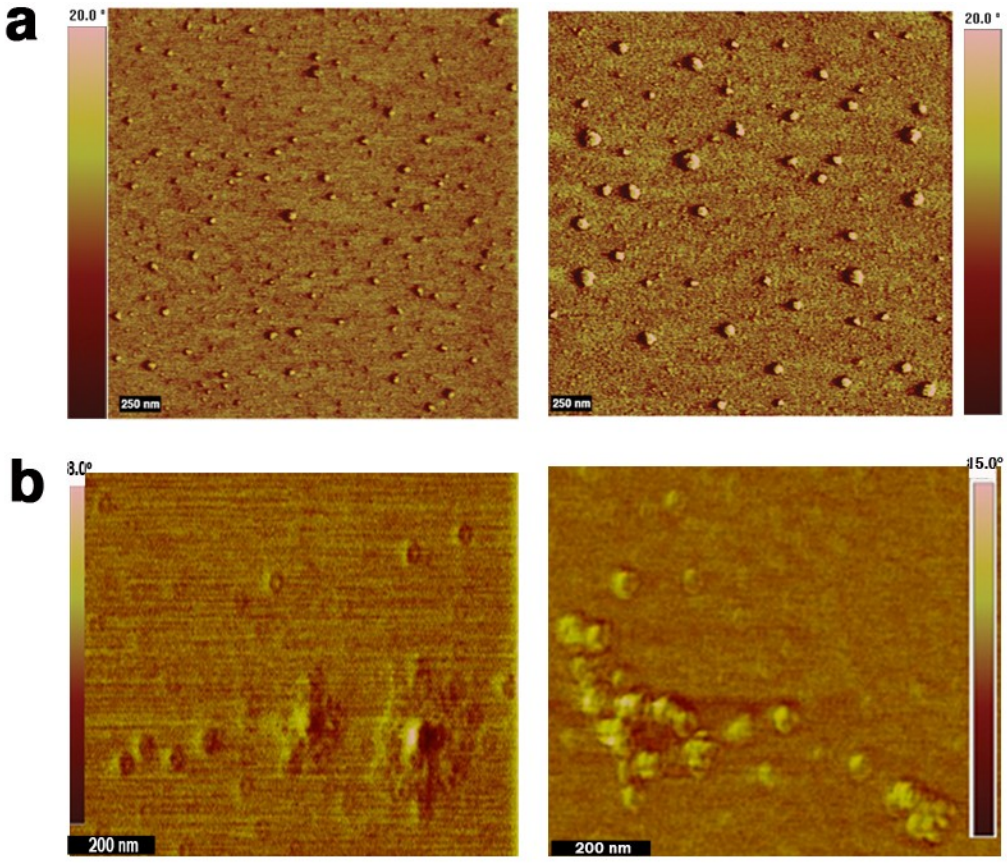

Figure 4.11 AFM characterization of DNA−polymer conjugates organized on 3D cubes. **a,** AFM images for **C2a$_o$-PD$_2$** (left) and **C4a$_o$-PD$_4$** (right) at a 3D concentration of 50 nM. Phase images shown. **b,** AFM images for **C2a$_o$-PD$_2$** (left) and **C4a$_o$-PD$_4$** (right) at a 3D concentration of 10 nM. Phase images shown.

AFM imaging of the site-specifically organized DNA−polymer conjugates onto **C** also displayed distinct differences depending on the architecture being imaged. Samples of **C2a$_o$-PD$_2$** and **C4a$_o$-PD$_4$** were prepared at both 10 and 50 nM concentrations for AFM imaging (Fig. 4.11). At 50 nM, aggregates were observed, likely the result of interactions between the polymer chains organized onto the DNA scaffolds and drying effects on the mica surface (Fig. 4.11a). Analysis of these particles revealed average heights of 1.5 ± 0.3 nm (**C2a$_o$-PD$_2$**) and 2.2 ± 0.4 nm (**C4a$_o$-PD$_4$**). In an effort to reduce aggregation effects, C4ao-PD4 and C4ao-PD4 were imaged at 10 nM (Fig. 4.11b). Fewer aggregate domains were observed, and analysis at this concentration produced height values of 0.8 ± 0.1 nm (**C2a$_o$-PD$_2$**) and 0.9 ± 0.20 nm (**C4a$_o$-PD$_4$**). Taking into consideration an

average height of 0.6 ± 0.2 nm recorded for DNA-only structure **dsC**, overall height comparisons between **C2a$_o$-PD$_2$** and **C4a$_o$-PD$_4$** support the site-specific organization of the DNA−polymer conjugate **PD** onto these 3D DNA scaffolds. To our knowledge, these studies constitute the first examples of using three-dimensional scaffolds to organize block copolymers in a programmable way in 3D-space. This approach is expected to significantly increase the morphological range possible with block copolymers.

4.3.4 Initial assessment of nuclease stability

To gain insight into the sensitivity of the DNA cube to nucleases, with and without organized synthetic polymer, these architectures were studied under conditions that more closely mimic the physiological environment. Each structure (**C**, **C2a$_o$-PD$_2$**, and **C4a$_o$-PD$_4$**) was prepared and subjected to digestion with a 10% solution (v/v) of fetal bovine serum (FBS), which contains a milieu of nonspecific nucleases commonly found in the *in vitro* assays. A control double-stranded DNA **NC** was digested by FBS (37 °C) in 2 h (Fig. 4.12a). The single-stranded DNA structure **C** shows a similar FBS digestion profile (Fig. 4.12b) as compared to **NC**.

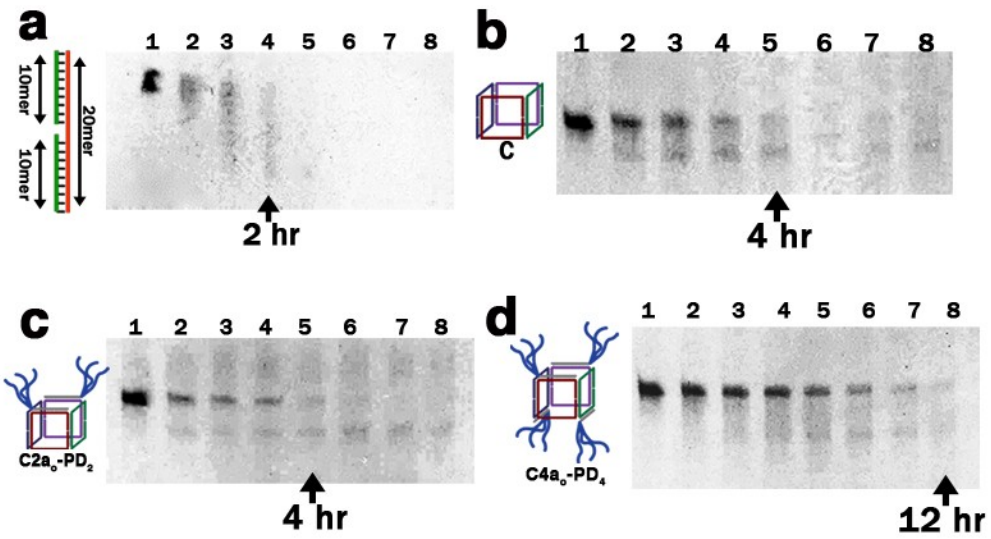

Figure 4.12 FBS digestion. Denaturing PAGE analysis (12%) of time points taken from FBS assay preformed on (**a**) control structure NC, (**b**) **C**, (**c**) **C2a$_o$-PD$_2$** and (**d**) **C4a$_o$-PD$_4$**. In each experiment: lane 1 - 0 h, lane 2 - 0.5 h, lane 3 - 1 h, lane 4 - 2 h, lane 5 - 4 h, lane 6 - 6 h, lane 7 - 8 h and lane 8 - 12 h.

The nuclease profile of structures where the synthetic polymer had been site-specifically organized onto the 3D-DNA scaffold were next examined. Analysis of **C2a$_o$-PD$_2$** after addition of 10% FBS revealed a digestion pattern (Fig. 4.12c) similar to that of **C**. The 80-nucleotide component strands were digested by the 4 h time point, indicating that functionalization with two polymers is not sufficient to prevent nuclease activity. On the other hand, structure **C4a$_o$-PD$_4$**, which displays two polymers on each single stranded face, shows more stability up to a 12 h time point, as evidenced by the continued presence of the component strands (Fig. 4.12d). It is likely that the initial degradation product formed from the Cube (**C**), **C2a$_o$-PD$_2$** and **C4a$_o$-PD$_4$** is the same and relates to exonuclease attack at one or more of the nicked positions within each respective 3D structure. Further nuclease analyses and development of methods to block or functionalize the nicked sections of the cube structures are currently being explored to provide long-term stability under biological conditions. However, these nuclease results are encouraging, in that the specific arrangement of polymers on two of the cubic faces is sufficient to hinder nuclease binding. Ultimately, this feature will help to extend the lifetime of such structures in drug delivery and bioimaging applications.[39-41]

4.4 Conclusions

A method to build 3D-DNA structures that represents a departure from previous approaches has been introduced in this chapter. This method starts with a minimum number of DNA strands, and assembles them in excellent yield to give a 3D-scaffold that contains a large number of single-stranded arms. This well-defined 3D-DNA "frame" can then be used as a core structure onto which a number of other materials can be patterned, to create core−shell biohybrid structures. Ring-opening metathesis polymerization (ROMP) is used to generate block copolymers that are covalently attached to a DNA strand. Site-specific hybridization of these DNA-polymer chains on the single-stranded arms of the 3D-DNA scaffold gives efficient access to a range of biohybrid DNA-block copolymer cages, where single polymer chains are programmably positioned in three dimensions on a DNA core. Polymer-coated DNA cages are also found to be more nuclease-resistant than unfunctionalized DNA structures. Thus, these DNA-programmed block copolymers structures bring together the functionality, biocompatibility, and self-assembling potential of block copolymers with the fine control of geometry, positioning, and responsive character of DNA cages. As such, they will be a promising platform for exploring new applications in biology and materials science.

4.5 Experimental section

4.5.1 General

StainsAll®, acetic acid, tris(hydroxymethyl)-aminomethane (Tris), formamide and urea were used as purchased from Aldrich. Acetic acid and boric acid were purchased from Fisher Scientific and used without further purification. Nucleoside (dA, dC, dG and T) derivatized 1000Å LCAA- CPG supports with loading densities between 25-40 μmol/g and reagents used for automated DNA synthesis were purchased from Bioautomation Corporated. The 1,6-hexanediol phosphoramidite (**C6**) was purchased from ChemGenes Corporated (cat. # clp-1120). Sephadex G-25 (super fine, DNA grade) was purchased from Glen research. Mung Bean Nuclease (MBN, source: Mung Bean

Sprouts) and Exonuclease VII (ExoVII, source: recombinant) were purchased from BioLynx Incorporated. Fetal bovine serum (FBS) and phosphate buffered saline (PBS) were purchased from Wisent Corporated. 1xTBE buffer is composed of 0.09M Tris and Boric acid (TB) and 2 mM EDTA with a pH ~8.3. 1xTAEMg buffer is composed of 45 mM Tris, 12.5 mM $Mg(OAc)_2 \cdot 6H_2O$ and 2 mM EDTA. The pH was adjusted to 8 using glacial acetic acid. All analytical denaturing and native PAGE experiments were visualized using a solution of StainsAll (50 mg) in formamide:water (250 mL each).

4.5.2 Instrumentation

Standard automated oligonucleotide solid-phase synthesis was performed on a Mermade MM6 synthesizer from Bioautomation. Gel electrophoresis experiments were carried out on an acrylamide 20 X 20 cm vertical Hoefer 600 electrophoresis unit. Enzymatic digestions were conducted using a Flexigene Techne 60 well thermocycler. Dynamic Light Scattering (DLS) experiments were performed on a DynaPro (model MS) molecular-sizing instrument. Matrix Assisted Laser Desorption Ionization (MALDI) spectrometry was performed on a Bruker Daltonics Autoflex MALDI- TOF MS using AnchorChip target plates. The matrix used was 50% 3-hydroxypicolinic acid (10 mg/ml) in H2O/MeCN (9:1) and 20% diammonium citrate (10 mg/ml) in water.

4.5.3 Oligonucleotides prepared for 3D DNA Cube Assembly

DNA synthesis was performed on a 1 μmole scale, starting from the required nucleotide modified 1000 Å LCAA-CPG solid-support. Additionally, a 1,6 hexanediol phosphoramidite (**C6**) was site-specifically incorporated into each sequence and coupled onto the growing oligonucleotide chain as an artificial base with a prolonged coupling time of 5min. For 3'-amine (3'-NH2) containing DNA, a 1000 Å LCAA-CPG solid-support functionalized with an alkyl amine was purchased from Glen Research Corporated (cat. # 20-2958-41). Coupling efficiency was monitored after removal of the dimethoxytrityl (DMT) 5′-OH protecting groups. All sequences were fully deprotected in concentrated ammonium hydroxide (25 ^{o}C, 1.5 hours followed by 60 ^{o}C, 1 hour). Crude products were purified on 12 or 20% polyacrylamide/8M urea polyacrylamide gels (PAGE; up to 20 OD260 of crude DNA per gel) at constant current of 30 mA for 2 hours, using the 1x TBE buffer. Following electrophoresis, the plates were wrapped in plastic

and placed on a fluorescent TLC plate and illuminated with a UV lamp (254nm). The bands were quickly excised, and the gel pieces were crushed and incubated in 12 mL of sterile water at 55 ^{o}C for 16 hours. Samples were then dried to ca. 1.5 mL, desalted using size exclusion chromatography (Sephadex G-25), and quantified (OD260) using UV-Vis spectroscopy. Strand purity was assessed by denaturing PAGE.

Table 4.1 Oligonucleotides prepared via solid-phase synthesis. A hexane (**6**) spacer was site-specifically incorporated into select sequences using a commercially available phosphoramidite.

Name	Sequence (5' → 3')
C1	TCGCTGAGTA**6**TCCTATATGGTCAACTGCTC**6**GCAAGTGTGGGCACGCA CAC**6**GTAGTAATACCAGATGGAGT**6**CACAAATCTG
C2	CTATCGGTAG**6**TCCTATATGGTCAACTGCTC**6**TACTCAGCGACAGATTT GTG**6**GTAGTAATACCAGATGGAGT**6**CAACTAGCGG
C3	CACTGGTCAG**6**TCCTATATGGTCAACTGCTC**6**CTACCGATAGCCGCTAG TTG**6**GTAGTAATACCAGATGGAGT**6**GGTTTGCTGA
C4	CCACACTTGC**6**TCCTATATGGTCAACTGCTC**6**CTGACCAGTGTCAGCAA ACC**6**GTAGTAATACCAGATGGAGT**6**GTGTGCGTGC
a'	CAGTTGACCATATA
b'	CCATCTGGTATTAC
D	CAGTTGACCATATA-NH_2
C5	TCGCTGAGTA**6**TCCTTTTTTTTTTTTTTCTC**6**GCAAGTGTGGGCACGCAC

	AC**6**GTATTTTTTTTTTTTTTAGT**6**CACAAATCTG
C6	CTATCGGTAG**6**TCCTTTTTTTTTTTTTTCTC**6**TACTCAGCGACAGATTTG TG**6**GTATTTTTTTTTTTTTTAGT**6**CAACTAGCGG
C7	CACTGGTCAG**6**TCCTTTTTTTTTTTTTTCTC**6**CTACCGATAGCCGCTAGT TG**6**GTATTTTTTTTTTTTTTAGT**6**GGTTTGCTGA
C8	CCACACTTGC**6**TCCTTTTTTTTTTTTTTCTC**6**CTGACCAGTGTCAGCAA ACC**6**GTATTTTTTTTTTTTTTAGT**6**GTGTGCGTGC
C9	TCGCTGAGTA**6**GTAGTAATACCAGATGGAGT**6**GCAAGTGTGGGCACGC ACAC**6**TCCTATATGGTCAACTGCTC**6**CACAAATCTG
C10	CACTGGTCAG**6**GTAGTAATACCAGATGGAGT**6**CTACCGATAGCCGCTA GTTG**6**TCCTATATGGTCAACTGCTC**6**GGTTTGCTGA
NC20	TCCTATATGGTCAACTGCTC
NC10a	CCATATAGGA
NC10b	GAGCAGTTGA

4.5.4 Assembly of DNA Cubes.

Equimolar amounts of strands C1− C4 (250 pmol each) were dried down together and then redissolved in 200 μL of 1xTAEMg buffer. This mixture was then subjected to an annealing protocol whereby strands were held at 95 °C for 5 min, then 80 °C for 3 min, cooled to 60 °C (2 min/°C), and finally slowly cooled to 4 °C (3 min/°C). Final cube **C** concentration was ca. 1.25 μM. Cubes **C1a**−**C3a** and **C4a$_o$** were prepared in an identical manner. All strand combinations to make each of the various DNA cubes are outlined in Table 4.2.

Table 4.2 Strand combinations to prepare each cubic DNA structure.

Structure	***Component strands***
C	C1, C2, C3, C4
C1a	C2, C3, C4, C5
C2a$_o$	C2, C4, C5, C7
C2a$_a$	C3, C4, C5, C6
C3a	C4, C5, C6, C7
C4a$_o$	C2, C4, C9, C10

4.5.4 Connectivity assessment using exonucleaseVII (ExoVII)

Enzymatic protocols used to carry out the characterization of **C** were performed as previously reportedS1-S4 (and as outlined in Chapter 2, section 2.5.6). The closed, cyclic connectivity of the 3D DNA cube was confirmed using Exonuclease VII (ExoVII) digestion. ExoVII is selective for the digestion of single- stranded open DNA, over that of cyclic closed DNA. In a typical experiment 20 pmoles of DNA (total), was placed in 10 uL of 1xTAEMg buffer and subjected to 2.5 U of ExoVII at 15 °C for 2 hrs.

4.5.5 Cryo-EM

A 5 μL aliquot of **dsC** (7 μM) was deposited onto a glow-discharged quantifoil grid housed in a FEI Vitrobot automated freezing station. The sample was allowed to adsorb onto the grid surface for ca. 20 seconds after which it was blotted (blot time 2 sec, blot force 4) and plunge frozen in liquid ethane at liquid nitrogen temperatures. Samples were transferred to a cryo holder and imaged using a Tecnai F20 Twin transmission electron microscope operating at 200 kV and extraction voltage of 3950 eV. Images were recorded on a Tietz F415 4,000×4,000 pixel charge-coupled device (CCD) camera with a magnification of 50,000 (2.23 Å/pixel) and typical underfocus values between 2 – 4 um. Illumination doses were kept between 40 – 100 e-/$Å^2$.

4.5.6 AFM

For AFM imaging, **dsC** was assembled in solution as described in section 4.6.4 and then diluted to concentrations of 10- 50 nM in 1xTAEMg buffer. AFM Imaging of **dsC** showed fewer concentration effects as compared to the polymer loaded architectures, as will be discussed in a subsequent section. In a typical sample preparation, 2 μL of **dsC** (50 nM) was deposited on freshly cleaved grade 1 mica surface. After waiting for 60 sec, the mica surface was rinsed with 50 μL of Millipore water, excess liquid was removed by wicking with filter paper and the sample was then dried under argon for 1-2days. AFM images were acquired at room temperature in tapping mode using a Multimode microscope equipped with a Nanoscope IIIa controller (Digital Instruments, Santa Barbara, CA). Silicon probes (model AC160TS from Asylum Research) with resonance frequency ~200-400 kHz and spring constant ~12-103 N/m or RTSEP NanoProbe tips (Veeco, Santa Barbara, CA) with resonance frequency 200-400 kHz, spring constant ~20-80 N/m (tip radius < 10 nm) were used. Images were processed by NanoScope® (DI) and

leveled by a 3rd order plane fit in order to correct the sample tilt.

4.5.7 Polymer Synthesis.

Unless otherwise stated, all reagents and solvents were purchased from Sigma-Aldrich Chemicals and used without further purification, and all reactions were carried out under an atmosphere of nitrogen at room temperature. Monomers **S1** and **S2** were prepared according to literature procedures.36 A dry Schlenk tube was charged with Grubbs' catalyst third generation (100.0 mg, 0.112 mmol, 1 equiv) under an argon atmosphere. Dry CH_2Cl_2 (5 mL) was added, and the mixture was stirred at room temperature for 5 min. A solution of NHS-monomer (**S1**, 39.3 mg, 0.112 mmol, 1 equiv) in dry CH_2Cl_2 (5 mL) was added, and the mixture was stirred for 30 min. A solution of PEG-monomer (**S2**, 731.9 mg, 0.338 mmol, 3 equiv) in dry CH_2Cl_2 (5 mL) was then added, and the reaction mixture was stirred for another 30 min before ethyl vinyl ether (1 mL, excess) was added to quench the polymerization (Scheme 1). The polymer was precipitated with petroleum ether (716 mg, 94%) and purified by column chromatography (CH_2Cl_2 −MeOH 100:0 to 80:20): polymer **P** (234 mg, 31%) was obtained as a brown amorphous solid. Ruthenium-containing byproduct was removed by successive extraction of an aqueous solution of polymer (10 mL) with $CHCl_3$−isopropyl alcohol 3:1 (3 × 10 mL). Organic layers were combined, dried (MgSO4), filtered, and concentrated under reduced pressure to afford the pure polymer **P** as a light brown solid. ^{1}H NMR (400 MHz, CD_2Cl_2, 298 K): δ = 7.44 (d, J = 6.1 Hz, 2H, H_B), 7.34 (t, J = 7.1 Hz, 2H, H_C), 7.28 (q, J = 6.8 Hz, 1H, H_A), 6.75 (d, J = 15.7 Hz, 1H, H_D), 6.35 (dd, J = 3.3, 15.7 Hz, 1H, H_E), 5.95-6.15 (m, 6H, H_F and H_G), 5.80 (bd, J = 5.5 Hz, 1H, H_I), 5.44 (d, J = 17.0 Hz, 1H, $H_{I'}$), 4.87-5.06 (m, 2H, $H_{\alpha'}$ and $H_{\beta'}$), 4.33-4.62 (m, 6H, H_α and H_β), 3.77 (t, J = 4.3 Hz, 6H, $H_{a'}$), 3.45-3.45 (m, 530H, H_a, $H_{c'}$ and $H_{d'}$), 3.33 (s, 9H, $H_{e'}$), 2.80 (s, 4H, H_c), 2.67 (bt, J = 6.0 Hz, 2H, H_b), 1.93-2.10 (m, 2H, $H_{\gamma'}$ and $H_{\delta'}$), 1.65-1.84 (m, 6H, H_γ and H_δ). GPC (DMF, 1 mL/min): Mp = 6678, PDI = 1.13.

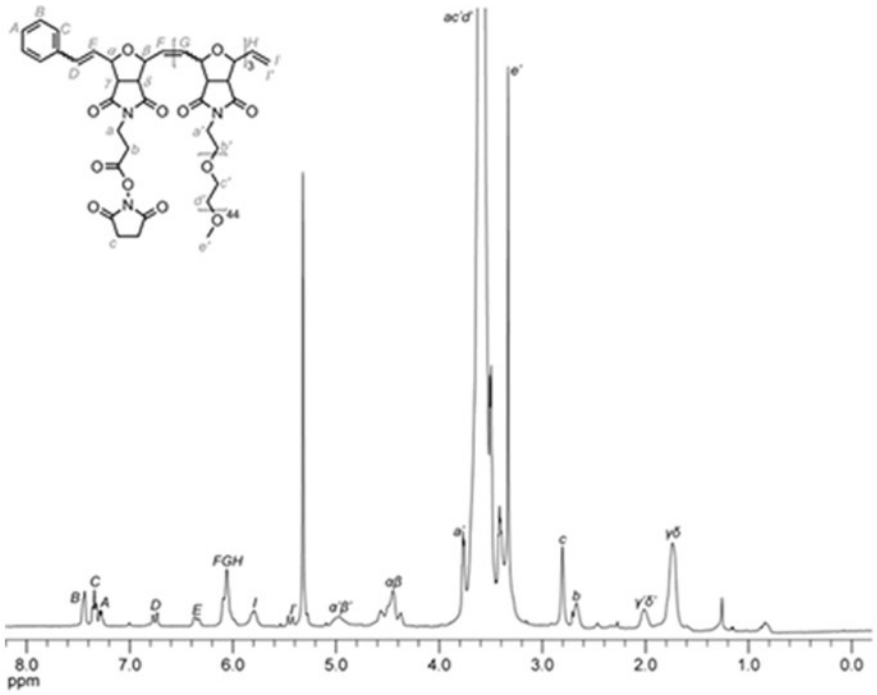

Fig. 4.12 ^{1}H-NMR spectrum for polymer P.

4.5.8 DNA−Polymer Conjugation.

In a typical conjugation reaction, 200 nmol of 3′-amine DNA (sequence D) was dried down under reduced pressure and heat. The DNA was then resuspended in 50 μL of a borate buffer (0.1 M, pH 8). NHS-activated polymer **P** (1 μmole) was weighed out in a 0.5 mL microcentrifuge tube and completely dissolved in 50 μL of acetonitrile. The DNA solution was then transferred to this tube, mixed, and allowed to react at room temperature for 2 days with agitation. The reaction mixture was reduced to dryness and dissolved in 75 μL of H_2O. Urea (8 M, 75 μL) was then added, and the mixture was loaded onto a 12% denaturing PAGE gel. The major product was purified by the crush and soak method, desalted using size exclusion chromatography (Sephadex G- 25), and quantified (OD260) using UV−vis spectroscopy.

4.5.9 Annealing DNA−Polymer Conjugate PD to 3D DNA Cubes.

In a typical assembly, DNA cube **C** (4 μL, 1.25 μM) was pipetted into a 0.5 mL microcentrifuge tube. DNA−polymer conjugate **PD** (1 μL, 20 μM) was added to **C** with slight mixing. 1xTAEMg buffer (5 μL) was added to make the final cube concentration

0.5 μM, and the mixture was allowed to stand at room temperature for 10 min. For each of the cubes containing poly(thymidine) tracts, the amount of DNA−polymer conjugate and 1xTAEMg buffer added was modified according to the number of binding sites available.

4.6 References

(1) Zheng, J.; Birktoft, J. J.; Chen, Y.; Wang, T.; Sha, R.; Constantinou, P. E.; Ginell, S. L.; Mao, C.; Seeman, N. C. *Nature* **2009**, *461*, 74.
(2) Aldaye, F. A.; Palmer, A. L.; Sleiman, H. F. *Science* **2008**, *321*, 1795.
(3) Lin, C.; Liu, Y.; Yan, H. *Biochemistry* **2009**, *48*, 1663.
(4) Rothemund, P. W. *Nature* **2006**, *440*, 297.
(5) Andersen, E. S.; Dong, M.; Nielsen, M. M.; Jahn, K.; Subramani, R.; Mamdouh, W.; Golas, M. M.; Sander, B.; Stark, H.; Oliveira, C. L.; Pedersen, J. S.; Birkedal, V.; Besenbacher, F.; Gothelf, K. V.; Kjems, J. *Nature* **2009**, *459*, 73.
(6) Douglas, S. M.; Dietz, H.; Liedl, T.; Hogberg, B.; Graf, F.; Shih, W. M. *Nature* **2009**, *459*, 414.
(7) Ke, Y.; Sharma, J.; Liu, M.; Jahn, K.; Liu, Y.; Yan, H. *Nano Lett.* **2009**, *9*, 2445.
(8) Endo, M.; Hidaka, K.; Kato, T.; Namba, K.; Sugiyama, H. *J. Am. Chem. Soc.* **2009**, *131*, 15570.
(9) Han, D.; Pal, S.; Nangreave, J.; Deng, Z.; Liu, Y.; Yan, H. *Science* **2011**, *332*, 342.
(10) Chen, J. H.; Seeman, N. C. *Nature* **1991**, *350*, 631.
(11) Shih, W. M.; Quispe, J. D.; Joyce, G. F. *Nature* **2004**, *427*, 618.
(12) Goodman, R. P.; Schaap, I. A.; Tardin, C. F.; Erben, C. M.; Berry, R. M.; Schmidt, C. F.; Turberfield, A. J. *Science* **2005**, *310*, 1661.
(13) He, Y.; Ye, T.; Su, M.; Zhang, C.; Ribbe, A. E.; Jiang, W.; Mao, C. *Nature* **2008**, *452*, 198.
(14) Andersen, F. F.; Knudsen, B.; Oliveira, C. L.; Frohlich, R. F.; Kruger, D.; Bungert, J.; Agbandje-McKenna, M.; McKenna, R.; Juul, S.; Veigaard, C.; Koch, J.; Rubinstein, J. L.; Guldbrandtsen, B.; Hede, M. S.; Karlsson, G.; Andersen, A. H.; Pedersen, J. S.; Knudsen, B. R. *Nucleic Acids Res.* **2008**, *36*, 1113.
(15) Zimmermann, J.; Cebulla, M. P.; Monninghoff, S.; von Kiedrowski, G. *Angew. Chem. Int. Ed.* **2008**, *47*, 3626.
(16) Bhatia, D.; Mehtab, S.; Krishnan, R.; Indi, S. S.; Basu, A.; Krishnan, Y. *Angew. Chem. Int. Ed.* **2009**, *48*, 4134.
(17) Severcan, I.; Geary, C.; Chworos, A.; Voss, N.; Jacovetty, E.; Jaeger, L. *Nat. Chem.* **2010**, *2*, 772.
(18) Fuks, G.; Mayap Talom, R.; Gauffre, F. *Chem. Soc. Rev.* **2011**, *40*, 2475.
(19) Vicent, M. J.; Dieudonne, L.; Carbajo, R. J.; Pineda-Lucena, A. *Expert Opin Drug Deliv* **2008**, *5*, 593.

(20) van Dongen, S. F.; de Hoog, H. P.; Peters, R. J.; Nallani, M.; Nolte, R. J.; van Hest, J. C. *Chem. Rev.* **2009**, *109*, 6212.
(21) Hawker, C. J.; Wooley, K. L. *Science* **2005**, *309*, 1200.
(22) Watson, K. J.; Park, S. J.; Im, J. H.; Nguyen, S. T.; Mirkin, C. A. *J. Am. Chem. Soc.* **2001**, *123*, 5592.
(23) Kwak, M.; Herrmann, A. *Angew. Chem. Int. Ed.* **2010**, *49*, 8574.
(24) Li, Z.; Zhang, Y.; Fullhart, P.; Mirkin, C. A. *Nano Lett.* **2004**, *4*, 1055.
(25) Gibbs-Davis, J. M.; Schatz, G. C.; Nguyen, S. T. *J. Am. Chem. Soc.* **2007**, *129*, 15535.
(26) Ding, K.; Alemdaroglu, F. E.; Borsch, M.; Berger, R.; Herrmann, A. *Angew. Chem. Int. Ed.* **2007**, *46*, 1172.
(27) Chien, M. P.; Rush, A. M.; Thompson, M. P.; Gianneschi, N. C. *Angew. Chem. Int. Ed.* **2010**, *49*, 5076.
(28) Kwak, M.; Minten, I. J.; Anaya, D. M.; Musser, A. J.; Brasch, M.; Nolte, R. J.; Mullen, K.; Cornelissen, J. J.; Herrmann, A. *J. Am. Chem. Soc.* **2010**, *132*, 7834.
(29) Pan, P. J.; Fujita, M.; Ooi, W. Y.; Sudesh, K.; Takarada, T.; Goto, A.; Maeda, M. *Polymer* **2011**, *52*, 895.
(30) Chien, M. P.; Gianneschi, N. C. *Small* **2011**, *7*, 2041.
(31) Jeong, J. H.; Park, T. G. *Bioconjugate Chem.* **2001**, *12*, 917.
(32) Alemdaroglu, F. E.; Alemdaroglu, N. C.; Langguth, P.; Herrmann, A. *Adv. Mater.* **2008**, *20*, 899.
(33) Patwa, A.; Gissot, A.; Bestel, I.; Barthelemy, P. *Chem. Soc. Rev.* **2011**, *40*, 5844.
(34) Giacomelli, C.; Schmidt, V.; Aissou, K.; Borsali, R. *Langmuir* **2010**, *26*, 15734.
(35) Yang, H.; McLaughlin, C. K.; Aldaye, F. A.; Hamblin, G. D.; Rys, A. Z.; Rouiller, I.; Sleiman, H. F. *Nat. Chem.* **2009**, *1*, 390.
(36) McLaughlin, C. K.; Hamblin, G. D.; Aldaye, F. A.; Yang, H.; Sleiman, H. F. *Chem. Commun.* **2011**, *47*, 8925.
(37) Kato, T.; Goodman, R. P.; Erben, C. M.; Turberfield, A. J.; Namba, K. *Nano Lett.* **2009**, *9*, 2747.
(38) Sankaran, N. B.; Rys, A. Z.; Nassif, R.; Nayak, M. K.; Metera, K.; Chen, B. Z.; Bazzi, H. S.; Sleiman, H. F. *Macromolecules* **2010**, *43*, 5530.
(39) Ko, S. H.; Liu, H. P.; Chen, Y.; Mao, C. D. *Biomacromolecules* **2008**, *9*, 3039.
(40) Bhatia, D.; Surana, S.; Chakraborty, S.; Koushika, S. P.; Krishnan, Y. *Nat. Commun.* **2011**, *2*.
(41) Walsh, A. S.; Yin, H.; Erben, C. M.; Wood, M. J.; Turberfield, A. J. *ACS Nano* **2011**, *5*, 5427.

4.7 Introduction to chapter 5

Development of a method to generate a 3D DNA structure with a maximal number of singe-stranded regions provided a unique scaffold with which to organize materials through hybridization of functionalized oligonulceotides. Although preliminary, the nuclease results suggested that there was some additional stability that resulted from coverage with large polymer chains and that the fate of such 3D DNA structures should be further assessed under biological conditions. To this point in the literature, it had been demonstrated that large poly-anionic materials (such as gold nanoparticle-DNA/RNA conjugates) were capable of cell uptake over a number of cell lines. In addition, recent reports had been published which indicated that 'naked' 3D DNA structures could also cross the cell membrane. These latter studies were, however, only performed on single structures with no variance on geometry. How, then, are these small anionic structures undergoing cell uptake? More importantly, is there a link between 3D DNA structure and a receptor mediated cell uptake response? In chapter 5, *in cellulo* experiments that explore how variance in shape affects cell uptake for 3D DNA structures are discussed.

Chapter 5: Cell Uptake Assessment for a 3D DNA Cube

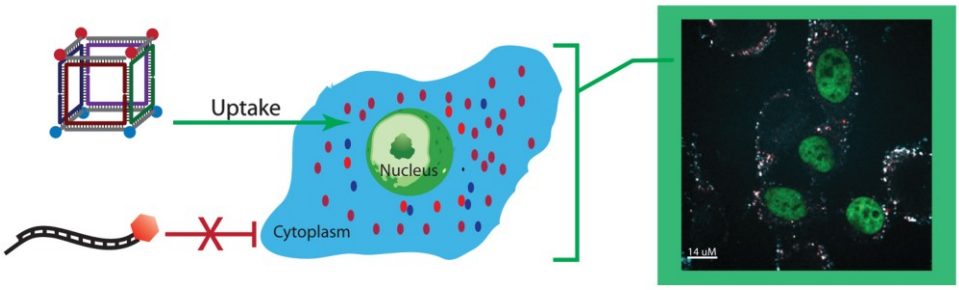

5.1 Abstract

In chapter 5, the cell uptake properties of DNA nanocubes assembled from four 80-base single strands and decorated with Cy3 and/or Cy5-modified complementary strands are investigated. It is demonstrated that these 3D DNA cubes efficiently accumulate in the cytoplasm of human cervical cancer cells (HeLa) without the aid of any transfection agent, whereas single stranded and double stranded DNA cytoplasmic accumulation is acutely absent. A sequence asymmetric DNA cube variant was also assembled, which showed excellent cell uptake when labeled with only a single fluorophore. This same DNA cube is also shown to be amenable to selective assembly of fluorescent molecules to yield efficient Förster resonance energy transfer (FRET). The results suggest that the intracellular accumulation of nucleic acid particles without the aid of viral or non-viral vectors could be achieved if DNA particles are packaged into compact globular particles. These molecules could thus represent a new class of selective cellular probes and drug delivery tools, and would assist the development of nucleic acid therapeutic routes.

5.2 Introduction

Nucleic acid therapeutics represent a promising avenue for the treatment of a spectrum of diseases. Several approaches are currently being examined, including the incorporation of gene units to compensate for the deficiency in a

protein, the delivery of small interfering RNA or antisense oligonucleotides to achieve gene silencing, or the introduction of genetic material from various pathogens as vaccines.[1-4] However, the success of nucleic acid therapeutic modalities has been severely hampered by physiological barriers that prevent delivery of these anionic macromolecules into cells.[5,6] Several strategies have been employed to overcome these challenges, including modifications to the phosphate backbone or the sugar moieties, and the use of transfection agents, such as viral vectors, cationic polymers, dendrimers or liposomes.[7-10]

Recently, studies have demonstrated that, if DNA strands are arranged into a dense core-shell structure, such as oligonucleotide-gold nanoparticle conjugates,[11,12] they can be efficiently taken up by a variety of cells without the need for viral or non-viral vectors. These large 'spherical nucleic acids'[13] have been shown to be able to regulate gene expression[14] and act as detection systems for mRNA in living cells[15]. Purely DNA-based constructs, such as DNA nanotubes[16,17] or origami[18] have also been shown to accumulate intracellularly. In the latter case, DNA-origami nanotubes decorated with cytosine-phosphate-guanine (CpG) sequences elicit a strong immune response in spleen cells without toxic effect.[18] The cellular uptake for smaller DNA-based structures, such as tetrahedra[19,20] or icosahedra[21,22] has also been observed. Although uptake efficiencies vary within these structures, this raises the possibility that packaging DNA strands into compact three-dimensional structures can enhance their cellular uptake and intracellular accumulation. However, assembly yields are often low yielding and constructs lack regions that can be functionalized in a geometrically well-defined manner. In addition, methods so far do not generate a range of geometries, and thus do not provide the opportunity to study the shape dependence of DNA uptake.

The 'DNA-minimal' assembly strategy previously reported in chapter 4 generates discrete 3D DNA structures in high-yield and contains a maximal amount of single-stranded regions for further functionalization.[23] Structures produced in this manner are thus excellent candidates for both packaging functional nucleic acids and geometrically positioning ligands or chemical probes

on the nanometer length scale. Fundamental investigations into the cell uptake profile of such structures are thus highly desirable.

In chapter 5, preliminary investigations into the cellular internalization and accumulation of 3D DNA cubes are reported. Single-stranded sites within the cubic structure are annealed to both Cy3 and Cy5 labeled DNA strands, incubated with a variety of cell lines and cell uptake investigated by confocal microscopy (CFM) and flow cytometry. The design for DNA cube assembly is also tuned to generate a structure that is fully sequence asymmetric. This allows both hybridization of a single fluorescent-labeled strand and the selective incorporation of double-stranded regions on structures to be tested for cell uptake. In all cases, DNA cubes efficiently accumulate in the cytoplasm of human cervical cancer cells (HeLa) without the aid of any transfection agent. Conversely, single stranded and double stranded DNA cytoplasmic accumulation is acutely absent or minimal under these experimental conditions.

5.3 Results and discussion

5.3.1 Assembly of various 2D and 3D DNA structures

Recently, an assembly strategy that simplifies the design of 3D-DNA structures to produce monodisperse structures in high yield was developed.[23] As shown in Fig. 5.1a, the hybridization of an 80-mer DNA strand to a second strand promotes cyclization of two ends to form pseudo-catenated dimer **1**. Addition of a third strand results in open trimer construct **2**. DNA cube structure **C1** is constituted of four such DNA strands (C1a - C1d), with the fourth strand hybridizing with the first to generate a closed 3D structure. Each cyclized strand thus constitutes the face of the final three-dimensional assembly. In its present design, **C1** has four arms with identical sequences **a** on its top face and four with sequence **b** on its bottom face (Fig. 5.1a). This 3D DNA structure is thus designed to combine with a different number of complementary DNA strands, yielding molecules with a cubic topology but with different rigidity/flexibility and an approximate size of 6-7 nm[23]. Heating the correct combinations of component

DNA strands to 95°C and cooling them slowly to room temperature yielded structure **C1** in near quantitative yield as shown in the native PAGE analysis in Fig. 5.1b.

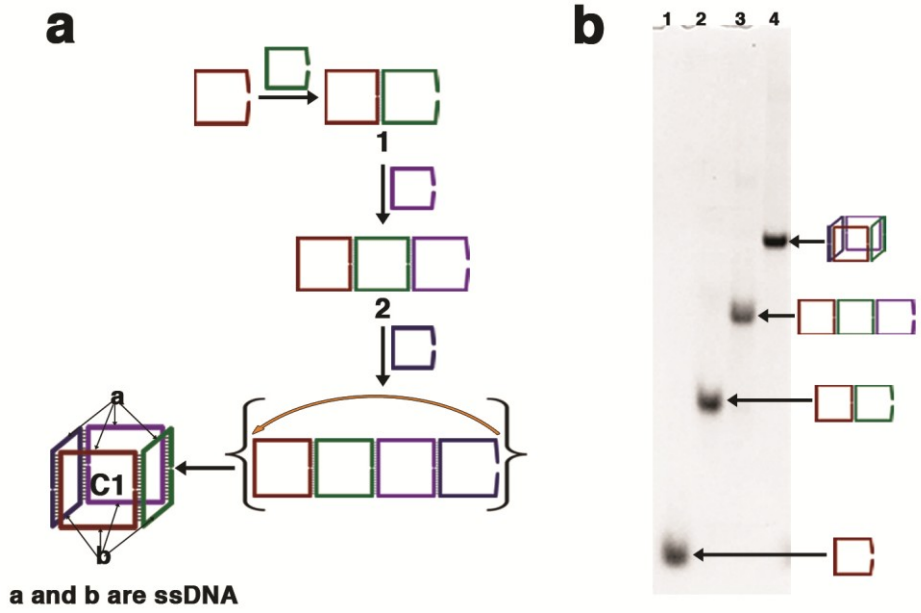

Figure 5.1. Assembly and characterization of DNA cube C1 a, Schematic representation of the assembly of DNA structures. Starting from an 80mer component strand, dimer **1**, trimer **2** and closed-cube **C1** can be prepared. **b,** Native PAGE analysis of structures **1, 2 and C1**; Lane 1 – 80mer component strand, lane 2 – **1**, lane 3 – **2** and lane 4 – **C1**. Schematic representation for **C1** shows the placement of 20mer single-stranded sequences **a** and **b**.

5.3.2 Cell uptake results for DNA cube C1

The design of the single-stranded regions in **C1** DNA allowed for hybridization with 18mer complementary sequences containing Cy3 or Cy5 fluorophores (a'Cy3 and b'Cy3). As shown in Fig. 5.2aii, this structure could be annealed to Cy3 containing complement strand a'Cy3 to create a multi-labeled derivative **C1**·**Cy3**, which allowed for tracking during cellular internalization studies. Strands a'Cy3 and b'Cy3 have theoretical melting temperatures (Tm) of 48 and 44 °C, respectively, when hybridized to their complement sequences on the cubic structure (see Table 5.1). Single- and double-stranded DNA conjugated to Cy3 (Fig. 5.2ai) were used as controls for each cell uptake study.

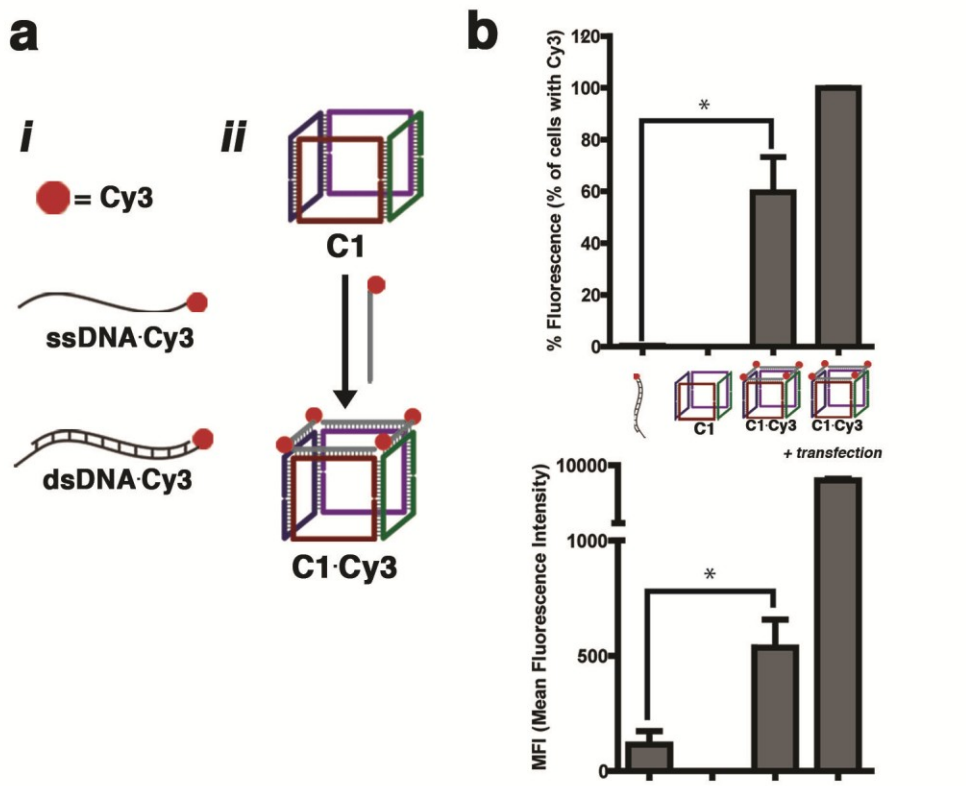

Figure 5.2 Cy3 labeled structures and flow cytommetry results. a, Schematic representation of Cy3 labeled i) control strands and ii) Cubic DNA structure with 4 labels (**C1·Cy3**). **b,** HeLa cells were incubated in the presence of dsDNA+Cy3, **C1**, **C1·Cy3**, and lipoplexed **C1·Cy3**. The percentage of cells carrying fluorescent particles (left) and the Mean Fluorescence Intensity (MFI, right) were calculated ($p<0.05$) and plotted.

To gain insight into the effectiveness of intracellular internalization, DNA cube **C1·Cy3** (10 μM) and control samples were added to exponentially dividing HeLa cells. After 6 hours of incubation at 37°C, Cy3 content was analyzed using a specialized flow cytometry technique, Flow Activated Cell Sorting (FACS). Within this incubation period, significant intracellular presence of **C1·Cy3** was observed, with approximately 60% of cells exhibiting accumulation of this DNA cube in the absence of a transfection agent (Figure 5.2b-*top*). In contrast, very few cells incubated with Cy3-labeled double-stranded DNA exhibited intracellular accumulation. Quantifying the signal exhibited by Cy3 positive cells, a significant increase in fluorescence intensity was observed when cells are incubated with **C1·Cy3** particles as compared to cells incubated with Cy3-labeled dsDNA (5.2b-*bottom*). Incubating **C1.Cy3** in a select number of other cell lines tested the

reproducibility of this data. Intracellular accumulation of the DNA cube occurs in two normal fibroblast cell lines (WI-38 and MRC-5) and an immortal cell line (GM847) (Fig. 5.3). Interestingly, when DNA cube **C1·Cy3** was incubated with hepatocellular carcinoma cells (Huh-7), cellular accumulation of DNA cube particles was not observed. As will be discussed in subsequent sections, this may suggest that these cells lack a receptor or family of receptors that are important for the internalization of DNA cube structures.[24]

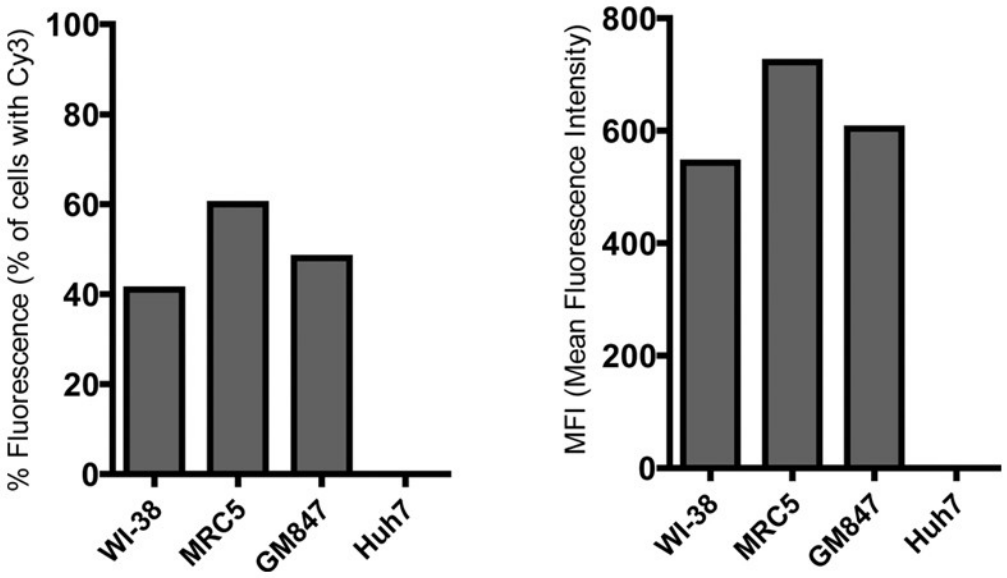

Figure 5.3 Intracellular accumulation of C1·Cy3 in different cell lines. Normal fibroblast cell lines (WI-38 and MRC-5), immortal cell line (GM847) and hepatocellular carcinoma cells (Huh-7 were incubated with **C1·Cy3** and cellular accumlulation assessed by FACS. *Left* - % of cells exhibiting Cy3 fluoresence and *right* – mean fluorescence intensity (MFI) collected by FACS.

A time course for the intracellular accumulation of **C1·Cy3** in HeLa cells was also determined using flow cytometry. **C1·Cy3** was incubated with HeLa cells for 0, 6, 24, 48, and 72 hours and Cy3 content analyzed at each time point using FACS. After 24 hours, almost all cells (~100%) contained **C1·Cy3** particles (Fig. 5.4). Interestingly, after 72 hours of incubation a sustained level of intracellular accumulation **C1·Cy3** was observed without any obvious cytotoxicity or deterioration in cellular viability. Taken together, these results demonstrate the sustained and preferential intracellular accumulation of DNA cube particles.

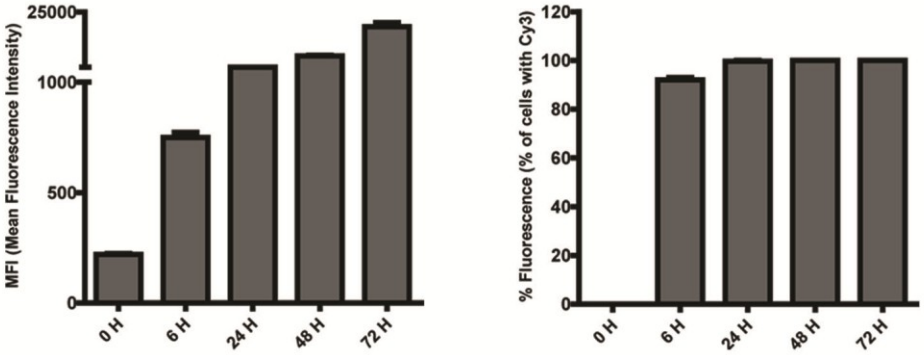

Figure 5.4 Time course for the intracellular accumulation of C1·Cy3. HeLa cells were incubated in the presence of **C1·Cy3** for 0, 6, 24, 48, and 72 hours and then analyzed using FACS. Subsequently, the percentage of cells carrying fluorescent particles and the MFI were calculated.

Confocal fluorescence microscopy (CFM) was next used to confirm the subcellular localization of DNA cube **C1** and try and assess its structural integrity upon crossing the plasma membrane. For this, cube **C1** was assembled with complementary Cy3-labelled strands alone (**C1·Cy3**), complementary Cy5-labeled strands alone (**C1·Cy5**), or both Cy3- and Cy5-labelled complementary strands (**C1·Cy3/5**, Fig. 5.5a). Each structure was characterized by native PAGE analysis (Fig. 5.5b) and shown to cleanly hybridize with each respective fluorophore labeled strands (a'-Cy3 and/or b'-Cy5, see section 5.5.2 for sequence details).

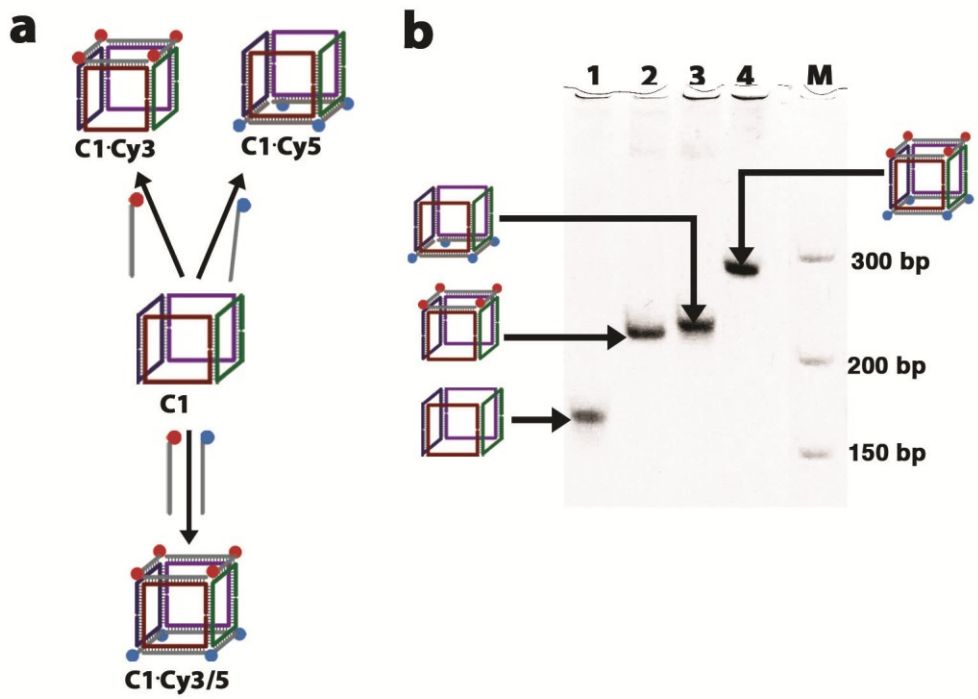

Figure 5.5 Dual fluorophore labeling of C1. a, Selective hybridization of Cy3 (red) and Cy5 (blue) modified strands either the top- and bottom-faces, or both, of cube **C1** generates mono-labeled structures **C1·Cy3** and **C1·Cy5**, and dually labeled structure **C1·Cy3/Cy5**. **b,** Native PAGE (6%) characterization of Cy-labeled structures; Lane 1 – C1, lane 2 - **C1·Cy3**, lane 3 – **C1·Cy5**, lane 4 - **C1·Cy3/Cy5** and lane M – molecular weight marker (bp).

Exclusive cytoplasmic localization of DNA cubes **C1·Cy3** and **C1·Cy5** was observed using CFM (Figure 5.6a and b, respectively). In each image the fluorescently labeled structures appear to be located within the cytoplasm, as indicated by the overlaid bright field and dark field channels (Cy3 + Cy5 + GFP + DIC), but are not found in the nucleus. Both of the fluorescently labeled 3D DNA structures thus appear to be efficiently taken up into the cell. One means of testing whether the DNA cubes remain intact upon crossing the cell membrane, was to assemble dually labeled structure **C1·Cy3/5** (Fig. 5.6c). CFM images of this sample should exhibit a distribution of Cy3 and Cy5 emission that overlaps. Indeed, the Cy3 and Cy5 signals where colocalized when dually labeled DNA cube **C1·Cy3/5** was introduced, where foci containing both signals were prominent (Figure 5.6c). Although the resolvable features in CFM are diffraction limited (~300 nm), this data indicates that intracellular accumulation of DNA

cubes is exclusively cytoplasmic, structures do not penetrate the nucleus and suggests particle integrity remains intact upon cellular entry.

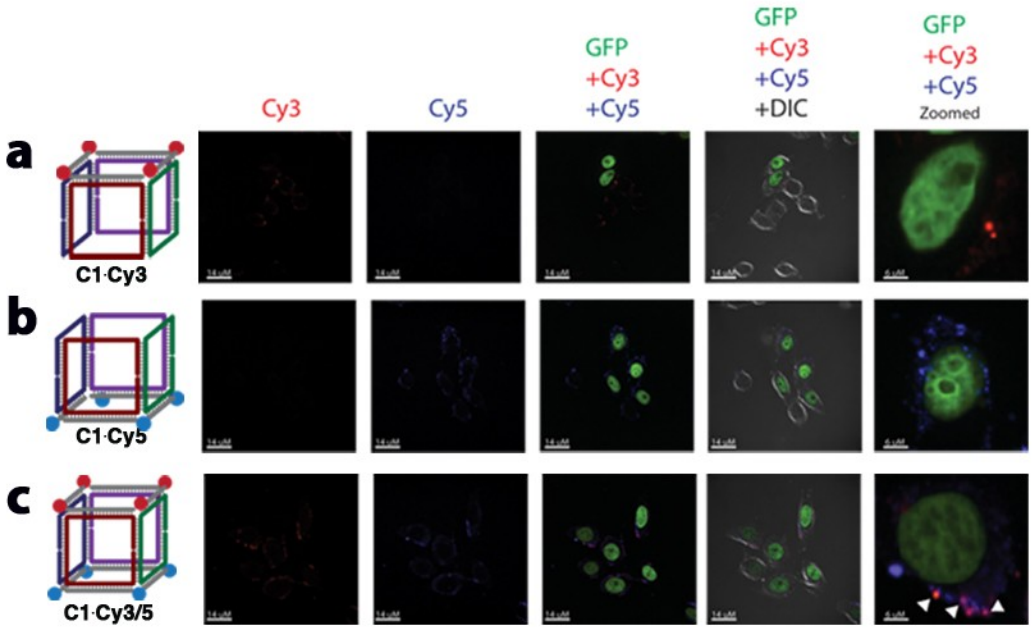

Figure 5.6 Confocal microscopy results for C1·Cy3, C1·Cy5 and C1·Cy3/Cy5. HeLa cells were incubated in the presence of labeled **C1** structures (**C1·Cy3, C1·Cy5** or **C1·Cy3/Cy5**) for 6 hours and then examined by confocal microscopy (CFM). Cy3 and Cy5 channels are individually shown. Cells express histone proteins with a green fluorescent protein (GFP) in the nucleus, allowing this structure to be independently imaged. DIC represents the bright field image. **a,** Images obtained for **C1·Cy3**. **b,** Images obtained for **C1·Cy5**. **c,** Images obtained for **C1·Cy3/Cy5**. Arrows on the zoomed in merged field of view indicate individual colocalization foci where the Cy3 and Cy5 signals overlap.

5.3.3 Preparation and cell uptake of a fully asymmetric DNA cube

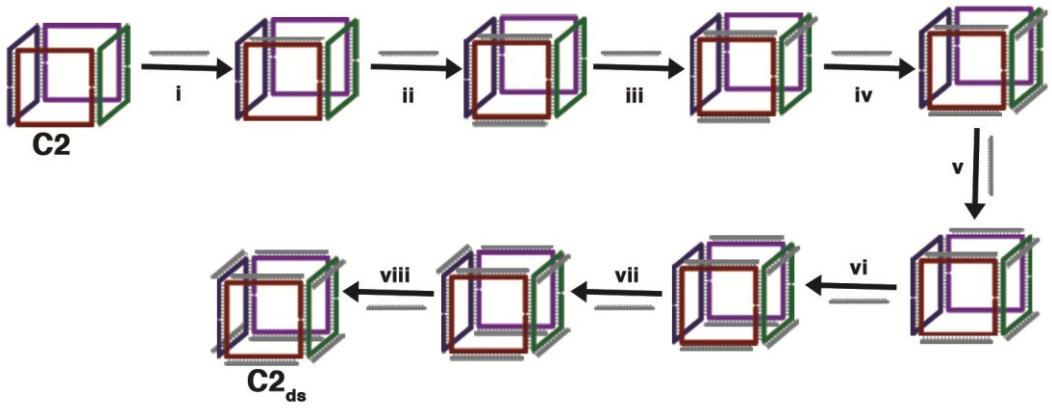

Figure 5.7 Fully asymmetric DNA cube design. Each of the 8 single-stranded regions can be individually hybridized with a complement strand. Sequential addition of each 20mer complement strand (i – viii, shown in grey above the arrow) generates fully double-stranded DNA cube **C2**.

The DNA cubes studied thus far have included a high degree of sequence symmetry within each face to accommodate multiple binding of fluorophore labeled strands. In turn, cell uptake studies could only be performed on multiply labeled structures. In Chapter 4, binding to specific single-stranded regions was eliminated by using poly(thymine) insertions. The poly(adenine) complement strand is, however, not stable enough to prepare selectively labeled double-stranded structures. With these factors in mind, a completely asymmetric system was designed. For example, each of the single-stranded sequences shown schematically in Fig. 5.7 is unique, allowing sequential hybridization of complementary strands (steps i - viii) to yield the fully double-stranded 3D DNA product $\mathbf{C2_{ds}}$. With this type of structure the potential effects of polyvalency on the cellular uptake process for the DNA structures could be explored. Such a 3D DNA structure is also unprecedented in that it allows for complete control over the arrangement of different strands, which can be functionalized with various chemical groups, in a geometrically well-defined manner.

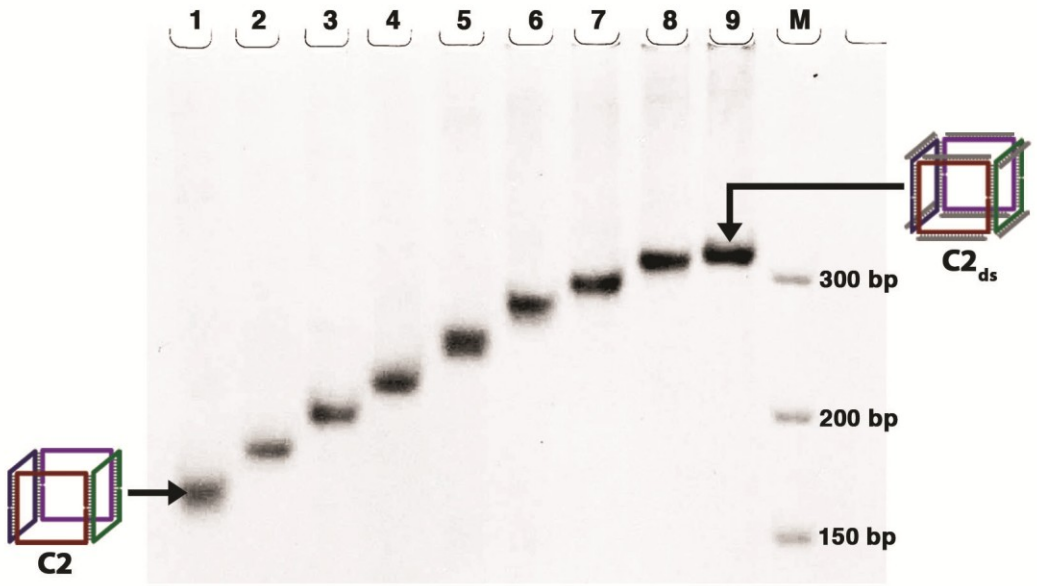

Figure 5.8 Native PAGE characterization for asymmetric DNA cube C2. Native PAGE analysis of DNA cubes hybridized to various combinations of complement strands **c** – **j**; Lane 1 – **C2**, lane 2 – **C2** + **c**, lane 3 – **C2** + **c/d**, lane 4 – **C2** + **c/d/e**, lane 5 – **C2** + **c/d/e/f**, lane 6 – **C2** + **c/d/e/f/g**, lane 7 – **C2** + **c/d/e/f/g/h**, lane 8 – **C2** + **c/d/e/f/g/h/i**, lane 9 – **C2** + **c/d/e/f/g/h/i/j** and lane M – molecular weight marker.

Cube **C2** was assembled in the same way as partially symmetric structure **C1** at a concentration of 2.5 μM and in excellent yield (Fig. 5.8, lane 1). Addition of complement strands c-j to this asymmetric cube in a sequential manner resulted in structures with progressively slower mobility as analyzed by native PAGE (Fig. 5.8, lanes 2 – 9). Fully double-stranded cube $\mathbf{C2_{ds}}$ now contains 8 different 20mer single-stranded regions that can be selectively annealed with individual complement strands.

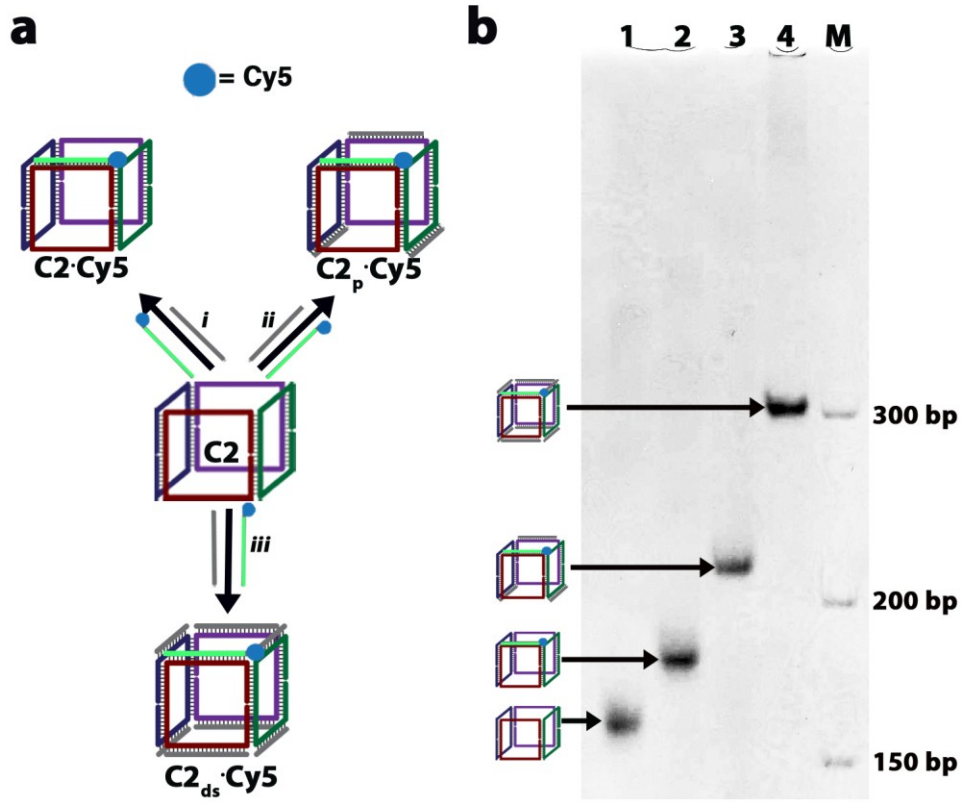

Figure 5.9 Design and characterization of Cy5 monolabeled cube C2. a, Schematic representation of monolabeled **C2** structures with c'Cy5 that contain varying placement of double-stranded DNA regions. **b,** Native PAGE analysis of DNA cubes hybridized to various combinations of complement strands **c** – **j**; Lane 1 – **C2**, lane 2 – **C2·Cy5**, lane 3 – **$C2_p$·Cy5**, lane 4 – **$C2_{ds}$·Cy5** and lane M – molecular weight marker (bp).

Due to the asymmetric arrangement of single-stranded sites on **C2**, cubes with single fluorescent tags could be assembled. This strategy allowed for cell uptake studies to be performed on a mono-labeled structure instead of polyvalent structure **C1**. Cy5 was initially chosen as the fluorescent tag due to its excellent emission properties, which would make detection easier via FACS or CFM. It should also be noted that 20mer complement strand c'Cy5 was designed to be more GC rich (Tm ≈ 59 °C based on calculation using Oligo Analyzer) to ensure tight binding labeled strand to the cubic structure. As shown in Fig. 5.9ai, a single Cy5 labeled strand (c'Cy5) can be hybridized to only one edge of **C2** to generate the flexible structure **C2·Cy5**. Sequestering the 7 remaining sites with complement strands produces fully double-stranded **$C2_{ds}$·Cy5** (Fig. 5.9aii). In addition, the design of **C2** allowed for selectivity in how ss- and ds-sequences

might be arranged with respect to one and other. Thus, partially ss/ds **C2$_p$·Cy5** was designed (Fig. 5.9aiii) to address if flexibility might play a role in the cell uptake for these 3D DNA structures. Each cube derivative was generated in excellent yield as analyzed by native PAGE (Fig. 5.9b).

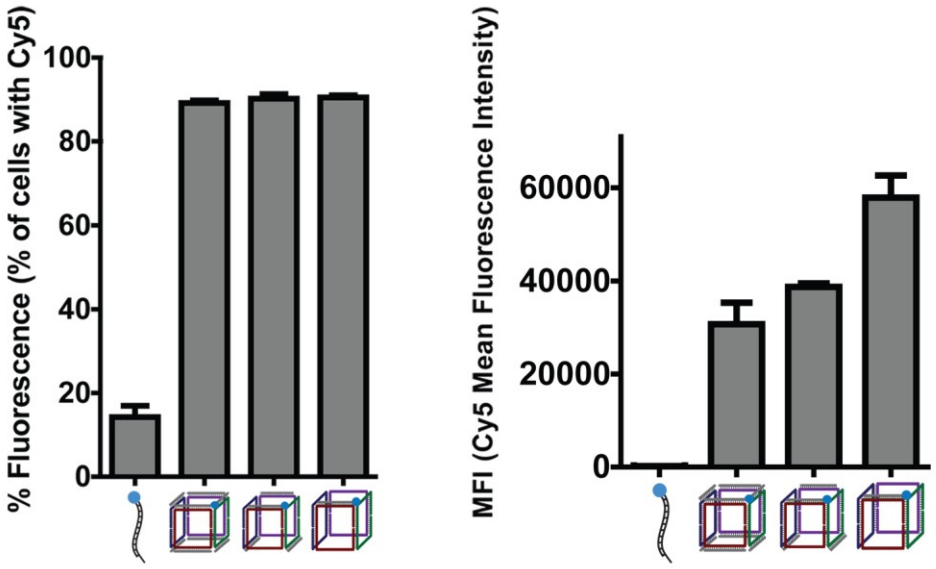

Figure 5.10 Cell uptake results for Cy5 monolabeled structures. HeLa cells were incubated in the presence of dsDNA+Cy5, **C2·Cy5**, **C2$_p$·Cy5** and **C2$_{ds}$·Cy5**. The percentage of cells carrying fluorescent particles (left) and the Mean Fluorescence Intensity (MFI, right) were calculated ($p<0.05$) and plotted. Each experiment performed in triplicate.

Each Cy5 monolabeled cubic structure was again incubated, along with a dsDNA control, for 6 hours with exponentially dividing HeLa cells. Subsequent analysis using FACS revealed high levels of accumulation for each 3D structure, with Cy5 emission being detected in greater than 80 % of the cells analyzed and limited response due to the dsDNA control (Fig. 5.10-*left*). Interestingly, calculating the signal for Cy5 positive cells revealed a distinct trend in cell uptake between each of the 3 structures tested (Fig. 5.10-*right*). The predominantly single-stranded structure **C2·Cy5** showed the highest MFI of all three structures. The calculated MFI for partially single-stranded structure **C2$_p$·Cy5** and fully double-stranded **C2$_{ds}$·Cy5** were comparable, but still noticeably less than that observed for **C2·Cy5**. This trend would appear to indicate that there is some level

of ‘compaction’ of the flexible single-stranded sections that play a role in how efficiently the 3D DNA structures are able to gain access into the cell. More detailed studies are currently underway to determine the exact structures of each DNA cube so as to be able to better investigate any shape dependence on the observed cell uptake.

5.3.4 Mechanistic thoughts on DNA cube cell uptake

Taken together, the data presented in the above sections suggests that compact three-dimensional DNA cubes cross the plasma membrane and accumulate in the cytoplasm. While a definitive mechanism for cell uptake is still under investigation, DNA cube accumulation was exclusively observed in the cytoplasm into distinct foci, suggesting that cellular uptake is achieved through receptor mediated endocytosis.[25] Recent studies have indicated that cellular uptake of dense DNA structures could be mediated by scavenger surface receptors or the anionic ligand-binding receptor (ALBR).[21,26] Scavenger receptors (SRs) form a large family of pattern recognition receptors (PRRs) and have been shown to play an important role in innate immune defense mechanisms.[27] SRs bind to a wide range of molecular patterns including liposaccharides, bacterial DNA, and double stranded RNA.[27] DNA cube structures presented here are highly structured three-dimensional objects; however, they are far less DNA-dense than DNA gold nanoparticles, or DNA origami structures, raising the possibility that the mechanism for their uptake could differ from the one responsible for internalization of dense DNA structures.[19] Interestingly, for DNA cube **C1·Cy3** with hepatocellular carcinoma cells (Huh-7), preliminary studies indicated cellular accumulation of DNA cube particles was not observed (Fig. 5.3)[24], suggesting that these cells might lack a receptor or family of receptors that are crucial for the internalization of DNA cube structures. These experiments need to be repeated, however, with the singly labeled cube to compare uptake profiles. Also of note, is the efficient uptake observed for flexible structure **C2·Cy3** (Fig. 5.10), which suggests that some level of single-stranded DNA compaction may be contributing to an overall structure that may more selectively interact with receptors. Nguyen and Shatz have demonstrated that in self-assembled structures where synthetic

vertices are used, interaction between the ion clouds of neighbouring duplexes can impart significant overall stabilization.[28,29] Given the flexible nature of single-stranded DNA,[30] it is proposed that both the amount and geometric arrangement of ssDNA within the cubic structures could play a role in how readily duplexes are able to interact via this above described mechanism, which would contribute to the overall shape recognized in biological media. Taken together, it is hypothesized that receptors that are able to distinguish size, shape, and DNA-density, could be involved in the cellular uptake of rigid DNA cube particles, but the exact mechanism involved is still not fully understood. The important implication is that this approach of assembling DNA strands into compact objects may be a new method to bring DNA into cells without the aid of transfection agents, which have shown toxicity.[7]

5.3.5 Assembly of a cube able to undergo FRET

Although the colocalization studies performed by CFM indicated that the labeled cube derivatives remained intact after cell entry (Fig. 5.6c), an alternative approach would be to design a dually fluorophore labeled system that could undergo Förster resonance energy transfer (FRET). FRET has been extensively used over the past decade in biochemistry and molecular biology to reveal molecular conformation, proximity and orientation on the nanometer length scale within living systems.[31,32]

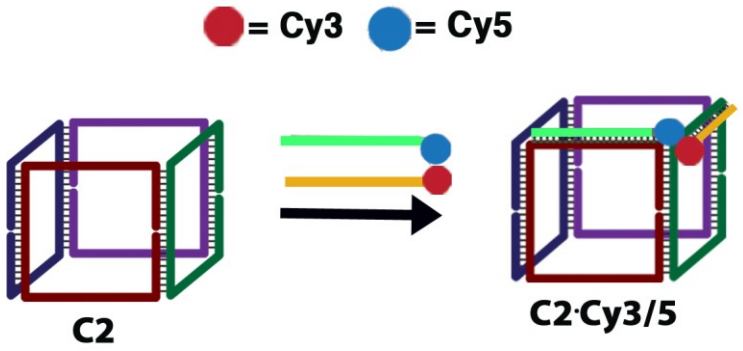

Figure 5.11 Cube C2 labeling with Cy3/Cy5 for FRET analysis. Due to the sequence arrangement on the top-face of the **C2**, strand **c'** is labeled at the 5' end with Cy5 (**c'Cy5**) and strand **d'** labeled at the 3' position with Cy3 (**d'Cy3**). Hybridization of these strands to **C2** results in structure **C2·Cy3/5**, which is now amenable to investigation using FRET detection.

The sequence asymmetry inherent to DNA cube **C2** allows for selective placement of fluorophores (Cy3 and Cy5) on this structure. Efficient FRET between the donor fluorophore (Cy3) and acceptor fluorophore (Cy5) by non-radiative dipole-dipole coupling is distance dependent,[33] thus requiring close spatial positioning of the two labeled DNA strands on **C2**. As shown in Fig. 5.11, this requirement is best met by placing strands **c'Cy5** and **d'Cy3** such that they meet at one of the cubes corners. Depending how the DNA duplexes are oriented at this flexible junction point, the distance between fluorophores is estimated to be 3-5 nm, which is well within the range for FRET to occur.

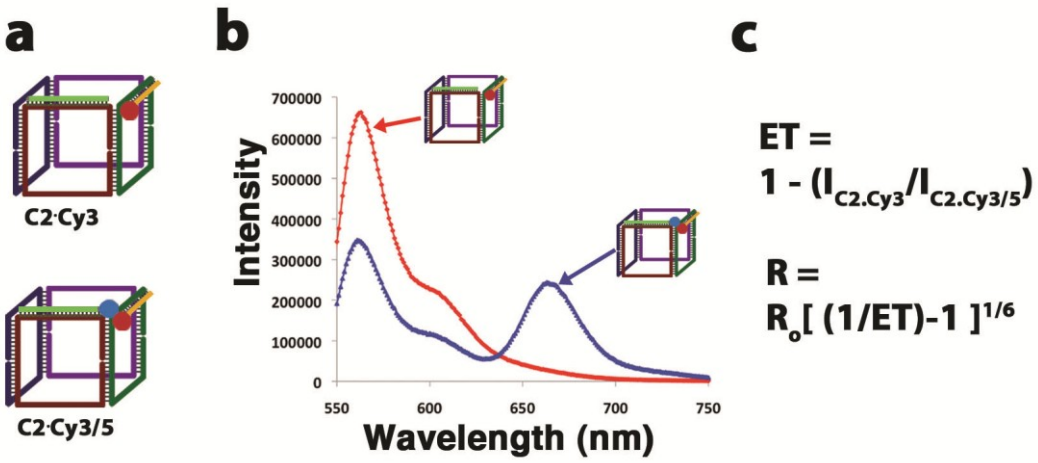

Figure 5.11 Cube C2 labeling with Cy3 and Cy5 for FRET analysis. a, Mono-fluorophore labeled **C2** derivatives used to assess FRET. **b,** Typical emission spectra recorded for **C2·Cy3** and **C2·Cy3/5** overlaid to visualize efficient FRET. Cy3 was excited at 540 nm and spectra scanned from 545 – 750 nm. **c,** Equations used to calculate energy transfer (ET) and FRET distance (R) for **C2·Cy3/5**. ET calculated from the change in intensity (I) at λ_{max} = 564 nm between **C2·Cy3** and **C2·Cy3/5** ($I_{C2.Cy3}$ and $I_{C2.Cy3/5}$, respectively).

Steady-state fluorescence measurements were performed on each of the assembled structures in Fig. 5.11a at 1 μM in 1xTAMg buffer (pH 8). As shown in Fig 5.11b, excitation of donor structure **C2·Cy3** at 540 nm generates an emission profile (red trace) of the Cy3 label with λ_{max} = 564 nm. Upon excitation of donor-acceptor structure **C2·Cy3/5**, the intensity at 564 nm is significantly reduced, with concomitant appearance of Cy5 emission centered at ca. 667nm

(Fig. 5.11b, blue trace). The emission curves obtained provide clear evidence that FRET occurs between fluorescent labels **c'Cy5** and **d'Cy3** that have been site-specifically annealed to **C2**. From the reduction in emission intensity of Cy3 at the λ_{max}, energy transfer (ET) efficiency and the average distance (R) between Cy3 and Cy5 could be calculated based on the simplified equations found in Fig. 5.11c.[33] A Forster radius (R_o), defined as the distance between donor and acceptor molecules at 50% ET,[33] of 5.4 nm for the Cy3/C5 was derived from similar DNA-based usage of this FRET pair.[34] From triplicate experiments, R was calculated to be 4.4 ± 0.3 nm for **C2·Cy3/5**.

Preparation of a 3D DNA structure able to undergo FRET, in tandem with CFM and FACS characterization, will allow for further elucidation of structural integrity after cell uptake. These investigations are ongoing for the DNA cube along with other 3D DNA structures.

5.4 Conclusions

In this chapter it has been demonstrated that plasma membrane crossing and cytoplasmic accumulation is significantly enhanced when DNA is packaged in compact, well-defined cubes. Furthermore, the mechanism for cellular uptake may be a result of selective uptake via pattern recognition receptors. While multivalent fluorophore cubes were initially tested, it has been demonstrated that mono-labeling is sufficient to ensure efficient cellular uptake in HeLa cells. Moreover, the sequence asymmetric design of cube **C2** allows site-specific DNA hybridization of different chemical modalities in geometrically well-defined fashion. This is shown by the positioning of Cy3 and Cy5 to produce a cube that can undergo efficient FRET. While the mechanism for cellular uptake is still under investigation, these DNA cages may be useful as vehicles to achieve efficient and selective delivery of therapeutic oligonucleotides and act as switchable, responsive probes of intracellular activity.

5.5 Experimental

5.5.1 General

StainsAll®, acetic acid, tris(hydroxymethyl)-aminomethane (Tris), formamide and urea were used as purchased from Aldrich. Acetic acid and boric acid were purchased from Fisher Scientific and used without further purification. Nucleoside (dA, dC, dG and T) derivatized 1000Å LCAA-CPG supports with loading densities between 25-40 μmol/g and reagents used for automated DNA synthesis were purchased from Bioautomation Corporated. The 1,6-hexanediol phosphoramidite (**C6**) was purchased from ChemGenes Corporated (cat. # clp-1120). Sephadex G-25 (super fine, DNA grade) was purchased from Glen research. Oligofectamine, DMEM media and PROLONG Gold Antifade was purchased from Invitrogen Corporated. 1xTBE buffer is composed of 0.09M Tris and Boric acid (TB) and 2 mM EDTA with a pH ~8.3. 1xTAMg buffer is composed of 45 mM Tris and 12.5 mM $Mg(OAc)_2 \cdot 6H_2O$. The pH was adjusted to 8 using glacial acetic acid. All analytical denaturing and native PAGE experiments were visualized using a solution of StainsAll (50 mg) in formamide:water (250 mL each).

5.5.2 Oligonucleotides used for DNA nanostructure assembly

DNA synthesis was performed on a 1 μmole scale, starting from the required nucleotide-modified 1000 Å LCAA-CPG solid-support. All phosphoramidites (DMF-dG, Ac-dC, bz-dA and T) were purchased from Bioautomation in 1 gram quantities. Additionally, a 1,6-hexanediol phosphoramidite (**C6**) was site-specifically incorporated into each sequence and coupled onto the growing oligonucleotide chain as an artificial base with a prolonged coupling time of 5min. Coupling efficiency was monitored after removal of the 5′-OH protecting groups using UV/Vis readers calibrated to detect the signal for the dimethoxytrityl (DMT) cation. All sequences were fully deprotected in concentrated ammonium hydroxide (25 ^{o}C, 1.5 hours followed by 60 ^{o}C, 1 hour) as per the manufacturers protocol. Crude products were purified on 12 or 20% polyacrylamide/8M urea polyacrylamide gels (PAGE; up to 20 OD_{260} of crude DNA per gel) at constant current of 30 mA for 2 hours, using the 1x TBE buffer. Following electrophoresis, the plates were wrapped in plastic and placed on a fluorescent TLC plate and illuminated with a UV lamp (254nm). The bands were quickly excised, and the gel pieces were crushed and incubated in 12 mL of sterile water at 55 ^{o}C for 12-16 hours. Samples were then dried to ca. 1 mL, desalted using size exclusion chromatography

(Sephadex G-25), quantified (OD_{260}) using UV-Vis spectroscopy and analyzed by analytical denaturing PAGE. Fluorophore labeled strands, **a′Cy3**, **b′Cy5** and **d′Cy3**, were purchased from IDT and used without further purification. Fluorophore labeled strand **c′Cy5** was prepared from commercially available (Glen Research Company, cat# 10-5915) Cy5™ Phosphoramidite (1-[3-(4-monomethoxytrityloxy)propyl]-1'-[3-[(2-cyanoethyl)-(N,N-diisopropylphosphoramidityl]propyl]-3,3,3',3' tetramethylindodicarbocyanine chloride)

Table 5.1 Oligonucleotides prepared via solid-phase synthesis. A hexane (**6**) spacer was site-specifically incorporated into select sequences using a commercially available phosphoramidite.

Name	Sequence (5' → 3')
C1a	TCGCTGAGTA**6**TCCTATATGGTCAACTGCTC**6**GCAAGTGTGGGC ACGCACAC**6**GTAGTAATACCAGATGGAGT**6**CACAAATCTG
C1b	CTATCGGTAG**6**TCCTATATGGTCAACTGCTC**6**TACTCAGCGACA GATTTGTG**6**GTAGTAATACCAGATGGAGT**6**CAACTAGCGG
C1c	CACTGGTCAG**6**TCCTATATGGTCAACTGCTC**6**CTACCGATAGCC GCTAGTTG**6**GTAGTAATACCAGATGGAGT**6**GGTTTGCTGA
C1d	CCACACTTGC**6**TCCTATATGGTCAACTGCTC**6**CTGACCAGTGTC AGCAAACC**6**GTAGTAATACCAGATGGAGT**6**GTGTGCGTGC
C2a	TCGCTGAGTA**6**GCCTGGCCTTGGTCCATTTG**6**GCAAGTGTGGGC ACGCACAC**6**CGCACCGCGACTGCGAGGAC**6**CACAAATCTG
C2b	CTATCGGTAG**6**CTGTACATGGAGCGTCTAGC**6**TACTCAGCGAC AGATTTGTG**6**GTAGCTCATGCTTGGCAGAT**6**CAACTAGCGG
C2c	CACTGGTCAG**6**CCACCAGCTAGATGTTGAAG**6**CTACCGATAGC CGCTAGTTG**6**CGCTCTTCTATACTGGCGGA**6**GGTTTGCTGA
C2d	CCACACTTGC**6**TGAGGTAGACCATAATGATG**6**CTGACCAGTGT CAGCAAACC**6**CTCGTCAACTGGTATATCCT**6**GTGTGCGTGC
a'	AGCAGTTGACCATATAGG
b'	CTCCATCTGGTATTACTA
c'	CAAATGGACCAAGGCCAGGC
d'	ATCATTATGGTCTACCTC
e'	CTTCAACATCTAGCTGGTGG

f'	GCTAGACGCTCCATGTACAG
g'	GTCCTCGCAGTCGCGGTGCG
h'	GGATATACCAGTTGACGA
i'	TCCGCCAGTATAGAAGAGCG
j'	ATCTGCCAAGCATGAGCTAC
a'Cy3	AGCAGTTGACCATATAGG-**Cy3**
b'Cy5	CTCCATCTGGTATTACTA-**Cy5**
c'Cy5	**Cy5**-CAAATGGACCAAGGCCAGGC
d'Cy3	ATCATTATGGTCTACCTC-**Cy3**

5.5.3 Assembly of DNA nanostructures

In general, equimolar amounts of each strand were combined in 1xTAMg buffer at final 3D concentrations of 2.5 μM. Samples were then subjected to an annealing protocol whereby strands were held at 95 ºC for 5 minutes then 80 ºC for 3 minutes, cooled to 60 ºC (2 min/ºC) and finally slowly cooled to 4 ºC (3 min/ºC). For cell studies, DNA cubes were additionally concentrated using microcon centrifugal filtration devices (10K MWCO). Before concentration, filter devices were washed with autoclaved Milli-Q water (2 x 450 μL) by centrifugation at 13,400 rpm and 4 °C for 15 minutes. Cube samples were then centrifuged (13,400 rpm, 10 minutes, 4 °C). The final volumes for each sample were then adjusted with 1xTAMg buffer to give an overall 3D concentration of 20 μM. Structures were analyzed by PAGE under native conditions. Table 5.2 shows each of the individual strand combinations used to assemble the various derivatives of DNA cubes **C1** and **C2**.

Table 5. 2 Strand combinations to prepare all cubic DNA structures. Brackets indicate strands, which were annealed with heat/cool protocol. Additional strands added at room temperature and allowed to anneal for 15 minutes.

Structure	*Component strands*
C1	(C1a, C1b, C1c, C1d)
C1·Cy3	(C1a, C1b, C1c, C1d) + 4x a'Cy3
C1·Cy5	(C1a, C1b, C1c, C1d) + 4x b'Cy5
C1·Cy3/5	(C1a, C1b, C1c, C1d) + 4x a'Cy3, 4x b'Cy5
C2	(C2a, C2b, C2c, C2d)
$C2_p$	(C2a, C2b, C2c, C2d) + c', e', h', j'
$C2_{ds}$	(C2a, C2b, C2c, C2d) + c' - j'
C2·Cy3	(C2a, C2b, C2c, C2d) + d'Cy3
C2·Cy5	(C2a, C2b, C2c, C2d) + c'Cy5
C2·Cy3/5	(C2a, C2b, C2c, C2d) + c'Cy5, d'Cy3

5.5.4 Cell lines utilized for uptake studies

HeLa-GFP cells were a generous gift form Dr. Stephane Richard. GM847, MRC5, WI-38, and Huh-7 cells were a generous gift from Dr. Chantal Autexier. HeLa-GFP cells express a GFP-tagged histone protein that is expressed exclusively in the nucleus. Cells were grown in Dulbecco's Modified Eagle Medium (DMEM) (Invitrogen) supplemented with FBS (10%) and antibiotic/antimycotic. Cells were passaged every 3-4 days (or at 95% confluency) at a ratio of 1:4.

5.5.5 Confocal microscopy

Confocal cell imaging was performed with a Quorum WaveFX-X1 Spinning Disc Confocal System. Typically, HeLa cells were counted and seeded at a density of 25,000 cells/well in an 8-well slide. Cells were allowed to recover for 24 hours at 37°C with 5% CO_2. Subsequently, cells were washed once with serum-free DMEM media and then 200 µl of serum-free DMEM media was added. DNA nanocubes (9.4 µM) and control nucleic acid preparations (9.4 µM) were diluted up to 100 µl with serum-free media and added to the appropriate well to a total volume of 300 µl. Cells were incubated for 4 hours, at that

point each well was supplemented with 100 μL of serum-enriched DMEM media. Cells were further incubated for 2 hours (for a total of 6 hours post-DNA addition). Cells were then washed 3 times with phosphate-buffered saline (PBS) and fixed in with a 2% paraformaldehyde/PBS solution. Cells were further washed thrice with PBS. Fixed cells were then mounted with Prolong Gold®(Invitrogen) and visualized after curing overnight at 4°C.

5.5.6 Flow cytometry

For the analysis of DNA uptake in cells we performed fluorescence activated cell sorting (FACS) on HeLa-GFP (and other cells lines). Cells were exposed to DNA nanocubes (9.4 μM) and control nucleic acid preparations (9.4 μM). Briefly, cells were seeded at 125,000 cells/well in a 6-well plate. After 24 hours cells were exposed to cube preparations in the presence or in the absence of Oligofectamine (Invitrogen, USA). Cells were further incubated at 37°C in a 5% CO_2 for 6, 24, 48, or 72 hours. Subsequently, cells were collected by trypsinization, washed with cold PBS, and fixed with 2% paraformaldehyde. Cell counting was performed on a FACS LSR Fortessa flow cytometer (BD, USA) and data analysis was concluded with the FACSDiva software (BD, USA).

5.6 References

(1) Watanabe, T.; Umehara, T.; Kohara, M. *Adv. Drug Deliv. Rev.* **2007**, *59*, 1263.

(2) Schiffelers, R. M.; Ansari, A.; Xu, J.; Zhou, Q.; Tang, Q.; Storm, G.; Molema, G.; Lu, P. Y.; Scaria, P. V.; Woodle, M. C. *Nucleic Acids Res.* **2004**, *32*, e149.

(3) Rice, J.; Ottensmeier, C. H.; Stevenson, F. K. *Nat Rev Cancer* **2008**, *8*, 108.

(4) Meyer, M.; Wagner, E. *Hum Gene Ther* **2006**, *17*, 1062.

(5) Harada-Shiba, M.; Yamauchi, K.; Harada, A.; Takamisawa, I.; Shimokado, K.; Kataoka, K. *Gene Therapy* **2002**, *9*, 407.

(6) Karikó, K.; Bhuyan, P.; Capodici, J.; Weissman, D. *Journal of Immunology* **2004**, *172*, 6545.

(7) Chan, J. H.; Lim, S.; Wong, W. S. *Clin Exp Pharmacol Physiol* **2006**, *33*, 533.

(8) Kurreck, J. *Eur. J. Biochem.* **2003**, *270*, 1628.

(9) Sliva, K.; Schnierle, B. S. *Virol J* **2010**, *7*, 248.

(10) Singha, K.; Namgung, R.; Kim, W. J. *Nucleic Acid Therapeutics* **2011**, *21*, 133.

(11) Cutler, J. I.; Zhang, K.; Zheng, D.; Auyeung, E.; Prigodich, A. E.; Mirkin, C. A. *J. Am. Chem. Soc.* **2011**, *133*, 9254.

(12) Giljohann, D. A.; Seferos, D. S.; Patel, P. C.; Millstone, J. E.; Rosi, N. L.; Mirkin, C. A. *Nano Lett.* **2007**, *7*, 3818.

(13) Cutler, J. I.; Auyeung, E.; Mirkin, C. A. *J. Am. Chem. Soc.* **2012**, *134*, 1376.

(14) Rosi, N. L.; Giljohann, D. A.; Thaxton, C. S.; Lytton-Jean, A. K. R.; Han, M. S.; Mirkin, C. A. *Science* **2006**, *312*, 1027.

(15) Seferos, D. S.; Giljohann, D. A.; Hill, H. D.; Prigodich, A. E.; Mirkin, C. A. *J. Am. Chem. Soc.* **2007**, *129*, 15477.

(16) Ko, S. H.; Liu, H. P.; Chen, Y.; Mao, C. D. *Biomacromolecules* **2008**, *9*, 3039.

(17) Hamblin, G. D.; Carneiro, K. M.; Fakhoury, J. F.; Bujold, K. E.; Sleiman, H. F. *J. Am. Chem. Soc.* **2012**, *134*, 2888.

(18) Schuller, V. J.; Heidegger, S.; Sandholzer, N.; Nickels, P. C.; Suhartha, N. A.; Endres, S.; Bourquin, C.; Liedl, T. *ACS Nano* **2011**, *5*, 9696.

(19) Walsh, A. S.; Yin, H.; Erben, C. M.; Wood, M. J.; Turberfield, A. J. *ACS Nano* **2011**, *5*, 5427.

(20) Li, J.; Pei, H.; Zhu, B.; Liang, L.; Wei, M.; He, Y.; Chen, N.; Li, D.; Huang, Q.; Fan, C. *ACS Nano* **2011**, *5*, 8783.

(21) Bhatia, D.; Surana, S.; Chakraborty, S.; Koushika, S. P.; Krishnan, Y. *Nat. Commun.* **2011**, *2*.

(22) Chang, M.; Yang, C. S.; Huang, D. M. *ACS Nano* **2011**, *5*, 6156.

(23) McLaughlin, C. K.; Hamblin, G. D.; Hanni, K. D.; Conway, J. W.; Nayak, M. K.; Carneiro, K. M.; Bazzi, H. S.; Sleiman, H. F. *J. Am. Chem. Soc.* **2012**, *134*, 4280.

(24) Akazawa, D.; Date, T.; Morikawa, K.; Murayama, A.; Miyamoto, M.; Kaga, M.; Barth, H.; Baumert, T. F.; Dubuisson, J.; Wakita, T. *Journal of Virology* **2007**, *81*, 5036.

(25) Gu, Z.; Biswas, A.; Zhao, M.; Tang, Y. *Chem. Soc. Rev.* **2011**, *40*, 3638.

(26) Patel, P. C.; Giljohann, D. A.; Daniel, W. L.; Zheng, D.; Prigodich, A. E.; Mirkin, C. A. *Bioconjugate Chem.* **2010**, *21*, 2250.

(27) Areschoug, T.; Gordon, S. *Cell Microbiol* **2009**, *11*, 1160.

(28) Eryazici, I.; Prytkova, T. R.; Schatz, G. C.; Nguyen, S. T. *J. Am. Chem. Soc.* **2010**, *132*, 17068.

(29) Stepp, B. R.; Gibbs-Davis, J. M.; Koh, D. L.; Nguyen, S. T. *J. Am. Chem. Soc.* **2008**, *130*, 9628.

(30) Chen, H.; Meisburger, S. P.; Pabit, S. A.; Sutton, J. L.; Webb, W. W.; Pollack, L. *Proc. Natl. Acad. Sci. USA* **2012**, *109*, 799.

(31) Periasamy, A. *J Biomed Opt* **2001**, *6*, 287.

(32) Jares-Erijman, E. A.; Jovin, T. M. *Nat Biotechnol* **2003**, *21*, 1387.

(33) Wu, P.; Brand, L. *Anal Biochem* **1994**, *218*, 1.

(34) Ha, T.; Rasnik, I.; Cheng, W.; Babcock, H. P.; Gauss, G. H.; Lohman, T. M.; Chu, S. *Nature* **2002**, *419*, 638.

Chapter 6: Conclusions, contributions to original knowledge and future Work

6.1 Conclusions and contributions to original knowledge

The work published from chapter 2 (***Nature Chemistry*, 2009**) explores how cyclic metal-DNA structures can be quantitatively assembled into the first 3D metal-nucleic structure. This ability to position transition metals within a three-dimensional framework can lead to metal–DNA hosts with applications for the encapsulation, sensing, modification and release of biomolecules and nanomaterials. Moreover, this established that the 2D DNA polygons can be selectively modified prior to 3D assembly, making this modular approach amenable to further synthetic alteration with various ligands that can be tuned to coordinate a variety of different transition metals. With this, transition metals have the potential to bring much needed functionality, such as redox, photoactivity, magnetic and catalytic properties, as well as increased stability to previously passive 3D DNA constructs.

Towards expanding the range of 3D geometries, sequence symmetry, in tandem with selective synthetic modification, was explored in chapter 3. Here, a simple and quantitative method to generate DNA cages of deliberately designed geometry from readily available starting strands was described. By balancing the incorporation of sequence uniqueness and symmetry in a face-centered approach to 3D construction, a triangular (TP), rectangular (RP), and pentagonal prisms (PP) could be assembled without compromising the potential for nanostructure addressability. This published methodology (***Chemical Commun*ications, 2011)** is important within the field of structural DNA nanotechnology, as it gives researchers a means to selectively re-use sequences with their design, thus limiting the amount of unique strands required for 3D DNA assembly. It is also demonstrated where the limits of sequence symmetry are for assembly.

Taken together, chapters 2 and 3 provide methods to assemble of 3D DNA structures containing single-stranded sites as a new approach in DNA

nanotechnology to give quantitative yields, room temperature assembly, assembly at higher concentrations and ease of functionalization.

In chapter 4, a method to build 3D-DNA structures that represents a departure from previous approaches developed in structural DNA nanotechnology was introduced. This method starts with a minimum number of DNA strands, and assembles them in excellent yield to give a 3D-scaffold that contains a large number of single-stranded arms. This well-defined 3D-DNA "frame" could then be used as a core structure onto which site-specific hybridization of DNA-polymer conjugates can be accomplished. This results in a range of biohybrid DNA-block copolymer cages. Polymer-coated DNA cages were found to be more nuclease-resistant than unfunctionalized DNA structures. Given the fact that the field of DNA nanotechnology typically uses highly DNA dense and double-stranded structures, this published work (***Journal of the American Chemical Society*, 2012**) provides an alternative 'DNA-economic' strategy for 3D DNA assembly. Design and development of 3D DNA structures in this manner should yield opportunities for maximal addressability and 3D-organization of components on the nanometer length scale.

Increasing interest in biology and medicine has driven discovery into functional DNA-based nanostructures. This has made it ever more important to develop ways to make DNA-based materials compatible and stable under biological conditions. Toward this goal, it was demonstrated in chapter 5 that plasma membrane crossing and cytoplasmic accumulation is significantly enhanced when DNA is packaged in compact, well-defined cubes. Furthermore, the mechanism for cellular uptake may be a result of selective uptake via receptors that are capable of discriminating DNA shape. While the mechanism for cellular uptake is still under investigation, the work developed in this chapter (**manuscript under preparation**) illustrates how DNA cages may be useful as vehicles to achieve efficient and selective delivery of therapeutic oligonucleotides and act as switchable, responsive probes of intracellular activity. Moreover, the sequence asymmetric design developed allows site-specific DNA hybridization of different chemical modalities in geometrically well-defined fashion. Control over

3D DNA geometry and positioning of biomacromolecules will allow exploration into how variance in shape affects cell uptake for 3D DNA structures.

Overall, this dissertation has enabled the development of more 'DNA-minimal' approaches to generating 3D DNA structure. These use DNA strands that have been synthetically modified, and result in highly efficient assembly, maximal single-stranded DNA sites within structures and much higher assembling concentrations. Taken together, these methods for 3D DNA assembly could be used to guide the organization of synthetic materials that are engineered for increased biocompatibility, cell penetration ability, and decreased toxicity. The synergistic arrangement of nucleic acids and synthetic components will be useful to address challenges of precise molecular patterning and chemical construction.

6.2 Suggestions for future work

With respect to chapter 2, future work will explore the incorporation of various ligand environments capable of selectively binding different metals within the 3D DNA structures. Recent advancements in our lab have actually led to the development of a terpyridine modification and DNA templation to create mixed-ligand environments for selective metal coordination in 1D structures.[1] Also, due to the advancements in chapter 3, it will be possible to expand the range of metal-containing 3D DNA geometries. Study of the properties of these metal-DNA hybrids, using electrochemical or luminescence based techniques, will reveal fundamental insight the synergistic behaviour of such synthetic insertions within a well-defined 3D nanoscale scaffold. In addition, each of the DNA polygons created in chapters 2 and 3 are amenable to conjugation with various synthetic and biomacromolecules at either the 5' or 3' terminal positions. These structures could prove essential for both mimicking and studying polyvalent effects. For example, various numbers of polymers or peptides could be conjugated to the 2D polygons and assembled into geometrically well-defined arrangements.

Numerous further studies can be envisaged that utilize the 'DNA-minimal' approach to 3D DNA assembly outlined in chapters 4 and 5. Most obvious, is that the geometries assembled with this approach can be expanded (preliminary work has been done towards this) and more detailed structural studies using cryo-

EM/single-particle construction performed to gain insight into overall structure in solution. The asymmetric sequence design outlined in chapter 5 for the DNA cube offers a unique scaffold that can be used in future work to site-specifically, and in a geometrically well defined fashion, position DNA-conjugated materials with nanometer precision. The positive results obtained so far with the *in cellulo* results illustrated in chapter 5, will allow future exploration on how variance in shape may affect cell uptake for 3D DNA structures. More specifically, the packaging or integration of functional nucleic acids, such as antisense or siRNA oligonucleotides, into 3D geometries may prove to be an effective measure for delivering and investigating novel cellular probe and drug delivery designs within the field of structural DNA nanotechnology. We could also go one step further here and completely replace the single-stranded portions of each 3D structure with synthetic molecules, such as peptides, biomimetic DNA polymers or conjugated molecules, towards examining the properties of such hybrid materials.

Some of the major challenges in working towards applications based on 3D DNA nanostructures are assessing their long-term stability under biological conditions, determining whether/how they can 'escape' endosomal entrapment and tracking their movement in the cell. Although preliminary work from our lab suggests that covalent closure of the phosphodiester backbone at the nicked junctions within each 3D structure is enough to cause nuclease stability (specifically to exonucleases), these methods are in a way 'clunky'. This is to say that synthetic modification at these positions to a) stabilize junctions and b) increase nuclease resistance could be done in manner that additionally imparts a functional role. Such modifications may include polymers or peptides that could also serve as targeting moieties for specific receptor-mediated uptake. Another route to non-covalent closure at the nicked junctions is to selectively modify component strands with metal binding ligands that can be templated to form an octahedral environment for coordination to metals such as ruthenium. One may gain stability and optical activity (luminescence) along with nuclease resistance.

6.3 References

(1) Yang, H.; Rys, A. Z.; McLaughlin, C. K.; Sleiman, H. F. *Angew. Chem. Int. Ed.* 2009, *48*, 9919.

Appendix 1- Stable Gold Nanoparticle Conjugation to Internal DNA Positions: Facile Generation of Discrete Gold Nanoparticle-DNA Assemblies

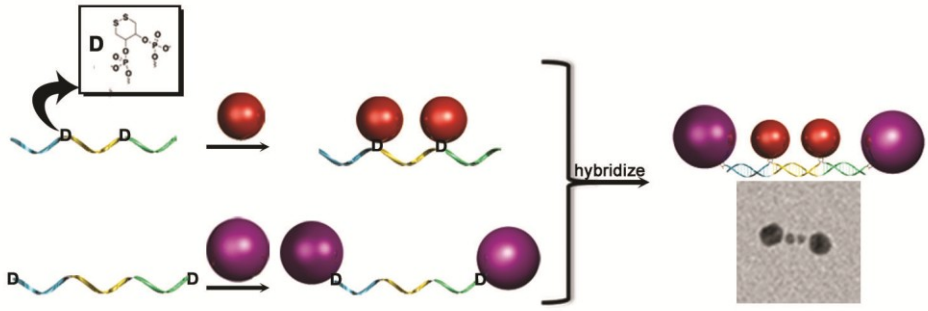

Reproduced with permission from; "Stable gold nanoparticle conjugation to internal DNA positions: facile generation of discrete gold nanoparticle-DNA assemblies", Wen, Y., McLaughlin, C. K., Lo, P. K., Yang, H. and Sleiman, H. F. Bioconjugate Chem., **2010**, 21, 1413-1416. American Chemical Society (2010).

A1.1 Abstract

A straightforward strategy to stably anchor one or more gold nanoparticles (AuNPs) at both the internal and terminal positions of single-stranded DNA is presented. Discrete DNA-AuNP conjugates are isolated using a noncovalent extension strand strategy that helps to resolve prepared species by agarose gel electrophoresis (AGE). These are used to assemble well-defined AuNP squares and rectangles. Two complementary bis-AuNP-labeled DNA conjugates are then prepared. One of these places two smaller (5 nm) AuNPs at defined internal positions within a DNA strand, and the other places two larger (13 nm) AuNPs at each of its terminal positions. We show the self-assembly of these bis-AuNP conjugates into a tapered tetrameric gold nanoparticle "antenna" structures of

direct relevance to engineered "hot spots" and surface enhanced Raman scattering (SERS) substrates.

A1.2 Introduction

Gold nanoparticle assemblies have recently attracted considerable interest as a class of materials with novel optical, electronic, catalytic, and sensing applications.[1,2] In particular, their ability to exhibit single electron transport and to act as plasmon "antennae" for focusing light to nanoscale volumes may lead to their incorporation in future nanoelectronic and nanophotonic devices and as sensitive reporters in biodetection and bioimaging strategies.[3] These properties arise directly from the geometric arrangement of the particles within the assembly.[1,4-10] In order to investigate these phenomena and to incorporate nanoparticles into devices and biosensing schemes, methods to systematically organize gold particles (AuNPs) into well-defined assemblies are essential.

Toward this goal, the DNA-directed organization of AuNPs can provide a high degree of control, due to its programmable self-assembly parameters.[4,11-24] However, the 1:1 conjugation of a DNA strand onto a gold nanoparticle is still synthetically challenging. It typically relies on bringing together gold nanoparticles with a DNA strand that is end-labeled with a single thiol unit, in a 1:1 ratio. This leads to a statistical mixture of unlabeled, singly labeled, and multiply labeled nanoparticles that are usually difficult to separate, unless the DNA strand is very long (e.g., >80 bases). Moreover, because the conjugation is through a single gold-thiol bond, these conjugates are typically labile and tend to lose their DNA labels in a relatively short time. Finally, strategies to conjugate nanoparticles to internal positions of a DNA strand in a stable manner are necessary, in order to expand the range of gold-DNA assemblies. Solutions have been put forward to address some of these problems individually;[25-32] however, there remains a need for a single strategy that gives ready access to these conjugates with stability, ease of separation, and internal conjugation, and as a result increases their applications range.

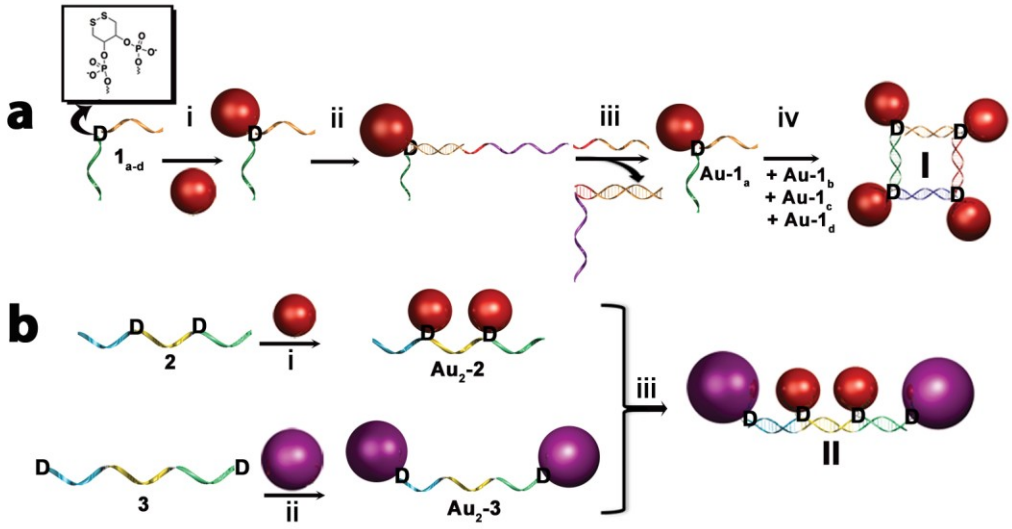

Figure A1.1 Site-specific conjugation of AuNPs to internal and external DNA positions using a cyclic disulfide. (A) Sequence **1a**, modified internally with cyclic disulfide **D** (inset), is conjugated to AuNPs (step i). Upon addition of extension strand (step ii), the conjugate can be isolated by electrophoresis, and a displacement strand (step iii) is used to obtain the DNA-AuNP conjugate. Four such monoconjugates **Au-1a-d** are annealed to give discrete AuNP tetramer **I** (step iv). (B) Selective functionalization of **D**-modified strands **2** (step i) and **3** (step ii) with two different sizes of nanoparticles generate dimers that can be further assembled into linear tetrameric structure **II**.

We report here the first example of site-specific and stable conjugation of gold nanoparticles at any internal position within DNA strands. This is achieved through incorporation of a cyclic disulfide group (**D**, inset Fig. 6.1a) within a DNA strand, which serves as a chelating anchor to stably position AuNPs. Moreover, we achieved ready separation and purification of the AuNP-DNA conjugates through the use of a noncovalent extension strategy. This involves hybridization with a partially cDNA strand (**EXT**) that helps to increase the separation between conjugated and unconjugated nanoparticles by electrophoresis, followed by strand displacement of **EXT** (Fig. 6.1). Thus, AuNP mono-conjugates can be isolated even when the DNA strand is relatively short.

Using this strategy, we designed an internally bis-labeled DNA strand that can capture two AuNPs within a single DNA sequence **2** (Fig. 6.1b). This creates AuNP dimers that can now be used for further self-assembly. By combining bis-

AuNP labeling at internal and terminal (**3**) positions, we can create a nanoparticle "antenna" tapered structure, containing two larger nanoparticles at its two ends and two smaller particles in the middle. Such tapered structures have been predicted to exhibit strong focusing of light in their middle gap through plasmon coupling,[7] with a number of applications in nanophotonics and as surface enhanced Raman scattering substrates. However, they have not been previously generated. Thus, the anchoring of gold nanoparticles on any position within a DNA strand can be achieved and gives access to gold nanoparticle groupings with programmability, stability, and positional and geometric control.

A1.3 Results and discussion

Oligonucleotides **1a-d**, **2**, and **3** containing gold nanoparticle anchoring units were obtained in high yields by standard automated solid-phase synthesis, with site-specific incorporation of a chelating cyclic disulfide **D** as its commercially available phosphoramidite precursor (Fig. 6.1 inset). AuNP conjugation methods were first developed using the singly modified DNA strands **1a-d** that had **D** placed in the middle of the sequence space (Fig. 6.1a). As an example, sequence **1a** was added to 5 nm AuNPs in different molar ratios and left overnight at room temperature in a phosphate buffered saline (PBS) solution. Samples were analyzed by agarose gel electrophoresis (AGE) to determine product composition (Fig. 6.2a). These (lanes 1-4) resulted in diffuse bands of only slightly reduced mobility compared to the 5 nm AuNP marker (lane M). While it was possible that no reaction had taken place between the AuNP and **D** under these conditions, we hypothesized that gold conjugates were formed but may have been inadequately separated by electrophoresis. Previous approaches have used longer conjugating DNA strands to help resolve AuNP-DNA conjugates with electrophoresis[12] or anion-exchange HPLC separation[20].

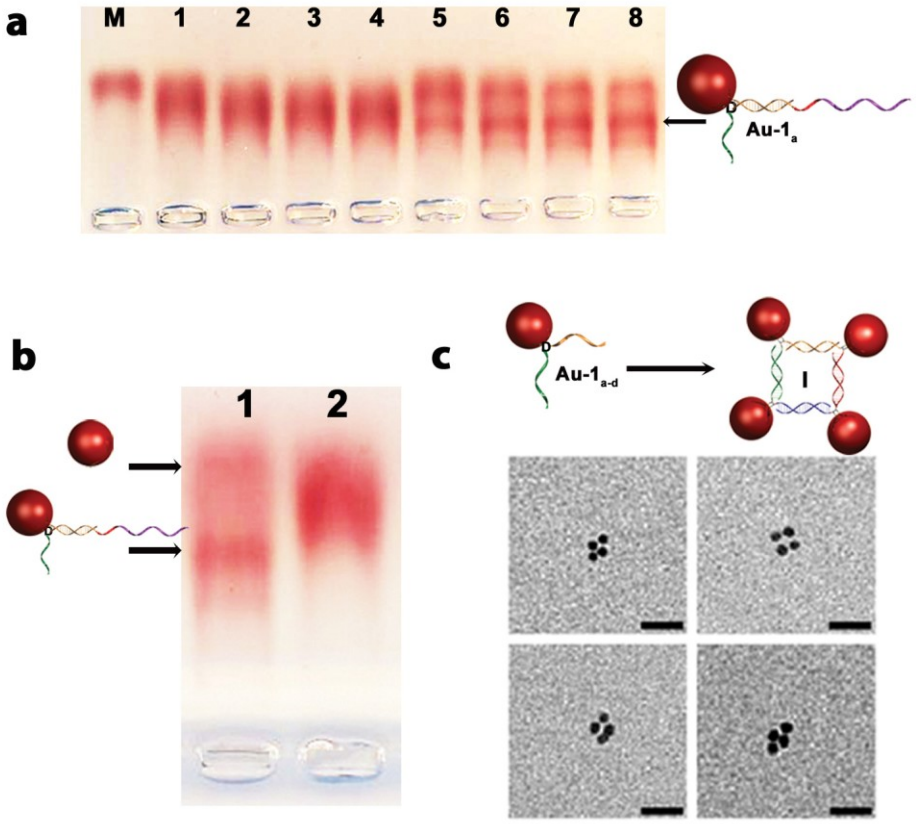

Figure A1.2 AuNP conjugation to internal singly-D modified DNA. (A) 3% agarose gel electrophoresis (AGE, 0.5× TBE) analysis of conjuga- tion between AuNPs (5 nm) and **1a** at various molar ratios (**1a**/AuNP) in the absence (lanes 1-4) and presence (lanes 5-8) of **EXT-1a**. Lane M, 5 nm AuNP; lane 1, 1:1 ratio **1a**/AuNP; lane 2, 2:1 ratio; lane 3, 3:1 ratio; lane 4, 4:1 ratio. Lanes 5-8 contain same ratios of **1a**/AuNP, respectively, except the correct ratio of **EXT-1a** was added prior to AGE analysis. (B) 3% AGE analysis of **1a**/**EXT-1a**/AuNP mixture (2: 2:1) in the absence (lane 1) and presence (lane 2) of **DISP-1a**. (C) Representative TEM fields of view of square structure I assembled from **Au-1a-d**. Scale bars are 20 nm.

Here, we used a noncovalent method for lengthening the conjugating DNA strands. A partially complementary extension (**EXT**) strand is designed to hybridize to the DNA sequence on the gold nanoparticles (Fig. 6.1a). This temporarily increases the size of the DNA strand on the nanoparticle and allows better electrophoretic separation of the monoconjugates from the unconjugated gold nanoparticle.[16] After separation by AGE, the extension strand can be removed by the addition of displacement (**DISP**) strand that possesses a larger region of complementarity. Addition of the appropriate **EXT-1a** sequence to each sample prior to AGE analysis results in the formation of two discrete bands (Fig.

6.2a, lanes 5-8), one with the same mobility as unconjugated AuNPs and one with retarded mobility, that is assigned to the **Au-1a** monoconjugate.

To test the displacement strategy, we conjugated **1a** to 5 nm AuNPs in a 2:1 (DNA/AuNP) molar ratio and added the **EXT- 1a**. After a 10 min incubation period, half of the sample was loaded directly onto a 3% agarose gel. This sample showed two well-separated bands for the unconjugated and the monoconjugated AuNPs (Fig. 6.2b, Lane 1), consistent with temporary lengthening of the conjugating DNA strand. To the second half was added **DISP-1a**, which is fully complementary to **EXT-1a**. This results in a single diffuse band of increased mobility (Fig. 6.2b, lane 2), consistent with displacement of **EXT-1a** from the conjugate and reduced resolution of the unconjugated and the monoconjugated AuNPs.

To confirm the gel band assignment and demonstrate the ability of the internal AuNP monojugates to undergo further organized assembly, we designed an additional set of **D**-labeled sequences (**1b-d**), which, once conjugated to AuNPs, could be hybridized together to yield square particle grouping **I** (Fig. 6.1a). Conjugation of these sequences to AuNPs and isolation of monoconjugates **Au-1a-d** was carried out as above. Quantification of these isolated products **Au-1a-d** was based on the AuNP absorbance at 520 nm, and samples were then mixed in an approximate stoichiometric fashion (1:1:1:1). Characterization of the resulting gold nanoparticle assembly **I** by transmission electron microscopy (TEM) (Fig. 6.2c and section 6.5.7, Fig. 6.5) revealed a number of discrete particle groupings with the expected cyclic tetramer geometry, formed in a yield of ~40%. The TEM analysis in Fig. 6.2c reveals some distortion of the AuNP groupings from the expected square geometry. Unlike our previous system where a rigid organic vertex helps to define the DNA junctions,[16] the vertices in this design are more flexible, leading to increased conformational mobility in the DNA-AuNP conjugates. In addition, structural distortions of DNA-nanoparticle assemblies have been previously noted during TEM imaging on hydrophobic substrates.[23] Using a similar strategy, we also created DNA strands where the **D**-label was asymmetrically positioned in the sequence, such that its AuNP

conjugate carries two DNA arms of different lengths. These conjugates were used to generate rectangular particle groupings with the same efficiency as the square groupings above (see section 6.5.7, Fig. 6.6). In this manner, a variety of discrete gold nanoparticle assemblies can be readily obtained, using the site-specific insertion of a single **D** group within the interior sequence space of single-stranded DNA components.

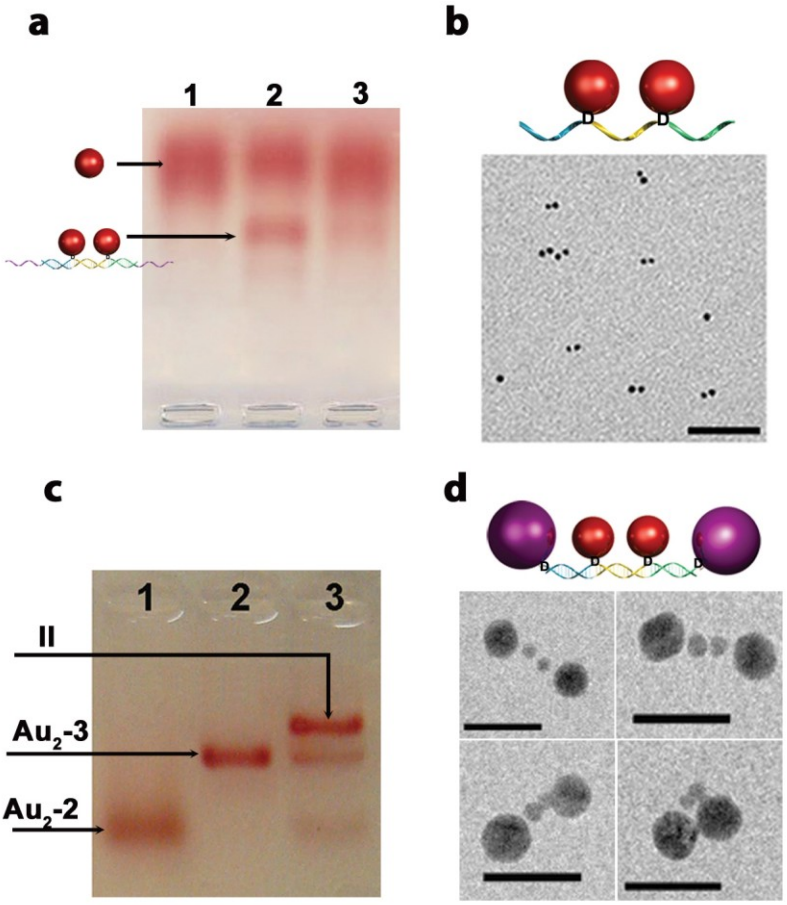

Figure A1.3 Characterization of Au2-2 conjugation and assembled nanostructure II. (A) AGE analysis (3%, 0.5× TBE) of doubly-**D** modified **2** conjugation with AuNPs (5 nm) (**2**/AuNP ratio is 2:1) in the absence (lane 1) and presence (lane 2) of **EXT-2**. Lane 3 shows the mobility after addition of the correct amount of **DISP-2**. (B) Representative TEM field of view for **Au2-2** (scale bar) 100 nm). (C) AGE analysis (2.5%, 0.5× TBE) of isolated structures **Au2-2** (lane 1), **Au2-3** (lane 2), and assembled tetrameric AuNP nanostructure **II** (lane 3). (D) Representative TEM field of view for **II** (scale bar) 20 nm).

To test whether a single DNA strand could selectively conjugate to two gold

nanoparticles, we designed doubly labeled sequence **2** (Fig. 6.1b), which is capable of binding two 5 nm AuNPs. As an example, incubation of **2** with 5 nm AuNPs in a 2:1 ratio (AuNP/DNA) produced a band of reduced electrophoretic mobility upon addition of the extension strand **EXT-2** (Fig. 6.3a, lane 1), which we assigned to the AuNP dimer. Isolation of this band, followed by removal of extension strand **EXT-2** with added **DISP-2**, gave **Au2-2**. This dimer contains one internal DNA single strand between the two nanoparticles, as well as two external single-stranded DNA sections on each particle, that are available for further hybridization (Fig. 6.1b). After isolation of this band, TEM analysis was used to confirm the **Au2-2** dimer assignment. A typical TEM field of view for **Au2-2** is shown in Figure 2b, which reveals a number of dimer structures that are formed in high yield (~75%). Additional evidence for the formation of these single-stranded DNA-AuNP dimers came from testing the assembly of two such dimers, containing complementary external DNA strands, into a AuNP square structure (See section 6.5.7, Fig. 6.7). Thus, by placing the cyclic disulfide group **D** within each sequence, access to stable, AuNP modified DNA strands can be achieved. More importantly, the relative position of each AuNP can be easily tuned on the DNA strand, as is the case when comparing structures **Au-1** and **Au2-2** (Fig. 6.1), while retaining single- stranded regions that can now be used to further hybridize materials in a site-specific and programmable manner.

Interestingly, in the case of internal DNA modification with AuNPs such as for **Au-1** and **Au2-2**, increasing the relative ratio of DNA/AuNP from 1:1 to 3:1 did not appear to generate distinct polyconjugated structures as is normally observed when thiol modifications are made at the termini of DNA.[12]

With selective control over the position of AuNPs at internal positions within a DNA sequence, we next attempted to introduce a higher degree of complexity in the assembled nanostructures. Specifically, we designed DNA sequence **3**, the complementary sequence of **2**, to contain **D** at both the 3′- and 5′-positions. In this way, we could conjugate 13 nm nanoparticles to the two ends of this sequence to form AuNP dimer **Au2-3**. **Au2-3** is expected to hybridize with **Au2-2** to form linear tetrameric structure **II**, containing two large 13 nm particles

on its two ends and two smaller 5 nm particles in internal positions (Fig. 6.1b). Motivation for this "antenna" structure came from recent simulations that have shown that tapered structures such as **II** are expected to exhibit strong focusing of light in their middle gap through plasmon coupling,[7] with important implications in engineered "hot spots" for surface-enhanced Raman scattering (SERS).[6]

In a similar fashion to the conjugation of **1** and **2**, doubly 5′-3′ **D**-modified **3** was conjugated to 13 nm AuNPs, resulting in a band of reduced electrophoretic mobility. After isolation of this band, TEM imaging was used to confirm assignment of the AuNP dimer **Au2-3**. Typical TEM fields of view for **Au2-3** (See section 6.5.7, Fig. 6.8) reveal a significant number of dimer products with yields of ~75%. Reanalysis of structures **Au2-2** and **Au2-3** by AGE (Fig. 6.3c, lanes 1 and 2, respectively) showed the clean isolation of each product.

Hybridization of discrete structures **Au2-2** and **Au2-3** in a 1:1 ratio generated the desired "antenna" tetrameric architecture **II** in good yield, as evidenced by the band of reduced mobility in Figure 3c, lane 3. Direct evidence of the tapered structure by TEM analysis (Fig. 6.3d and see section 6.5.7, Fig. 6.9) indeed reveals the formation of tetramer structure **II** in ~38% yield and shows the arrangement of the 5 nm AuNPs placed on the interior and two 13 nm AuNPs that book-end the construct. Similar to the TEM analysis of **I**, distortion in some of the AuNP assemblies **II** is observed, due to the drying conditions on the hydrophobic TEM substrate. It should be noted here that, while bulk optical measurements on these assemblies would yield ensemble averages for all conformations, single-molecule optical measurements on individual assemblies (e.g., surface enhanced Raman scattering) coupled with TEM imaging are expected to provide a better correlation between individual structures and optical activity.[9]

Unlike other DNA-based systems for arranging AuNPs, the stability afforded by the cyclic disulfide insertion, in conjunction with the ability to easily isolate site-specifically labeled AuNP-DNA constructs that contain single-stranded regions, introduces a high degree of programmability and modularity into this approach. In this way, fewer restrictions exist in comparison to end-monoconjugation, and the stable dimer products can be readily isolated by

electrophoresis and further assembled into any number of spatial arrangements via their single-stranded regions.

A1.4 Conclusions

In conclusion, we have introduced a facile method to stably and site-specifically append one or more AuNPs to either the interior sequence space, or to terminal (5′ or 3′) positions of single-stranded DNA. Insertion of this anchoring group within a DNA sequence led to the generation of AuNP-DNA constructs that contain single-stranded regions, which can be designed to assemble into discrete polygons of spatially well- defined AuNPs. This method was further explored to generate a tetrameric linear construct that contains well-defined positioning of two different sizes of AuNPs (5 and 13 nm). This facile conjugation strategy has the potential to enable the construction of any number of discrete metal nanoparticles, with varied sizes and spatial arrangements, based on the preparation of stably held conjugated AuNP-DNA synthons and their programmed self-assembly. Such discrete structures will be valuable model systems for fundamental physics investigations of optical and electronic properties of nanoparticles and for the generation of surface-enhanced Raman scattering substrates for sensitive biological detection.

A1.5 Experimental

A1.5.1 General

Tris(hydroxymethyl)-aminomethane (Tris), boric acid, acetic acid, ethylenediamine- tetraacetic acid, NaCl, $MgCl_2.6H_2O$, StainsAll®, formamide, and ethidium bromide were purchased from Aldrich. 1,2-Dithiane-4-O-Dimethoxytrityl-5-[(2-cyanoethyl)- N,N-diisopropyl]-phosphoramidite (DTPA) was purchased form Glen Research Corporation. 5-ethylthiotetrazole, CPG and reagents used for automated DNA synthesis were purchased from ChemGenes. Sephadex G-25 (super fine DNA grade), was purchased from Amersham Biosciences. Microcon® size-exclusion centrifugal filter devices were purchased from Millipore. Citrate coated gold nanoparticles were either made in-house or purchased from Ted Pella. The ligand bis(*p*-sulfonatophenyl) phenylphosphine dihydrate dipotassium salt (BSPP) was purchased from Strem

Chemicals. 400 mesh Formvar-carbon coated copper grids for transmission electron microscopy imaging were purchased from Electron Microscopy Sciences.

A1.5.2 Instrumentation

Standard automated oligonucleotide solid-phase synthesis was performed on either a Perspective Biosystems Expedite 8900 DNA synthesizer or MM6 Mermade Synthesizer (Bioautomation). UV-vis experiments were conducted on a Varian Cary 300 biospectrophotometer. Gel electrophoresis experiments were carried out on an acrylamide 20 × 20 cm vertical Hoefer 600 electrophoresis unit or 7 × 8 cm horizontal Owl separation minigel system. TEM was performed using a Philips CM 200 kV electron microscope.

A1.5.3 Oligonucleotides used for DNA nanostructure assembly

Modified oligonucleotides were constructed on CPG supports (1000 Angstrom) using conventional phosphoramidite chemistry. Products were cleaved from the support by treatment with concentrated NH_4OH for 16 h at 55 °C. The NH_4OH solution was carefully pipetted out and dried down to yield the crude DNA mixture. The crude mixture was purified on 24% polyacrylamide/7 M urea gels using 0.09 M Tris-borate-EDTA buffer (pH 8.3). Gels were illuminated briefly with UV light to visualize DNA bands which were excised, crushed and incubated in 10 mL of sterile water at 55°C (16 hours). The tubes were then vortexed and briefly centrifuged to condense acrylamide. The supernatant was removed and the volume brought to ca. 1 mL under heat/reduced pressure in a speedvac system. DNA samples were then desalted using Sephadex G-25 size exclusion media. Quantification was determined based on UV-vis absorbance at 260 nm.

For the sequences modified by one or more **D** inserts in the middle, the first arm, of appropriate sequence, was initially grown on the solid support using standard automated solid phase oligonucleotide synthetic protocols. **D** was then incorporated using a modified protocol in which the coupling and deprotection times were extended to ten and two minutes, respectively. Subsequently, the second arm was synthesized using standard synthetic protocols.

Table A1.1 DNA prepared for AuNP Conjugation Experiments. Cyclic disulfide (**D**) inserted via standard phosphoramidite chemistry.

Name	Sequence (5' → 3')
$\mathbf{1_a}$	AATTGATATGTCACGAATAACACAAATCGGTCAGTAATCT**D**C TTGAAGGTAGCAAACGACAGGTCCAAATGAAGATACGAA
$\mathbf{1_b}$	TCATTGCTTCAGTATCTAAGTAGTAGTGACCACTAGCTCT**D**TT CGTATCTTCATTTGGACCTGTCGTTTGCTACCTTCAAC
$\mathbf{1_c}$	AGAGCTAGTGGTCACTACTACTTAGATACTGAAGCAATGA**D**T GAGGCAGATAAGGATAGGACTTTTGGAGACTACGACGGA
$\mathbf{1_d}$	AGATTACTGACCGATTTGTGTTATTCGTGACATATCAATT**D**TC CGTCGTAGTCTCCAAAAGTCCTATCCTTATCTGCCTCA
EXT-1_a	TTTTTTTTTTTTTTTTTTTTTTTTTTTTTTTTTTTTTTTTTTTAGA GCTAGTGGTCACTTCGTATCTTCATTTGGACCT
DISP-1_a	AGGTCCAAATGAAGATACGAAGTGACCACTAGCTCT
2	TCAGTATCGTATCTTT**D**TCCTTGGACCTGTCGTGTTT**D**TTGCCT TCTCTACTTC
EXT-2	TTTTTTTTTTTTTTTTTTTTTTTTTTTTTTTTTATCCACACGACAG GTCCAACGGCATTTTTTTTTTTTTTTTTTTTTTTTTTTTT
3	**D**TTGAAGTAGAGAAGGCATTTAACACGACAGGTCCAAGGTTT AAGATACGATACTGATT**D**
EXT-3	TTTTTTTTTTTTTTTTTTTATCCAGAACACGACAGGTCCAAGG TCGGCA TTTTTTTTTTTTTTTTTT
DISP-3	TGCCGACCTTGGACCTGTCGTGTTCTGGAT

A1.5.4 Confirmation of hybridized structures by native PAGE

Annealed structures **I** and **II** were initially verified by polyacrylamide gel electrophoresis (PAGE) under non-denaturing conditions. In a typical experiment, samples of each building block in the correct molar ratios (final assembly 1.2×10^{-10} moles; 30 μL PBS) were added in PBS (pH 7.4, 10mM, 100 mM NaCl) and incubated at room temperature for 10 minutes. All of the final assemblies were characterized using 7 % native polyacrylamide gel (run at constant current of 10 mA, 4 °C and visualized using StainsAll®). As an example, Figure 6.4 shows the hybrdization of both square structure **I** and linear tetra-**D** mfunctionalized **II**. Strand **1a** alone showed a band of relatively high mobility (Fig. 6.4a, lane 1). The assemblies of two, three, and four building blocks showed well-defined, single bands of steadily decreasing mobility. This behavior is consistent with the clean and quantitative formation of discrete duplex assemblies containing the desired number of building blocks in each case. The addition of the fourth

building block is expected to result in both duplex formation and subsequent cyclization (lane 4 in Figure 6.4a). In addition, a second band of low mobility was detected, suggesting the concomitant formation of a small amount of higher order oligomeric species.

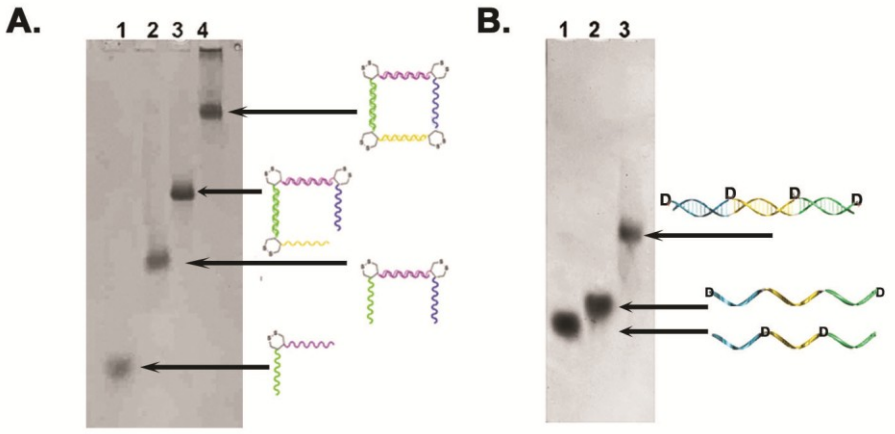

Figure A1.4 Native polyacrylamide gel (7%, 1x TAEMg) analysis of the assembly products. (a) Structure **I** was assembled by the sequential addition of **1a-d** (lanes 1-4, respectively) in PBS solution at room temperature . (b) Sequences **2** and **3** are annealed at room temperature in PBS solution to yield the tetra-subsituted nanostructure **II** in an excellent yield.

A1.5.5 Preparation and Phosphination of AuNPs

AuNPs were prepared by citrate reduction methods in the presence (5 nm)[33] or absence (13 nm)[34] of tannic acid as co-reductant. Both types of citrate coated AuNPs were further stabilized against aggregation via addition of BSPP.[34] Briefly, 20 mg of BSPP was added to the 10 mL of AuNP solution and left overnight on a vortex mixer at low speed. Sodium Chloride (solid) was added slowly to the colloidal gold solutions until a colour change was observed from burgundy to purple. Resulting mixtures were centrifuged at 4000 rpm for 30 min and the supernatant removed and discarded. The pelleted AuNPs were then resuspended in 100 μL of a BSPP solution (2.5 mM). AuNPs were quantified by assaying the optical absorbance at 520 nm.

A1.5.6 General Protocol for AuNP-DNA Conjugation

In general, 1 x 10^{-11} moles of AuNPs (3.3 uM) were used in conjugation experiments for both 5 and 13 nm AuNPs. Varying molar ratios of DNA based on the above moles of AuNPs were used for conjugation experiments to account for any inaccuracy in the quantified AuNP solutions. Typically, appropriate DNA volumes, based

on the required moles, were taken from stock solutions and dried to completion. The DNA was then resuspended in an appropriate volume of PBS (10 mM, 100mM NaCl) that would bring the AuNP concentration to 3.3 uM. AuNPs were added to the resuspended DNA with slight mixing and samples were left overnight at room temperature. The resulting AuNP-DNA conjugates were loaded onto an agarose gel (3% for 5 nm and 2.5% for 13 nm) and run at 10V/cm in 0.5x TBE running buffer. In the case of conjugates requiring extension strands, the appropriate **EXT** strand was added in the correct molar ratio (initially dried down and resuspended in a minimal volume of PBS) with slight mixing and left to stand at room temperature for 10 minutes prior to being loaded onto an agarose gel. Monoconjugate bands were isolated after AGE by electroelution into glass fiber backed with dialysis membrane (MWCO 10000). After removal of the dialysis membrane, the glass fiber containing the AuNP conjugates were placed into a 0.6 μL centrifuge tube that had a small hole fitted in the bottom with a syringe needle. This centrifuge tube was then placed into a 1.5 mL centrifuge tube and spun at 500 rpm for 5 minutes. The AuNP-DNA conjugates were then carefully pipetted into a clean centrifuge tube. Quantification of monoconjugates was estimated by obtaining the absorbance at 520 nm and samples stored at 4 ^{o}C. If necessary, monoconjugate solutions were further concentrated using microcon filtration devices (MWCO 3000). From the estimated concentrations, the correct molar ratio of the appropriate displacement strand could be calculated that is required to remove the extension strands.

A1.5.7 General Protocol for TEM

TEM was performed using a Philips CM 200 kV electron microscope. 3 - 5 μL of dilute sample in 0.5xTBE buffer was spotted on the surface of Formvar-coated copper TEM grids. The sample was left on the grid for 3 min to allow particles to adsorb to the surface before touching the edge of the grid with a filter paper to wick off excess moisture and salts. Grids were then allowed to air-dry prior to analysis. Additional TEM support for all hybridized AuNP structures can be found in Fig. 6.5-6.9.

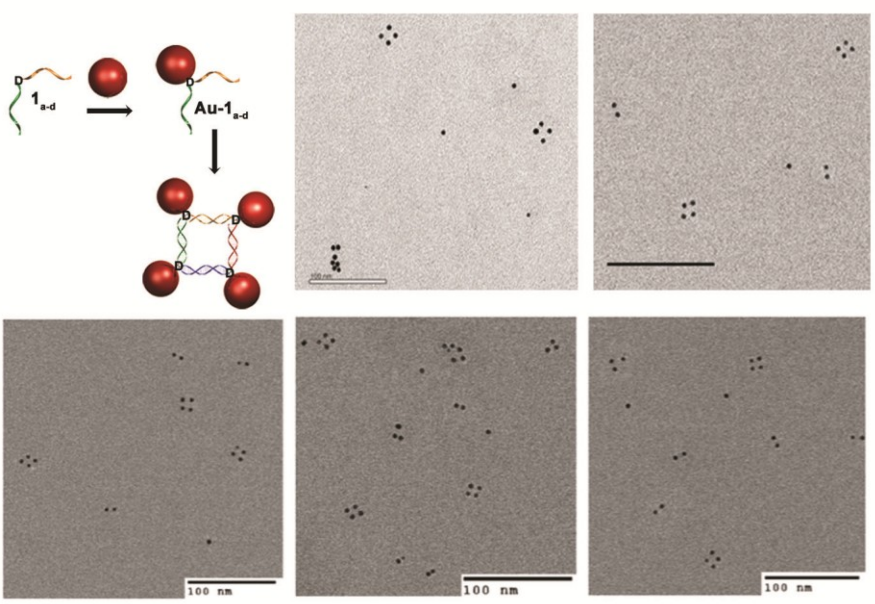

Figure A1.5 Additional TEM fields of view obtained for I. Square **I** was produced from **Au-1a-d** in ca. 41% yield.

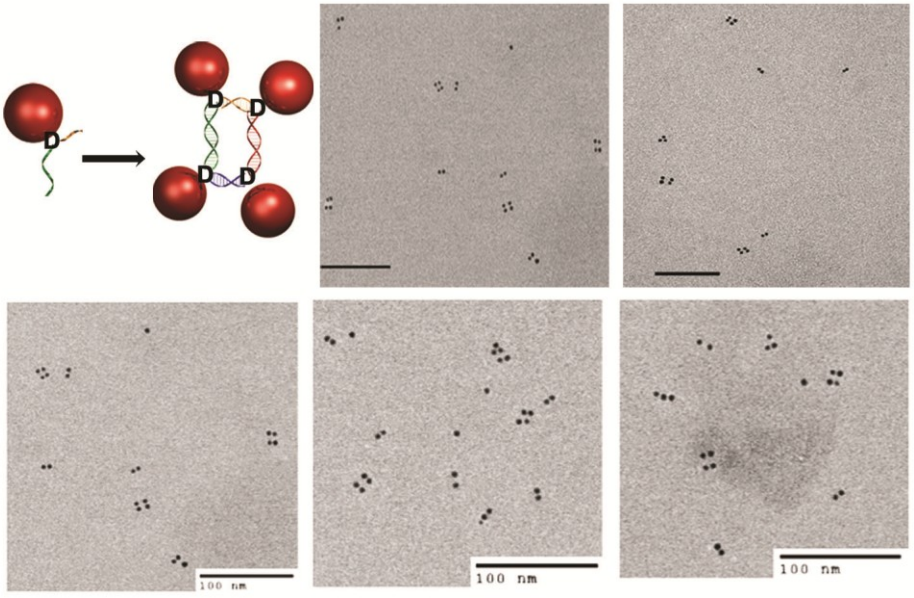

Figure A1.6 Additional TEM fields of view obtained for structure III. The rectangular AuNP structure **III** was prepared in ca. 37% yield.

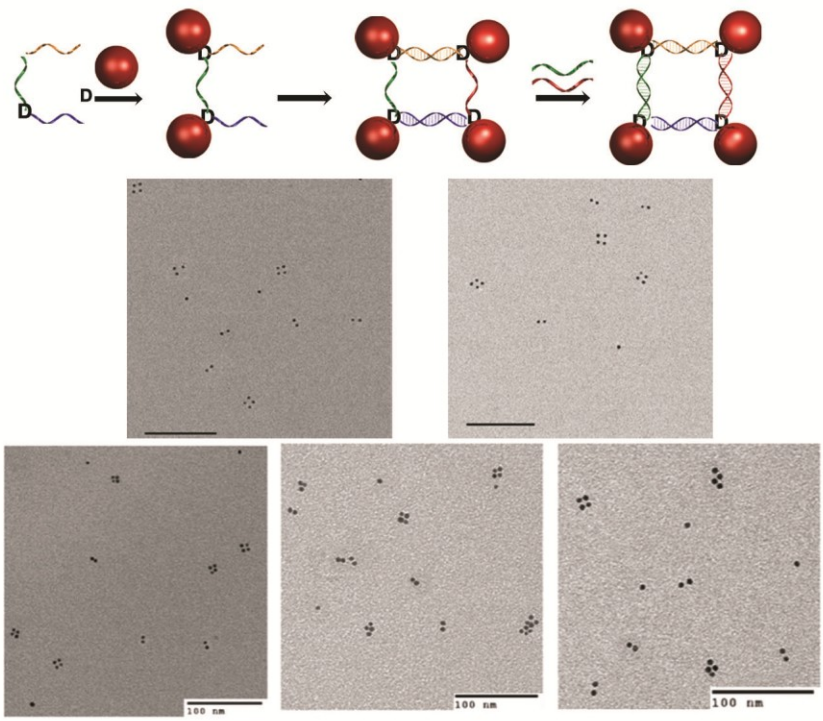

Figure A1.7 Additional TEM fields of view obtained for structure IV. The square AuNP structure **IV** was prepared in ca. 48% yield.

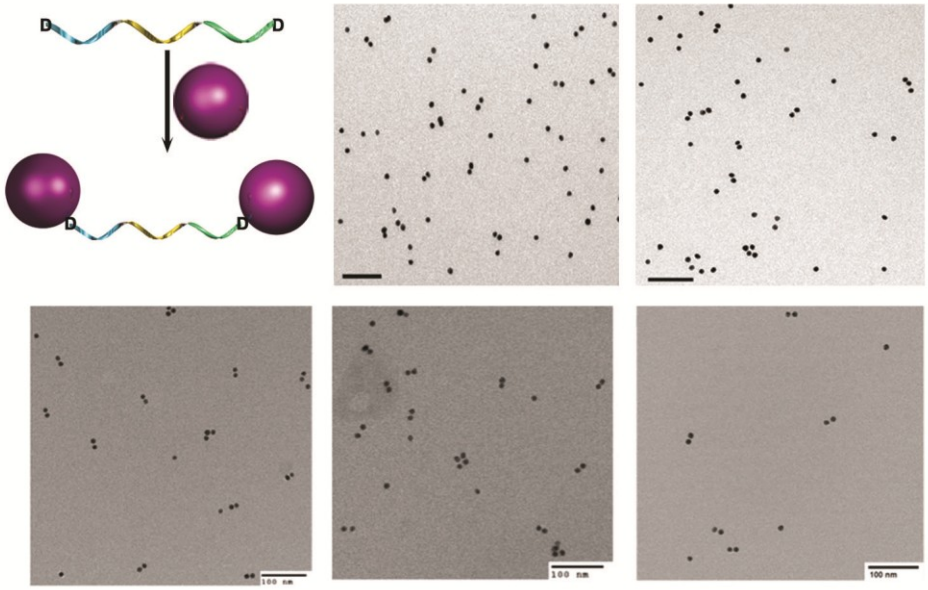

Figure A1.8 Additional TEM fields of view obtained for Au2-3. The dimer of 15 nm AuNPs **Au2-3** was produced in ca. 75% yield.

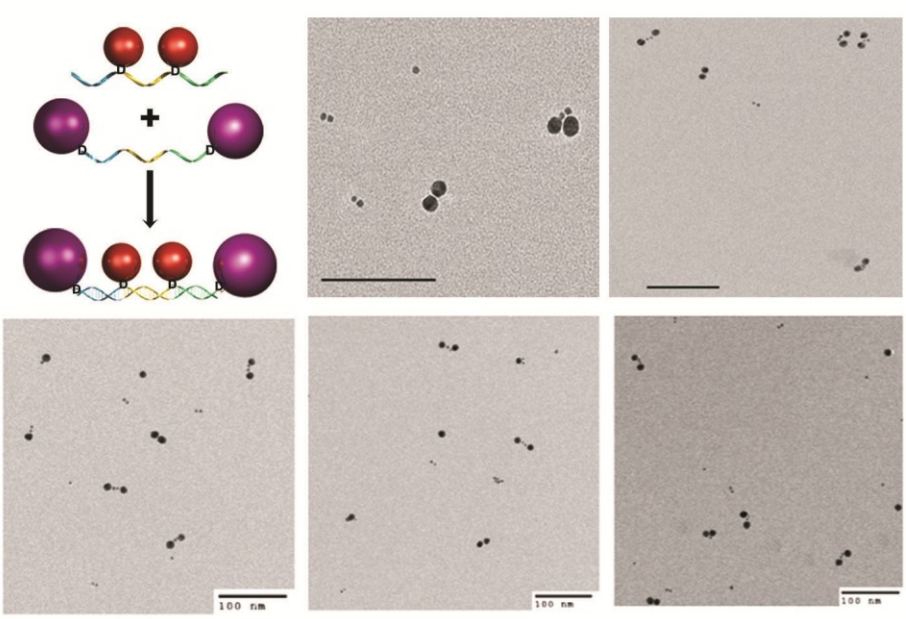

Figure A1.9 Additional TEM fields of view obtained for structure II. The tetrameric mixed AuNP structure **II**, prepared from **Au2-2** and **Au2-3**, was produced in ca. 38% yield.

A1.6 References

(1) Nie, Z. H.; Petukhova, A.; Kumacheva, E. *Nat. Nanotechnol.* 2010, *5*, 15.

(2) Sperling, R. A.; Rivera Gil, P.; Zhang, F.; Zanella, M.; Parak, W. J. *Chem. Soc. Rev.* 2008, *37*, 1896.

(3) Wilson, R. *Chem. Soc. Rev.* 2008, *37*, 2028.

(4) Mirkin, C. A.; Letsinger, R. L.; Mucic, R. C.; Storhoff, J. J. *Nature* 1996, *382*, 607.

(5) Reinhard, B. M.; Siu, M.; Agarwal, H.; Alivisatos, A. P.; Liphardt, J. *Nano Lett.* 2005, *5*, 2246.

(6) Ghosh, S. K.; Pal, T. *Chem. Rev.* 2007, *107*, 4797.

(7) Chien, W. Y.; Szkopek, T. *Opt. Express* 2008, *16*, 1820.

(8) Li, W. Y.; Camargo, P. H. C.; Lu, X. M.; Xia, Y. N. *Nano Lett.* 2009, *9*, 485.

(9) Lim, D. K.; Jeon, K. S.; Kim, H. M.; Nam, J. M.; Suh, Y. D. *Nat. Mater.* 2010, *9*, 60.

(10) Myroshnychenko, V.; Rodriguez-Fernandez, J.; Pastoriza-Santos, I.; Funston, A. M.; Novo, C.; Mulvaney, P.; Liz-Marzan, L. M.; Garcia de Abajo, F. J. *Chem. Soc. Rev.* 2008, *37*, 1792.

(11) Alivisatos, A. P.; Johnsson, K. P.; Peng, X. G.; Wilson, T. E.; Loweth, C. J.; Bruchez, M. P.; Schultz, P. G. *Nature* 1996, *382*, 609.

(12) Zanchet, D.; Micheel, C. M.; Parak, W. J.; Gerion, D.; Alivisatos, A. P. *Nano Lett.* 2000, *1*, 32.

(13) Deng, Z. X.; Tian, Y.; Lee, S. H.; Ribbe, A. E.; Mao, C. D. *Angewandte Chemie-International Edition* 2005, *44*, 3582.

(14) Zheng, J. W.; Constantinou, P. E.; Micheel, C.; Alivisatos, A. P.; Kiehl, R. A.; Seeman, N. C. *Nano Lett.* 2006, *6*, 1502.

(15) Aldaye, F. A.; Sleiman, H. F. *Angew. Chem. Int. Ed.* 2006, *45*, 2204.

(16) Aldaye, F. A.; Sleiman, H. F. *J. Am. Chem. Soc.* 2007, *129*, 4130.

(17) Lee, J. H.; Wernette, D. P.; Yigit, M. V.; Liu, J.; Wang, Z.; Lu, Y. *Angewandte Chemie-International Edition* 2007, *46*, 9006.

(18) Lee, J. S.; Lytton-Jean, A. K.; Hurst, S. J.; Mirkin, C. A. *Nano Lett.* 2007, *7*, 2112.

(19) Bidault, S.; Abajo, F. J.; Polman, A. *J. Am. Chem. Soc.* 2008, *130*, 2750.

(20) Claridge, S. A.; Liang, H. W.; Basu, S. R.; Frechet, J. M.; Alivisatos, A. P. *Nano Lett.* 2008, *8*, 1202.

(21) Park, S. Y.; Lytton-Jean, A. K.; Lee, B.; Weigand, S.; Schatz, G. C.; Mirkin, C. A. *Nature* 2008, *451*, 553.

(22) Nykypanchuk, D.; Maye, M. M.; van der Lelie, D.; Gang, O. *Nature* 2008, *451*, 549.

(23) Mastroianni, A. J.; Claridge, S. A.; Alivisatos, A. P. *J. Am. Chem. Soc.* 2009, *131*, 8455.

(24) Sharma, J.; Chhabra, R.; Cheng, A.; Brownell, J.; Liu, Y.; Yan, H. *Science* 2009, *323*, 112.

(25) Letsinger, R. L.; Elghanian, R.; Viswanadham, G.; Mirkin, C. A. *Bioconjugate Chem.* 2000, *11*, 289.

(26) Li, Z.; Jin, R.; Mirkin, C. A.; Letsinger, R. L. *Nucleic Acids Res.* 2002, *30*, 1558.

(27) Dougan, J. A.; Karlsson, C.; Smith, W. E.; Graham, D. *Nucleic Acids Res.* 2007, *35*, 3668.

(28) Sharma, J.; Chhabra, R.; Andersen, C. S.; Gothelf, K. V.; Yan, H.; Liu, Y. *J. Am. Chem. Soc.* 2008, *130*, 7820.

(29) Sharma, J.; Chhabra, R.; Yan, H.; Liu, Y. *Chem. Commun.* 2008, 2140.

(30) Stakenborg, T.; Peeters, S.; Reekmans, G.; Laureyn, W.; Jans, H.; Borghs, G.; Imberechts, H. *J. Nanopart. Res.* 2008, *10*, 143.

(31) Mei, B. C.; Oh, E.; Susumu, K.; Farrell, D.; Mountziaris, T. J.; Mattoussi, H. *Langmuir* 2009, *25*, 10604.

(32) Suzuki, K.; Hosokawa, K.; Maeda, M. *J. Am. Chem. Soc.* 2009, *131*, 7518.

(33) D. A. Handley (1989) *Colloidal Gold: Principles, Methods and Applications Vol. 1* (Hayat, M. A., Ed.) pp 13-22, Academic press, San Diego.

(34) T.A. Taton (2002) Preparation of Gold Nanoparticle–DNA Conjugates. *Current Protocols in Nucleic Acid Chemistry.* pp 12.2.1-12.2.12.

Appendix 2- Self-Assembly of 3D DNA Structures Using either a Modular Linking Strand or Clip-by-Clip Approach

A2.1. Introduction

This appendix is a detailed experimental methods section that encompasses the assembly strategies developed in chapters 2-5. Specifically, it is intended to distill the pertinent elements of the DNA assembly strategies developed within this thesis. As such, this appendix is broken down into 2 parts; 1 – assembly 3D DNA assembly using linking strands (Chapters 2 and 3 material) and 2 – A DNA economic approach to 3D construction using a Clip-by-Clip strategy (Chapter 4 and 5 material). To help reduce redundancy, references are made throughout this appendix to Figures or Tables within each respective chapter. In addition, the DNA-transition metal work described in Chapter 2 has been previously published in this methods style.[1]

Here, the focus is placed on DNA synthesis/purification, self-assembly and characterization of each system via polyacrylamide gel electrophoresis (PAGE). Throughout the Methods section, notes are placed within the text to give further details/tricks found while developing these strategies. It is the author's hope that the additional detail outlined below will help to better cohesively organize the experimental methods developed within this thesis work.

A2.2. Materials

A2.2.1 Solid Phase DNA synthesis

1. Standard reagents and phosphoramidites for automated solid- phase DNA synthesis are currently being purchased almost exclusively through Bioautomation Corporated. Initial work was performed using an isobutyryl protected deoxyguanosine and benzoyl protected deoxycytosine. The former required long deprotection times (upwards of 16 h) and has since been replaced by the N-dimethylformamidine protected version. In addition, an acetyl protected version of deoxycytosine is now being used so that fast-deprotection with a

mixture of ammonium hydroxide and methyl amine (1:1 by volume) can be employed. Numerous reports and literature can be found on the Glen Research website (www.glenresearch.com) that overview these base modifications.

2. Functionalized controlled pore glass (CPG) supports are also almost exclusively obtained through Bioautomation. Typical loading densities of ca. 30 mmol/g are used along with 1,000 Angstrom pore sizes. A first generation universal support was initially used and required lithium chloride for full deprotection. This has since been replaced with a second-generation version UnyLink support that does not require additional chemical treatment.

6. Concentrated ammonium hydroxide (NH_4OH) solution (28%, Fisher Scientific).

7. Sephadex G-25 (superfine DNA grade) (Amersham Bio-sciences) in pre-packed columns are used to desalt DNA strands synthesized in Chapters 2 – 5. A similar product from Glen Research has since replaced this.

A2.2.2. Polyacrylamide Gel Electrophoresis (PAGE)

1. TB (10×): 900 mM tris (hydroxymethyl)-aminomethane (Tris) and 900 mM boric acid, pH 8. Store at room temperature.

2. TB (1×): prepared by tenfold dilution of TB (10×).

3. TAMg (10×): 400 mM Tris, 126 mM $Mg(OAc)_2 \times 6H_2O$, and ca. 14 mM glacial acetic acid, pH 8 (adjusted with small amounts of glacial acetic acid). Autoclaving extends the longevity of this buffer and helps to prevent bacterial growth. EDTA can be added to this buffer ONLY if it is not being used for cell uptake or nuclease studies i.e. EDTA can chelate metals required for proper nuclease function or metal-coordination.

4. TAMg (1×): prepared by tenfold dilution of TAMg (10×). For running buffer purposes, dilution is typically done with MiliQ water. For assembly (especially biological samples), the 10xTAMg buffer is diluted with autoclaved water.

5. 40% Acrylamide/bis solution (Fisher Scientific or Bioshop) (WARNING: the unpolymerized solution is a neurotoxin and care should be taken to avoid exposure) and N,N,N ′,N ′- tetramethylethylenediamine (TEMED, Sigma–

Aldrich).

6. Denaturing polyacrylamide gel electrophoresis (PAGE) solution (24%, 100 mL): mix 42.04 g urea, 10 mL TB (10×), and 60 mL 40% acrylamide solution and add water to adjust the volume to 100 mL.

7. Native PAGE solution (8%, 100 mL): mix 10 mL TAMg (10×) and 20 mL 40% acrylamide solution and add water to adjust the volume to 100 mL.

8. Ammonium persulfate (APS).

9. Gel combs: preparative 1.5-mm-thick single lane comb (Hoefer) and 20-lane 0.75-mm-thick comb (Hoefer). Various analytical combs have been used throughout of the years of data acquisition. The 20-lane comb has almost exclusively been used for analytical denaturing and native PAGE experiments in Chapters 3 -5.

10. Denaturing PAGE loading solution: 8 M solution of urea in H_2O.

11. Native PAGE loading solution: mixture of glycerin and H_2O (7:3 v/v).

12. Dye mixture: 1 mL formamide, 10 mM Na_2EDTA, pH 8.0, 0.1% (w/v) bromophenol blue, and 0.1% (w/v) xylene cyanol.

13. Stains-All solution: 10% (w/v) solution of StainsAll (Sigma– Aldrich) made in formamide (98%): H_2O (1:1 v/v). This solution should be kept in the dark to prolong its lifetime.

14. Autoclaved H_2O.

A2.2.3. 3D DNA assembly

1. The sequences synthesized and used for each 3D assembly strategy can be found in Tables 2.1, 3.1, 4.1 and 5.1 within the respective chapters of the thesis.

A2.3. Methods

A variety of geometrically well-defined 3D DNA structures can be prepared by the following methods. The focus will be on how to synthesize and purify sequences necessary for modular 3D DNA asssembly (Figure A2.1) and clips necessary for assembling structures with longer tracts of single-stranded regions

via a clip-by-clip strategy (Figure A2.2).

In chapter 2, the single-stranded regions (10 bases in length) of triangles **T1** and **T2** were designed to be completely sequence asymmetric, as shown in Figure A2.1a. This design thus required three different linking strands LS to form the final prismatic structure. Later, it was found out that this strategy could be simplified by selective use of sequence symmetry, which then only required one LS to create a closed structure (Figure A2.1b). It really is up to the assembler as to how much sequence symmetry is used within the LS design. On one hand, full symmetry allows for easier sequence design while still being able to generate geometrically diverse structures. The flip side of this is that orientational control between the two polygons (**T1** and **T2**, for example) is lost. The most effective use of this assembly strategy likely lies somewhere in the middle between fully asymmetric and symmetric (Figure A2.1c). For example, one could develop a linking strand that is asymmetric between two polygons as shown in Figure A2.1c. As long as the sequences are strong enough to hold together the two polygons, the orientation of the duplex regions should be known. After this, a second symmetric linking strand can be added to hybridize to the remaining single-stranded polygonal edges. This strategy would limit the required sequences and retain control in orienting the top and bottom polygons. Orientation between the polygons and could be tested using the insertion of an appropriate FRET pair.

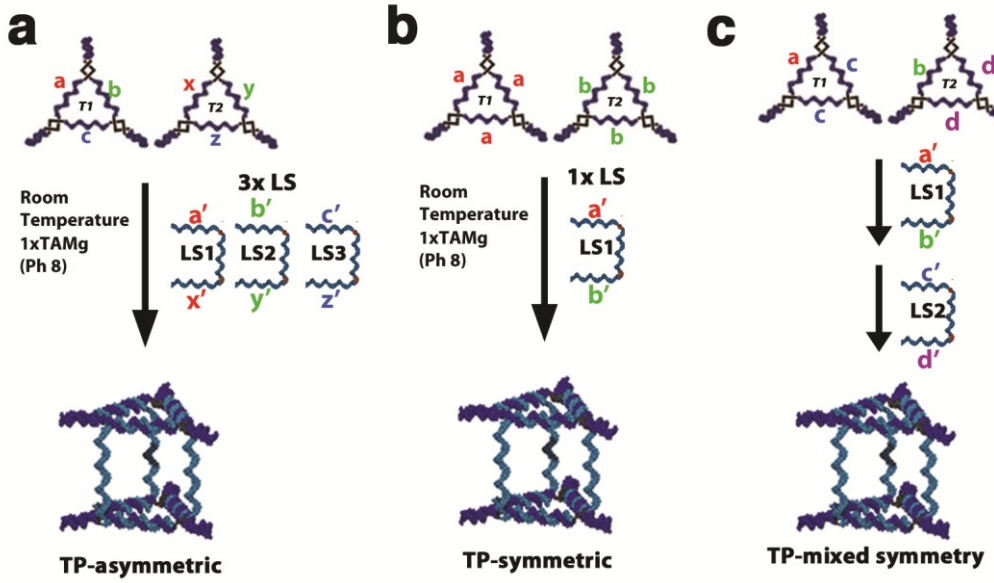

Figure A2.1 3D DNA assembly strategy using linking strands with and without sequence symmetry. a) As an example, asymmetric triangles **T1** and **T2** are assembled into a closed triangular prismatic structure at room temperature using three different linking strands (**LS**). **b)** Using selective sequence symmetry within the triangles, a single linking strand is used to form the 3D DNA structure. **c)** Mixing in an asymmetric linking strand LS1, before adding a second asymmetric LS2, allows for orientation between the polygons to be controlled.

The second part of this section describes a 3D-DNA construction method that assembles a minimum number of DNA strands in quantitative yield, to give a scaffold with a large number of single-stranded arms (Figure A2.2). This DNA frame can be used as a core structure to organize materials in 3D due to the 20mer binding regions, which remain available for further hybridization. For example, Figure A2.2a outlines the modular addition of clips to generate an open tetramer that then folds onto itself to create the cubic DNA structure used in Chapters 4 and 5. This step-by-step scheme is used mainly for illustrative purposes, as the clips are almost always added together in a single pot and annealed together to generate the final structure (Figure A2.2b). As will be outlined in the Methods section, numerous annealing protocols have been developed to form clip-by-clip structures in a facile and efficient manner.

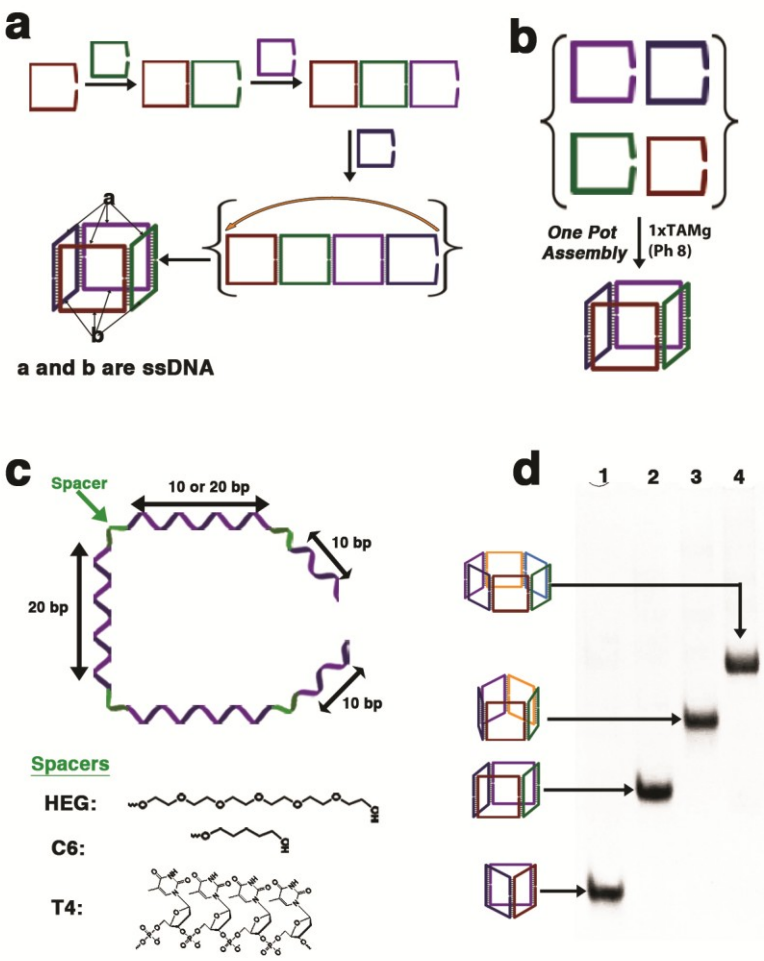

Figure A2.2 3D DNA assembly using a clip-by-clip strategy. a) Schematic representation of the clip-by-clip 3D DNA assembly strategy. Successive addition of each clip in a modular fashion creates higher order intermediates. When the open tetramer is generated, the ends close up to form the fully catenated cubic structure, which contains single-stranded edges (a and b in this case) available for further hybridization. **b)** A more typical one-pot assembly of all four clips to generate the cubic DNA structure. **c)** Various clip designs that have been developed, including dimensions, and chemical spacers used to provide enough flexibility for 3D structure formation. **d)** Assembly and native PAGE (6%) analysis of a triangular prism (lane 1), cube (lane 2), pentagonal prism (lane 3) and hexagonal prism (lane 4) assembled using the clip-by-clip strategy. Each structure was formed from clips modified with a HEG spacer. Each resulting single-stranded region within the structures is 20 bp in length.

Admittedly, this clip-by-clip methodology has gone through numerous iterations – especially when it comes to the actual clip design. The typical dimensions of a DNA clip are outlined in Figure A2.2c. Each vertical edge of a 3D DNA structure is held together by base paring between two 10mers onto the back edge of a second clip (20 bases length). The remaining single-stranded edges

after assembly have been currently designed to be 10 or 20 bases in length. With an appropriate G:C content, the 20mer binding sites can be designed to have denaturation values close to 65^{o}C. The most important design feature is the spacer unit (displayed in green within Figure A2.2c). A variety of spacers have been inserted, which include hexaethyleneglycol (HEG), hexanediol (C6) and a tetra-deoxythymidine (T4). While the T4 spacer has worked well for a triangular prism (with 20mer ssDNA regions) and numerous structures with 10mer ssDNA regions, intermolecular product formation has been observed. This intermolecular byproduct formation has been mainly seen in forming cubes, or higher order structures i.e. pentagonal prism, hexagonal prism, that utilize clips with T4 spacers and contain ssDNA regions of 20 bases in length. Insertion of the HEG and C6 spacers generates clips that display better assembling properties and can be used to make large, flexible 3D structures in excellent yield. As an example, HEG modified clips can be assembled into a triangular, cubic, pentagonal and hexagonal prism in excellent yield. Each of these structures contains multiple 20mer ssDNA regions that can be further used for functionalization (Figure A2.2d). As is outlined in Chapter 2, careful consideration should taken to which spacer (HEG or C6) is used when metal coordination chemistry is employed.

A2.3.1. Solid-Phase DNA Synthesis and Purification of a DNA Clip

1. This section assumes that one is synthesizing a clip to be used in the clip-by-clip strategy (usually 80 bases in length, see Tables 4.1 and 5.1 in Chapters 4 and 5, respectively). Shorter sequences, as required by the modular 3D DNA assembly strategy (see Tables 2.1 and 3.1 in Chapters 2 and 3, respectively), are synthesized and purified in a similar fashion with only slight modifications to this experimental section (see Note 1). Strands with site-specific insertion of HEG or C6 are made on 1,000 Å CPG in 1 μmole quantities. DNA strands are synthesized on a solid support until the required modification is to be inserted. Synthesis is then halted and the 5′ dimethoxytrityl (DMT) protecting group is removed. A coupling adaptor is attached to the solid support along with a 1 mL disposable syringe. The HEG or C6 phosphoramidite (10 μmole, 200 μL) and ethylthiotetrazole (0.2 M in acetonitrile, 200 μL , commercially available) are

micropipetted onto the the solid-phase column (see Note 2). Coupling is performed by slowly moving the liquid across the column via syringe for 8 minutes, after which the phosphoramidite mixture is removed and disposed of. The solid support is placed back on the synthesizer and standard washing, capping, and oxidation steps are performed before continuation of DNA synthesis (see Note 3). Successful insertion of HEG or C6 is monitored by the DMT cation response that occurs after addition of subsequent bases.

2. After synthesis, oligonucleotides are deprotected and cleaved from the solid support by placing the CPG in a screw-cap vial and adding 1 mL of concentrated NH_4OH. The vials are shaken at room temperature for 1 h after which they are placed in a heating bath (60°C) for 2 h and periodically shaken to assist in deprotection (see Note 4).

3. The NH_4OH solutions are transferred to 1.5-mL centrifuge tubes and samples are dried to completeness under vacuum (see Note 5). The samples are then resuspended in 200 – 600 µL of autoclaved H_2O, vortexed gently to ensure dissolution and kept at 4°C until purification (see Note 6). 200 µL of DNA solution is taken and 200 µL 8M urea is added. This will be loaded onto a denaturing gel for purification.

A2.3.2. Purification and Quantification of DNA

1. These instructions assume the use of a Hoefer SE-600 gel system, but are easily adaptable to other formats. Glass plates (20 × 15 cm) are washed extensively with water (soap can be used if plates are extra dirty). Before gel preparation, the plates are rinsed with ethanol (95%) and assembled using 1.5-mm spacers and the casting unit. A preparative 1.5-mm-thick comb is used for preparative PAGE.

2. Prepare a 1.5-mm-thick, 8% gel by mixing 17 mL of the 24% PAGE/urea solution with 33 mL of 1xTB buffer. Mix this solution and add 50 mL TEMED and 50 mg APS (see Note 7). Pour the gel, insert the comb, and wait for polymerization (ca. 10 min). After polymerization, invert the gel, remove the comb, and wash all gel lanes with H_2O.

3. After allowing the gel to set for ca. 30 min, add running buffer TB (1×) to upper and lower chambers of the gel unit and clean lanes with a syringe (see Note

8). Carefully add the 400 µL solution of DNA/urea using a micropipette with loading tip. Add ca. 20 µL of the dye mixture to a small gel lane.

4. Complete assembly of the gel unit and connect to power supply. Run gel at 250 V (30 mA) for 30 min (see Note 9), then change voltage to 500 V and continue to run for 1 h.

5. After the gel has completed running, remove buffer from upper chamber of the gel unit. Carefully remove the glass plates from gel and transfer to a piece of plastic wrap.

6. Place wrapped gel on top of a 20×20 fluorescent TLC plate. Remove upper plastic so that the gel is exposed on one side, irradiate with short wavelength UV light (254 nm) using a hand-held UV lamp, and quickly excise DNA band from the gel (see Note 10) using a sterilized razor blade. Place the excised gel portion into a 15-mL sterilized tube (see Note 5).

7. Using a sterilized pipette tip, crush the excised PAGE band, add 13 mL of autoclaved H_2O and shake well. Place the tube into a Dewar flask filled with in liquid nitrogen until a crackling sound is heard (usually after about 5 minutes) (see Note 11). Take tube out of liquid nitrogen (carefully bringing to room temperature) and place in 60°C bath overnight (see Note 12). Shake periodically to assist in DNA extraction.

8. Remove aqueous layer from the 15-mL tube and reduce volume to ca. 1 mL by evaporation on a Speed-Vac (see Note 13).

9. Wash the storage buffer from the pre-packed Sephadex columns with ca. 30 mL of H_2O. Add DNA solution (1mL) and allow the column to drain completely. Add 400 µL of autoclaved water and allow this drain. Add 1.5-mL autoclaved H_2O and collect at least four 1.5 mL fractions in plastic tubes (see Note 14).

10. Using a microplate reader, assay collected DNA fractions and record absorbance at 260 nm to obtain each concentration (see Note 15).

A2.3.3. Analytical Denaturing PAGE Characterization of Synthesized Clip

1. Prepare a 0.75-mm-thick (20 lane), 8% analytical denaturing PAGE using a similar method as in Subheading 3.2, step 2, but with 8.5 mL 24% denaturing

PAGE solution and 16.5 mL 1xTB buffer.

2. Prepare 10 pmol of each clip in a total volume of 5 µL water (see Note 16) and add 5 µL 8M urea loading solution. Load the samples to each lane of the gel. Load the dye mixture (10 µL) to monitor the running of gel.

3. Run denaturing PAGE at 250 V for 30 min followed by 500V for 1 h. Stain the gel using Stains-All solution (see Note 17). The purified DNA should run as a single band on the gel.

A2.3.4. Assembly of 3D DNA Cube Using a Clip-by-Clip Strategy

1. Equimolar amounts of strands C1− C4 (250 pmol each, see Table 4.1 for sequence details) are added to a PCR microcentrifuge tube (ca. 250 µL total volume for these tubes). 1xTAMg buffer (20 µL) is added to these strands and the total volume brought to 200 µL with autoclaved water.

2. The above mixture is then subjected to an annealing protocol whereby strands are held at 95 °C for 5 min, then 80 °C for 3 min, cooled to 60 °C (2 min/°C), and finally slowly cooled to 4 °C (3 min/°C) (see Note 18). Final cube concentration is ca. 1.25 µM.

3. Prepare 0.75-mm-thick (20 lane) native PAGE (6%) using a method similar to that in Subheading 3.3, step 1, but using 18.75 mL 8% native PAGE solution diluted with 6.25 mL of 1xTAMg buffer. Polymerize gel with 25 mg APS and 25 µL or TMED.

4. Run native PAGE at 250 V and 60 mA for 3 hr at room temperature (see Note 19) and then stain with Stains-All (see Note 17). This native gel demonstrates the assembly of a cube assembled using the Clip-by-Clip strategy (see Figure A2.2d above for native PAGE example).

A2.3.5. Assembly and characterization of Triangular Prism using sequence symmetry

1. This section will outline the assembly of a sequence symmetric triangular prism from triangles **T1** and **T2** (see Note 20). First, stock solutions of each polygon, **T1** and **T2**, were made by taking 0.70 nmole of the component strands (see Table 3.1 for sequence details) and adding them together with 10 µL of 10xTAMg buffer.

The total volume was then adjusted to 100 μL with autoclaved water. A 10 minute hybridization time at room temperature was allotted before use. The final concentration of **T1** and **T2** stock solutions is thus 7 μM.

2. For triangular prism (**TP**) assembly, a stock solution of linking strand **LS1** (see Table 3.1 for sequence) was prepared in 1xTAMg buffer at a concentration of 21 μM. The step-wise 3D assembly of **TP** is achieved by taking 1 μL of **T1** (7 μM) and adding 1 μL of **LS1** (21 μM). After a 3-5 minute wait time at room temperature, the triangle is pre-loaded with 3 linking strands now ready for binding with the second polygon. The second triangle **T2** (1 μL, 7 μM) is then added to the mixture, with an additional 3-5 minute wait time, to generate single-stranded 3D prism **TP** (see Note 21). Top up the solution to a total volume of 5 μL with 1xTAMg buffer (Based on quantitative assembly, the [3D] is now 1.4 μM). All of the assembly steps can be carried out at room temperature.

3. Prepare a native PAGE (6%) as outlined in sub-heading A2.3.4, step 3.

4. To characterize **TP**, take 2 μL of the above solution and add 8 μL of 1xTAMg buffer (see Note 22). Add 2 μL glycerin loading solution to the sample and load onto the 6% gel. Into a different lane add the dye mixture (ca. 10 μL) to monitor the running of gel.

5. Run native PAGE at 250 V and 60 mA for 5 hr at 10°C (see Note 23) and then stain with Stains-All (see Note 17). This native gel demonstrates the assembly of **TP** using a sequence symmetric linking strand (see Figures 3 for native PAGE example).

A2.4. Notes

1. Purification conditions for strands of length between 30 and 50 bases are typically done using a 12 or 15 % PAGE solution to obtain best separation results. For these lengths of strands, with modifications and performed on a 1 μmole scale, half of the column is loaded onto the gel for purification. Refer to ref. 2 for recommended PAGE purification conditions with respect to oligonucleotide length.

2. Early DNA synthesis protocols were based on the use of a Biosystems Expedite 8900 instrument. All current synthesis is being performed on a Bioautomation

MerMade MM6 machine. Because the column designs are different between instruments, off-column couplings are now being performed in a glove box to reduce contact with moisture and oxygen. Also, Mermade synthesizers require a Female luer x female luer adapter (Cole-Palmer, WU-45501-22).

3. These steps can be directly modified and automated within the synthesizer script file.

4. These are manufacturer protocols for cleavage/deprotection. To ensure full deprotection, especially for longer strands (>60 bases), it is recommended that incubation time at 60 ^{o}C be increased to 3 – 5 h.

5. Effort should be taken to use only sterilized plastic ware and, if possible, materials that are certified RNase–DNase free.

6. Depending on how well your synthesis looks will determine how much DNA is loaded onto the gel for purification. As an example, synthesis of an 80mer clip (1 μmole scale) with four good off-column couplings of HEG, should be resuspended after deprotection in 600 μL of autoclave water. The DNA (200 μL) is then mixed with 8 M urea (200 μL) and purified by denaturing PAGE. The remaining 400 μL (2/3 of a 1 μmole synthesis) of impure DNA is frozen until required for additional purification.

7. Excess APS or TEMED can cause rapid cross-linking of the gel matrix and lead to non-homogenous pore sizes. This can result in uneven migration of DNA. Be patient and take your time casting gels.

8. Gel lanes should be extensively washed to remove any unpolymerized acrylamide that can cause unwanted mobility effects in PAGE or failure of the sample to penetrate the gel matrix (see reference 2 for further details).

9. The initial 30 min at 250 V helps to “stack” the DNA within the gel matrix, leading to a uniform and condensed band. This step helps toward reliable excision from gel without taking the n−1 products.

10. Care should be taken to avoid prolonged exposure of DNA (<15 s) to the short wavelength UV light as degradation can occur.

11. Freezing in liquid nitrogen has been found to help extract the DNA. This is likely due to rapid expansion of the gel matrix upon cooling. Do not drop frozen

tubes and this can lead to cracking of the plastic and subsequent contamination of the DNA.

12. If you are in a time crunch, it is unnecessary to do the extraction overnight. The author has done extractions for as little as 4 h and still retained high recovered yields for DNA.

13. The current protocols for size-exclusion are quite exact, so try and get as close to 1 mL as possible for the final volume that will be loaded onto the column.

14. If the initial volume added was 1 mL, your DNA should be concentrated in fraction 2. It is not recommended to combine fractions 2 and 3, as the latter may contain trace amounts of urea or buffer. One can dry down fraction 3 and keep it for the next time size exclusion is performed.

15. Currently, DNA is quantified in 96 well plates. A typical dilution factor might be 50x with a total volume of 100 μL i.e. 4 uL DNA + 196 μL H_2O.

16. This is based only on the authors experience using a 20 lane comb and StainsAll visualization. DNA strands of 80 bases in length can be visualized well after loading 10 pmole. Tune this amount according to the length of DNA being assayed.

17. Times vary depending on how fresh the StainsAll solution is and how evenly one wants the gel to be stained. For publication gels, the author typically leaves gels in solution overnight.

18. This anneal program works well, but takes 4 h. The following anneal protocol works just as well for all structures assembled using HEG or C6 modified clips and takes only 2 h: 95 ^{o}C – 5 min, 80 ^{o}C – 90 sec, cooled to 60 ^{o}C (1min/^{o}C) and slowly cooled to 4 ^{o}C (90 sec/^{o}C).

19. Run times should be lengthened to 4-5 h for better resolution of double-stranded and larger structures. Also, make sure the bottom chamber of the gel box is filled with 1xTAMg to prevent heating of the gel during the run.

20. Although there are some differences here between the method outlined in Chapter 2, these conditions can be directly applied to either the asymmetric version or any system that contains phenanthroline insertions.

21. Although **TP** assembly is outlined in a modular fashion, all strands can be added together quickly to get the same result. See Chapter 3 for discussion on the assembly.

22. This 10 μL total volume is simply to make loading onto the gel easier.

23. Most native PAGE analyses are currently run by the author at room temperature (ca. 22 ^{o}C). The 10 ^{o}C temperature may be unnecessary and was a vestige of the work developed in Chapter 2.

A2.5. Reference

(1) Yang, H.; Lo, P. K.; McLaughlin, C. K.; Hamblin, G. D.; Aldaye, F. A.; Sleiman, H. F. *Methods. Mol. Biol.* **2011**, *749*, 33.

(2) Albright, L.M.; Slatko, B.E. Appendix 3B, denaturing polyacrylamide gel electrophoresis. *Current Protocols in Nucleic Acid Chemistry*. **2003**, A.3B.1-A.3B.5. John Wiley and Sons, Inc